PNL-10187
UC-[redacted]
2030

Experimental Data and Analysis to Support the Design of an Ion-Exchange Process for the Treatment of Hanford Tank Waste Supernatant Liquids

D. E. Kurath
L. A. Bray
K. P. Brooks
G. N. Brown
S. A. Bryan
C. D. Carlson
K. J. Carson
J. R. DesChane
R. J. Elovich
A. Y. Kim

December 1994

Prepared for Westinghouse Hanford Company
and the U.S. Department of Energy
under Contract DE-AC06-76RLO 1830

Pacific Northwest Laboratory
Operated for the U.S. Department of Energy
by Battelle Memorial Institute

Battelle

PNL-10187

DISCLAIMER

PACIFIC NORTHWEST LABORATORY
operated by
BATTELLE MEMORIAL INSTITUTE
for the
UNITED STATES DEPARTMENT OF ENERGY
under Contract DE-AC06-76RLO 1830

Printed in the United States of America

Available to DOE and DOE contractors from the Office of Scientific and Technical Information, P.O. Box 62, Oak Ridge, TN 37831; prices available from (615) 576-8401. FTS 626-8401.

Available to the public from the National Technical Information Service, U.S. Department of Commerce, 5285 Port Royal Rd., Springfield, VA 22161.


The contents of this report were printed on recycled paper

PNL-10187
UC-[redacted]
2030

EXPERIMENTAL DATA AND ANALYSIS TO SUPPORT THE DESIGN OF AN ION-EXCHANGE PROCESS FOR THE TREATMENT OF HANFORD TANK WASTE SUPERNATANT LIQUIDS

D. E. Kurath
L. A. Bray
K. P. Brooks
G. N. Brown
S. A. Bryan
C. D. Carlson
K. J. Carson
J. R. DesChane
R. J. Elovich
A. Y. Kim

December 1994

Prepared for
Westinghouse Hanford Company
and the U.S. Department of Energy
under Contract DE-AC06-76RLO 1830

Pacific Northwest Laboratory
Richland, Washington 99352

EXECUTIVE SUMMARY

BACKGROUND

Hanford's 177 underground storage tanks contain a mixture of sludge, salt cake, and alkaline supernatant liquids. The insoluble sludge consists of metal oxides and hydroxides and contains the bulk of many radionuclides. The water-soluble salt cake, the residuum from extensive evaporation of aqueous solutions, consists primarily of sodium salts. The supernates are concentrated aqueous solutions of sodium and potassium nitrates. Most of the water-soluble radionuclides, such as ^{137}Cs, are in salt cake and supernate.

Disposal options for these wastes are high-level waste (HLW) glass for disposal in a repository or low-level waste (LLW) glass for onsite disposal. Systems-engineering studies show that economic and environmental considerations preclude disposal of these wastes without further treatment. Difficulties inherent in transportation and disposal of relatively large volumes of HLW make it impossible to vitrify all of the tank waste as HLW. Potential environmental impacts make direct disposal of all of the tank waste as LLW glass unacceptable. Although the pretreatment and disposal requirements are still being defined, most pretreatment scenarios include retrieval of the aqueous liquids, dissolution of the salt cakes, and washing of the sludges to remove soluble components. Most of the cesium is expected to be in the aqueous liquids, which are the focus of this report on cesium removal by ion exchange.

The main objectives of the ion-exchange process are removing cesium from the bulk of the tank waste (i.e., decontamination) and concentrating the separated cesium for vitrification. Because exact requirements for removal of ^{137}Cs have not yet been defined, a range of removal requirements will be considered. This study addresses requirements to achieve ^{137}Cs levels in LLW glass between 1) the Nuclear Regulatory Commission (NRC) Class C (10 CFR 61) limit of 4600 Ci/m^3 and 2) 1/10th of the NRC Class A limit of 1 Ci/m^3 (i.e., 0.1/m^3. The required degree of separation of cesium from other waste components is a complex function involving interactions between the design of the vitrification process, waste form considerations, and other HLW stream components that are to be vitrified.

REPORT OBJECTIVE

This report summarizes much of the data necessary for the design of an ion-exchange process that will remove cesium from Hanford tank waste supernates and sludge wash waters. It includes information on the expected feed compositions, process performance criteria, equilibrium behavior, and kinetic behavior of two ion-exchange resins: Duolite™ CS-100, a phenol-formaldehyde resin, and R-F, a resorcinol formaldehyde resin developed by researchers at the Savannah River Site (SRS). A preliminary engineering analysis presents the results of efforts to model equilibrium, column loading, and elution. Significant areas that are not covered include resin production, shelf life, mechanical stability, column hydraulics, and removal of other radionuclides of potential interest (^{90}Sr, ^{99}Tc, and transuranic components).

SUMMARY OF RESULTS

In general, R-F resin was much more selective for cesium than CS-100, roughly 6-fold to 12-fold at 25°C and up to 20-fold under some conditions at 40°C. Equilibrium behavior suggests that low temperature, concentrated feeds, and low potassium favor the highest cesium loading. As temperature fell from 40°C to 10°C, the average selectivity for cesium doubled for CS-100 and increased by about 40% for R-F. The amount that could be processed per unit volume of exchanger diminished by 30% to 35% for CS-100 and 25% to 30% for R-F when complexant concentrate (CC) was diluted from 7M to 3M sodium. Potassium decreased the cesium loading on both resins. The amount of potassium ($[Na^+]:[K^+]$ = 7.4) in Double-Shell Slurry Feed (DSSF) significantly reduced the cesium column distribution ratio (Cs λ) of both resins. Equilibrium Cs λ for CS-100 was 25 with DSSF ($[Na^+]:[K^+]$ = 7.4, 7M Na, $[Na^+]:[Cs^+] = 10^5$, 25°C) versus 38 with CC waste simulant ($[Na^+:[K^+]$ = 200, 7M Na, $[Na^+]:[Cs^+] = 10^5$, 25°C). At the same conditions, Cs λ for R-F was 170 with DSSF and 400 with CC waste.

The rate-limiting step in loading 200 mL bench-scale columns with Neutralized Current Acid Waste (NCAW) simulant (5M Na, low K) appears to be diffusion in the particle phase. The breakthrough curves showed little to no dependence on the velocity of the fluid through the exchanger bed, and mass-transfer coefficients were nearly independent of the flow rate. The shape of

the breakthrough curve is largely a function of the residence time of the feed in the column.

In loading the bench-scale columns with DSSF simulants, the rate-limiting step appears to be diffusion in the particle phase with an element of film diffusion. The slope of the breakthrough curves was less dependent on the feed velocity than would be expected if loading were completely controlled by film diffusion. The apparent difference in the significance of film diffusion may be because DSSF is more viscous than NCAW; diffusion in viscous liquids is slower.

When the loading process is limited by diffusion in the particle phase, the breakthrough curves of 200 mL columns can be expected to be reasonably similar to those of full-scale columns at similar feed composition, operating temperature, and flow rate (column volumes [cv]/h). Theoretically, the column dimensions have no impact when loading is particle-phase-controlled. Columns are commonly designed with length to diameter ratio (L:D) >1.5 to minimize problems associated with channeling and feed distribution. A larger L:D may be chosen for processing of more concentrated feeds, such as DSSF, in which film diffusion plays a significant role, or to provide a higher feed velocity, thereby reducing the thickness of the diffusion layer and improving the loading rate.

Both resins could be eluted with nitric acid or formic acid. Eluting at a slower rate, raising the temperature, or decreasing the acid concentration can minimize the amount of chemicals added as eluant. Although using less-concentrated acid adds fewer chemicals to the system, the volume of eluant is larger. Elution of R-F resin required (at similar process conditions) fewer moles of acid per volume of waste processed because its selectivity for cesium was higher.

Significant channeling of eluant occurred during many runs with R-F resin (batch BSC-187, produced in 1988) in 200 mL columns. During elution, the resin shrinks ≈35% and tends to adhere to itself, pulling away from the column walls. The result is usually a poor elution curve, requiring excessive quantities of eluant, and incomplete elution of the cesium. In some cases, elution was continued even though the resin had shrunk. The resin apparently

was not very sticky; lightly stirring the resin and allowing the column to settle provided excellent elution profiles. It is not known if channeling will be a problem in full-scale columns, in which the resin might settle under its own weight.

Channeling did not occur during elution of a new batch of R-F resin (BSC-210), which did not agglomerate. The reason(s) for the different elution performance of the two batches of resin remain unknown.

Published data suggest that both resins lose capacity at a rate of 2% to 3% per loading/elution cycle. However, the estimate for R-F was based on only 7 cycles, and the data for CS-100 were obtained in 1979, when the resin was made by a different manufacturer.

Comparison of equilibrium data for CC waste (high-organic) to NCAW (low-organic) suggests that the complexants have little effect on the equilibrium behavior of the resins. The organic complexants are probably present as anions and do not participate in the exchange reaction. They would be expected to bind with divalent ions (e.g., strontium) but not with monovalent ions (e.g., cesium).

It is possible, although not likely, that repeated exposure to the complexants could foul the resins. Resin fouling with inorganic precipitates is a potential problem, especially during the processing of concentrated waste streams (DSSF at 7M sodium). Many tank wastes are at approximately 40°C, and they generate significant amounts of precipitate when cooled to room temperature. Adequate dilution is one potential solution, although aluminum hydroxide ($Al(OH)_3$) in waste streams that are low in free hydroxide might precipitate on dilution.

ION EXCHANGE PROCESS ANALYSIS

Decontamination requirements were estimated for several waste types and for NRC Class C, A, and 1/10th of Class A limits in LLW glass. The decontamination factor (DF) to meet 1/10th of Class A limits ranges from about 900 for an average single-shell tank (SST) waste supernate (5M sodium feed) to about 55,200 for NCAW. The DF requirement for a blended aqueous phase (all supernates and sludge wash solutions) from an enhanced sludge wash (ESW)

process was about 1700. For Class C limits, the only waste requiring cesium removal is NCAW, and the required DF is approximately 2.

A limited effort directed at defining the compositional limits of the eluate indicates that the ratio of the total moles of monovalent cations (Na^+, K^+, Rb^+) to moles of cesium must be <1500. This number is reached by assuming that 1) the sodium that would normally be added as frit (glass formers) is replaced by sodium in the eluate and 2) sludge from an ESW process is loaded at 50 wt% waste oxides in an HLW glass with a frit composition of 92 wt% SiO_2 and 8 wt% Na_2O. The ratio will remain unverified until the rest of the tank waste treatment system has been defined. The two areas of primary importance in setting the eluant composition are 1) the quantity of washed solids to be vitrified as HLW glass and 2) the characteristics of the HLW glass.

Preliminary examination of a 4-column carousel operation indicated that R-F resin requires about 10% of the total number of column loadings required by CS-100 for a given quantity of waste. For processing an NCAW feed of average composition, the eluate from an R-F loading would have a total cation to cesium mole ratio of about 11; the eluate from CS-100, about 65. For processing a typical DSSF feed, the eluates would have ratios of about 100 and 1200 for R-F and CS-100, respectively. Large DFs are expected to be difficult to achieve with a regenerable system because of the increasing elution requirements with DF. However, a laboratory-scale system achieved DFs in excess of 10,000 for two cycles with SRS waste simulant on R-F resin.

IMPLICATIONS FOR SYSTEM DESIGN

Processing of waste at sodium concentrations >7M will be difficult at 25°C. The DSSF simulant used was near its solubility limit at 7M sodium and 25°C, and higher concentrations would carry increased risks of precipitation and fouling of the resins. Loading the resins with DSSF was partially limited by film diffusion, whereas the less concentrated NCAW was not, probably because NCAW is less viscous. Perhaps more significant is that R-F resin floated in DSSF at 8M sodium; thus, a restraining device in the columns would be required to keep the bed from fluidizing and mixing.

Some processing conditions favor cesium loading and others favor higher flow rates. Lower temperature favors cesium loading, but will probably lower the loading rate, since the diffusion rate is expected to diminish with temperature. Conversely, processing at a higher temperature would increase the diffusion rate and the solubility of the waste components, thereby minimizing precipitation problems, but decreasing capacity. Concentrated feeds favor cesium loading, but reduce the loading rate in DSSF column runs. Detailed trade-off studies are required to define the optimum processing conditions.

A preliminary examination of the column-loading characteristics suggests that use of CS-100 will require larger columns or more columns than will R-F. CS-100 is less selective for cesium, and breakthrough of the cesium during loading would result in lower DFs. A slower flow rate will reduce the extent of early breakthrough, but the columns will have to be correspondingly larger to maintain process rates. Use of columns in series will effectively increase the length of the column and result in higher DFs.

A preliminary examination of the elution data indicates that the moles of acid required for elution to a given cesium concentration (C/C_0) can be minimized by reducing acid concentration and flow rate (which together will increase elution time) and raising temperature. If elution time exceeds the time required to load the columns, continuous operation will be impossible.

ACKNOWLEDGMENTS

Pacific Northwest Laboratory (PNL) is collaborating with universities, national laboratories, and industry to develop ion-exchange materials for the pretreatment of nuclear wastes stored at Hanford. The authors would like to acknowledge the contributions to this effort of Ronald M. Orme and Michael J. Klem, Westinghouse Hanford Company; Dr. Jane Bibler, Westinghouse Savannah River Company; Mr. John Burningham, Boulder Scientific Co.; Dr. Rodney S. Skeen and William G. Richmond, PNL, for providing an ion exchange column model; Dr. N.H. Linda Wang, Purdue University, and Dr. R.D. Whitley, Purdue Research, for providing the VERSE-LC© liquid chromatography computer program and the concomitant consultation to implement the model; and Audrey H. Ignatov and Robbie L. Tidwell, PNL, for editorial and organizational support.

CONTENTS

FIGURES

TABLES

NOTE: The data contained in this report can be found in PNL Laboratory Record Book Numbers 54337, 54704, 54462, 54705, 55172, and 55026.

1.0 INTRODUCTION

1.1 BACKGROUND

Hanford's 177 underground storage tanks contain sludge, salt cake, and alkaline supernate. The insoluble sludge consists of metal oxides and hydroxides and contains the bulk of many radionuclides. The water-soluble salt cake, the product of extensive evaporation of aqueous solutions, consists primarily of dried sodium salts. The supernate consists of concentrated aqueous solutions of sodium and potassium nitrate salts. The salt cake and supernate contain most of the water-soluble radionuclides, such as ^{137}Cs. The disposal options for these wastes are high-level waste (HLW) glass for disposal in a repository or low-level waste (LLW) glass for onsite disposal.

Systems engineering studies show that economic and environmental considerations preclude disposal without further treatment. Problems associated with transportation and disposal of relatively large volumes of HLW preclude vitrification and direct disposal of all tank waste in the HLW repository. Direct disposal of all tank waste as LLW glass appears to be unacceptable because of potential environmental impacts. Although the pretreatment and disposal requirements are still being defined, most pretreatment scenarios include retrieval of the aqueous liquids, dissolution of the salt cakes, and washing of the sludges to remove soluble components. Most of the cesium is expected to be in the aqueous liquids, the focus of the ion-exchange process.

The main process objectives associated with the cesium ion-exchange process are removing cesium from the bulk of the tank waste (i.e., decontamination) and concentrating the separated cesium for vitrification. Because the exact requirements for removal of ^{137}Cs have not yet been defined, a range of removal requirements will be considered. This study addresses ^{137}Cs-removal requirements for LLW glass between the Nuclear Regulatory Commission (NRC) Class C (10 CFR 61) limit of 4600 Ci/m^3 and 1/10th of the NRC Class A limit of 1 Ci/m^3 (i.e., 0.1 Ci/m^3). The required degree of separation of cesium from other waste components for disposal as HLW is a complex function involving interactions among the design of the vitrification process, waste-form considerations, and other HLW-stream components to be vitrified.

The technology for cesium recovery from high-level alkaline wastes and sludge wash waters is being developed at the Hanford Site in Richland, Washington (Bray et al. 1993); the Savannah River Site at Aiken, South Carolina (Bray et al. 1990; Bibler et al. 1990); and the West Valley Demonstration Project in West Valley, New York (Bray et al. 1984). Pacific Northwest Laboratory (PNL)[1] used this technology as a starting point for experimental studies and analyses of simulated and actual Hanford tank wastes to evaluate the performance of existing and emerging ion-exchange materials and processes.

1.2 SCOPE

This report covers most of the relevant data and analyses associated with the removal of cesium from Hanford tank waste. It focuses on two ion-exchange resins: CS-100, a phenol-formaldehyde resin developed by Rhom and Haas, and R-F, a resorcinol-formaldehyde resin developed at SRS and produced by Boulder Scientific. This report includes the equilibrium and kinetic data required to design and optimize the ion-exchange process.

Data associated with the zeolites and the newly developed crystalline silico-titanates (CSTs) are not included because the focus of the work is on the development of an ion-exchange system using a resin that can be regenerated. Bray et al. have reported on the performance of zeolites (1984) and CSTs (1993).

1.3 PURPOSE/OBJECTIVES

The overall objectives of the PNL ion-exchange program are to provide experimental data and analyses that will be used to design an ion-exchange process for the removal of cesium from Hanford tank wastes. The work is directed at meeting the following specific objectives:

- evaluation and selection of ion-exchange materials for plant-scale implementation;

---

(1) PNL is operated for the U.S. Department of Energy by Battelle Memorial Institute under Contract No. DE-AC06-76RLO 1830.

- determination and evaluation of equilibrium behavior, including the effect of competing cations, organic complexants, waste concentration, temperature, and pH for application to a wide range of aqueous tank wastes;
- determination and evaluation of column-loading data, including the effect of flow rate, residence time, temperature, and waste concentration;
- determination of the stability of selected ion exchangers in the chemical and radiolytic environment likely to be encountered in actual processing;
- establishment of engineering-scale data for the design and scale-up of ion-exchange equipment; and
- development of preliminary flowsheets to support the design of process and facility.

This report summarizes data and analyses performed by PNL pertaining to the removal of cesium from Hanford tank wastes by use of R-F and CS-100 organic resins. This report is not all-inclusive; additional work is needed to support final resin selection and engineering analyses.

1.4 EXPERIMENTAL AND ENGINEERING APPROACH

The experimental and engineering work is conducted in the framework of the general approach to the development of nuclear waste treatment processes (bench- to pilot- to plant-scale), which is similar to that commonly employed in the chemical process industry. The conventional approach is modified to make extensive use of waste simulants, with small amounts of actual wastes used to verify the results. This is necessary to minimize the use of actual radioactive waste, which is difficult and costly to obtain and work with; confirmation tests with actual wastes are planned.

The experimental approach is directed at the definition and understanding of three major areas: 1) equilibrium behavior, 2) kinetic behavior, and 3) chemical and radiolytic material stability. Equilibrium behavior is studied by repeated batch contacts using small quantities of exchanger and waste simulants to which trace amounts of ^{137}Cs was added for analytical purposes. Equilibrium data are important because the equilibrium behavior defines the maximum loading performance that can be expected from a

given combination of waste and exchanger and contributes to defining the runs to be performed with lab-scale columns. Kinetic behavior is important because the rate at which a process approaches equilibrium has a direct bearing on process rate and equipment size. Material stability is important for choosing the best exchanger, since the exchangers must withstand the chemical and radiolytic environment encountered in plant-scale operation.

Extensive analysis of the data by empirical correlations and more fundamental methods maximizes the useful information derived from the experimental work. Such analyses provide a means of interpolating or extrapolating the results to a range of process conditions and guide the direction of additional experiments to fill gaps or confirm models. The equilibrium data were analyzed by developing correlations that provide an easy, although limited, method of predicting the behavior of the exchangers. A more involved and general approach is to develop thermodynamic models for ion exchange. Premilimanry thermodynamic models for CS-100 and R-F were developed by OLI Systems, Inc., for use in the Environmental Simulations Program (ESP). The models are in preliminary development and therefore are not presented in this report. The kinetic data were analyzed with equations developed from a differential mass balance and solved with a mathematics package. This analysis provides the fundamental parameters for accurate scale-up of laboratory-scale kinetics for use in pilot-scale and plant-scale columns.

2.0 ION EXCHANGE FUNDAMENTALS AND THEORY

This section gives a theoretical background for the ion-exchange equilibrium and kinetics of cesium and for scale-up of the ion-exchange columns. Section 2.1 focuses on characterizing equilibrium behavior, Section 2.2 presents a fundamental perspective of ion-exchange kinetics, and Section 2.3 addresses some of the key issues associated with scale-up.

2.1 EQUILIBRIUM BEHAVIOR

An important step toward designing the large-scale ion-exchange process is to understand the sodium-cesium exchange properties of the resins and how the process parameters influence exchange. The ionic equilibrium of cesium was measured in Neutralized Current Acid Waste (NCAW) and Complexant Concentrate (CC) simulants on R-F and CS-100 resins under different process conditions, such as varying $[Na^+]$, $[Na^+]:[Cs^+]$, and temperature. Section 5.1 correlates the equilibrium data to provide additional, design-relevant information. The correlations are intended to provide a simple method of predicting cesium column distribution ratio (λ) at specified temperature, $[Na^+]:[Cs^+]$, and $[Na^+]$. This section develops the equation used for the correlations and lays theoretical foundations for understanding how pH and competing ions, such as potassium, affect ion exchange.

This overview of ion-exchange equilibrium behavior is divided into five parts, addressing 1) ion exchange, with particular emphasis on organic exchangers and the influence of pH; 2) the thermodynamic equilibrium constant, a fundamental measure of equilibrium; 3) practical means of characterizing equilibrium, including isotherms and empirical correlations; 4) limitations to the correlations, and 5) approaches to modeling nonideality and multicomponent ion exchange.

2.1.1 General Description of Ion Exchange

Ion exchange is the process by which certain ions in the liquid phase, such as Cs^+, are selectively removed by exchange with ions associated with a solid phase. The solid phase is also called the "resin" and the liquid phase, the "solution."

In the case of tank waste, the liquid phase is a high ionic-strength alkaline solution containing many different ions. The organic resins are milled polymeric particles, 0.3 to >1 mm in diameter, consisting of functional ionic groups joined by crosslinking. In the absence of these crosslinks, the polymer would dissolve in the liquid. Thus, the resin may be considered an immobilized liquid phase containing functional groups capable of ion exchange.

The nature of ion exchange is directly related to the chemical properties of the functional groups that constitute the active sites. Whether a certain chemical group will exchange ions with the surrounding medium depends to a large extent on its degree of dissociation, or ionization; nonionized sites do not participate in ion exchange. The acid-dissociation constant, K_a, characterizes the dissociation according to

$$K_a = \frac{[H_3O^+]\,[A^-]}{[HA]} \qquad (2.1)$$

where $[H_3O^+]$ = hydronium ion concentration
$[A^-]$ = conjugate base concentration
$[HA]$ = undissociated acid concentration.

The pK_a is defined as $-\log_{10}(K_a)$. The pK_a values for p-toluic carboxylic acid and phenol are 4.4 and 9.9, respectively. Assuming that those values are close to the pK_as of the functional groups in the CS-100 resin (carboxylic and phenolic) and the R-F resin (phenolic only), one can illustrate the relation between solution pH and ion exchange.

Ionization, which must precede ion exchange, is a function of pH. Taking the log of both sides of Equation (2.1) and rearranging provides a relation between the pH of the solution in contact with the active sites and the pK_a

$$pK_a = pH - \log_{10}\frac{[A^-]}{[HA]} \qquad (2.2)$$

As shown in Equation (2.2), which is the classic Henderson-Hasselbalch equation, the resin is significantly nonionized when pH is close to pK_a. For example, 50% of the sites are ionized at pH = pK_a, and even more sites are dissociated when pH < pK_a. Since CS-100 has an additional carboxyl group (pK_a 5 ≈ 4.4), it might be expected to operate in a broader pH range than R-F resin (pK_a ≈10). Ion exchange can still occur at pH <pK_a, but the number of dissociated sites can be increased by increasing the pH. For 99% dissociation of a specific functional group, the pH must be 2 units in excess of the pK_a.

2.1.2 Definition of the Thermodynamic Equilibrium Constant

Although a number of monovalent and divalent ions are present in the tank wastes, and the high ionic strength, Donnan potential, and steric exclusion effects impart nonideality to the cesium ion-exchange system, the following discussion assumes ideal, binary equilibrium between sodium and cesium ions as a first approximation. Approaches to modeling multicomponent ion exchange and nonideality are discussed toward the end of this section.

The binary exchange reaction of cesium with sodium may be written as

$$\overline{Na} + Cs^+ \rightleftarrows Na^+ + \overline{Cs} \qquad (2.3)$$

where the bar ($^-$) = association with the resin.

The thermodynamic equilibrium constant is the fundamental measure of equilibrium behavior. For the sodium/cesium exchange described by Equation (2.3), the general form of the equilibrium constant is as follows:

$$K^\circ = \frac{a_{\overline{Cs}}^{\nu_{Na}} \, a_{Na}^{\nu_{Cs}}}{a_{\overline{Na}}^{\nu_{Cs}} \, a_{Cs}^{\nu_{Na}}} \qquad (2.4)$$

where a = activity, and
ν = valence.

Substituting the activity coefficients and concentrations into Equation (2.4), and using the fact that both sodium and cesium are monovalent ($\nu = 1$), the equilibrium constant becomes

$$K^\circ = \frac{\gamma_{\overline{Cs}}[Cs]_s \, \gamma_{Na}[Na]_l}{\gamma_{\overline{Na}}[Na]_s \, \gamma_{Cs}[Cs]_l} \tag{2.5}$$

where γ = activity coefficient

$[Cs]_l$ = the concentration of Cs^+ in solution, M

$[Na]_l$ = the concentration of Na^+ in solution, M

$[Cs]_s$ = the concentration of Cs^+ in the resin, M

$[Na]_s$ = the concentration of Na^+ in the resin, M.

2.1.3 Isotherms

More practical descriptions of the equilibrium behavior, including so-called isotherms, are in common use. Equilibrium data are often reported as K_d, which is defined as

$$K_d = \frac{[Cs]_s}{[Cs]_l} = \text{mL/g of exchanger} \tag{2.6}$$

where Cs = the concentration of cesium per mole of exchanger.

The determination of K_d from experimental data is given in Equation (4.1).

The separation factor is defined as

$$\alpha = K_{eq} = \frac{[Cs]_s \, [Na]_l}{[Cs]_l \, [Na]_s} \tag{2.7}$$

which is equal to K_{eq}, the thermodynamic equilibrium constant for ideal solution behavior ($\gamma = 1$) and monovalent ion exchange ($v = 1$). For monovalent ion exchange, the separation factor is equal to the selectivity coefficient.

The separation factor can be used as the starting point in the derivation of a Langmuir-type isotherm for ion exchange. If the total ion-exchange capacity, Q, is equal to the sum of the $[Na^+]$ and $[Cs^+]$ adsorbed on the resin, rearrangement of Equation (2.7) gives

$$[Cs]_s = \frac{Q\, K_{eq}[Cs]_l}{\left\{[Na]_l + K_{eq}[Cs]_l\right\}} \qquad (2.8)$$

which is in the form of the Langmuir isotherm for gas adsorption (Langmuir 1918).

The assumptions made to arrive at Equation (2.8) were similar to those of the derivation of the Langmuir isotherm. Three assumptions in the Langmuir derivation are that 1) the energy of adsorption is constant over the entire surface, 2) the adsorbed molecules do not interact, and 3) adsorption is limited to a single monolayer (Coulson and Richardson 1991). The derivation of Equation (2.8) is based on the thermodynamic equilibrium constant, which implicitly assumes a constant change in free energy for the reaction. Equation (2.8) also assumes that the ions adsorbed to the resin do not interact with each other (ideal behavior) and that ion exchange is limited to the total capacity of the resin.

The asymptotic behavior of Equation (2.8), hereafter referred to as the Langmuir isotherm, can be useful for interpreting equilibrium data. For low concentrations of cesium in the liquid ($[Cs]_l << [Na]_l/K_{eq}$), Langmuir-type behavior can be expressed as a linear relationship between $[Cs]_s$ and $[Cs]_l$:

$$[Cs]_s = \frac{Q\ K_{eq}[Cs]_l}{[Na]_l} \qquad (2.9)$$

and a log-log plot of $[Cs]_s$ vs. $[Cs]_l$ with a slope of 1. This is referred to as a linear isotherm.

When cesium concentrations in the feed are high ($[Cs]_l >> [Na]_l/K_{eq}$), the cesium concentration in the resin becomes constant as the ultimate capacity of the resin is approached:

$$[Cs]_s = Q \qquad (2.10)$$

To determine the values of K_{eq} and Q, Equation (2.8) can be rearranged to the following form:

$$\frac{1}{[Cs]_s} = \frac{[Na]_l}{Q\ K_{eq}[Cs]_l} + \frac{1}{Q} \qquad (2.11)$$

A plot of $1/[Cs]_s$ vs $[Na]_l/[Cs]_l$ results in an intercept of 1/Q and a slope of $1/(K_{eq}Q)$. The value of Q can be determined directly from the y-intercept, and K_{eq} can be determined from the slope and the value of Q. At the low cesium concentrations used in the experiments, the sodium concentration essentially remains at its initial value.

A different approach is necessary if the slope of the low-concentration equilibrium data on log-log coordinates is significantly different from 1. The Langmuir isotherm will model the data poorly, since it restricts the slope to 1. The exponent can vary in the Freundlich isotherm (Freundlich 1926):

$$[Cs]_s = K[Cs]_l^n \qquad (2.12)$$

where K and m are empirically derived constants.

The Freundlich isotherm has one potential drawback. It does not account for finite capacity of the ion-exchange materials and, therefore, will fit the data only at low to moderate cesium concentrations. For data that span a range of cesium concentrations, exhibiting Freundlich behavior at low concentration and saturation (Langmuir-type behavior) at high concentration, a combination Langmuir-Freundlich isotherm can be used (Koble and Corrigan 1952).

$$[Cs]_s = \frac{K_1[Cs]_l^m}{K_2 + [Cs]_l^m} \qquad (2.13)$$

where K_1, K_2, and n are empirical constants.

The goal of this work is to provide a simple equation to predict the column distribution ratio at specified temperature, $[Na^+]:[Cs^+]$, and $[Na^+]$. The disadvantage of the Langmuir, Freundlich, and Langmuir-Freundlich isotherms is that the temperature, sodium concentration, or both do not appear explicitly in the equations. (Because the Langmuir isotherm is based on thermodynamics, it can be made temperature-explicit, as shown below.) Attempts at correlating the Freundlich isotherm parameters, K and n, with temperature and $[Na^+]$ met with only partial success. No attempt was made to correlate the Langmuir-Freundlich parameters because trends were not apparent. Apart from undertaking a fundamental thermodynamic analysis involving activity coefficients, improvements over the Langmuir and Langmuir-Freundlich isotherms could be accomplished only by developing a more general empirical method of correlation.

The Langmuir equation can be used as a starting point to develop a basis for empirical correlation of the equilibrium data with temperature,

$[Na^+]/[Cs^+]$ ratio, and $[Na^+]$. The Langmuir isotherm explicitly states that $[Cs]_s$ is proportional to $1/[Na]_1$. The temperature dependence of the equilibrium data can be obtained by examination of the temperature dependence of K_{eq}.

$$K_{eq} = \exp\left(\frac{-\Delta G^\circ_{rxn}}{RT}\right) \tag{2.14}$$

Rearranging Equation (2.8) and combining it with Equation (2.14) gives

$$\frac{[Cs]_s}{[Cs]_1} = \frac{Q \exp\left(\frac{-\Delta G^\circ_{rxn}}{RT}\right) / [Na]_1}{\frac{[Cs]_1}{[Na]_1} \exp\left(\frac{-\Delta G^\circ_{rxn}}{RT}\right)} \tag{2.15}$$

The left-hand side of Equation (2.15) is the column distribution ratio, Cs λ. The Cs λ is related to K_d (Equation 2.6) as follows:

$$Cs\ \lambda = K_d \rho_b \tag{2.16}$$

where ρ_b = the bed density of the exchanger.

The units of Cs λ ($K_d \rho_b = [Cs]_s/[Cs]_1$) are volume of liquid per volume of resin.

Neglecting the term with the exponent in the denominator ($[Cs]_1/[Na]_1$ is generally small) of Equation (2.15) suggests a correlation of the form

$$\lambda = C_1 [Na]_1^{C_2} \exp\left(\frac{C_3}{T}\right) \tag{2.17}$$

where C_1, C_2, and C_3 = constants to be obtained by nonlinear regression of the equilibrium data.

The disadvantage of Equation (2.17) is that the dependence of $[Cs]_s$ on $[Cs]_l$ is forced to be linear. Analysis of the experimental data showed that this is not the case; cesium concentration on the resin exhibited Freundlich behavior with respect to cesium in the liquid [see Equation (2.12)]. The correlation for λ should, therefore, have a power-law dependence on $[Cs]_l$.

Since the equilibrium data were taken under conditions of varying $[Na^+]:[Cs^+]$, temperature, and $[Na^+]$, it is desirable to have all three variables included in the correlation for Cs λ. Equation (2.17) can be generalized to include dependence on $[Na^+]:[Cs^+]$ and allow for Freundlich behavior by the following:

$$\lambda = C_1 [Na]_l^{C_2} \left(\frac{Na}{Cs}\right)^{C_3} \exp\left(\frac{C_4}{T}\right) \qquad (2.18)$$

Equation (2.18) gives the form of the empirical correlation used in Section 5.1 to correlate Cs λ for CS-100 and R-F resins with NCAW and CC waste simulants. These correlations will be useful for estimating Cs λ and column-loading parameters for wastes of different composition. For a specific $[Na^+]$ and temperature, the Freundlich isotherm can be reconstructed by rearrangement of Equation (2.18).

2.1.4 Limitations of the Empirical Correlations

The limitation of empirical correlations, such as Equation (2.18), is that they are valid only under the experimental conditions at which the correlated data were taken. The Cs λ were measured over specific ranges of $[Na^+]$, $[Na^+]:[Cs^+]$, and temperature, as well as for specific waste compositions. Specifically, the correlations do not account for the presence of other monovalent and divalent ions. Thus, the correlations for Cs λ are expected to be most accurate for those concentrations and temperatures. The correlations and their ranges of validity are presented in Section 5.1.

2.1.5 Multicomponent and Thermodynamic Modeling

Although the binary (sodium-cesium) isotherms provide a convenient method of correlating the cesium ion-exchange data, multicomponent isotherms are more appropriate. Bray and colleagues showed that the cesium distribution coefficient decreased as the potassium concentration was increased. Potassium is one of many cations that can occupy ion-exchange sites that could be selective for cesium. This interference by potassium and the dependence of Cs λ on $[Na^+]$ demonstrate the multicomponent nature of ion exchange. A simple multicomponent model based on Langmuir-type adsorption behavior for monovalent ion exchange is given by Equation (2.19).

$$\overline{C_i} = \frac{a_i C_i}{1 + \sum b_j C_j} \qquad (2.19)$$

where $(\bar{})$ = concentration on the resin
i = the species of interest
Σ = over all adsorbing species.

A potential disadvantage of using adsorption models, such as Equation (2.19), to describe ion exchange is that ion exchange is physically more complicated than adsorption. The adsorption equations may correlate cesium ion-exchange behavior over the range of concentrations investigated, but only a detailed thermodynamic model will give reliable information that can be extrapolated to other process conditions. Multicomponent isotherms were not investigated as a means of correlating the cesium equilibrium data, because not all of the necessary equilibrium cation concentrations were available.

In thermodynamic modeling of cesium ion exchange, two issues require particular attention: 1) the high ionic strength of the tank wastes (approximately 10 and 25 M for NCAW and CC waste simulants, respectively) precludes the use of dilute-solution theories for the calculation of liquid-phase activity coefficients; and 2) the model should allow for multicomponent ion exchange of monovalent and divalent ions.

The Environmental Simulations Program, OLI Systems, Inc., appears to be a good software candidate for thermodynamic modeling. It is a comprehensive chemical process modeling tool designed to model multicomponent aqueous concentrations up to 40M. ESP is already being used by Westinghouse Hanford Company (WHC) and PNL to model the equilibrium behavior of the tank wastes and to design process flow sheets.

2.2 KINETIC (DYNAMIC) BEHAVIOR

Similar to the study of ion-exchange equilibria, the kinetic (or dynamic) characteristics of an exchanger also are essential for designing an ion-exchange system. The kinetics of the exchanger will impact the size and shape of the column as well as its operating flow rate. Unfavorable exchange rates may require that more columns be placed in series and that the columns be taken offline more frequently than would be predicted by equilibrium data. An unfavorable elution rate can cause other complications, such as increased volume of eluant.

2.2.1 Elements of Exchanger Kinetics

The kinetics of ion exchange involves several steps. In order for ion exchange to take place, the ions must 1) travel from the bulk liquid phase to the particle surface, 2) travel from the particle surface to the exchange sites, 3) exchange with the counterion at the sites, 4) travel back through the particle to the particle surface, and 5) travel back through the solid-liquid interface to the bulk liquid phase.

The ion to be exchanged is originally in the bulk of the fluid passing through the ion-exchange media (see Figure 2.1). For a flowing fluid near the resin surface, the change in ion concentration occurs over a thin stationary region, or film, immediately adjacent to the surface. Thus, the ions must diffuse across the concentration gradient from the bulk fluid to the surface of the ion exchanger. For macroporous resins, diffusion from the surface of the particle to an interior ion-exchange site occurs primarily through the pores. The situation with gel-type exchangers, such as CS-100 and R-F, is more complex; diffusion of water into the bead causes it to swell as the water surrounds the ionic constituents of the resin and equalizes the osmotic

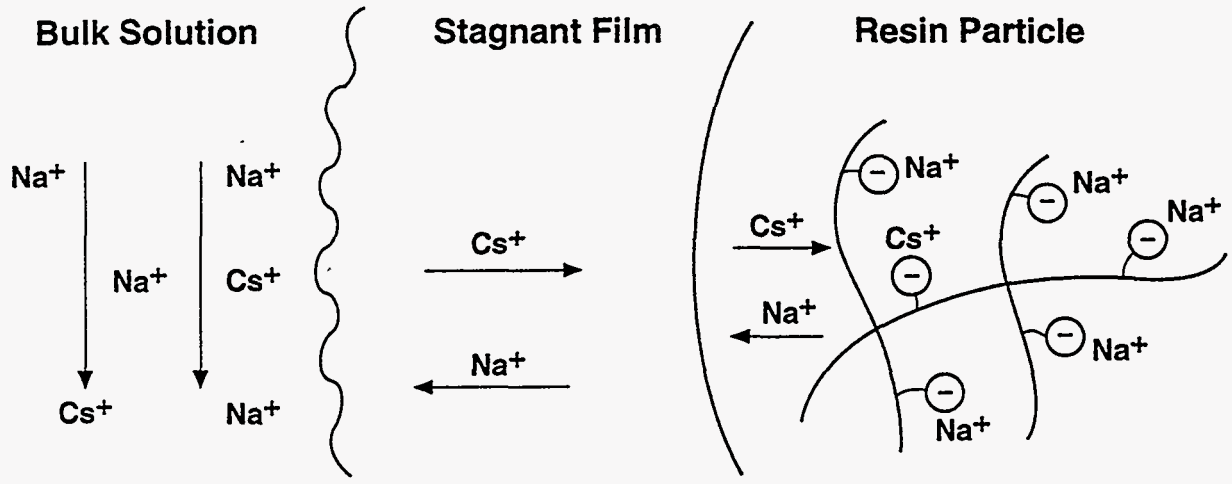

FIGURE 2.1. Elements of Exchanger Kinetics

electroneutrality between all ions must be satisfied. Thus, the counterion pressure between the solution and the resin. Ions travel along a concentration gradient through this aqueous phase of the bead, moving between the exchange sites toward the bead center. During this process, must diffuse outward through the particle phase and the film layer to the bulk fluid. One of these processes may be much slower than the others; it is referred to as the rate-limiting step. The rate-limiting step alone can determine the overall exchange rate, greatly simplifying the mathematical analysis. In simple ion exchange, adsorption and desorption at the exchange site are generally faster than diffusion through the film and particle (Helfferich 1962). Thus, it becomes a matter of determining whether mass transport is limited by diffusion of ions in the particle phase (particle-diffusion control) or diffusion of ions in the film phase (film-diffusion control). In particle-diffusion control, the ion concentration in the film phase is constant because diffusion occurs so quickly; the concentration gradient is in the particle phase. In film diffusion, the concentration gradient is in the film phase (see Figure 2.2).

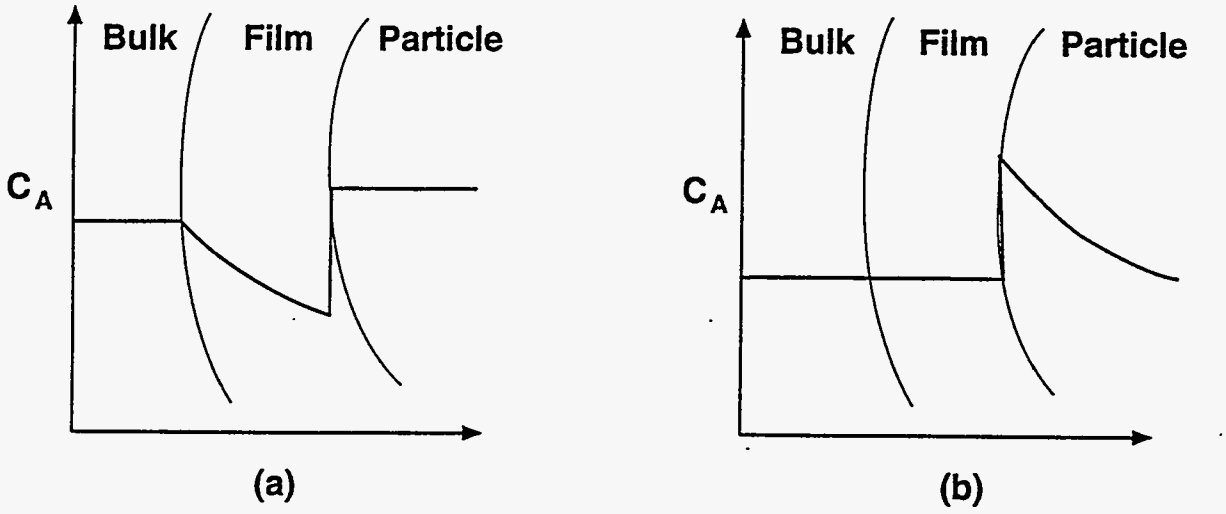

FIGURE 2.2. Illustration of the Concentration Gradients for Mass Transport Limitations in the (a) Film Phase and in the (b) Particle Phase

The Helfferich (He) number provides a qualitative method of comparing the effects of several exchange parameters on the relative importance of each diffusion mechanism.

$$He = \frac{\overline{C}\overline{D}\delta}{CDr_0}(5+2\alpha) \qquad (2.20)$$

where C and D = the overall concentration and diffusivity in the liquid
$\overline{C}$ and $\overline{D}$ = the resin capacity and diffusivity
δ = the thickness of the film layer
r_0 = the particle radius
α = the separation factor.

An He number much greater than 1 indicates that film diffusion limits the rate of exchange; much less than 1, particle phase diffusion; and close to 1, both effects could be important. Film-diffusion control therefore prevails with an exchanger with high capacity ($\overline{C}$) and selectivity (α), dilute solutions

(small C), small particles (r_0), and a low degree of mixing (large δ). Estimates of the Helfferich number for R-F and CS-100 resins will be provided in Section 5.2.

2.2.2 Modeling Exchanger Kinetics

Several levels of complexity can be used to describe the ion-exchange kinetic process. The simplest is the linear driving force approach, in which the flux of ions is based on the concentration difference in the film or particle and a mass-transfer coefficient. For both particle- and film-diffusion control, the diffusion rates (in equivalents) of the exchanging counterions are assumed to be constant and equal. The mass-transfer coefficient is constant with respect to resin loading, time, and concentration. No resin particle shape is assumed.

It is instructive to analyze the empirical mass-transfer coefficient correlations for a packed bed of spherical particles (Perry and Chilton 1973). The particle-phase mass-transfer coefficient can be represented as

$$k_p a = \frac{15\bar{D}}{r_0^2} \tag{2.21}$$

Particle-phase mass transfer is a function of the diffusivity (ionic mobility) in the particle and the square of the particle radius. Thus, the mass-transfer rate can be increased only by using smaller particles or changing the characteristics of the resin. The flow rate of the liquid has no impact on the mass-transfer rate.

The film-phase mass-transfer coefficient can be represented as

$$k_f a = 2.62\sqrt{\frac{Dv}{r_0^3}} \tag{2.22}$$

Liquid-phase characteristics, such as liquid diffusivity and superficial velocity, become important. Viscosity of the liquid also affects film-limited mass transfer through the diffusivity term. The film mass-transfer

coefficient is less dependent on particle radius than is particle-phase mass transfer: $r_o^{-1.5}$ versus r_o^{-2}.

The description of the mass transfer can be improved by assuming Fick's law. In this case, the concentration flux (J) at any point through the film or particle can be described by the gradient of the concentration, as follows:

$$J=-D\nabla C \tag{2.23}$$

The transport equations must be solved to describe the concentration gradient within the particle or film. The shape of the resin particle then becomes important.

For both Fick's law and linear driving force approaches, the ionic mobility is assumed constant. This assumption of equal diffusivity of both counterions can be relaxed to improve the validity of the model. The Nernst-Planck model (Helfferich 1962) adds complexity. There, diffusivity is not constant with respect to location or time; instead, overall diffusivity is based on each ion's electrical charge, concentration, and diffusivity. As a result, ions of lower diffusivity and charge will slow the exchange process to maintain electrical neutrality with ions of higher diffusivity and charge.

Those assumptions and others can be relaxed to better describe the effect of kinetics in ion exchange. However, many factors besides kinetics, such as dispersion and equilibria, must be taken into account to accurately model experimental data. Each additional level of complexity requires the use of more parameters (which are often not well quantified) and further increases in computation time. For these reasons, the linear driving force model, rather than more complex approaches, is used in Section 5.2 to describe the exchange kinetics.

2.2.3 Column Operation: General Principles

Principles of ion-exchange kinetics and equilibria combine to build an understanding of ion exchange in a column configuration. Unlike batch ion exchange, fresh feed is continuously added to the process in a column operation. As ion exchange progresses, the cesium in the resin near the inlet

of the column loads to equilibrium with the cesium in the feed; consequently the liquid and resin farther down the column equilibrate at lower concentrations of cesium, so that the concentrations leaving the column may be very low. During the ion-exchange process, a concentration gradient forms down the column axis. As the column loads, more of the column will be in equilibrium with the feed composition and the cesium concentration gradient will move further down the column. A sample loading curve at various times is shown in Figure 2.3.

The column approach to ion exchange can remove cesium to a much lower level with less exchanger than the batch-contacting method. For the concentration of cesium in the liquid to approach zero, its concentration must also approach zero in the solid. In a batch-type system, that is possible only if the amount of resin is infinite or through repeated contacts. In a column system, effluent purity is based only on the concentration of cesium on the solid at the egress of the bed, which may be at only trace levels during much of the loading phase.

The ionic concentration gradient moving down the column can be described as a wave whose size and shape depend on equilibrium and kinetic behavior of

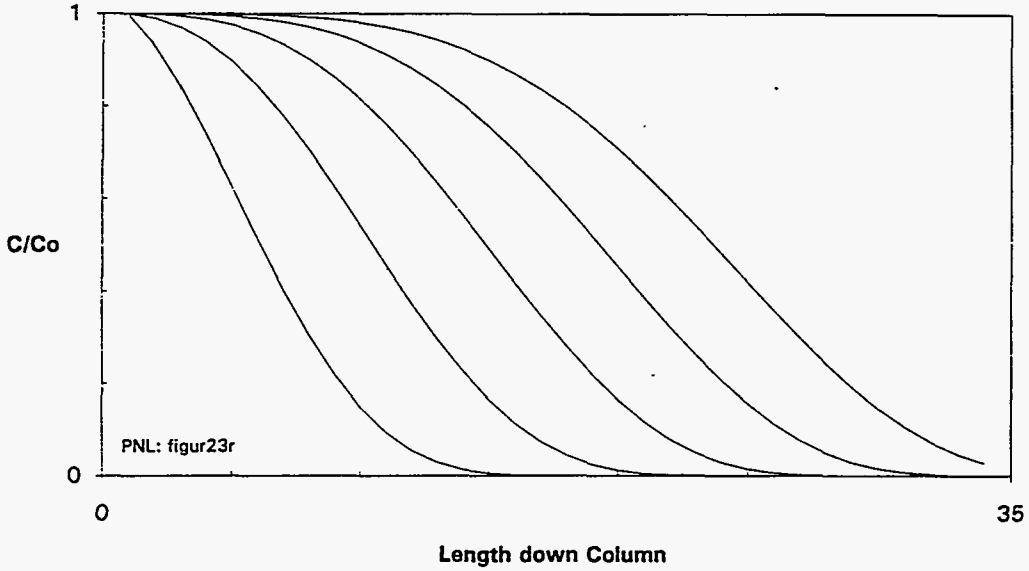

NOTE: After a certain distance, the shape approaches a constant pattern.

FIGURE 2.3. Sample Concentration Gradient in the Liquid for a Self-Sharpening Exchanger at Equal-Time Intervals During the Loading Process

the exchanger. A favorable equilibrium (in which the ion of interest loads on the column preferentially to its counterion) will produce a self-sharpening wave; an unfavorable equilibrium, a nonsharpening wave.

Once established, the self-sharpening wave of the concentration gradient will remain nearly constant, independent of column length (see Figure 2.3). Its S-shaped concentration profile results from a balance between equilibrium and mass-transport effects. Equilibrium promotes a step-function change in the cesium concentration as the wave moves. However, the ion exchanger cannot respond instantaneously to the sharp changes in cesium concentration. Thus, mass-transport effects will tend to spread the ion-exchange curve, forming an S-shaped wave. The result is premature initial breakthrough from the column and a longer time to reach complete loading. For systems that require high purity effluent, understanding the effects of mass transport is crucial to designing an optimum system that will maintaining high purity.

The active zone of a nonsharpening wave increases in length as it moves down the column (Figure 2.4). In many cases, the resin will not be fully loaded at the inlet when cesium breakthrough begins. Thus, maintaining high purity would be very difficult with such an exchanger. The mass-transport effects are additive with the equilibrium behavior to stretch out the shape of

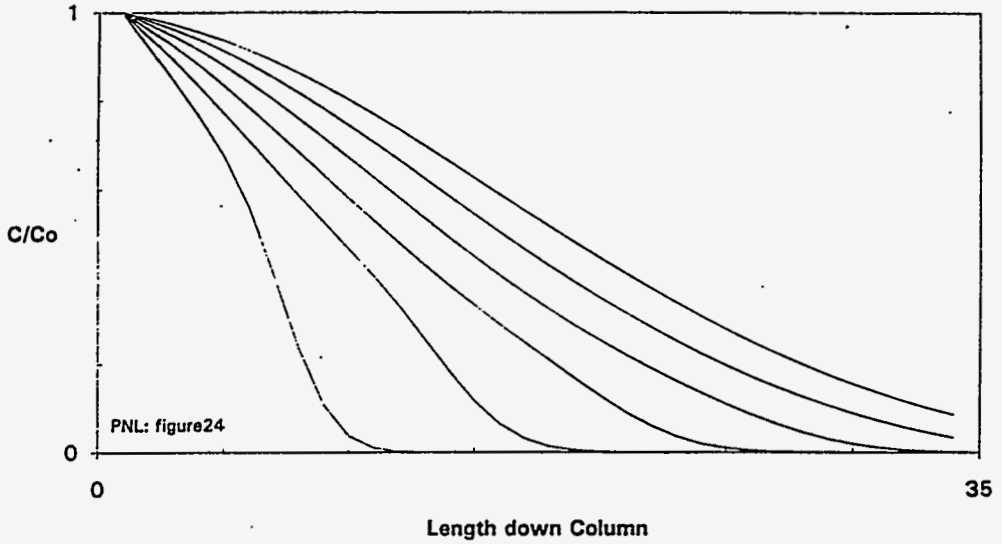

FIGURE 2.4. Sample Concentration Gradient in the Liquid for a Nonsharpening Exchanger at Equal-Time Intervals During the Loading Process

the curve. This makes the two effects more difficult to separate than in the case of the self-sharpening wave. Most elution techniques result in nonsharpening waves (Helfferich 1962).

Breakthrough curves from laboratory-scale column experiments provide information about the equilibrium behavior of the resin. The column distribution ratio of an exchanger (λ) can be approximately determined from the breakthrough curve under certain operating conditions. An example would be the case where the breakthrough curve, or concentration profile, is a step function and every mole of cesium that enters the column loads on the exchanger. Assuming that all the cesium fed to the column is loaded onto the exchanger (breakthrough has not occurred), the following mass balance holds:

moles of cesium fed = moles of cesium on resin

or in equation form:

$$[Cs]_o V_l = [Cs]_s V_b^* \tag{2.24}$$

where V_e = the volume of feed passed through the column

V_b^* = the volume of exchanger fed that is completely loaded

$[Cs]_o$ = the concentration of cesium in the feed.

When all the cesium in the column is totally loaded with cesium, V_b^* = the total volume of the bed (V_b). Equations 2.16 and 2.24 can be combined to give the column distribution ratio

$$\lambda = \frac{[Cs]_s}{[Cs]_l} = \frac{V_l}{V_b} \tag{2.25}$$

Consequently, the column distribution ratio is equal to the number of column volumes of cesium that loaded onto the bed. This derivation assumes that the breakthrough curve is a step function (infinitely fast mass-transfer rates, but the result is approximately true for finite rates of mass transfer. The typical concentration profile is an S-shaped curve with Cs λ approximately

equal to the column volumes of feed processed at C/C_0 = 50%. The moles of cesium that have passed through the column at C/C_0 = 50% are approximately equal to the moles of ion-exchange sites on the bed that remain available for cesium exchange.

Although the effects of mass transfer on self-sharpening waves can be identified as a broadening of the concentration gradient, the differences in film-diffusion control versus particle-diffusion control on the breakthrough curve are much more subtle. Pure film diffusion results in an earlier breakthrough than occurs with particle-diffusion control. Thus, in log-probability coordinates, the curve is slightly concave up rather than a straight line. The effects of particle-diffusion control are opposite. The initial breakthrough occurs later and requires a longer time to reach 100% breakthrough; the curve is slightly concave down. These effects in general are observed only at small C/C_0; however, they may be important if high cesium decontamination factors (DF) are required.

$$\frac{C}{C_0} = (1 - e^{-kt}) \qquad (2.26)$$

2.2.4 Kinetics During Elution of the Column

Elution is generally a nonsharpening-wave phenomenon. The cesium ion prefers remaining on the resin to being removed. In general, resins that are more selective during loading are more difficult to elute. Therefore, elution is more complex to model, and the column equilibrium λ cannot be approximated with the 50% breakthrough point. Integration under the C/C_0 curve is the only way to determine the amount of cesium that has come off the column.

During elution, mass transfer and equilibrium behavior determine the shape of the curve. Mathematical complexity requires that the two bounding cases be examined separately. The first case is that of mass-transfer control only; equilibrium behavior being unimportant. The cesium removal rate is based on the concentration of cesium on the resin, which is constant down the axis of the column. The breakthrough curve begins at a relatively high value and decreases rapidly in proportion to the loading on the exchanger

(Figure 2.5). The higher the mass-transfer coefficient, the sharper the elution curve will be. Loss of ions from the column after the peak can be described as an exponential decay. The rate of cesium elution is independent of the eluant flow rate or concentration. Thus, the lowest flow rate and eluant concentration possible are preferable.

When equilibrium dominates, the elution curve will rise quickly to a constant value, which can be related to the equilibrium between the eluant and the cesium. The curve will remain stable until the cesium in the solid isdepleted below the equilibrium value. A faster flow rate or higher eluant concentration would reduce the elution time; however, the total quantity of eluant required will not change.

2.2.5 Methods for Determining the Rate-Limiting Step

By adjusting the appropriate experimental conditions of the laboratory column run, it should be possible to determine the rate-limiting step for mass transfer. If film diffusion is the rate-limiting step [see Equation (2.22)] the mass-transfer coefficient will increase with the superficial velocity in the column. If the process is limited by particle diffusion, increasing the

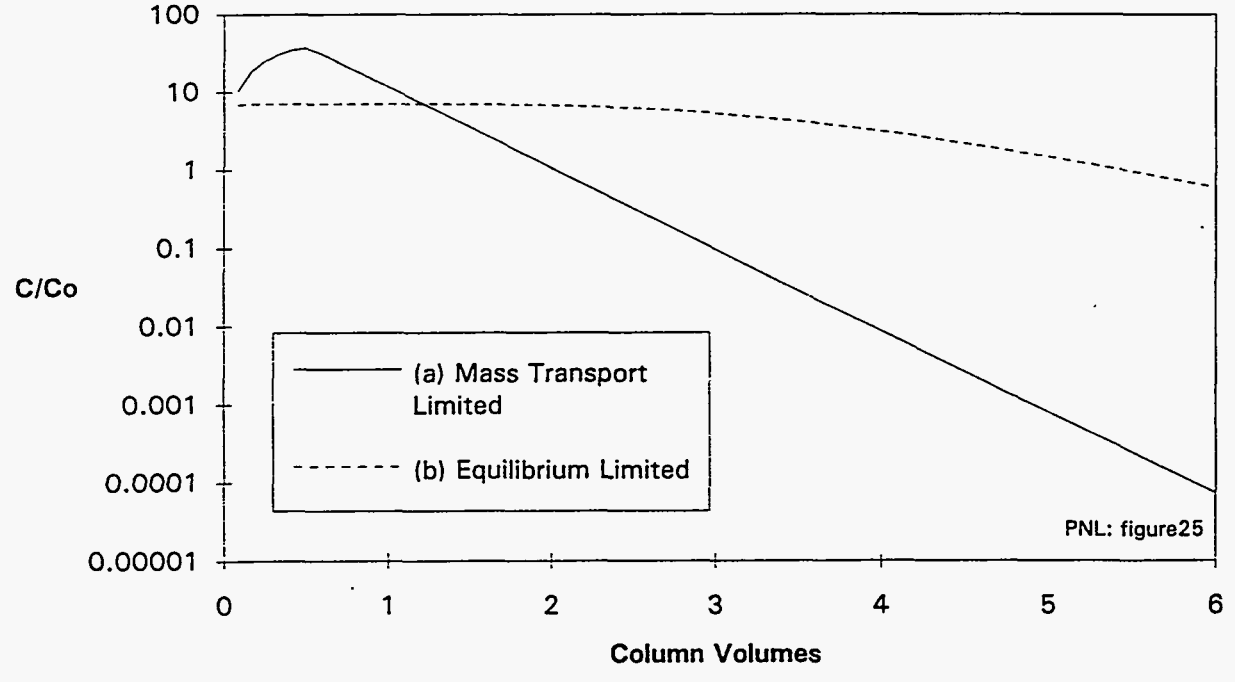

FIGURE 2.5. Sample Elution Curves. (Run (a) is a mass transport limited process; run (b) is a kinetic limited process.)

velocity will not affect the mass-transfer coefficient. The effect of film diffusion is secondary to that of increased flow rate (in cv/h) on the slope of the breakthrough curve. Therefore, identification of changes in slope of the breakthrough curve due to film limitation requires that curves be compared at the same cv/h. For example, a column flowing at 20 mL/min can be compared to a column flowing at 40 mL/min only if the second column contains twice the volume of resin.

The rate-determining step can also be inferred from the results of a "stop-flow" test, in which the flow is halted and restarted during column loading. The behavior of C/C_0 after the column is restarted provides information about the mass-transfer mechanism. If the exchange rate is controlled by diffusion in the particle phase, diffusion of cesium ions within the particles continues even after flow is stopped. Highly concentrated cesium on the outer layers of the resin particles will diffuse toward the particle centers, thereby leveling the concentration gradient in the particle and reducing the C/C_0 on the surface. The result is a decrease in C/C_0 when the column is restarted. As the run continues, the concentration gradients in the particles are reestablished, and the breakthrough curve will slowly approach the shape it would have had without interruption. If the exchange rate is controlled by film diffusion, the halt in flow might temporarily decrease the C/C_0, but after flow is reestablished, the breakthrough curve will rapidly return to its initial level.

A change in particle size is another important method for identifying mass-transfer control phase. If the mass-transfer coefficient increases with the inverse of particle diameter to the 1.5 power, the process is controlled by film diffusion. If it increases with the inverse of the square of the diameter, the process is controlled by particle-diffusion.

Hydrodynamics may complicate identification of the rate-limiting step by affecting the concentration profile in much the same as film or particle diffusion. Hydrodynamic effects include dispersion and channeling. Dispersion is caused by molecular diffusion and eddy currents. Molecular diffusion is the motion of ions in a concentration gradient and is usually significant when flow rates are low and active zones are sharp.

Random packing of the exchange material causes eddy dispersion. The liquid tends to travel at different rates through the various interparticle spaces, and as neighboring stream paths separate and join, the concentration in any given element of solution changes slightly. Unlike molecular diffusion, eddy dispersion is proportional to the flow rate and occurs mostly at higher flow rates. The significance of these effects will be explored in Section 5.2.

Channeling is much the same as eddy dispersion, but occurs on a macroscopic scale. Liquid traverses the path of least resistance (the lowest pressure drop). If packing irregularities or resin shrinkage have caused uneven distribution of exchanger, liquid will bypass the resin. Early breakthrough may result.

2.3 SCALE-UP CONSIDERATIONS

Both batch equilibrium experiments and column experiments play a part in the process of scale-up. Batch equilibrium experiments alone can provide initial rough estimates of column-loading behavior. Improved understanding of column performance requires a knowledge of column kinetics, which includes effects of both equilibrium and mass transfer. Hydrodynamic effects, if important, require additional testing. The following sections describe the role of the various laboratory experiments in column design and scale-up.

2.3.1 Batch Equilibrium Experiments

The nondimensional value (λ), which is calculated from the batch equilibrium experiments, represents the number of bed volumes of waste at a particular concentration that can be loaded onto one bed volume of ion-exchange material. The number of bed volumes loaded can be scaled directly from laboratory experiments to a full-sized column, since this is a reflection of equilibrium behavior only. This is only an approximation, but it can be accurate in a multicolumn system. The flow rate will change the rate of column loading; the column size will change the quantity of cesium loaded, but the value of λ will remain the same.

In design of a full-scale column, λ can be used to balance flow rate and column size. Decreasing the flow rate and increasing the column size will

have similar effects: increased time between elutions. A good rule of thumb is that loading time should be approximately equal to the time required for washing, elution, and regeneration time. With the loading time set, the choice of column size is then a trade-off between capital equipment costs and operating costs (time to complete a job at a given flow rate).

The equilibrium values determined from laboratory experiments cannot be used to determine the time when cesium begins to appear in the effluent (e.g., $C/C_0 = 0.001$). That would be determined by the column kinetics. Equilibrium data alone provide no information about the λ value at other ionic strengths, ion ratios, temperatures, or resin types. Any variations in these parameters during operation will change the λ, the amount of feed processed, and the loading time. Extrapolation to different process conditions and waste types requires modeling or correlation of the data. This effort was undertaken and is described in Section 5.1 of this report.

2.3.2 Column Kinetics Experiments

If the ion-exchange process is limited by diffusion in the particle, scale-up from a small laboratory-scale experiment to a full-scale column can be done directly, based only on column residence time. This can be demonstrated by dimensional analysis of the column transport equations.

If one assumes that dispersive effects are negligible, the transport equations can be written such that the solution is not a function of the size or flow rate of the column. One begins with the mass-balance and linear driving force equations:

$$\frac{\partial C_A}{\partial t} + v_z \frac{\partial C_A}{\partial z} + \frac{(1-\epsilon)}{\epsilon} \frac{\partial \overline{C_A}}{\partial t} = 0 \qquad (2.27)$$

$$\frac{\partial \overline{C}_A}{\partial t} = k_p a (\overline{C}_A^* - \overline{C}_A) \qquad (2.28)$$

where v_z = interstitial velocity
z = distance down the column
ε = interparticle porosity
C_A = concentration of ion A in the liquid
$\overline{C}_A$ = concentration in the solid phase.

The starred (*) concentration is the concentration in the solid in equilibrium with the liquid phase, $k_p a_i$ represents the mass-transfer coefficient times the specific area of the resin, assuming particle-phase diffusion control.

If these equations are recast in terms of

$$x = \frac{z}{L}\,;\ \tau = \frac{L}{V_z}\,;\ \theta = \frac{t}{\tau} \tag{2.29}$$

where x = dimensionless length
τ = residence time in the bed
θ = dimensionless time of operation, they then become

$$\frac{\partial C_A}{\partial \theta} + \frac{\partial C_A}{\partial x} + \frac{(1-\epsilon)}{\epsilon}\frac{\partial \overline{C_A}}{\partial \theta} = 0 \tag{2.30}$$

$$\frac{\partial \overline{C}_A}{\partial \theta} = \tau k_p a\,(\overline{C}_A^* - \overline{C}_A) \tag{2.31}$$

Since ε and $k_p a$ are independent of column size, Equations 2.30 and 2.31 will remain unchanged for a given exchanger and set of experimental conditions if τ is held constant. The solution to these equations (i.e., the breakthrough curve) will then be identical for a laboratory-scale and a full-scale column.

The West Valley Demonstration Project (Kurath 1989) successfully used such a scale-up approach. This project used ion exchange to remove ^{137}Cs from the neutralized supernate from the PUREX process. During the design, PNL used

200-mL laboratory columns containing zeolite (IE-96) to scale-up to the production sized 1700-L columns at West Valley. The breakthrough curves for the laboratory-scale columns and the production unit were nearly identical at similar residence times. Thus, the residence-time scale-up approach was valid, and diffusion was particle-phase-limited for those particular experimental conditions.

The ability to scale up from laboratory to production scale for a particle-phase controlled process does have a limit; the diameter of the laboratory-scale ion-exchange column must not be too small. Because of the space constraint imposed by the column wall, the packing density of a resin is lower near the wall of a column than at its center, and higher flow rates are therefore possible near the wall of the column. In most cases, the quantity of liquid flowing in such channels is insignificant, and dispersion within the column is sufficient to prevent the liquid from bypassing the resin entirely. However, for columns with diameters of less than 20 particle diameters, early breakthrough may occur of too much liquid bypasses the resin.

In the case of particle-phase control, the ratio of column length to diameter (L:D) ideally has little effect on the loading of the column. Mass-transfer characteristics will be determined solely by residence time in the column and not by its shape, since the L:D affects only the velocity of liquid. However, there may be other reasons to carefully consider the L:D. A higher L:D will reduce the impact from channeling or poor distribution of the feed, but it also will increase the pressure drop in the column. The L:D may be determined by available facility space.

If mass transport is controlled by diffusion in the film, the rate of cesium uptake will be a function of flow rate, because k_f (analogous to k_p) is velocity dependent. If diffusion is film-phase control and the full-scale column is longer than the experimental column, the breakthrough curve of the full-scale unit will be sharper than that of the experimental column, and the full-scale column will perform better than the laboratory-scale column at the same residence time. Thus, direct scale-up from a laboratory scale column is an acceptable, although conservative approach.

If film diffusion controls the resin utilization and the DF can be increased by increasing the column L:D for a given residence time. Increasing the L:D provides for a higher interstitial velocity, which will increase the mass transfer coefficient and therefore improve column kinetics. Regardless of which is the rate-limiting step, the use of multiple columns in series will increase resin utilization and DF. Even at high flow rates, the first column will have earlier breakthrough, but no breach in the DF will occur because the cesium leaving the first column will load on the downstream columns. The first column can then be fully loaded before being taken offline for elution. The complexity and cost of additional columns is often outweighed by the improved cesium DF, loading rate, and loading efficiency. Table 2.1 summarizes important column and operational characteristics and their impact on ion-exchange performance.

One limitation of directly using experimental column-run data for scale-up is that the temperature, concentration, particle size, and solution viscosity must be the same at both scales. The shape of the breakthrough curve and the location of mass-transfer control changes with those variables. Thus, column experiments, which are relatively expensive, performed under one set of conditions cannot be used to describe column breakthrough at different conditions. Only by use of a model is it possible to extrapolate to other conditions. The mathematical model will be of further use during scale-up and optimization of process parameters. Experiments are still required, but the use of models will greatly reduce their number.

2.3.3 Characteristics of Operation Specific to Elution

Columns can be loaded either upflow or downflow. Because the resin should not be fluidized during loading, they are generally loaded downflow. Elution similarly can be either done upflow or downflow. Co-current elution is often preferred because the piping and valving for loading and elution are nearly the same. Although counter-current elution requires additional piping, it provides greater elution efficiency. In counter-current elution, the eluant is fed through the bottom of the column, and the resin at the bottom of the column contains the least cesium. The reduced concentration of cesium on the solid at the column exit improves the cesium DF for the next loading.

2.3.4 Limitations of the Laboratory Experiments Performed

Several other important issues must be considered before the columns can be properly scaled up. These cannot be or have not been addressed by the batch and kinetic experiments.

The pressure drop in the column will impact the size of equipment and may restrict the column's shape or flow rate. To estimate the pressure drop in the full-scale columns, the pressure drop in the laboratory-scale columns must be accurately measured or the resin particle size and shape must be better quantified. Better characterization of particle size and shape would allow the use of pressure-drop correlations.

Channeling in the columns may cause early breakthrough, inefficient use of the resin, or a breach in the DF. The potential for channeling as it pertains to column L:D and shrinking and swelling of the resin must be understood before a resin can be implemented in a full-scale column.

Removal of resin from the column is another issue that must be addressed in column design. After many cycles of loading and elution, the resin degrades and eventually must be replaced. This issue needs to be investigated with pilot-scale to full-scale columns that duplicate the expected production-scale design.

Resin fines are produced when the resin is moved and by mechanical and chemical wear during normal operation. The fines can pass through the ion-exchange bed and into the effluent, and if loaded with cesium, can reduce the process DF. Current laboratory studies have not addressed this issue.

TABLE 2.1. Column Scale-Up Considerations

Column Characteristic	Advantages	Disadvantages	Limitations
Increased column length	1. Sharper breakthrough 2. Higher mass transfer if film-diffusion-limited	Higher pressure drop.	1. After reaching a constant pattern, additional length doesn't improve breakthrough. 2. Will not improve breakthrough for elution (nonsharpening).
Decreased particle size	1. Improved kinetics 2. Higher equilibrium capacity in some cases 3. Improve tailing problem if particle-diffusion-limited.	1. Higher pressure drop 2. Small particles are more difficult to work with 3. Smaller fines will reduce DF performance.	1. Mechanical constraints limit maximum pressure drop.
Decreased flow rate	1. Sharper breakthrough 2. Lower pressure drop 3. No improvement if elution is controlled by equilibrium	Lower throughput or larger column required.	Reduced effect of improvement if film diffusion present.
More columns in series	1. Allows higher flow rate with same DF 2. Kinetics of the exchanger less important. 3. Better utilization of resin capacity.	More equipment, resulting in higher maintenance and capital cost.	None
Increased L:D	1. Improved kinetics for film diffusion limitations (sharper breakthrough) 2. Improved flow distribution	Greater pressure drop	1. Less channeling up to a point. If diameter is very small, channeling will increase due to wall effects. 2. May not improve mass transfer if particle phase limited or during elution.
Increased column volume	Longer time between elutions	Larger equipment	Higher shielding requirements.

3.0 BASES AND ASSUMPTIONS

3.1 WASTE COMPOSITIONS

An estimate of the composition of the liquid fraction for the double-shell tank (DST) wastes [NCAW, Double-Shell Slurry Feed (DSSF), and CC] is shown in Table 3.1. (Simulant compositions used in the PNL experimental program are listed in Section 4.2). The estimates are averages of several tank compositions and were derived from the inventories given in Boomer (1993).

Tables 3.2 and 3.3 provide, respectively, a summary of the cesium inventories in the aqueous phase and the inventories of major competing cations (Na, K) (Boomer 1993).

The compositions of the aqueous phases (see Table 3.4) reflect a likely range of ion exchange feeds. The $[Na^+]:[Cs^+]$ ranges from a low of 9800 for NCAW to a high of 4.41E+05 for aqueous solutions expected from the dissolution and washing of single-shell tank (SST) wastes. The $[Na^+]:[K^+]$ ranges from a low of 10 for NCRW supernate to a high of 1600 for aqueous solutions expected from the dissolution and washing of SST wastes. The DSSF $[Na^+]:[K^+]$ is an average number; the waste in Tank 241-AW-101 has the highest concentration of potassium, with $[Na^+]:[K^+] = 7.4$.

Because wash factors were applied, the inventories in Table 3.4 are slightly less than the total inventories in Table 3.1. Wash factors account for the fact that incomplete washing and adsorption of some of the components by the solids in the tanks will leave behind some soluble materials. These data are presented with the footnotes on the tables. Additional information on the wastes and the sources of the data may be obtained in the references (Boomer 1993).

TABLE 3.1. Supernatant Compositions

Waste Component	NCAW Supernate, M	DSSF Supernate, M	CC Supernate, M
Al	1.69E-01	1.16E+00	1.09E+00
Ba	1.06E-05	4.41E-05	1.97E-04
Ca	1.56E-04	1.74E-03	9.62E-03
Cd	2.38E-05	5.04E-05	
Cr	1.42E-02	8.99E-03	2.60E-02
Cs[(a)]	4.05E-04	8.52E-05	1.22E-04
Cu	2.43E-05	6.68E-05	
Fe	2.27E-04	4.11E-04	2.73E-02
K	7.29E-02	6.81E-01	4.40E-02
Mg	6.84E-05	4.37E-04	6.74E-03
Mo	7.10E-04	5.87E-04	2.77E-03
Na	3.43E+00	9.99E+00	1.08E+01
Ni	3.51E-05	1.94E-04	5.30E-03
Rare Earths (La)	6.50E-05	7.55E-08	1.60E-03
Si	1.13E-02	5.88E-03	
Sr		5.54E-07	9.35E-05
UO2	2.90E-03	5.93E-04	1.25E-05
Zn	9.83E-05	2.61E-04	8.00E-04
Cl-	3.10E-03	1.89E-01	1.72E-01
CO3-2	8.51E-02	9.65E-02	7.00E-01
F-	5.97E-02	1.01E-01	1.13E-01
NO2-	4.10E-01	2.11E+00	9.99E-01
NO3-	9.00E-01	3.04E+00	3.71E+00
OH-(total)	2.04E+00	8.53E+00	7.61E+00
PO4-3	6.95E-02	7.60E-03	6.32E-02
SO4-2	1.61E-01	2.69E-02	7.63E-02
TOC (g/l)	1.22E+00	3.09E+00	2.45E+01
137CsBa (Ci/L)	1.92E+00	2.69E-01	4.05E-01
90Sr (Ci/L)		6.38E-04	1.08E-01
99Tc (Ci/L)	3.26E-04	9.69E-05	2.85E-04
241Am (Ci/L)		9.38E-06	3.70E-04
239/240Pu (Ci/L)		1.15E-05	1.11E-04
Volume (m^3)	6.74E+03	4.82E+04	1.80E+04
$[Na^+]:[Cs^+]$	8.50E+03	1.17E+05	8.85E+04
$[K^+]:[Cs^+]$	1.36E+02	9.05E+03	3.89E+02

(a) The values in Table 3.1, which are based on 1991 inventories, are higher than those in Table 3.2, in which the radionuclide inventories are decayed to December 1995.

TABLE 3.2. Cesium Inventory in Hanford Supernates

Waste Type	^{137}Cs,Ci	Mass of ^{137}Cs, kg	Total Mass, kg	Isotopic Ratio	Fraction Assumed Soluble	Mass in aqueous phase, total	Moles in aqueous phase, total
	(1)(2)(3)	(4)	(5)	(6)	(7)	kgs	(8)
NCAW	1.15E+07	133	350	0.38	0.97	340	2530
NCRW	3.52E+05	4.1	11	0.37	0.5	5.5	40
PFP	1.70E+05	2.0	7	0.28	0.95	6.7	50
CC	6.49E+06	75	285	0.26	0.99	282	2110
DSS/DSSF	1.18E+07	136	545	0.25	1	545	4070
Subtotal	3.03E+07	350.0	1198	0.29		1178	8800
SSTs	1.60E+07	185	900	0.205	0.75	675	5040
Total	4.63E+07	535	2098	0.255		1854	13840
ESW[9]	4.63E+07	5.35E+02	2.10E+03	2.55E-01		1.85E+03	1.38E+04

(1) Cesium inventories from page D-51, WHC-EP-0616, except for SST inventory, which was obtained from page 4-13 of WHC-EP-0616. The decay daughters not included. Multiply by 1.95 to obtain curies of ^{137}Cs as given on pages D-51 and 4-13 of reference.
(2) Radionuclides decayed to end of 1995.
(3) Numbers may not be consistent with the Integrated Data Base.
(4) Divide curies by 86.6 Ci/g and 1000 g/kg to obtain mass.
(5) Reference unknown.
(6) Mass of ^{137}Cs/total mass of cesium.
(7) Wash factors obtained from page G1-24 of WHC-EP-0616; do not reflect probability that sludge-leaching operations will solubilize additional cesium.
(8) Average molecular weight of cesium isotopes assumed to be 134 g/mole for this conversion.
(9) Enhanced Sludge Wash (ESW).

TABLE 3.3. Inventory of Sodium and Potassium in Hanford Supernates

Waste Type	Mass of sodium (kg)	Moles of sodium	Mass of potassium (kg)	Moles of potassium	Fraction Na Assumed Soluble	Fraction K Assumed Soluble
	(1)(2)		(1)(2)		(3)	(4)
NCAW	5.89E+05	2.56E+07	2.21E+04	5.66E+05	0.97	0.93
NCRW	4.55E+05	1.98E+07	7.06E+04	1.81E+06	0.72	0.78
PFP	5.98E+04	2.60E+06	1.64E+03	4.21E+04	0.91	0.99
CC	4.51E+06	1.96E+08	3.13E+04	8.03E+05	0.99	0.99
DSSF	1.13E+07	4.91E+08	1.31E+06	3.36E+07	1	1
Subtotal	1.69E+07	7.35E+08	1.44E+06	3.68E+07	---	---
SSTs	5.17E+07	2.25E+09	5.99E+04	1.54E+06	0.99	0.9
Total	6.86E07	2.98E+09	1.50E+06	3.38E+07		

(1) Mass of sodium and potassium in DSTs from page D-51, WHC-EP-0616.
(2) Mass of sodium and potassium in SSTs from page D-35, WHC-EP-0616 (total of the normalized TRAC data).
(3) Percent assumed soluble from page G1-24 of WHC-EP-0616. These values are not wholly consistent with the solid/liquid split on page D-51. The potassium split for SST waste differs from that on page G1-24 of WHC-EP-0616, where none of the potassium is assumed soluble. DSSF Fraction assumes all DSSF is soluble salts.

TABLE 3.4. Inventories of Major Cations in Hanford Supernates

Waste Type	Na aqueous phase (moles)	K aqueous phase (moles)	$[Na^+]:[Cs^+]$	$[K^+]:[Cs^+]$	[Na+]:[K+]	Volume at 5M Na (L)	Volume at 5M Na (gal)	$[Cs^+]$ @ 5M Na (Ci/L) (b)	$[Cs^+]$ @ 5M Na (moles/L)
NCAW	2.48E+07	5.27E+05	9.80E+03	208	47	4.97E+06	1.31E+06	2.318	5.10E-04
NCRW	1.42E+07	1.41E+06	3.47E+05	3.44+04	10	2.85E+06	7.52E+05	0.124	1.44E-05
PFP	2.37E+06	4.17E+04	4.77E+04	840	57	4.74E+05	1.25E+05	0.359	1.05E-04
CC	1.94E+08	7.95E+05	9.21E+04	380	240	3.88E+07	1.02E+07	0.167	5.43E-05
DSSF	4.91E+08	3.36E+07	1.2E+05	8260	15	9.83E+07	2.60E+07	0.120	4.14E-05
Subtotal	7.27E+08	3.64E+07	8.26E+04	4100	20	1.45E+08	3.84E+07	0.209	6.05E-05
SSTs	2.23E+09	1.38E+06	4.41E+05	270	1610	4.45E+08	1.18E+08	0.036	1.13E-05
Total	2.95E+09	3.77E+07	2.13E+05	2700	78	5.90E+08	1.56E+08	0.078	2.34E-05
ESW (a)	3.21E+09	3.99E+07	2.32E+05	2900	80	6.42E+08	1.70E+08	0.072	2.15E-05

(a) Enhanced Sludge Wash. ESW inventories are the same as for the total of all of the waste types except for sodium. Based on an analysis of a nonradioactive leaching flowsheet an estimate of the additional sodium was included to account for the NaOH that might be used during the leaching of Aluminum compounds and Chromium.

(b) Radionuclides are decayed to 1995. Decay daughters are not included.

3.2 SEPARATION REQUIREMENTS

This section describes the development of separation criteria. Relevant to the development of a cesium ion-exchange process are 1) decontamination of the waste and 2) separation of cesium from the rest of the waste components.

3.2.1 Decontamination Requirements

The disposal criteria for ^{137}Cs considered are 1) Class C; 4600 Ci/m^3, 2) Class A, 1 Ci/m^3, and 3) 1/10th of the Class A limit. These limits are applied to the vitrified LLW waste form. These limits do not account for the influence of other radionuclides that may further restrict the cesium concentration through the sum of fractions rule.

In deriving ion-exchange performance criteria, it is convenient to derive a relationship between the limits in vitrified LLW and the ^{137}Cs concentrations in the aqueous stream. This conversion is achieved by assuming that the waste will be vitrified so that the Na_2O level in the LLW glass is 25 wt%. A density of 2.6 g/Ml (typical of glasses containing 25 wt% Na_2O) is assumed for the vitrified LLW. A volume reduction factor (volume of vitrified waste:volume of aqueous feed) can then be estimated.

Basis: 1 L of aqueous waste at 5 M sodium.

$$Vg/Vl = \frac{(\text{sodium concentration})(\text{oxide molecular weight})}{(\text{conversion factors})(\text{weight fraction of } Na_2O \text{ in glass})(\text{glass density})}$$

$$Vg/Vl = \frac{(5 \text{ mole } Na^+/L)(62 \text{ g/mole } Na_2O)}{(2 \text{ mole } Na^+/\text{mole } Na_2O)(1000 \text{ g/kg } Na_2O)(0.25 \text{ kg } Na_2O/\text{kg glass})(2.6 \text{ kg/L})}$$

$$= 0.42 \text{ L glass/L feed @ 5 M } Na^+$$

This conversion factor was used to estimate the ^{137}Cs concentration required to reach the limits for LLW glass summarized in Table 3.5.

TABLE 3.5. ^{137}Cs Limits[a]

	Limit in LLW glass, Ci/m^3	Limit in Aqueous LLW @ 5 M Na Ci/m^3
Class C	4600	1930
Class A	1	0.42
1/10th of Class A	0.1	0.04

[a] sum of fractions rule not considered; other radionuclides not considered

As an example, the limit in the aqueous vitrification feed at 5M Na^+, corresponding to the Class C limit in glass, can be calculated as follows:

$$\text{limit in feed} = (4600\ Ci/m^3)(0.42\ L \text{ of glass/L of feed @ } 5M\ Na^+)$$

$$= 1930\ Ci/m^3 \text{ in feed @ } 5M\ Na^+$$

In deriving the decontamination requirements, it is assumed that no cesium is lost from the system during vitrification of the LLW. However, some cesium is volatile at melter temperatures, and the portion that is volatilized will require recovery in the melter off-gas system. The recovered cesium is usually returned to the melter, but in this case it may be advantageous to send the recovered radionuclides to the HLW vitrification plant.

The limits for ^{137}Cs and the cesium concentrations given in Table 3.4 were used to estimate the cesium decontamination requirements for each waste type and each of the three limits (Table 3.6). For example, the cesium DF required for NCAW/Class A limits can be estimated as follows:

$$DF = (2318\ Ci/m^3)/(0.42\ Ci/m^3) = 5520$$

These decontamination factors are based on cesium concentrations in aqueous wastes with a sodium concentration of 5M. The only waste requiring cesium removal to meet Class C limits is the NCAW. The information in Table 3.6 suggests that NCAW is the only waste that would require treatment to meet the Class C limit. To meet the Class A limit, the DFs range from a low of 90 for SST waste to a high of 5520 for NCAW. The DFs required to meet 10% of the Class A limit are an order of magnitude higher.

TABLE 3.6. ^{137}Cs Decontamination Requirements[a]

	Class C 4600 Ci/m^3	Class A 1 Ci/m^3	1/10 Class A 0.1 Ci/m^3
NCAW	1.2	5520	55200
NCRW	0.06	290	2900
PFP	0.19	860	8600
CC	0.09	400	4000
DSSF	0.06	290	2900
DST (av)	0.11	500	5000
SST (av)	0.02	90	900
Total (av)	0.04	190	1900
ESW (av) (b)	0.04	170	1700

(a) Sum of fractions rule not considered, impact of other radionuclides not considered.
(b) Enhanced Sludge Wash. This stream contains additional sodium from aluminum leaching operations.

3.2.2 HLW Composition Requirements

This section estimates the extent to which cesium must be separated from the other waste constituents, especially the other major cations (i.e., Na^+, K^+), to minimize the quantity of HLW glass. The HLW composition limit is important in designing the ion-exchange process because it can impact how the process is run and the number of cycles required. Rigorous determination of the required separation is a complex optimization problem that remains to be solved. Instead, a simplistic analysis provides a rough estimate. This is probably as good as any other method, given the considerable uncertainty associated with many of the processes and waste streams.

The general approach to developing the frit (glass-forming chemicals) composition involves the solution to a nonlinear optimization problem (Hoza 1994). As shown in Figure 3.1, the leached solids from an ESW are assumed to be combined with the ion-exchange eluate, which may be acidic or alkaline, to yield a blended waste. The frit is added in such a way as to maximize the mass fraction of waste in the glass, subject to constraints on the glass waste form (e.g., durability, processability). Frit composition is varied as part of optimization. Optimal Waste Loading (OWL) software (Hoza 1994) has been developed to solve this problem.

To date, much process development has focused on vitrification of NCAW at 1150°C. A reference frit (WHC-SD-HWVP-DP-001, see Table 3.7) developed for that purpose is widely assumed to apply to the vitrification of other wastes. However, this approach does not permit optimization of waste loading in the glass because the frit composition is fixed and it adds a significant quantity of sodium to the HLW glass.

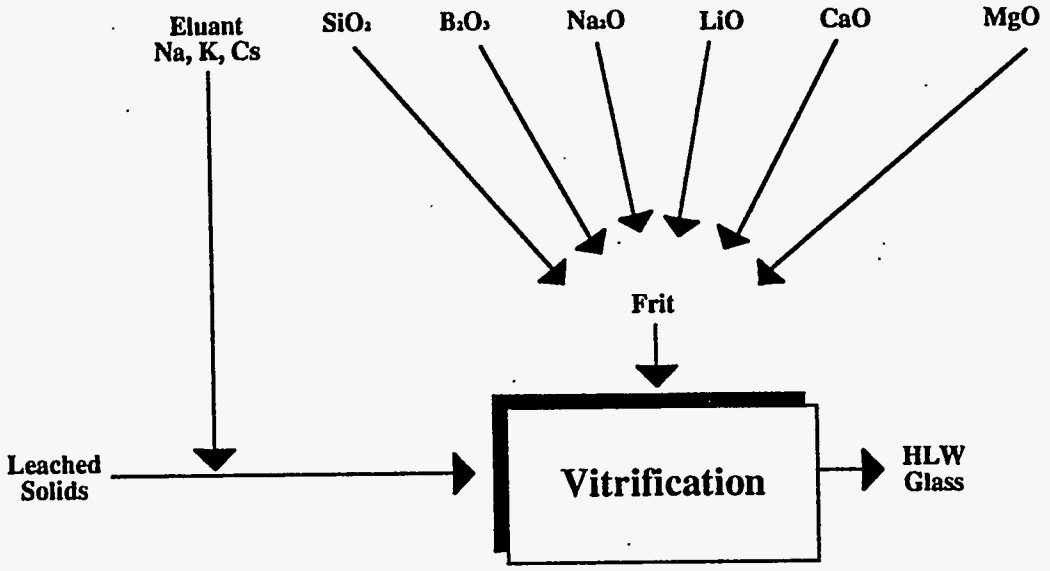

FIGURE 3.1. The Vitrification Process

TABLE 3.7. Reference Frit Composition

Component	Wt% of frit
SiO_2	70
B_2O_3	14
Na_2O	9
Li_2O	5
CaO	1
MgO	1

A simplistic analysis that yields a useful estimate of the separation requirement assumes that the sodium, potassium, and cesium sent to the melter can replace the sodium added in the frit. Assuming a waste loading of 25 wt% and a sludge mass that would produce 20,000 canisters of glass (1650 kg/can), the reference frit would add 2.2E+06 kg of Na_2O or 7.2E+07 moles of sodium to the glass. If sodium in the eluate can replace all of the sodium in the frit, an eluate $[Na^+]:[Cs^+]$ as high as 5200 would not impact the volume of glass.

Other types and formulations of glass containing less sodium are being evaluated, and their use could reduce the amount of sodium in the eluate that can be accommodated without increasing the amount of glass. For example, a glass consisting of 50 wt% waste oxides, 46% SiO_2, and 4% Na_2O is being considered for NCAW. The total amount of sodium in the glass is greatly reduced because fewer canisters are produced and the fraction of sodium in the frit is less. If this composition applied to all of the glass to be produced, the number of glass canisters would be about 10,000 at 50 wt% loading. About 5.32E05 kg or 2.12E07 moles of sodium would be added as frit. If all of the sodium in the frit can be replaced with sodium in the eluate, an eluate $[Na^+]:[Cs^+]$ as high as 1500 would not impact the total volume of glass. If the eluate with $[Na^+]:[Cs^+]$ = 1500 is considered separately, approximately 780 additional canisters (1650 kg/can) would be produced at 50 wt% waste-oxide loading.

As mentioned, these estimates on the allowable amount of sodium in the eluate are rough and are strongly dependent on the vitrification process and

the type of glass that will be produced. Some types of glass can tolerate large amounts of Na_2O; others, such as phosphate glasses, tolerate Na_2O poorly. Many types and formulations of glass are under consideration in the effort to increase waste loading and thereby reduce the volume of glass. This effort can greatly restrict the acceptable quantity of sodium in the eluate.

4.0 EXPERIMENTAL

Experimental cesium-recovery work completed in FY 1992 included the determination of cesium batch distribution coefficients and corresponding volume distribution ratios for three exchangers, CS-100, R-F Resin, and IONSIV IE-96, and two waste simulants, NCAW and CC. Work in FY 1993 included the initiation of ion-exchange column studies. Other studies this report include ion-exchange column and batch-equilibrium studies with DSSF simulant. Studies on radiation stability of CS-100 and R-F resins are being completed, and a summary of the results to date is included in Chapter 5.0.

4.1 ION-EXCHANGE SELECTION

The resins under consideration in this report are CS-100 and R-F. Duolite™ CS-100 resin is a granular organic condensation polymer of phenol and formaldehyde and contains phenol and carboxylic acid functional groups. It is made in France on special order (700-1000 ft^3) by Rohm and Haas, Cherry Hill, New Jersey. Its phenolic hydroxyl group, which provides selectivity for cesium over sodium, is weakly acidic and is activated at high pH. Although CS-100 has not been used in full-scale operation, it has been studied extensively. However, it has been manufactured by two different processes (pre-1982 and post-1981), and the early references may not apply to the resin as it is currently manufactured.

The R-F resin was first prepared by Drs. Jane Bibler and Richard Wallace of Westinghouse Savannah River Company (WSRC) (Patent No. A7460480). The resin is prepared by condensing the potassium salt of resorcinol with formaldehyde in an aqueous solution and drying the resulting gel at about 100°C. Boulder Scientific Co., Mead, Colorado, prepares commercial quantities for testing at Oak Ridge National Laboratory (ORNL), WSRC, and PNL. At high pH, R-F is more selective for cesium than is CS-100. Several studies of R-F resin have been completed, including those of Bibler et al. (1990) and Bray et al. (1990).

4.2 PREPARATION OF SYNTHETIC WASTES

The waste types selected for the initial cesium ion-exchange investigation were NCAW and CC. In that study, the organic content of the similant had no quantifiable effect on the cesium ion-exchange data, and those ion-exchange data can be applied to a broad range of tank-waste types containing similar molar proportions of sodium, cesium, and potassium. As shown in Table 4.1, CC waste simulant is high in sodium and contains organic complexants; its composition approximates that of Tank 241-AN-102 (Van Vleet 1993). The organic complexants were chosen from historical process information. Sodium gluconate was added because it is the only known iron-chelating agent effective in the pH 14 free-caustic region, and it may have been used in B-Plant operations. NCAW, modelled after the composition of Tank 241-AZ-101, represents a high-sodium waste with low organic content (Table 4.1).

A comparison of data from initial ion-exchange experiments with NCAW and CC simulants revealed the need for studies at a high potassium concentration and $[Na^+]:[Cs^+]$ of 10^5. Tank 241-AW-101 has the highest potassium level (1.07M) of the entire DST family; however, when the analytical results are scaled to a constant 10M sodium, Tank 241-AP-105 has the highest potassium concentration (1.35M). To model the highest $[K^+]:[Na^+]$ for the DST family, the potassium level in the simulant (DSSF-0) was fixed at 1.35M; other major constituents were combined as in Tank 241-AW-101. Rubidium was not added to the simulant because analytical data are unavailable. This formulation (10M Na) was soluble only above 50°C (the approximate equilibrium temperature in many DSTs), and sodium nitrate precipitated as the solution cooled to ambient temperature. The DSSF-0 simulant was soluble at 20°C only after dilution to 7M Na. This diluted DSSF-0 simulant (termed DSSF-7) was chosen for further study and is intended to model the worst-case removal of cesium from the DST family by ion exchange (see Table 4.1).

TABLE 4.1. Simulated Hanford Alkaline Waste Solutions

Species, Total	CC, M	NCAW, M	DSSF-7, M
Na	10.05	4.99	7.00
K	0.050	0.12	0.95
Rb	5.0E-05	5.0E-05	-
Cs	5.0E-04	5.0E-04	7.0E-05
Al	0.500	0.43	0.72
Ca	0.020	-	-
Fe	0.060	-	-
La	0.001	-	-
Mg	0.010	-	-
Mn	0.020	-	-
Mo	0.005	-	-
Ni	0.010	-	-
Si	0.005	-	-
Sr	7.0E-04	-	-
Zn	0.002	-	-
Zr	0.002	-	-
SO_4	0.10	0.15	0.008
OH (Total)	3.46	3.40	4.63
OH (Free)	0.94	1.68	1.75
CO_3	0.64	0.23	0.15
NO_2	1.50	0.43	1.51
NO_3	4.60	1.67	3.52
F	0.15	0.09	-
Cl	0.10	-	0.12
PO_4	0.03	0.025	0.014
Na_4EDTA	0.03	-	-
Citric Acid	0.064	-	-
$Na_3HEDTA \cdot 2H_2O$	0.038	-	-
Na_3NTA	0.007	-	-
Na Gluconate	0.30	-	-
Iminodiacetic	0.23	-	-
TOC (g/L)	46.00	-	-
Mole Ratio			
$[Na^+]:[Cs^+]$	2.00E+04	1.00E+04	1.00E+05
$[Na^+]:[K^+]$	2.00E+02	4.16E+01	7.41E+00
$[Na^+]:[Al^+]$	2.00E+01	1.16E+01	9.71E+00

Several difficulties that may be important to the overall process of removing cesium by ion exchange emerged during the formulation of the DSSF simulants. The problems centered around aluminum solubility, the actual meaning of the OH^- analytical data, and the specific gravity of the DSSF solution. Initially, DSSF-2 was prepared at 50°C in a 1 L batch (10M Na, 1.35M K, 1M Al, 5M OH^- total, and other major constituents as in tank AW-101) and diluted to 8M Na to determine if the material would remain in solution at 20°C. After two weeks at ambient temperature, a large amount of precipitate had accumulated; it was later identified by x-ray diffraction to be gibbsite ($Al_2O_3 \cdot 3H_2O_{(s)}$). As the pH of an aluminum-containing solution falls, a reversible reaction produces $Al(OH)_3$, which is irreversibly converted to gibbsite. It is likely that the hydroxide concentration of DSSF-2 was not high enough to keep aluminum in solution as $Al(OH)_4^-$; since each mole of Al requires 4M of OH^-, the solution was 5M in total OH^- and only 1M in free OH^-. The solubility of aluminum in radioactive sodium salt wastes at Hanford drops dramatically as free hydroxide falls below 1M (Barney 1976). From these results, it seems clear that diluting certain wastes with water may induce precipitate formation with potentially disastrous consequences.

At the initial formulation, it was thought that the OH^- value represented total hydroxide to be added to the solution. However, it now seems clear that the value is more accurately described as "free" hydroxide not bound to aluminum. In addition, since the OH^- value was obtained by titration, the presence of carbonate or tetrahydroxyaluminum anion may bias the analytical results. As a compromise, the DSSF-0 simulant was prepared with 6.6M total OH^- and 2.5M free OH^-. DSSF-7, produced by a 1.4x dilution with DSSF-0, is near the point of maximum aluminum solubility (1.75M free OH^-) (Barney 1976).

In initial batch equilibrium tests, CS-100 resin remained suspended in 8M Na DSSF-2 solution. The specific gravity of the solution and the resin may ultimately determine the minimum dilution factor.

4.2.1 Solution Radio-Tracer Analysis

Radio-tracer techniques were used to determine the extent to which an ion exchanger could extract cesium from solution and an acid could elute cesium from the resin. The synthetic alkaline waste solutions (NCAW and DSSF)

contain an amount of nonradioactive cesium nitrate that is equal to the total cesium content in the actual waste. The solution was then spiked with radio-tracer ^{137}Cs (purchased as CsCl in 1M HCl and containing about 0.4 mg ^{137}Cs/mL). The radiochemical activity of the "as-received" material is usually 12 mCi/mL, or 440 mGq/mL. For the sodium-iodide-well crystal-radiochemical-detector used in the laboratory, 1 μL of the stock tracer or 12 μCi of tracer is used to trace 1 L of feed. Four mL of feed or effluent are counted for batch equilibrium studies and column testing. During elution studies, the effluent sometimes exceeds the feed concentration. Such samples are diluted with water, a 4 mL aliquot analyzed, and the result corrected for the required dilution. The detection limit for the γ-counting system was determined by the T-Statistic method (Dixon and Massey 1969). The detection limit for the level of tracer used in these experiments was 700 counts or DF = 500.

4.3 BATCH EQUILIBRIUM MEASUREMENTS

A batch distribution coefficient is a measure of the overall ability of the solid phase to remove an ion from solution. For ion-exchange research and testing, measurement of batch distribution provides rapid and cost-effective comparison of a wide variety of conditions for their selectivity for specific radionuclides.

Cesium batch distribution coefficients were measured to evaluate five feed variables: sodium concentration, temperature, $[Na^+]:[Cs^+]$, potassium and rubidium concentrations, and dilution effects. The data are reported as radionuclide distribution coefficients (K_d) or λ, or both. K_d is expressed in mL/g (volume of solution/mass of dry exchanger) and represents a theoretical volume of solution that can be processed per mass of exchanger (see Equation 2.6). To convert to λ, multiplying K_d by the bed density of the exchanger (ρ_b) yields a value equivalent to the volume of solution per volume of exchanger (see Equation 2.24). In practice, the concentration of a radionuclide on the solid is more difficult to quantify than the concentration of unexchanged radionuclide in the liquid phase. For this reason, the following method is used for calculating K_d from experimental data:

$$K_d = \frac{C_0 - C_1}{C_1} \frac{V}{m \cdot F} \qquad (4.1)$$

where C_0 = initial concentration of the radionuclide in the solution (Ci or g of radionuclide/mL)

C_1 = final concentration of the radionuclide in the solution (Ci or g of radionuclide/mL)

V = volume of solution used in the batch equilibrium experiment

m = mass of ion exchange used in the batch equilibrium experiment

F = the F-factor of the ion exchange (mass dry ion exchanger/mass wet ion exchanger)

4.3.1 Preparation of Ion-Exchange Materials

An accurate and reproducible determination of the cesium distribution coefficient for various organic ion exchangers requires 1) a uniform basis for the mass of an ion exchanger and 2) accurate determinations of the mass. The most reproducible basis for determining mass is when the exchanger is completely dry (i.e., material oven-dried at 85°C for 24 h). Dry material is easier to weigh because damp material tends to form clumps. However, because drying may destroy exchange capacity, the ion-exchange materials are weighed as received, and a correction factor (F-factor) is applied to determine the dry weight. The F-factor is calculated by weighing a mass of sample, drying it at 85°C for 24 h, weighing the dried sample, and dividing the dried weight by the as-received weight.

4.3.2 Equipment Description

Obtaining batch-equilibrium data requires a constant-temperature shaker table, an analytical balance, and gamma-counting equipment.[1]

---

[1] The equipment and procedures are described in the latest revision of test procedure WTC-006-21, "Determination of Batch Sorption Ratios for Ion Exchange Materials Using Radionuclide Tracer Techniques."

4.4 COLUMN TESTING

The effect of process flow rate (superficial velocity and bed volumes/h) on cesium loading and breakthrough during column operation was measured. Other effects, such as temperature or feed variables ($[Na^+]:[K^+]$ and OH^-), may be the subject of future column tests. Required equipment includes a constant-temperature water bath, an analytic balance, temperature-controlled ion-exchange columns, and gamma-counting equipment.

4.4.1 Ion-Exchange Column System

The system consists of 1 to 6 glass ion-exchange columns, feed-storage bottles, pumps, and effluent-weighing bottles. As shown in Figure 4.1, each column has a capacity of 200 mL of ion-exchange material and is 2.54 cm in diameter and 41.9 cm tall (including head space for solution above the resin bed). The columns are equipped with water jackets connected to a water bath to maintain constant temperature. They may be run independently or connected in series. The feed solution is normally fed to the columns downflow, or from the top of the column. A pump located just upstream of the first column is used to control the flow rate. Each column's effluent is sampled as a function of time from a valve at the bottom of the column. The effluent from the final column is routed to the weighing bottle. The column volumes (cv) of effluent processed are determined by the effluent weight divided by the specific gravity of the feed. A 24,600 ± 0.1-g balance is used to weigh the effluent. The operation of the ion-exchange system for removing cesium containing ^{137}Cs-tracer from simulated NCAW or DSSF alkaline salt solution was varied as each test procedure was developed. The influent and effluent ^{137}Cs γ emission counting rates (C_0 and C, respectively) were measured to obtain the breakthrough curves (C/C_0 vs. cv) and to determine optimum performance of the ion-exchange columns as a function of time and feed flow.

4.4.2 Column System Configuration

Ion-exchange columns were operated as independent single columns or in a multicolumn array. Multicolumn operations were performed by connecting 2 to 6 columns in series. Each column test was operated 24 h/day until the objective of the test was met. Care was taken to minimize the amount of effluent

FIGURE 4.1. Ion-Exchange Column System

in the head space of each column so that the liquid-mixing area did not perturb the overall results. Back pressure in the 3-column system normally caused a relatively large volume of solution to accumulate above the second and third columns.

4.4.3 Column-Loading Conditions

The conditions for the initial column-loading tests were selected to determine the effect of the time-dependent variables (superficial velocity or bed volumes/h) on cesium loading. Temperature (25°C) and feed variables ([Na+], $[Na^+]:[Cs^+]$) were held constant during each test series. The ion-exchange system consisted of one to three 200 mL columns in series. The system was operated until the final column had a C/C_o of >0.90.

CS-100 and R-F resin were tested. The amount of material placed in each column (200 mL) was added by weight as determined by the following method: 1) The specific gravity of the material (grams of the dry exchanger in a known volume) was determined by weighing the as-received resin into a 200 mL volumetric cylinder containing 2M NaOH to a final resin volume of 100 mL and allowing the resin to equilibrate in the solution for 16 h; 2). The specific gravity was used to determine the mass of 200 mL of as-received resin to be used in the columns. A separate small sample (1 to 10 g) of as-received resin was dried at 85°C for 16 h to determine an F-factor when the resin was weighed (see Section 4.3.1).

To load the resin, a column was filled with 2M NaOH and the calculated quantity of resin added. Each column was then back flushed with 2M NaOH to remove resin fines before being connected in series. The temperature of the water-jacketed columns was maintained at 25±2°C. The ion-exchange system (the pump and one or three columns) was flushed and tested with at least 3 cv of 2M NaOH solution at a flow rate required for the specific test.

To initiate a test, the solution head above the resin was reduced to a minimum (<1 in.), the columns were connected as previously detailed, and the excess 2M NaOH above each exchange bed was removed through the bottom sampling valve. NCAW or DSSF feed was then started through the first column, and the liquid heads above each column reestablished to the minimum possible height.

When the last column was loaded to >90% breakthrough [^{137}Cs effluent count rate (C) ÷ ^{137}Cs feed count rate (C_0) = >0.90], the test was terminated. If the columns were not to be eluted immediately, they were stored in either feed solution or caustic wash. Elution was preceded by a downflow flush with 3 cv of 2M sodium hydroxide solution followed by 6 cv of water at 2 cv/h. The sodium hydroxide wash was used to remove residual sodium aluminate from the system to prevent precipitation of aluminum during water washing and acid elution. The cesium-loaded columns were then drained of water, detached, and individually eluted with formic acid or nitric acid (Section 4.4.4).

4.4.4 Column-Elution Conditions

Cesium-elution experiments were performed with cesium-loaded CS-100 or R-F resin. The experiments were designed to determine the effect of flow rate, temperature, and type of acid eluant on the cesium elution characteristics of the resin being tested. The acid types were limited to nitric and formic acids. The concentration of nitric acid was limited to <0.5M to minimize the potential for oxidation of the resin. To initiate the column-elution tests, the columns were first pretreated as described in the previous section. Nitric or formic acid was then started down through the column, and the liquid head above each column was reestablished and maintained at >1-in.

5.0 RESULTS AND ANALYSES

Chapter 5.0 presents and analyzes the results of the experiments described in Chapter 4.0 and includes additional information from published literature. Sections 5.1, 5.2, and 5.3, respectively, address the equilibrium behavior of the exchangers with NCAW and CC waste simulants, column-run data, and chemical and radiation stability.

5.1 EXCHANGER PROPERTIES AND EQUILIBRIUM BEHAVIOR

The physical characteristics and ion-exchange equilibrium properties of Duolite™ CS-100 and resorcinol-formaldehyde (R-F) resins provide useful background for the design and operation of large-scale ion-exchange columns. Areas where additional data are needed are noted. Section 5.1.1 briefly describes the chemical and physical characteristics of the resins. Section 5.1.2 summarizes the known physical data on the two resins. Section 5.1.3 presents an analysis of the equilibrium data (Cs λ) obtained with NCAW and CC waste simulants. This section discusses effects of the equilibrium $[Na^+]:[Cs^+]$, $[Na^+]$ (dilution), temperature, and pH on Cs λ. Correlations of Cs λ with the equilibrium $[Na^+]:[Cs^+]$, $[Na^+]$, and temperature show the impact of dilution on waste volume processed. Section 5.1.4 shows the effect of competing ions, such as potassium and rubidium, on the cesium column distribution ratio and presents the potassium column distribution ratios ($K \cdot \lambda$) with cesium-free NCAW simulant. Analysis of selected values of K λ provides information about the resin capacity and its selectivity for potassium over sodium. Another possible use for the binary potassium-sodium equilibrium data in the modeling of multicomponent systems is presented in Section 5.1.5. Section 5.1.6 briefly discusses thermodynamic modeling.

5.1.1 Exchanger Composition

The organic resins of interest, Duolite™ CS-100 and R-F, are milled or crushed particles ranging in size from 300 to >1000 microns. Both molecular structures are aromatic phenyl rings that have functional ionic groups and are

joined by methylene groups. Phenolic and carboxylic functional groups provide the ion-exchange capability for CS-100; the active sites for the R-F resin are phenolic. Both resins are condensate polymers (water is formed during the polymerization) with formaldehyde as the crosslinking agent.

5.1.2 Physical Properties

Table 5.1 summarizes the physical data and operating conditions for R-F and CS-100. Data were measured in our laboratory or taken from published sources. Most of the data for CS-100 comes from a technical data sheet provided by the manufacturer (Duolite International 1983) before Rohm and Haas acquired the rights to CS-100.

R-F resin appears to have a higher ion-exchange capacity than CS-100, but an accurate comparison is not possible at this time. Although analytical results were not available for CS-100, the technical data sheet states that the estimated capacity is >2 meq/g dry resin (Table 5.1). The estimated capacity of R-F resin is 3 or 4 meq/g dry resin: 3 meq/g as calculated from the quantities of sodium, cesium, potassium, and rubidium ions released during formic-acid elution; 4 meq/g based on hydrogen-ion uptake calculated from the amount of acid in solution, as measured by titration, before and after elution. Cation concentrations were based on atomic absorption analyses (flame AA). Since flame AA results showed good reproducibility, 3 meq/g dry resin, which is close to the reported value of 2.85 meq/g air-dried resin (Bibler et al. 1990), is most likely the better value for R-F exchange capacity.

The two resins are similar in many respects (Table 5.1). The density of both resins (CS-100 and batch BSC-187 of R-F) was measured at 0.46 g dry resin/mL swollen resin in water. Previous measurements indicated that the density was 0.34 and 0.36 g dry resin/mL swollen resin in 2M caustic (Bray et al. 1992; Bibler et al. 1990). Such variation in density is probably due to different degrees of resin swelling in different solutions; the resin expands as the pH or salt concentration of the solution increases. The R-F

TABLE 5.1. Exchange Resin Physical Data and Operational Conditions[a]

Criteria	Duolite™ CS-100	R-F Resin
Physical Data		
Ion-exchange capacity (meq/g dry resin)	>2[b]	2.85[c], 3.4[d]
Bulk density, Na form (g dry resin/ml swollen resin)	0.458[e]	0.461[e], 0.34[f], 0.36[g]
Void fraction	0.4	0.5[h]
Particle size (mm)	0.3-1.3 0.63[j]	0.26-0.42[i] 0.29, 0.34[j]
Volume change (H^+ to Na^+ form)	22-28%	43-54%
Volume change (Na^+ to H^+ form)	18-22%	30-35%[l]
Operational Conditions		
Chemical Stability		
Resistance to most acids	Excellent	Excellent
Resistance to alkalies	Good	Good
Maximum HNO_3 (at 25°C)	1 M	(k)
Optimum pH for Cs loading	≥12[m]	≥12[m]
Maximum temperature	80°C[o]	(n)

(a) CS-100 technical data sheet, unless otherwise noted.
(b) Estimate based on a capacity of >1 eq/l (CS-100 technical sheet) divided by the dry density.
(c) K-form of R-F resin contacted with 2M NaOH, Bibler et al. 1990.
(d) Based on the amounts of Na^+, Cs^+, K^+, and Rb^+ which were released from the resin during formic acid elution.
(e) BSC-210 batch of R-F resin and CS-100 were contacted with NaOH, rinsed with water, and dried for 24 h at 85°C.
(f) BSC-187 batch of R-F resin, Bray et al. 1992.
(g) Bibler et al. 1990.
(h) Estimate based on amount of water (0.7 ml) displaced by 1 g resin and the bulk density of the as-received resin (0.67 g/ml).
(i) As received from Boulder Scientific.
(j) Mass-average particle size based on sieve tray analysis.
(k) Unavailable at this time.
(l) Estimate based on volume shrinkage during acid elution (See Bray et al. 1990).
(m) Based on Cs λ-pH data presented below.
(n) Suggested limit from CS-100 technical sheet.
(o) Unavailable at this time, but probably close to 80°C.

resin shrinks by 30% to 35% during acid elution, and CS-100 shrinks an estimated 20%, based on the volume change from the hydrogen to the sodium form (Table 5.1) and assuming reversibility. Optimum pH for cesium loading is >12 for both resins. Chemical resistances and maximum operating temperatures are probably similar, since the resins have similar chemical structures (Section 5.1.1).

Dissimilar particle-size distributions in the CS-100 and R-F batches (BSC-187 and BSC-210) used in the experiments may contribute to the differences in equilibrium and kinetics. From Table 5.2, mass-average particle sizes can be calculated: 0.63, 0.34, and 0.29 mm for CS-100, BSC-187, and BSC-210, respectively. R-F particles are approximately one half the size of CS-100. This is important for the interpretation of the equilibrium and column data. Hubler[1] showed the cesium distribution coefficient (Cs Kd) for R-F to be a function of particle size, with an optimum size of 20 to 50 mesh (Table 5.3). Because the resins are chemically similar (Section 5.1.1), cesium equilibrium for CS-100 is also likely to be affected by particle size. Column kinetics is also a function of particle size, since the mass-transfer coefficient for particle-diffusion control typically varies inversely with the square of the particle radius (Section 2.2).

5.1.3 Cesium Equilibrium Behavior

The equilibrium of cesium between the resin and the liquid defines the limiting performance of the exchanger and is thereby important to the design and operation of the ion-exchange columns. The cesium λ value derived from batch equilibrium experiments (Cs $\lambda = K_d \rho_b = [Cs]_s/[Cs]_l$, concentrations based on volume) quantifies this relationship. As pointed out in Section 2.2, Cs λ represents the column volumes of feed that can be loaded onto the resin under

---

[1] Timothy L. Hubler, January 24, 1994. *Progress Report: Resorcinol-Formaldehyde Ion-Exchange Resins, internal communication*. Pacific Northwest Laboratory, Richland, Washington.

TABLE 5.2. Particle Size Distributions (Weight Percent) of R-F and CS-100

Particle Size	CS-100 (%)	R-F (BSC-187) (%)	R-F (BSC-210) (%)
<70	0.3	2	7.1
45-70	1.5	58	81.3
35-45	29.4	40	11.5
25-35	36.3.1	0	0
18-25	28.4	0	0
>18	4.1	0	0

TABLE 5.3. Effect of Particle Size on Cesium Batch Distribution Coefficients for Resorcinol-Formaldehyde Resin (55197-15-C)

Sample		Particle Size	Cs K_d
PNL	55197-15-C	>20 mesh	3945, 4051
PNL	55197-15-C	20-50 mesh	5467, 5276
PNL	55197-15-C	<50 mesh	4472, 4466
PNL	55197-15-C	very fine particles	2642, 2550

limited conditions. Knowledge of Cs λ values based on batch contacts with a specific waste would thus support sizing and configuration of the columns and scheduling of column regeneration for that waste. A broad understanding of how process conditions, such as temperature and potassium concentration, affect Cs λ would contribute to the application of ion exchange to decontamination of other wastes.

Cesium Cs λ for CS-100 and R-F was determined at 10°, 25°, and 40°C with simulated NCAW and CC wastes of various sodium and cesium concentrations (Bray et al. 1992). The following paragraphs examine their results.

Several process conditions, including $[Na^+]:[Cs^+]$, $[Na^+]$, temperature, and pH, affect equilibrium Cs λ for CS-100 and R-F resin. Correlations between Cs λ and those variables can be used to interpolate Cs λ at other process

process conditions, derive cesium isotherms for modeling, and demonstrate the impact of dilution on processed waste volume.

Cesium loading on the resin, as indicated by the Cs λ, is dependent on temperature, equilibrium $[Na^+]:[Cs^+]$, and $[Na^+]$ in the liquid. Appendix B shows Cs λ for both resins as a function of $[Na^+]:[Cs^+]$ at different $[Na^+]$ and temperature. Figures B.1 through B.6 plot Cs λ for NCAW, and Figures B.7 through B.12 plot Cs λ for CC waste. These graphs indicate three general features of cesium ion exchange: (1) for a specific $[Na^+]$, Cs λ increases with rising $[Na^+]:[Cs^+]$ (i.e., lower cesium concentration), (2) Cs λ increases with decreasing (by dilution) waste concentration, and (3) Cs λ increases with falling temperature.

R-F Loads More Cesium than CS-100. R-F resin loads more cesium than CS-100 at the same solution conditions. Figure 5.1 compares Cs λ for CS-100 and for R-F resin, using representative samples from Appendix B. Cs λ for R-F is higher than for CS-100, sometimes by more than a factor of 10. As expected from NCAW and CC waste results (Appendix B), R-F also loads more cesium than CS-100 with DSSF-7 simulant (Figure 5.2).

BSC-187 and BSC-210 Show Identical Csλ. Cesium λs for two batches of R-F (BSC-187 and BSC-210) with DSSF-7 are nearly identical (Figure 5.2). Apparently, the difference in particle size (Table 5.2) was not large enough to cause a measurable change in Cs λ. This finding also suggests that the R-F resin can be produced with consistent quality.

Sodium Saturation of Resin at High $[Na^+]:[Cs^+]$ Makes Isotherm Linear. Cs λ for R-F begins to level off when $[Na^+]:[Cs^+]$ exceeds 10^6 (Figure 5.1), because the resin is becoming saturated with sodium. Although competing cations are present, such behavior can be qualitatively explained by the binary equilibrium constant under ideal conditions (see Section 2.1):

$$K_{eq} = \frac{[Cs]_s\ [Na]_l}{[Cs]_l\ [Na]_s} \qquad (5.1)$$

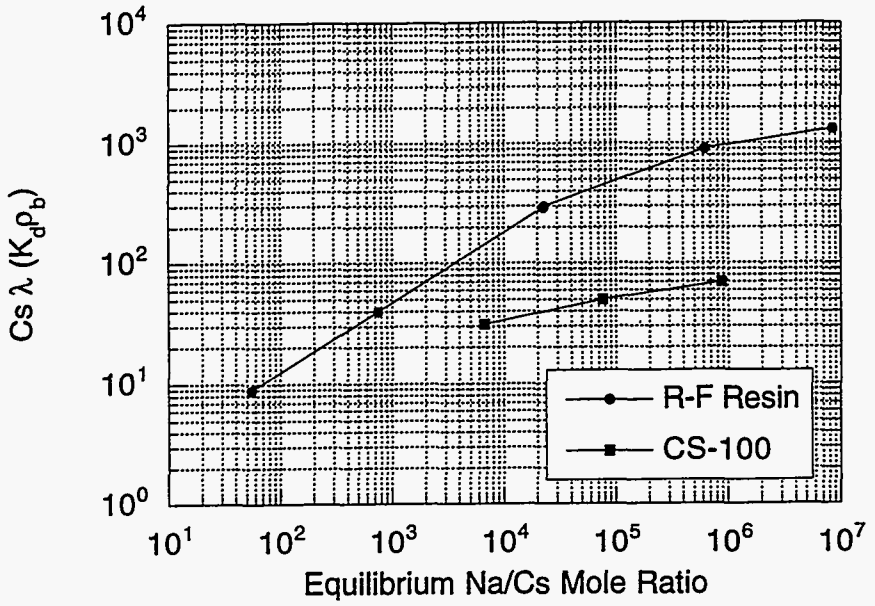

FIGURE 5.1. Cesium Equilibrium Behavior of the CS-100 and R-F Resins for NCAW at 25°C and 5M Na^+

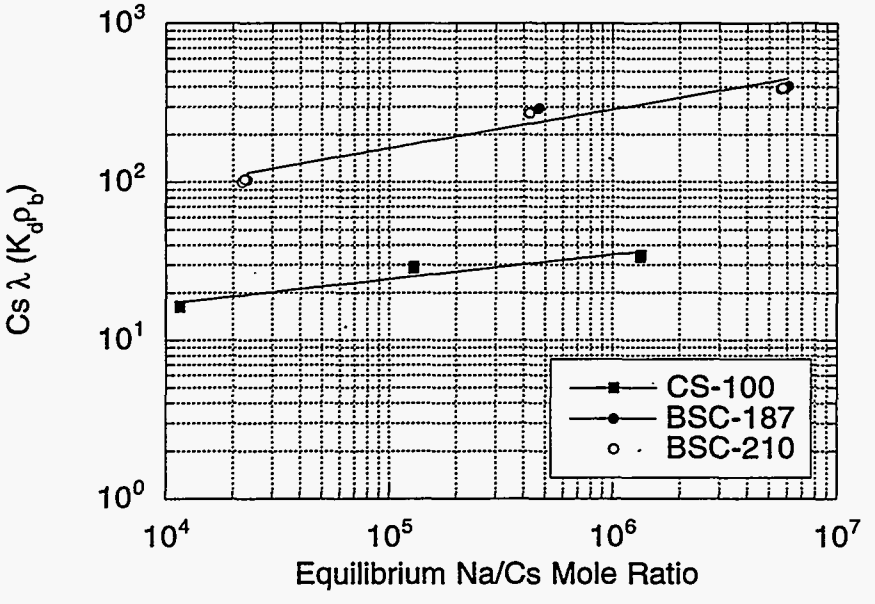

FIGURE 5.2. Cesium Equilibrium Behavior of the CS-100 and R-F Resins for DSSF at 25°C and 7M Na^+

Under ideal conditions (K_{eq} = constant), Cs λ is constant if $[Na]_l$:$[Na]_s$ is constant. Since $[Na]_l$ is effectively constant in the systems studied and $[Na]_s$ approaches a constant (Na saturation) at high $[Na^+]$:$[Cs^+]$, Cs λ also approaches a constant. The cesium is present in trace quantities such that the isotherm is linear. When $[Na^+]$:$[Cs^+]$ is high, the concentrations of cesium on the resin and in solution are linearly proportional, or $[Cs]_s$:$[Cs]_l$ (= Cs λ) = constant.

R-F and CS-100 Load More Cesium at Lower Temperatures. Both CS-100 and R-F take up more cesium at lower temperatures. Figures 5.3 and 5.4 plot Cs λ at $[Na^+]$:$[Cs^+]$ = 10^4 as a function of the reciprocal temperature (10^3/T) for two waste types. Cs λ increases with falling temperature; for example, at 5M Na^+, Cs λ for CS-100 approximately doubled as the temperature fell from 40°C to 10°C. Under the same conditions, Cs λ for R-F resin increased by a factor of about 1.4.

Impact of Temperature as Percentage is Larger for CS-100. At higher temperatures, R-F resin loads increasingly more cesium than CS-100. Table 5.4 shows interpolated cesium distribution coefficients for the two resins in NCAW, CC, and DSSF simulants at $[Na^+]$:$[Cs^+]$ = 10^4. The ratio of Cs λ values (last column in Table 5.4) indicates that R-F resin loads about 4 times as much cesium as CS-100 at 10°C and 8 times as much cesium at 40°C. The reason is that Cs λ for CS-100 is more sensitive to increases in temperature. Table 5.5 summarizes the slopes of the plots in Figures 5.3 and 5.4. For each case, the steeper slope for CS-100 shows that the impact of temperature (percentage basis) on Cs λ is greater for CS-100.

Effect of Temperature on Absolute Scale is Larger for R-F. Cesium λ values based on batch equilibrium data show that the absolute gain in column volumes that can be processed at lower temperatures is larger for R-F. The increase in Csλ as temperature is decreased from 40°C to 10°C in 3M Na^+ NCAW indicates that R-F resin could process an additional 92 cv, but CS-100 could process only an additional 33 cv. Although decreasing the temperature improves cesium loading, other effects of temperature which may alter column performance

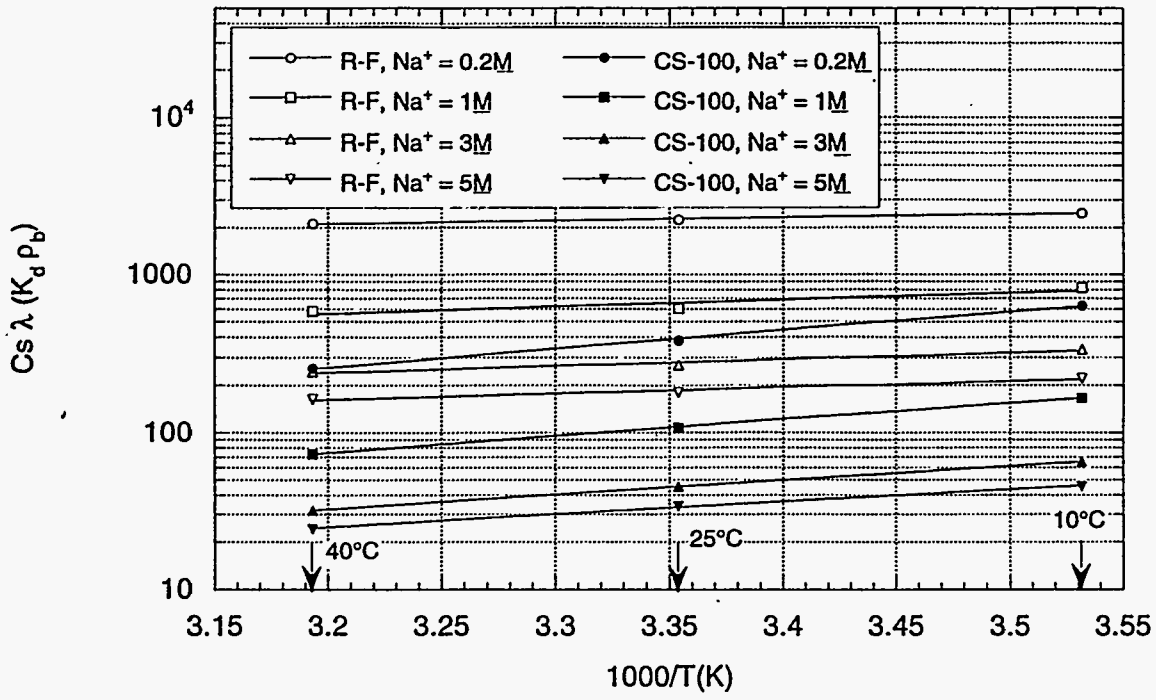

FIGURE 5.3. Cesium λ in NCAW as a Function of Temperature at Equilibrium $[Na^+]:[Cs^+] = 10^4$

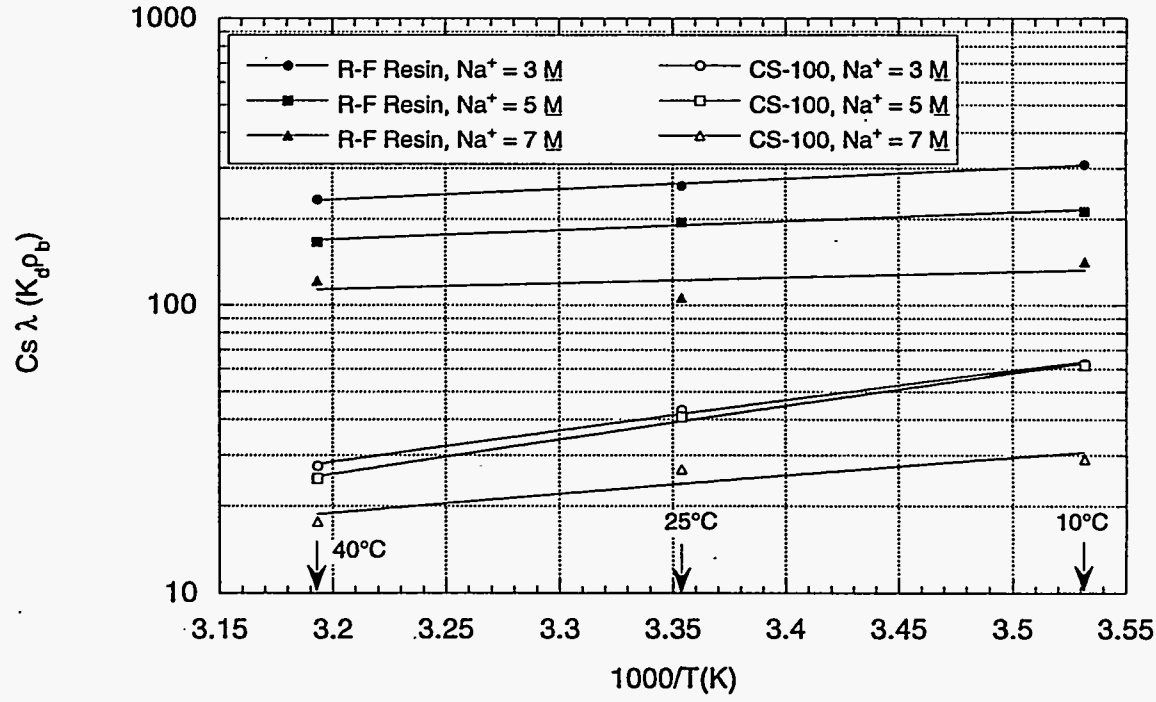

FIGURE 5.4. Cesium λ in CC Waste as a Function of Temperature at Equilibrium $[Na^+]:[Cs^+] = 10^4$

TABLE 5.4. Interpolated Cesium λ for CS-100 and R-F Resins at Equilibrium $[Na^+]:[Cs^+] = 10^4$ (a)

Waste	Na^+ (M)	T(°C)	Cs λ for CS-100	Cs λ for R-F Resin	Cs λ (R-F)/ Cs λ (CS-100)
NCAW	0.2	10	632	2487	3.9
NCAW	0.2	25	385	2243	5.8
NCAW	0.2	40	257	2126	8.3
NCAW	1.0	10	167	821	4.9
NCAW	1.0	25	108	603	5.6
NCAW	1.0	40	73	581	7.9
NCAW	3.0	10	65	336	5.1
NCAW	3.0	25	45	270	6.0
NCAW	3.0	40	32	244	7.6
NCAW	5.0	10	46	222	4.9
NCAW	5.0	25	34	182	5.3
NCAW	5.0	40	24	163	6.7
CC	3.0	10	63	310	4.9
CC	3.0	25	43	262	6.1
CC	3.0	40	28	234	8.5
CC	5.0	10	62	212	3.4
CC	5.0	25	41	195	4.8
CC	5.0	40	25	166	6.7
CC	7.0	10	29	142	4.9
CC	7.0	25	27	106	4.0
CC	7.0	40	18	122	6.9
DSSF(b)	7.0	25	15	75	5

(a) For CS-100, CC waste simulant, the Cs λ values were obtained by extrapolation outside the range of the data.
(b) For DSSF, Cs λ values are estimated from Figure 5.2.

TABLE 5.5. Temperature Dependence of Cs λ for the CS-100 and R-F Resins (Slopes of Figures 5.3 and 5.4)

	CS-100	R-F		
Na^+ (M)	NCAW	CC	NCAW	CC
0.2	2.664	-	0.466	-
1.0	2.429	-	1.034	-
3.0	2.117	2.437	0.957	0.837
5.0	1.849	2.690	0.909	0.717
7.0	-	1.458	-	0.468

(precipitation of dissolved solids, for example) must be considered before applying batch equilibrium data to column loading.

Dilution Increases Csλ. Figures 5.3 and 5.4 also show the downward shift of the Cs λ curves at higher $[Na^+]$, but Figure 5.5 more clearly shows the dependence of cesium λ on $[Na^+]$. Cs λ is plotted as a function of $[Na^+]$ in the solution at equilibrium $[Na^+]:[Cs^+]$ of 10^4 and 10^5. At lower $[Na^+]$ (i.e., for diluted wastes), Cs λ values are higher.

Cesium λ Unaffected by Anionic Organic Complexants. Figure 5.5 suggests that organic complexants (CC waste simulant) do not affect cesium equilibrium, consistent with the idea that anionic complexants do not participate in cation exchange. It is possible, although not likely, that repeated exposure to the complexants could foul the resin.

Csλ for Two Resins Show Similar Dependence on Sodium. Changes in cesium λ with $[Na^+]$ are similar for both resins. The slopes of the lines in Figure 5.5, based on a power-law curve fit, are nearly the same (-0.79 to -0.82). The behavior of Cs λ as a function of $[Na^+]$ is similar for the two waste types and for the two $[Na^+]:[Cs^+]$s. Thus cesium removal evidently can be predicted for a broad range of tank waste types (with relatively low potassium concentrations similar to those used in the waste simulants) by interpolation of cesium batch distribution data to specified $[Na^+]$ and $[Na^+]:[Cs^+]$.

Dilution Decreases Waste Volume Processed. The increase in Cs λ as sodium concentration is decreased suggests that dilution may increase the volume of waste that can be processed per volume of resin. However, a detailed examination indicates that dilution decreases the initial (actual) volume of waste that can be processed for a given volume of resin. The fractional change in the actual amount of waste processed is given by Equation (5.2).

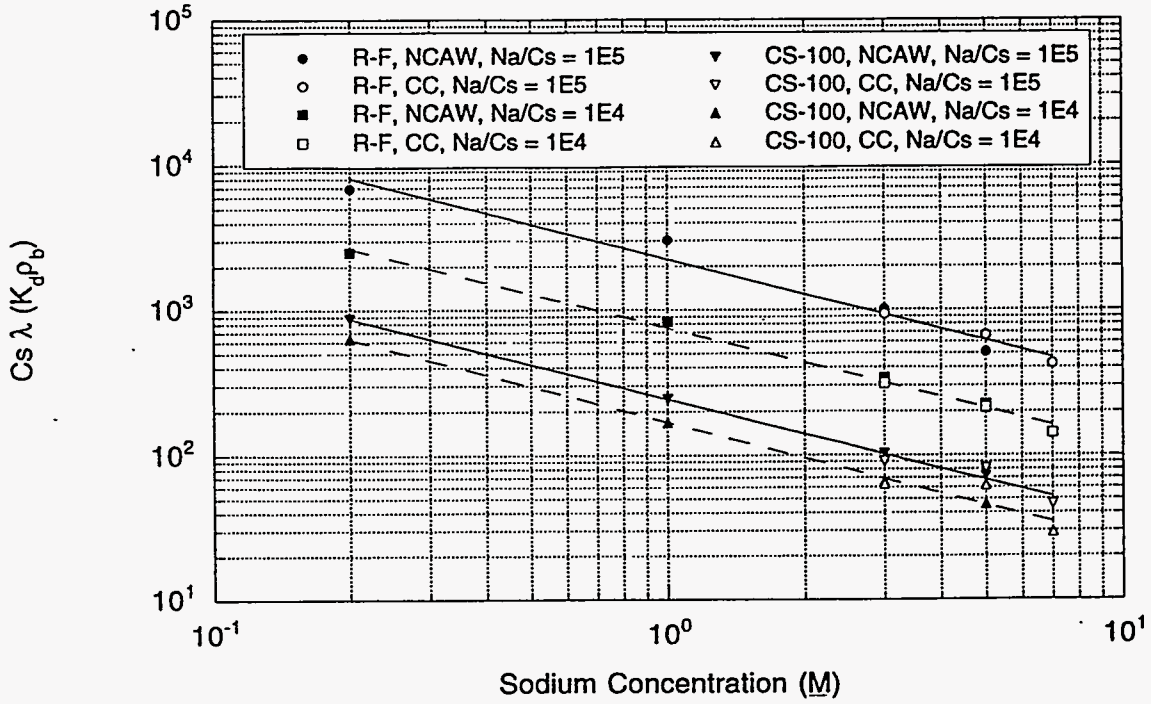

FIGURE 5.5. Cesium λ as a Function of Sodium Concentration at 10°C and Equilibrium $[Na^+]:[Cs^+] = 10^4$ and 10^5 (NCAW and CC Waste)

$$\Delta V = \frac{\lambda_1 - \frac{\lambda_2}{D}}{\lambda_1} \qquad (5.2)$$

where D = the dilution factor ($= V_2/V_1 = [Na]_1/[Na]_2$)

V_1 = the initial volume

V_2 = the final volume

For example, Cs λ for CS-100 increases from 46 (λ_1) to 167 (λ_2) when NCAW (10^4 $[Na^+]:[Cs^+]$) is diluted from 5M to 1M Na^+ at 10°C (Table 5.4), but the initial volume of waste that can be processed decreases by 27% ($\Delta V = 0.27$). For the same conditions ($\lambda_1 = 210$, $\lambda_2 = 750$), R-F resin could process 28% ($\Delta V = 0.28$) less of the initial feed. Depending on conditions, however, the reduction in waste processing capacity of the two resins can differ significantly with dilution. When CC waste is diluted from 5M to 3M Na^+ at 40°C, the

initial volume of waste that can be processed decreases by 33% for CS-100, but only 15% for R-F. Diluting the tank wastes as little as possible before cesium decontamination with R-F or CS-100 will minimize generation of secondary waste (resin and regenerant volumes). Figure 5.6 shows how the actual waste volume decreases with dilution (lower $[Na^+]$. The reference point for λ_{ref} is waste at 7M sodium and represents the column volumes of feed (at 7M Na) that could be processed per column volume if the waste were diluted to the indicated sodium concentration.

Cesium Distribution Coefficient is Maximized Above pH 12. Optimum pH for loading cesium is >12 for both resins. Figure 5.7 shows Cs K_d (= Cs λ/ρ_b) as a function of pH. Cesium K_d values at pH <2 for CS-100 appear to rise, contrary to expectations. Solution pH was varied and $[Na^+]$ was kept constant at 5M for the batch contacts by varying sodium hydroxide and sodium nitrate concentrations. Initial cesium concentration was 0.0005M and temperature was 25°C. Increasing Cs K_d with pH reflects the increasing number of ionized sites necessary for ion exchange. Since CS-100 and R-F both have phenolic

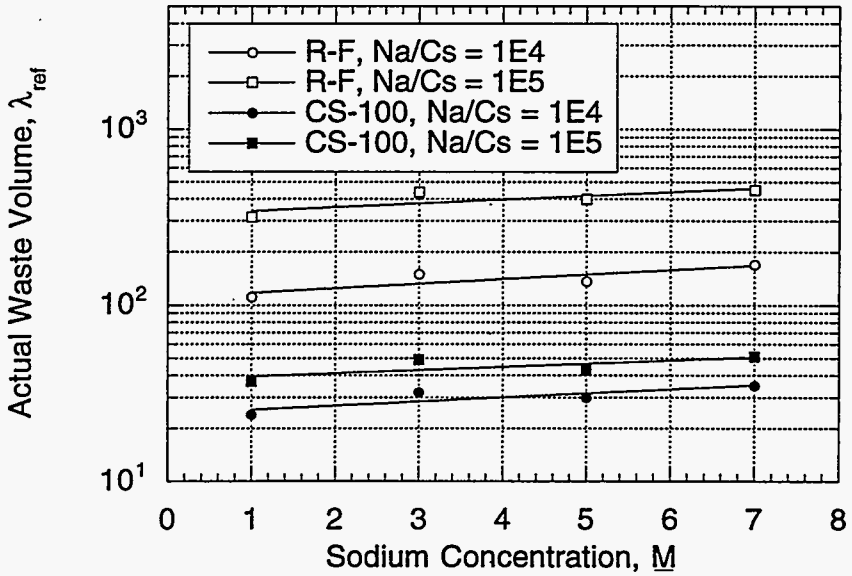

FIGURE 5.6. Effect of Dilution on Actual Volume of Waste Processed

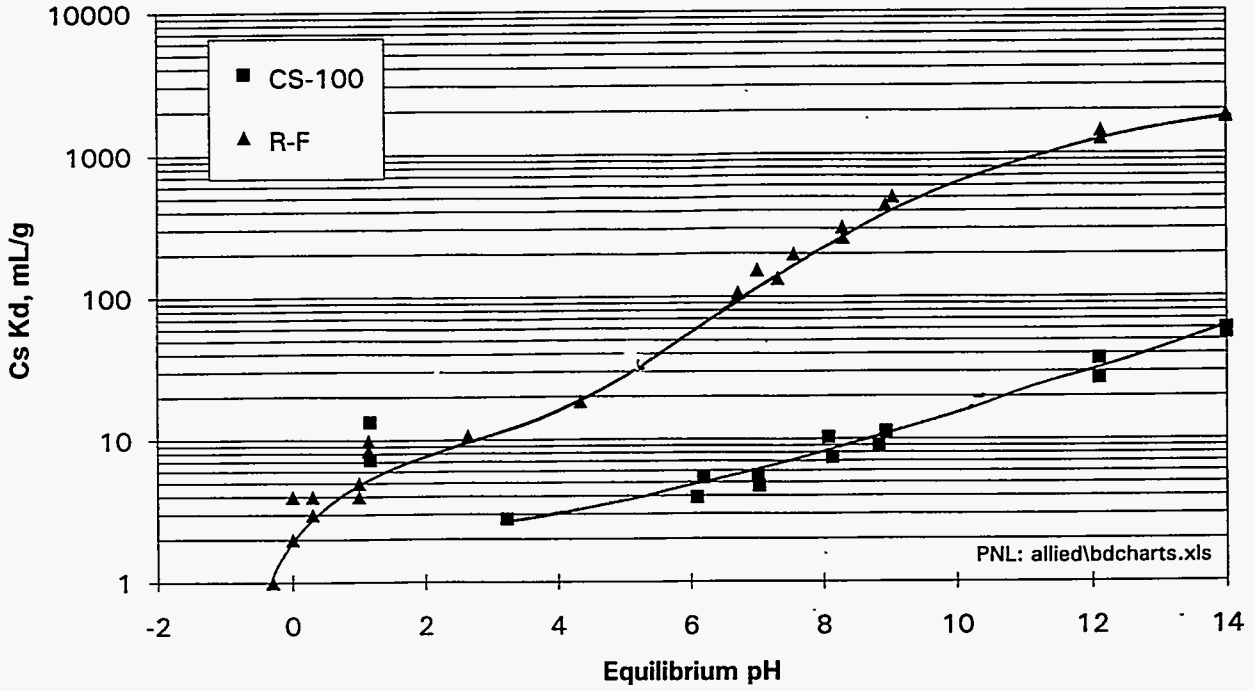

FIGURE 5.7. Resin Selectivities as a Function of pH at 25°C, 5M Na^+, Initial 0.0005M Cs^+

exchange sites ($pK_a \approx 10$), ion-exchange is maximized at pH >12 (see Section 2.1), as is cesium loading (Cs K_d).

Given the variety of cesium and sodium concentrations in the tank wastes, a method to estimate the cesium equilibrium behavior will facilitate column operation. Column volumes processed at 0.5 C/C_0 is equal to Cs λ for trace solutions of cesium loading at equilibrium without channeling or longitudinal dispersion (Popovich 1964). Since actual column-loading conditions may differ from those idealized conditions, the Cs λ value gives an approximation of the column volumes at 50% breakthrough.

In this section, the cesium λ for NCAW and CC waste simulants with the CS-100 and R-F resins are correlated with temperature, $[Na^+]$, and $[Na^+]:[Cs^+]$ using Equation (2.16). The correlations can be used to interpolate Cs λ levels at other conditions. However, each correlation was developed for data taken over specific ranges in temperature, $[Na^+]$, $[Na^+]:[Cs^+]$, and initial potassium concentration. The correlations should not be used outside those

ranges. Table 5.6 summarizes the ranges of validity for the correlations, and Table 5.7 gives the correlation constants (C_1, C_2, C_3, and C_4) and the r value. The r value, as defined by Equation (5.3), is used to measure the "goodness of fit."

TABLE 5.6. Ranges of Validity of the Correlations for Cesium λ

Correlation	Resin	Waste Type	$[Na^+]:[Cs^+]$	T(°C)	Na^+(M)	$[Na^+]:[Cs^+]$, Initial
1	CS-100	NCAW, CC	6.1E3-1.6E7	10-40	0.2-7	42-200
2	R-F	NCAW, CC	5.4E1-6.8E4	10-40	0.2-7	42-200
3	R-F	CC	5.6E5-3.0E8	10-40	3-7	200
4	R-F	NCAW	1.3E5-1.7E8	10-40	0.2-5	42

TABLE 5.7. Correlation Constants for Cesium λ[(a)]

Correlation	Resin	C_1	C_2	C_3	C_4	r value
1	CS-100	$8.563X10^{-4}$	-0.7613	0.1211	3181	0.980
2	R-F	0.1049	-0.7913	0.5106	1235	0.967
3	R-F	195.6	-1.008	0.0373	992.9	0.868
4	R-F	1.321	-0.8203	0.02911	2280	0.963

(a) For use with Equation (2.16):

$$\lambda = C_1 [Na]_1^{C_2} \left(\frac{Na}{Cs}\right)^{C_3} \exp\left(\frac{C_4}{T}\right) \qquad (2.16)$$

$$r = \sum_{i=1}^{n} \frac{\left(\frac{x_{avg}-x_i}{\sigma_x}\right)\left(\frac{y_{avg}-y_i}{\sigma_y}\right)}{n} \qquad (5.3)$$

where n = number of points

x_{avg} = average of the experimental Cs λ values

y_{avg} = average of the Cs λ values determined from the correlation

x_i = experimental Cs λ value

y_i = Cs λ value determined from the correlation

σ_x = standard deviation of the experimental values

σ_y = standard deviation of the correlated values

where $[Na]_1$ = $\underline{M}$ and T = degrees Kelvin.

For CS-100, Correlation 1 was obtained by fitting 63 Cs λ data points determined for NCAW or CC waste simulants. Figures 5.8 and 5.9 are scatter plots comparing the Cs λ values from Correlation 1 with the experimental values. Figure 5.9 is an expanded view of the lower part of Figure 5.8. The good fit of the data for both wastes (correlation r = 0.98) suggests that ion-exchange behavior of these two wastes with CS-100 will be similar.

Correlation of the Cs λ values for the R-F resin was more complicated than for CS-100. The R-F resin data required more than one correlation, apparently because the resin approached saturation with cesium over the range of $[Na^+]:[Cs^+]$ investigated. Although there were indications that the "goodness of fit" could be improved by several correlations over relatively short ranges of $[Na^+]:[Cs^+]$, for simplicity the data were divided into only two sets. Division at $[Na^+]:[Cs^+] = 10^5$ appeared to give the best results,

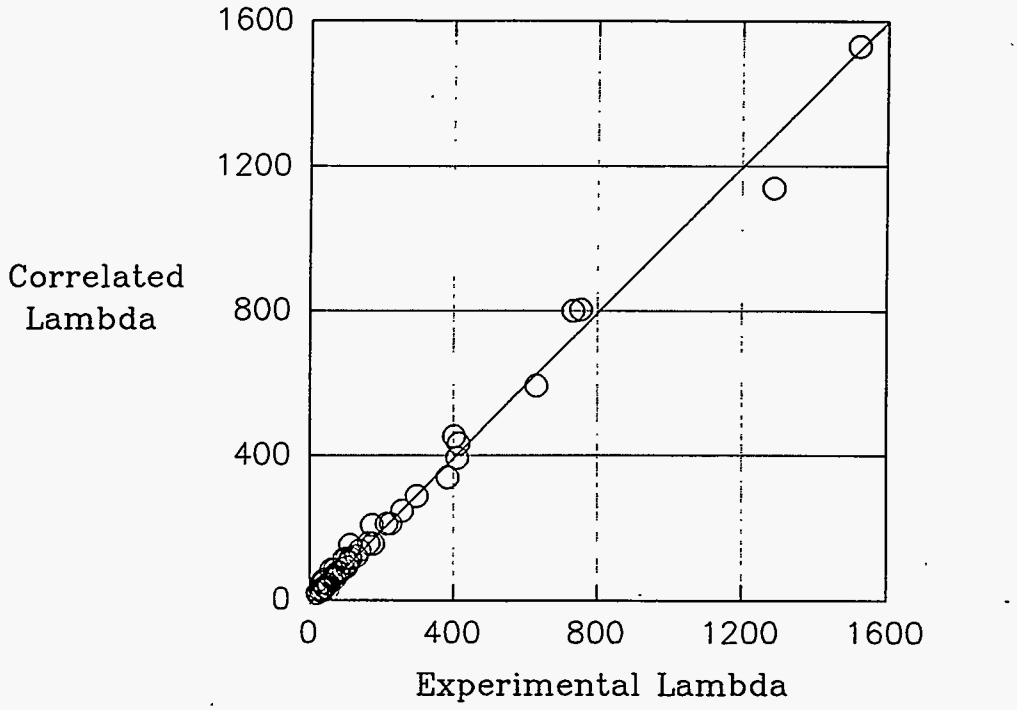

FIGURE 5.8. Cs λ Correlation 1: CS-100, NCAW, and CC Waste Simulants, Equilibrium $[Na^+]:[Cs^+]$ = 6.1E3-1.6E7

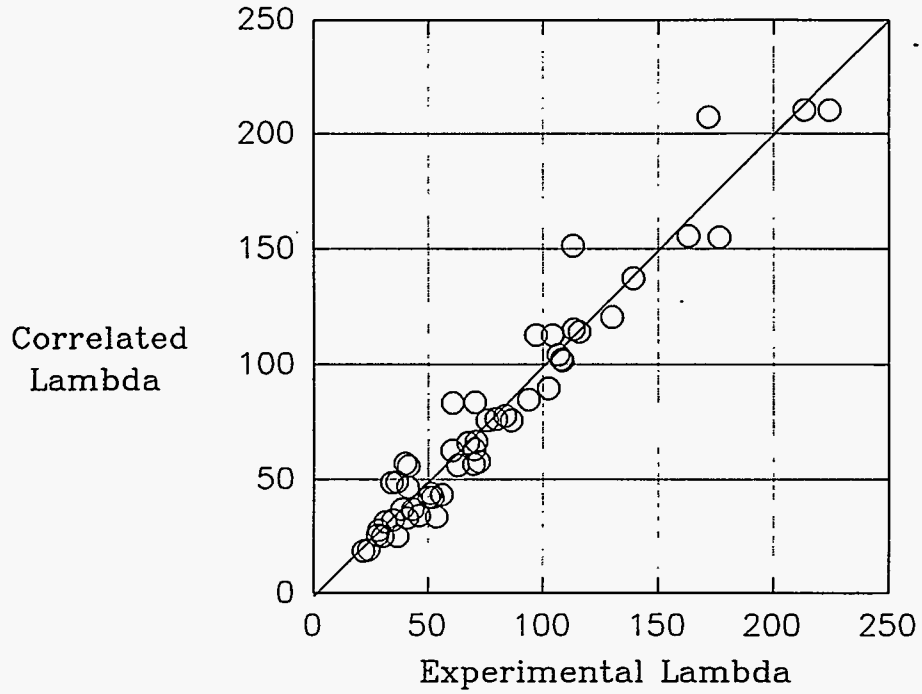

FIGURE 5.9. Cs λ Correlation 1: CS-100, NCAW, and CC Waste, Expanded View

probably because this value represents the transition where the resin begins to load with cesium (with diminishing $[Na^+]:[Cs^+]$). Four of the extremely high Cs λ values (two for $[Na^+]:[Cs^+] < 10^5$ and two for $[Na^+]:[Cs^+] > 10^5$) measured at 0.2M sodium in NCAW simulant were omitted so that most of the data could be fit. Correlation 2 was obtained for NCAW and CC waste simulants for $[Na^+]:[Cs^+] < 10^5$ (51 Cs λ values); for $[Na^+]:[Cs^+] > 10^5$: Correlation 3 for CC waste (36 points) and Correlation 4 for NCAW (34 points). Figures 5.10, 5.11 and 5.12 show that the correlations fit the Cs λ values reasonably well. Correlations 2 and 4 had a better fit ($r = 0.967$ and 0.963, respectively) than Correlation 3 ($r = 0.868$), but, as mentioned, some data were omitted to fit Correlations 2 and 4. Figures 5.13 and 5.14 compare Cs λ from the correlations with experimental values for NCAW simulant. The CS-100 correlation provides reasonable estimates of Cs λ (Figure 5.13). For R-F (Figure 5.14), Correlation 4 (high $[Na^+]:[Cs^+]$) represents the data better than Correlation 2 (low $[Na^+]:[Cs^+]$).

In summary, attempts to correlate cesium distribution coefficients with $[Na^+]$, $[Na^+]:[Cs^+]$, and temperature were generally successful. One correlation was sufficient for CS-100, but three correlations were needed for R-F resin. The correlations demonstrate three general trends in cesium ion-exchange for R-F and CS-100: (1) cesium loading, as indicated by Cs λ, rises with falling temperature, (2) cesium distribution coefficient increases with increasing $[Na^+]:[Cs^+]$, and (3) cesium distribution increases with dilution of wastes (lower $[Na^+]$). It cannot be overemphasized, however, that these correlations should be used only over the ranges of the original data (Table 5.6), including $[K^+]$. The correlations do not explicitly account for potassium, which also loads onto the resins (Section 5.1.4).

One use of the correlations developed above is to show the effect of dilution on the actual volume of waste that can be decontaminated of cesium. A general equation can be written that gives a reference λ (λ_{ref} = equivalent bed volumes of feed processed at a reference sodium concentration) as a function of the diluted sodium concentration:

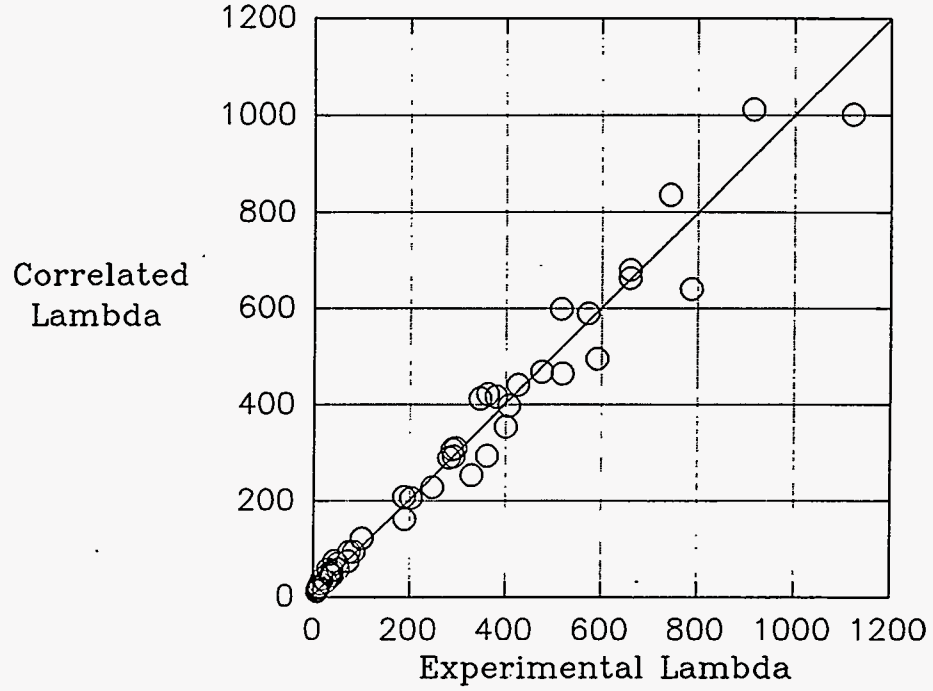

FIGURE 5.10. Cs λ Correlation 2: R-F Resin, NCAW, and CC Waste, Equilibrium $[Na^+]:[Cs^+]$ = 5.4E1-6.8E4

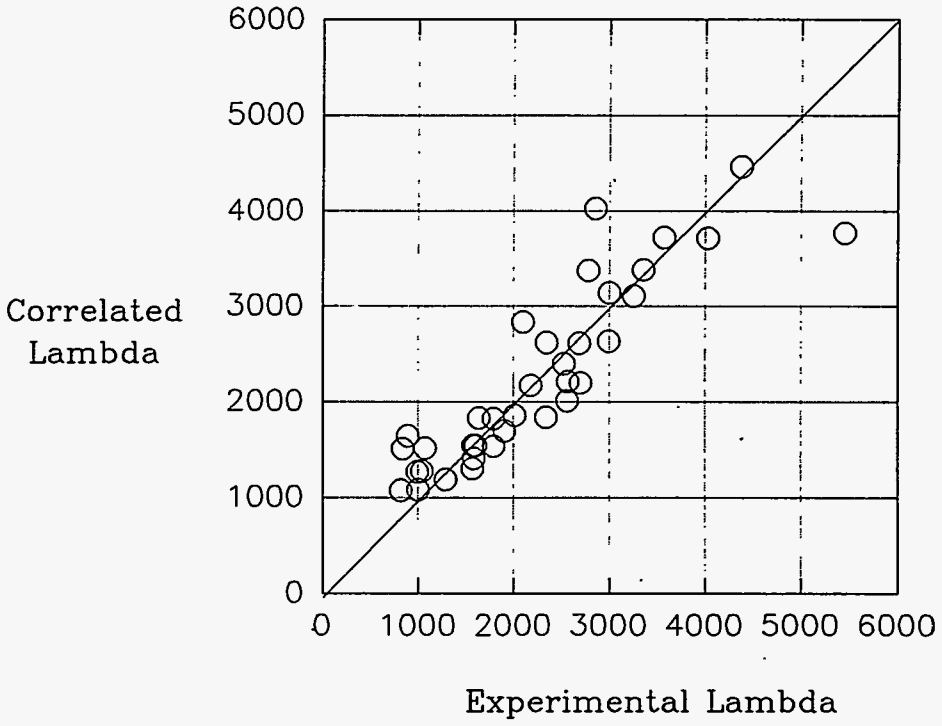

FIGURE 5.11. Cs λ Correlation 3: R-F Resin, CC Waste, Equilibrium $[Na^+]:[Cs^+]$ = 5.6E5-3.0E8

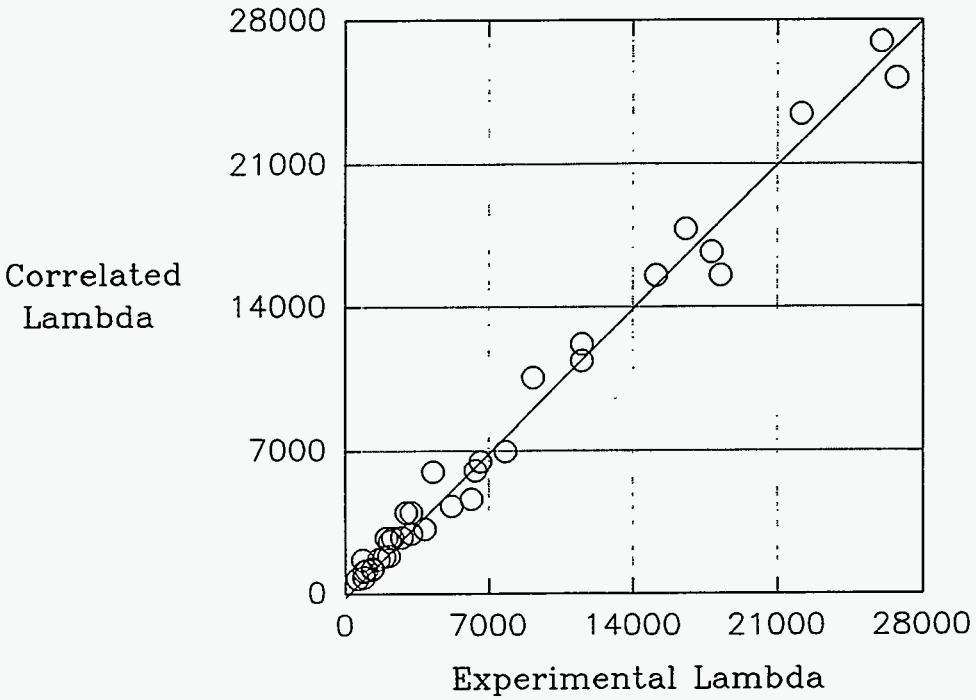

FIGURE 5.12. Cs λ Correlation 4: R-F Resin, NCAW, Equilibrium $[Na^+]:[Cs^+]$ = 1.3E5-1.7E8

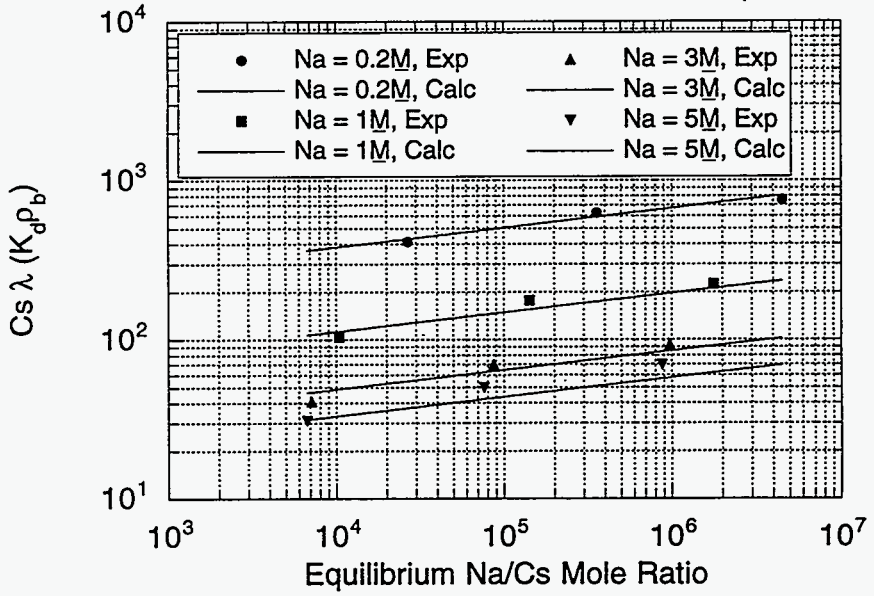

FIGURE 5.13. Comparison of CS-100 Cs λ Correlation with Experiment, NCAW, 25°C

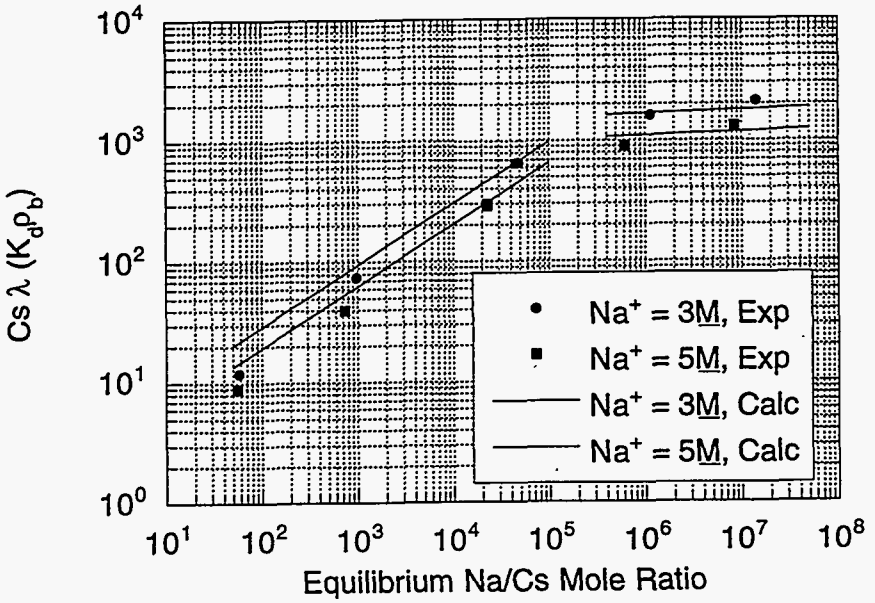

FIGURE 5.14. Comparison of R-F Cs λ Correlations with Experiment, NCAW, 25°C

$$\lambda_{ref} = \frac{K[Na]^{C_2}[Na]}{[Na]_{ref}} \qquad (5.4)$$

where $K = C_1([Na^+]:[Cs^+])^{C3}\exp(C_4/T)$ [part of correlation, Equation (2.16)]

$[Na]_{ref}$ = a reference sodium concentration corresponding to λ_{ref}

[Na] = diluted sodium concentration

The functional dependence of λ_{ref} on the diluted sodium concentration is $1+C_2$. The values of C_2 given in Table 5.7 show that the functional dependence of λ_{ref} ranges from about 0 to about 0.24. Since [Na] is a diluted concentration and therefore less than $[Na]_{ref}$, the actual amount of waste processed either stays the same ($C_2 = -1$) or decreases ($C_2 > -1$). Thus, the correla-

either stays the same ($C_2 = -1$) or decreases ($C_2 > -1$). Thus, the correlations confirm that, for most conditions studied, the amount of waste that can be processed (for a given amount of resin) decreases as the waste is diluted.

5.1.4 Equilibrium Behavior - Potassium λs

The competing effect of potassium reduces the cesium λ under certain conditions. For both resins, Cs λ was determined at 25°C with CC and NCAW adjusted to contain varying amounts of potassium. However, only the initial concentration of potassium was available; the equilibrium concentrations were not measured.

Increasing $[K^+]$ decreases the cesium λ for R-F resin, particularly at low cesium concentrations. In both NCAW (Figure 5.15) and CC Waste (Figure 5.16), Cs λ generally decreases as $[K^+]$ is increased (decreased initial $[Na^+]:[K^+]$). Competition from potassium is most significant when $[Na^+]:[Cs^+]$ is high, consistent with the idea that competition from other cations is more important at low cesium concentrations.

Potassium loading of CS-100 and R-F in cesium-free NCAW simulant was investigated. Potassium λs (K K_d values) were determined for 0.2-5M Na^+ using ^{42}K tracer at 25°C. The K K_d values were converted to K λ ($= K_d\rho_b$) using densities of 0.458 and 0.461 g/ml for CS-100 and R-F, respectively (Table 5.1). Experiments using the more concentrated wastes generally gave poor results because the amount of resin was too small to measurably change $[K^+]$. Consequently, the determination of the K_d values depended on the accurate measurement of a small difference between two large numbers. In some cases, negative values were obtained as a result of experimental error. Figures 5.17 and 5.18 plot K λ versus equilibrium $[Na^+]:[K^+]$ at different $[Na^+]$. The lines represent power-law curve fits. Except at 5M sodium, K λ for both resins increases with increasing $[Na^+]:[K^+]$, consistent with the trend of Cs λ with $[Na^+]:[Cs^+]$. The difference in the average K λ values for the two resins under the conditions studied was less than 3-fold. The R-F resin loads more potassium at 0.2M and 1M sodium than CS-100, as indicated by higher K λ.

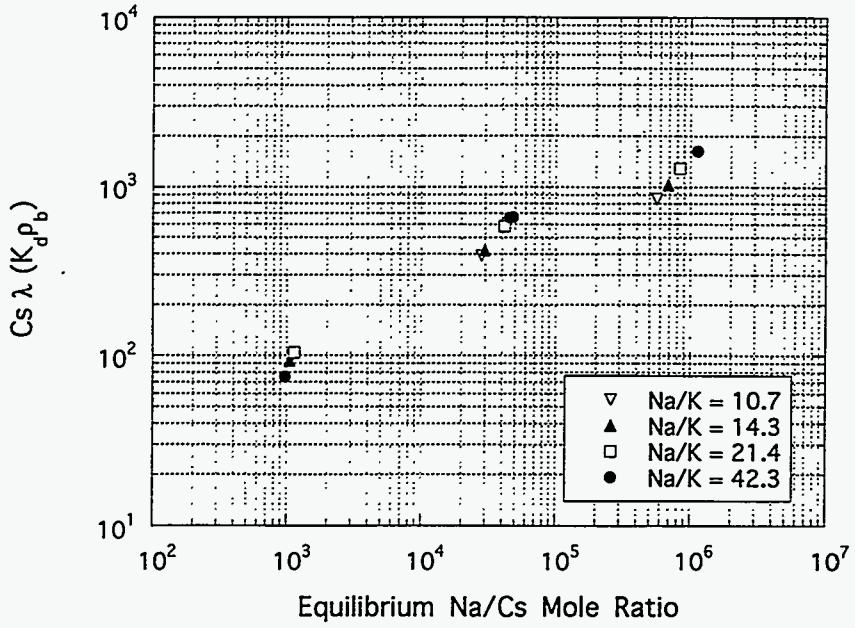

FIGURE 5.15. Cesium λs for R-F Resin at Different Initial Potassium Concentrations in NCAW Simulant at 3M Na^+, 2.2×10^{-5} initial $[Na^+]/[Rb^+]$, and 25°C

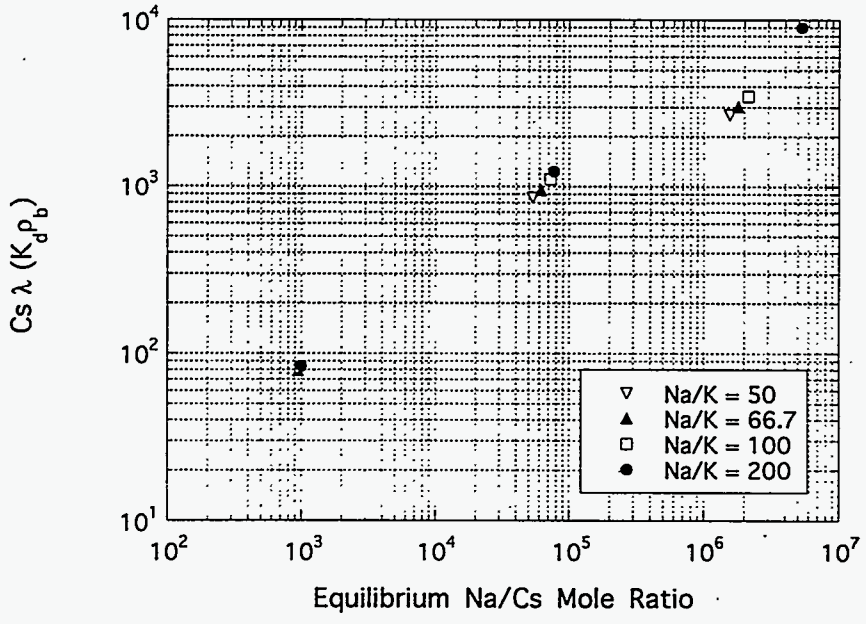

FIGURE 5.16. Cesium λs for R-F Resin at Different Initial Potassium Concentrations in CC Waste Simulant at 3M Na^+ and 25°C

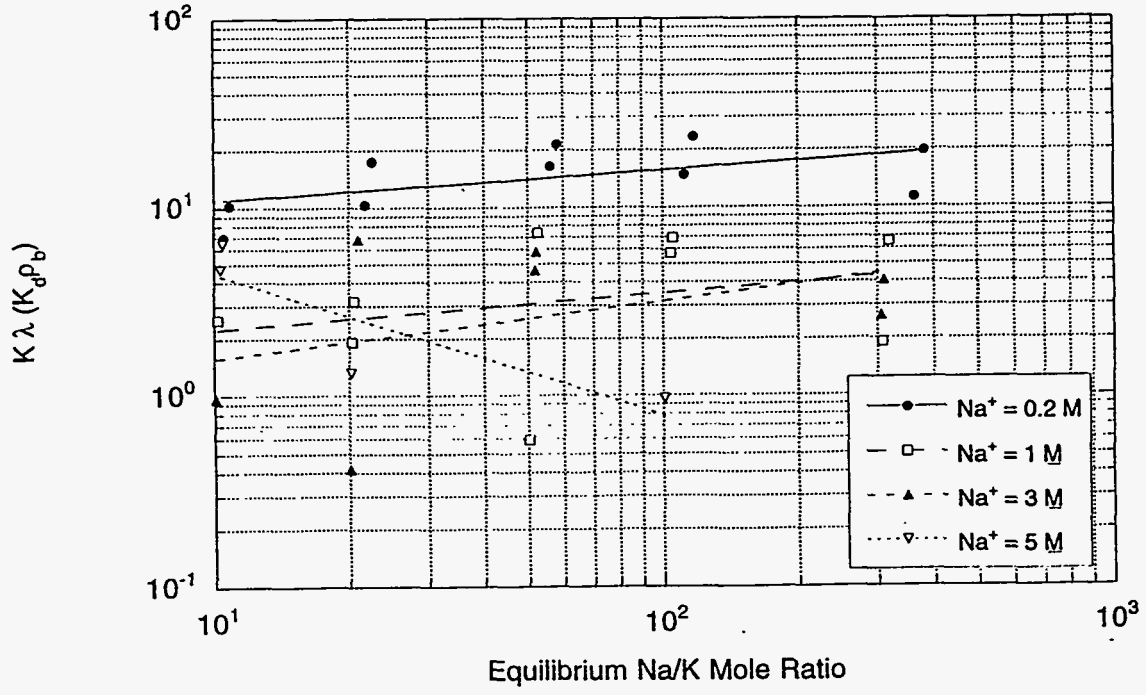

FIGURE 5.17. CS-100 Potassium λs in Cesium-Free NCAW Simulant at 25°C

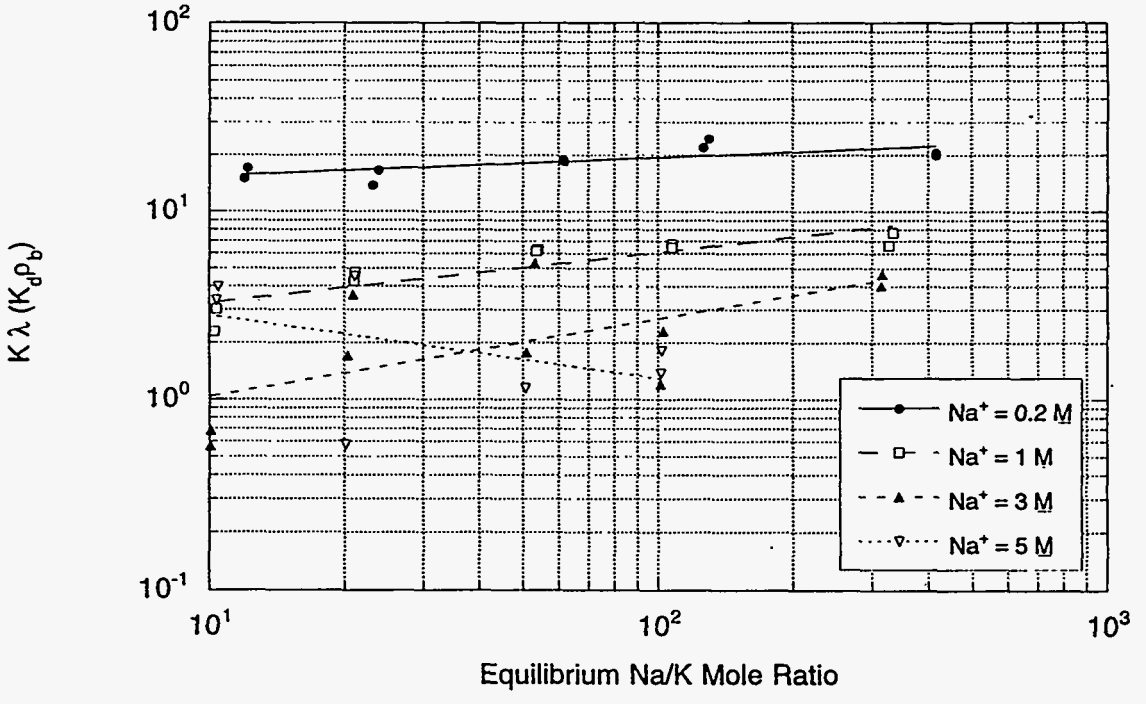

FIGURE 5.18. R-F Potassium λs in Cesium-Free NCAW Simulant at 25°C

Selected K λ values for both resins were analyzed to obtain apparent ion-exchange capacities and equilibrium constants. Average K λ values for 0.2M and 1M sodium were analyzed. The values at 3M and 5M sodium were not analyzed because of uncertainties in the data. The potassium concentration in the liquid, $[K]_l$, was calculated from Equation (5.5) and the potassium concentration on the resin, $[K]_s$, was calculated from Equation (5.6), assuming negligible change in sodium concentration. This assumption gives an estimated 1% error.

$$[K]_l = \frac{[Na]_l}{\left(\frac{Na}{K}\right)_l} \tag{5.5}$$

$$[K]_s = \frac{\lambda [Na]_l}{\left(\frac{Na}{K}\right)_l} \tag{5.6}$$

where $[K]_s$ = potassium concentration on the resin

$[Na]_l$ = sodium concentration in the liquid, assumed constant

$(Na/K)_l$ = equilibrium $[Na^+]:[K^+]$ in the liquid, based on the initial and final γ counts

A form of the Langmuir equation for ion exchange developed in Section 2.1 [see Equation (2.9)] was used to analyze the binary sodium-potassium data:

$$\frac{1}{[K]_s} = \frac{[Na]_l}{Q\, K_{eq} [K]_l} + \frac{1}{Q} \tag{5.7}$$

where $K_{eq} = [Na]_l[K]_s/\{[K]_l[Na]_s\}$

Q = the ion-exchange capacity

The inverse of potassium concentration on the resin was plotted against the equilibrium $[Na^+]:[K^+]$. Based on the linear-curve fit, the apparent ion-exchange capacity was calculated from the y-intercept, and the equilibrium constant (ideal behavior) was calculated from the slope and y-intercept. Figures 5.19 and 5.20 show the averaged data and correlations (in log-log coordinates).

Table 5.8 summarizes the ion-exchange capacities and equilibrium constants for the CS-100 and R-F resins at 25°C. The apparent capacity of the R-F resin is less than its total ion-exchange capacity (the total number of sites capable of exchanging ions) (Table 5.1). The apparent capacity from the analysis would equal the total capacity only under ideal conditions (dilute solution). Therefore, extrapolation of the isotherm cannot be expected to

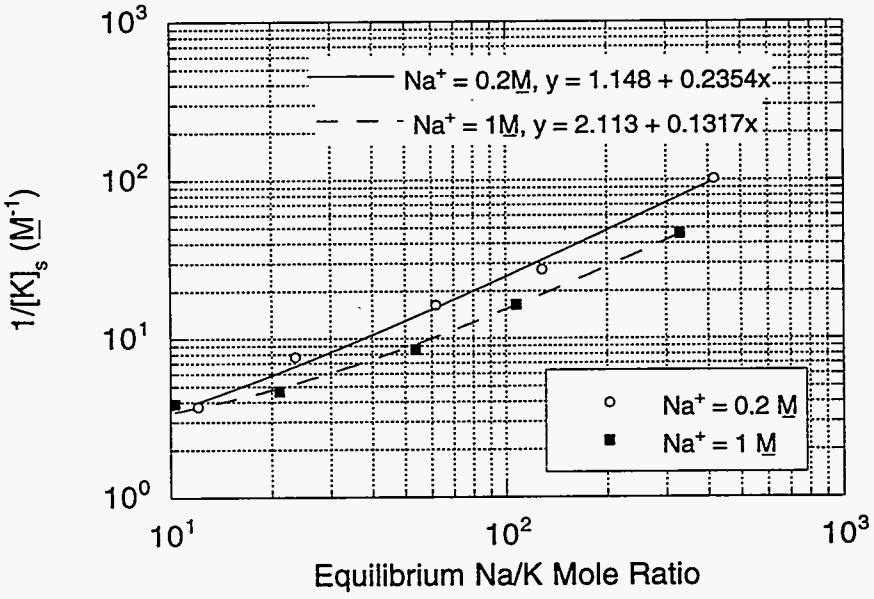

FIGURE 5.19. Correlation of the Potassium Equilibrium Data at 25°C for CS-100 Using the Langmuir Isotherm for Ion Exchange

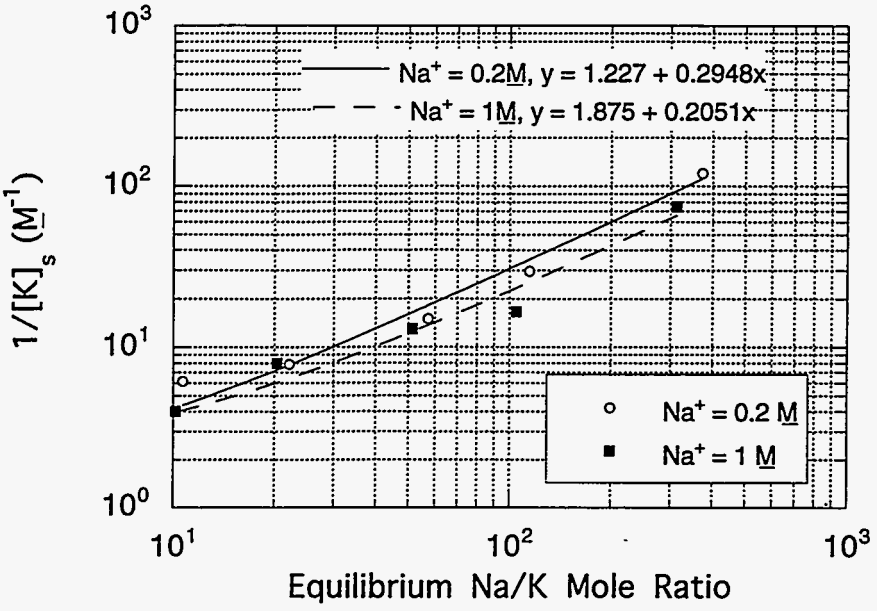

FIGURE 5.20. Correlation of the Potassium Equilibrium Data at 25°C for R-F Resin Using the Langmuir Isotherm for Ion Exchange

TABLE 5.8. Potassium Equilibrium Constants and Apparent Potassium Ion-Exchange Capacities

Resin	Sodium (M)	K_{eq}	Q (M resin)	Q (meq/g dry resin)[(a)]
CS-100	0.2	4.2	0.81	1.8
CS-100	1.0	9.1	0.53	1.2
R-F Resin	0.2	4.9	0.87	1.9
R-F Resin	1.0	16	0.47	1.0

(a) Estimate based on dry density of 0.458 for CS-100 and 0.461 for R-F.

yield the total ion-exchange capacity. Consistently, at the more dilute sodium concentration, the resin has a larger apparent capacity (approaching the total capacity). Surprisingly, both resins have about the same apparent capacity for potassium. The slightly higher equilibrium constants of R-F suggest that it is somewhat more selective for potassium over sodium than CS-100. To accurately quantify the apparent ion-exchange capacity and the equilibrium constant, the batch equilibrium measurements need to be extended to a much larger range of equilibrium $[Na^+]:[K^+]$, which includes regions where the resin is saturated with potassium and sodium.

One can now better understand why the Cs λ values are difficult to correlate. To date, the cesium distribution coefficients have been measured in waste simulants containing significant amounts of potassium (and rubidium); and the simultaneous equilibrium potassium concentrations were unavailable. For this reason, the empirical correlations that were developed neglected the effect of competing ions. The interference effect of potassium and rubidium and the dependence of Cs λ on sodium concentration demonstrate the multicomponent nature of ion exchange. An accurate characterization of cesium ion exchange requires a multicomponent analysis.

5.1.5 Multicomponent Modeling

A multicomponent description of ion exchange should account for all species that exchange with ions on the resin in significant quantity. In addition to sodium, cesium, and potassium (the minimum set of participating cations), rubidium, calcium, strontium, and other cations may also exchange.

A simple multicomponent model for monovalent ion exchange based on Langmuir-type adsorption behavior is given by Equation (5.8).

$$\overline{C_i} = \frac{a_i C_i}{1 + \sum_{j=1}^{n} b_j C_j} \tag{5.8}$$

where the bar = the concentration on the resin

i = the species of interest

n = number of adsorbing species.

If cesium-potassium-sodium exchange can be modeled as Langmuir-type adsorption, Equation 5.8 becomes

$$[Cs]_s = \frac{a_1 [Cs]_l}{1 + b_1 [Cs]_l + b_2 [K]_l + b_3 [Na]_l} \tag{5.9}$$

Data collection for determination of the cesium isotherm could be designed in one of two ways: (1) the equilibrium $[Cs^+]$ on the resin could be measured simultaneously as a function of the sodium, cesium, and potassium concentrations in the liquid, and the constants (a_i and b_j) could be found by nonlinear regression; (2) the equilibrium concentrations on the resin and in solution could be measured for the binary component systems, with one of the species in excess, such that its liquid concentration remained constant.

A potential disadvantage of using adsorption models, such as Equation (5.9), to describe ion exchange is that adsorption does not physically correspond to ion exchange. The adsorption equations may correlate the cesium ion-exchange behavior over the range of concentrations investigated, but only a detailed thermodynamic model will give reliable information that can be extrapolated to other process conditions.

5.1.6 Fundamental Thermodynamic Approach

Any thermodynamic model for cesium ion exchange of Hanford tank wastes must meet two primary criteria. First, the model must be valid for high ionic strength solutions. The high ionic strength of NCAW and CC waste simulants (approximately 10 and 25 molal, respectively) precludes the use of dilute solution theories for the calculation of liquid-phase activity coefficients. Secondly, the model must allow for multicomponent ion exchange. The ESP meets these requirements.

In a recent report ("Cesium Ion Exchange Model", produced for WHC, November 1993), the manufacturer demonstrated that a thermodynamic analysis of cesium ion exchange with ESP is feasible.[2]

5.2 COLUMN-LOADING AND ELUTION STUDIES

This section analyzes cesium-loading and column-elution data for CS-100 and R-F resins. Section 5.2.1 presents experimental loading data and compares them with breakthrough curves obtained by fitting the data to column-loading models. Section 5.2.2 describes the mathematics and results of the column-loading models. Section 5.2.3 presents cesium-elution data for CS-100 and R-F. Section 5.2.4 describes the equations for the elution model.

5.2.1 Column-Loading Experiments

Cesium-loading experiments were designed to determine the effect of flow rate on cesium-loading characteristics of CS-100 and R-F, with NCAW and DSSF simulant as feed. Table 5.9 summarizes the flow rates and column configurations used in the experiments. Two batches of R-F (BSC-187 and BSC-210) were investigated.

The breakthrough curves are represented in two ways. The first plots C/C_0 versus the number of column volumes of feed processed through the first

---

[2] The authors based their conclusions on analysis of equilibrium data for the CS-100 and R-F resins from Bray et al. 1992.

TABLE 5.9. Cesium-Loading Experiments

Test #	Resin Used	# of Columns in Series	Nominal Flow Rate mL/h,(cv/h)	Waste Type	Temperature (°C)
1	CS-100	1 (A)	1200 (6)	NCAW	25
3	CS-100	3 (C,D,E)	1200 (6)	NCAW	25
5	CS-100	3 (I,J,K)	600 (3)	NCAW	25
7	CS-100	3 (O,P,Q)	1800 (9)	NCAW	25
8	R-F (BSC-187)	3 (R,S,T)	1800 (9)	NCAW	25
9	R-F (BSC-187)	4 (U,V,W,X)	2700 (13)	NCAW	25
10	R-F (BSC-210)	1 (Y)	2600 (13)	NCAW	25
11	CS-100	2 (AA,BB,CC)	1200 (6)	DSSF-2	25
12	CS-100	2 (EE,FF,GG)	1200 (6)	DSSF-7	25
13	CS-100	2 (II,JJ,KK)	400 (2)	DSSF-7	25
14	R-F (BSC-187)	3 (MM,NN,OO)	1800 (9)	DSSF-7	25
15	R-F (BSC-187)	3 (PP,QQ,RR)	600 (3)	DSSF-7	25
16	R-F (BSC-210)	1 (SS)	2400 (12)	DSSF-7	25

NOTE: Runs 2, 4, and 6 were cancelled because resin had oxidized.

column in series, where one column volume is that of a single column (200 mL). This method conveniently compares breakthrough of the downstream columns to breakthrough of the first column. The second method normalizes the column volumes to reflect the actual volume of resin through which the solution has passed. (For example, one column volume for the breakthrough curve of the second column in series is 2 x 200 = 400 mL.) This method shows the effect of flow rate or fluid velocity on cesium breakthrough. The two methods of representing breakthrough curves can usually be easily distinguished. In the second method, the curves intersect at approximately 50% C/C_0; curves plotted by the first method usually do not intersect.

5.2.1.1 CS-100 Loading Studies Using NCAW

The initial cesium-loading test with CS-100 resin and NCAW simulant was performed with a single column (Test 1, Column A) at 6 cv/h, Figure 5.21. The initial detectable cesium breakthrough ($C/C_0 \approx 0.002$) occurred at 8 cv. The

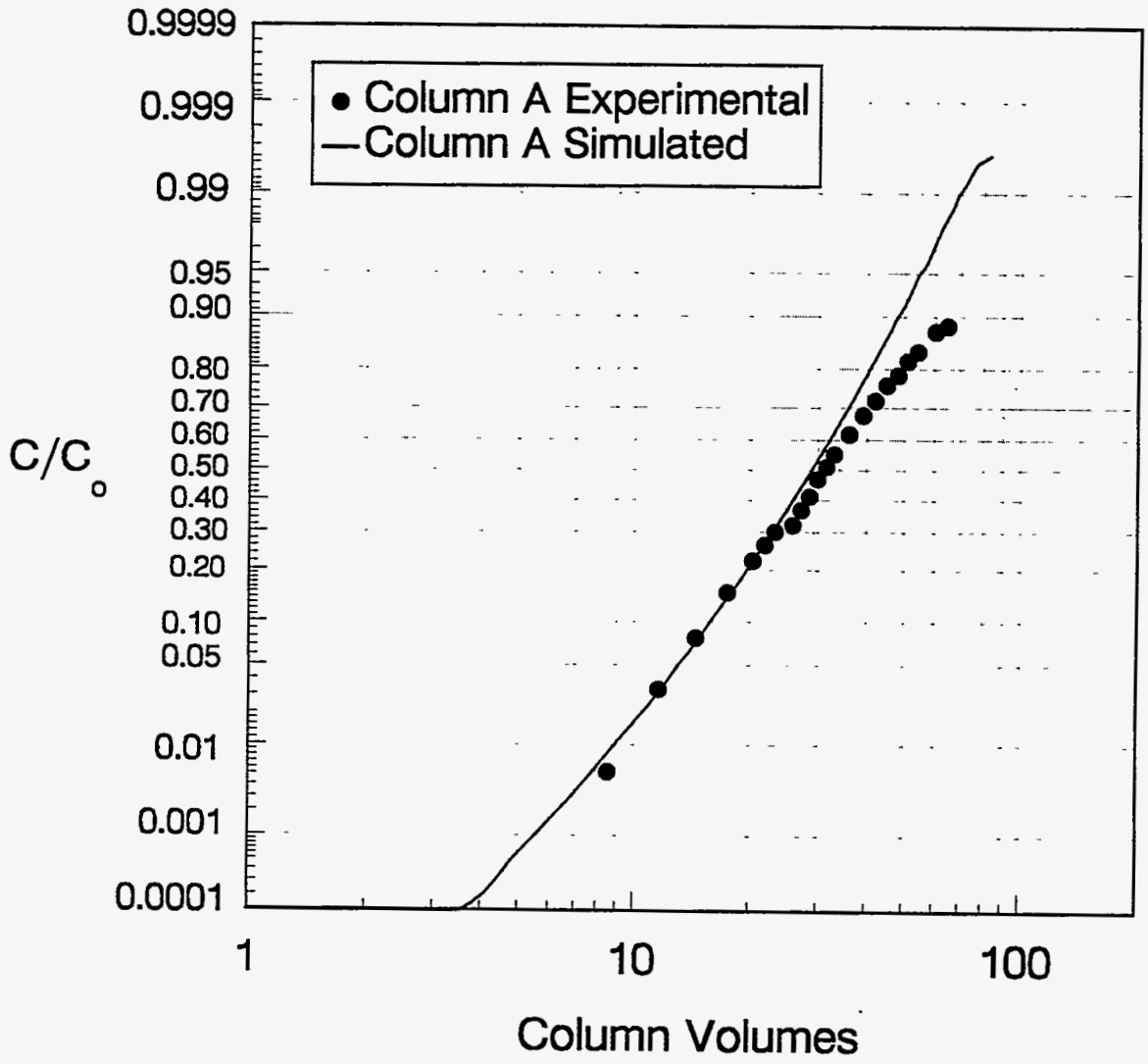

Resin: CS-100
Feed: NCAW
Flow rate: 6 cv/h, 1200 mL/h
Basis: 1 cv = 200 mL
Temperature: 25°C
Run 1: Column A

NOTE: There was a line plug at approximately 23 cv. The run was halted for approximately 30 min for repairs. This resulted in a drop in the effluent cesium concentration when it was restarted.

FIGURE 5.21. Cesium Ion-Exchange Column-Loading Experiment

Cs^+ 50% C/C_0 value was 30 cv, which agrees well with that predicted from the batch distribution data (Batch Cs λ = 34). The breakthrough curve is nearly a straight line in log-probability coordinates. The run was halted temporarily at approximately 23 cv. When it was restarted, the C/C_0 was less than would be predicted from extrapolation of earlier data; however, the breakthrough curve appeared to have recovered after less than 10 cv. This unplanned "flow interruption" test suggests the presence of mass-transfer effects, either in or outside the particle.

The next three tests with CS-100 (Tests 3, 5, and 7) involved three columns in series and different flow rates of NCAW simulant: 600, 1200, and 1800 mL/hr. Figures 5.22, 5.23, and 5.24 compare the breakthrough curves based on a 200-mL column volume. At each flow rate, breakthrough in the second column begins before 50% C/C_0 is reached in the first column. Although C/C_0 in the exit stream can be a poor indicator of the amount of cesium loaded on the resin, these results suggest that the resin in the first column cannot be fully loaded with cesium before it must be taken offline and regenerated, an effect examined in detail in Chapter 6.0. For the first column of each series, the number of column volumes at initial breakthrough (0.002 C/C_0) decreases from about 10 to 4 cv as the flow rate is increased from 600 to 1800 mL/hr. Initial breakthrough results were similar for downstream columns. The effect of flow rate on initial breakthrough is clearer when the breakthrough curves are normalized and shown on the same graph.

Figure 5.25 shows normalized cesium breakthrough curves for CS-100 at different flow rates of NCAW simulant. Increasing the flow rate (or decreasing residence time) increases the slope of the breakthrough curve and decreases the column volumes of feed processed before initial cesium breakthrough occurs. Initial breakthrough decreased from 20 cv to about 4 cv as flow rate was increased from 1 cv/h to 9 cv/h. The breakthrough curves intersect at ~0.5 C/C_0 and approximately 30 cv, which agrees well with the value expected from equilibrium Cs λ (Batch Cs λ = 34).

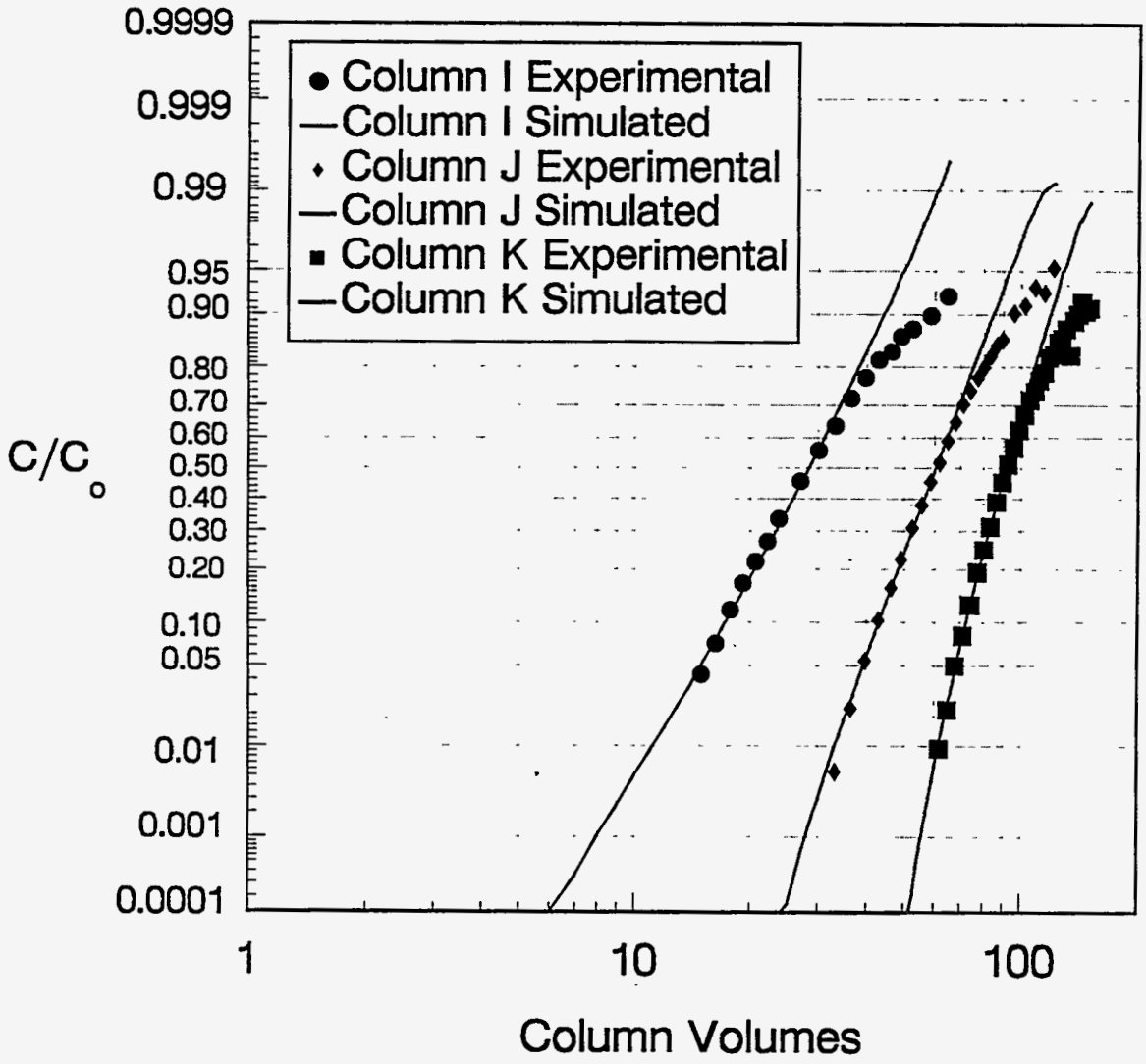

Resin: CS-100
Feed: NCAW
Flow rate: 3 cv/h, 600 mL/h
Basis: 1 cv = 200 mL
Temperature: 25°C
Run 5: Columns I, J, K (3 columns in series)

NOTE: Counting instrument drift caused the breakthrough curves to level off at a C/C_0 value <1.

FIGURE 5.22. Cesium Ion-Exchange Column-Loading Experiment

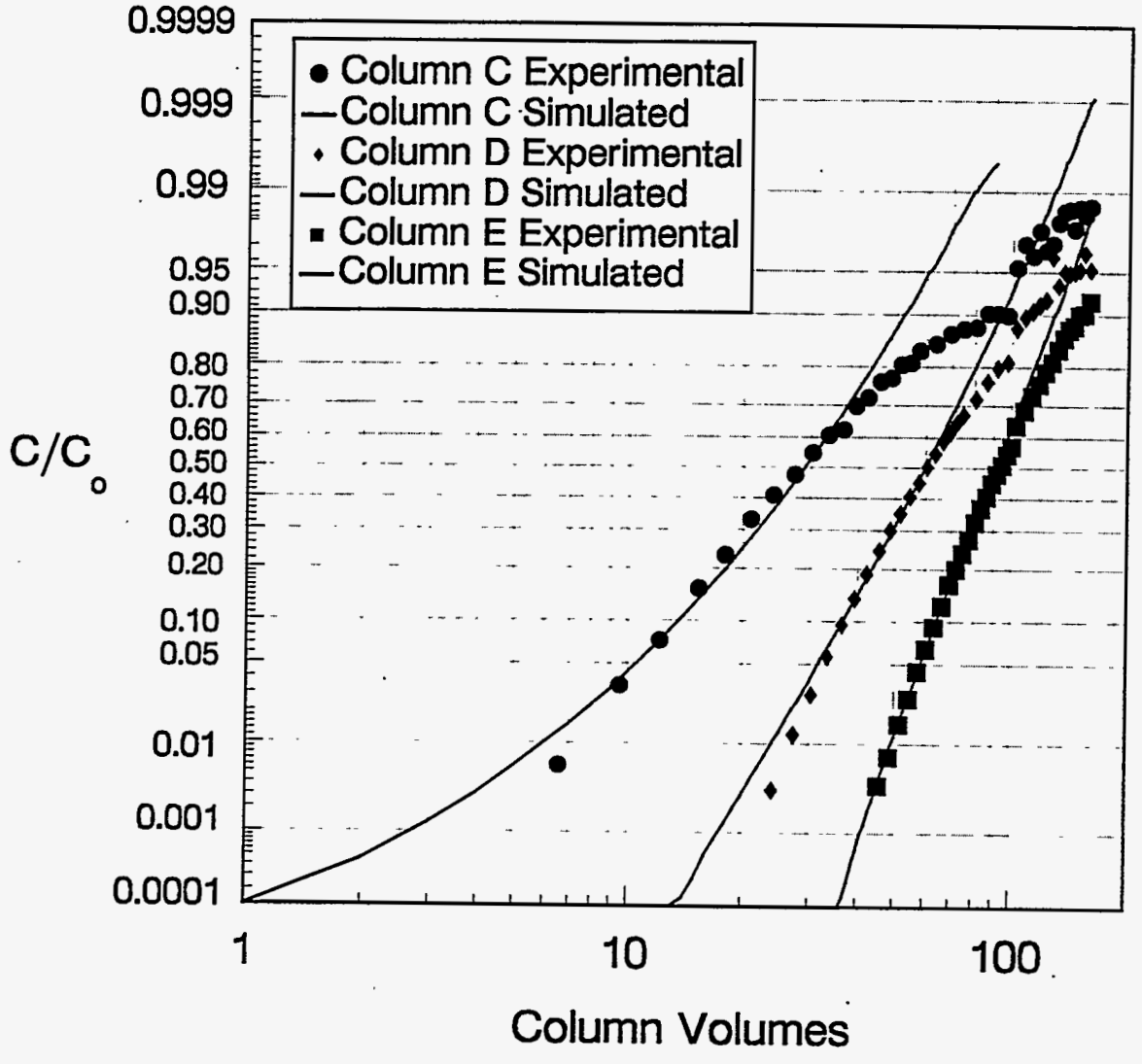

Resin: CS-100
Feed: NCAW
Flow rate: 6 cv/h, 1200 mL/h
Basis: 1 cv = 200 mL
Temperature: 25°C
Run 3: Columns C,D,E (3 columns in series)

NOTE: Counting instrument drift caused the breakthrough curves to level off at a C/C_0 value <1.

FIGURE 5.23. Cesium Ion-Exchange Column-Loading Experiment

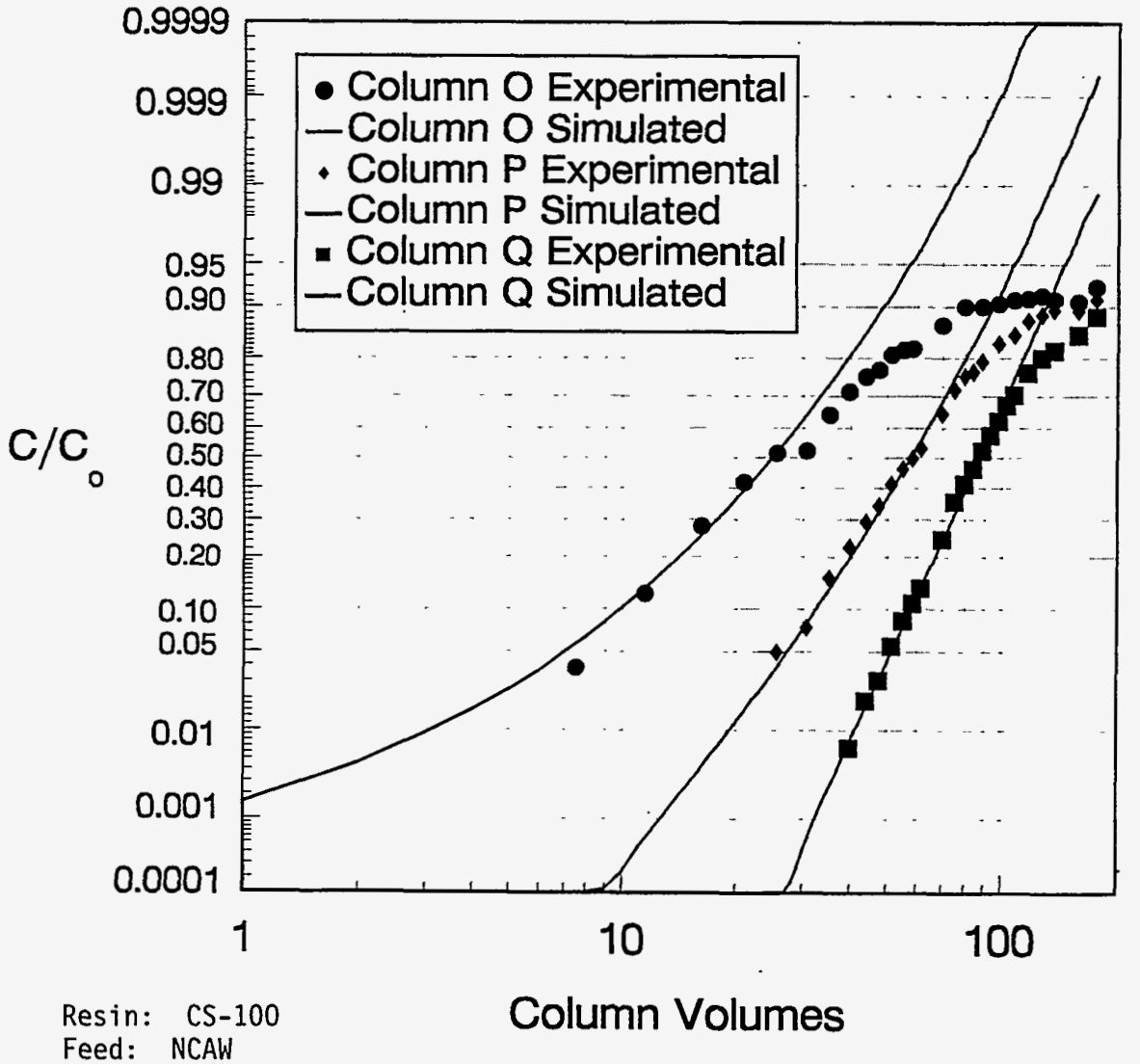

Resin: CS-100
Feed: NCAW
Flow rate: 9 cv/h, 1800 mL/h
Basis: 1 cv = 200 mL
Temperature: 25°C
Run 7: Columns O,P,Q (3 columns in series)

NOTE: Counting instrument drift caused the breakthrough curves to level off at C/C_0 <1. The run was halted for 45 min for repair of a line plug at 25 cv. After a second line plug at approximately 60 cv, the run was halted for 1.75 h and 200 mL was lost from the bottom of first column. At 157 cv, the run was stopped because the dipleg feed tube had come out of solution and the columns had become dry. They were backwashed with effluent for 1 h before proceeding with the run.

FIGURE 5.24. Cesium Ion-Exchange Column-Loading Experiment

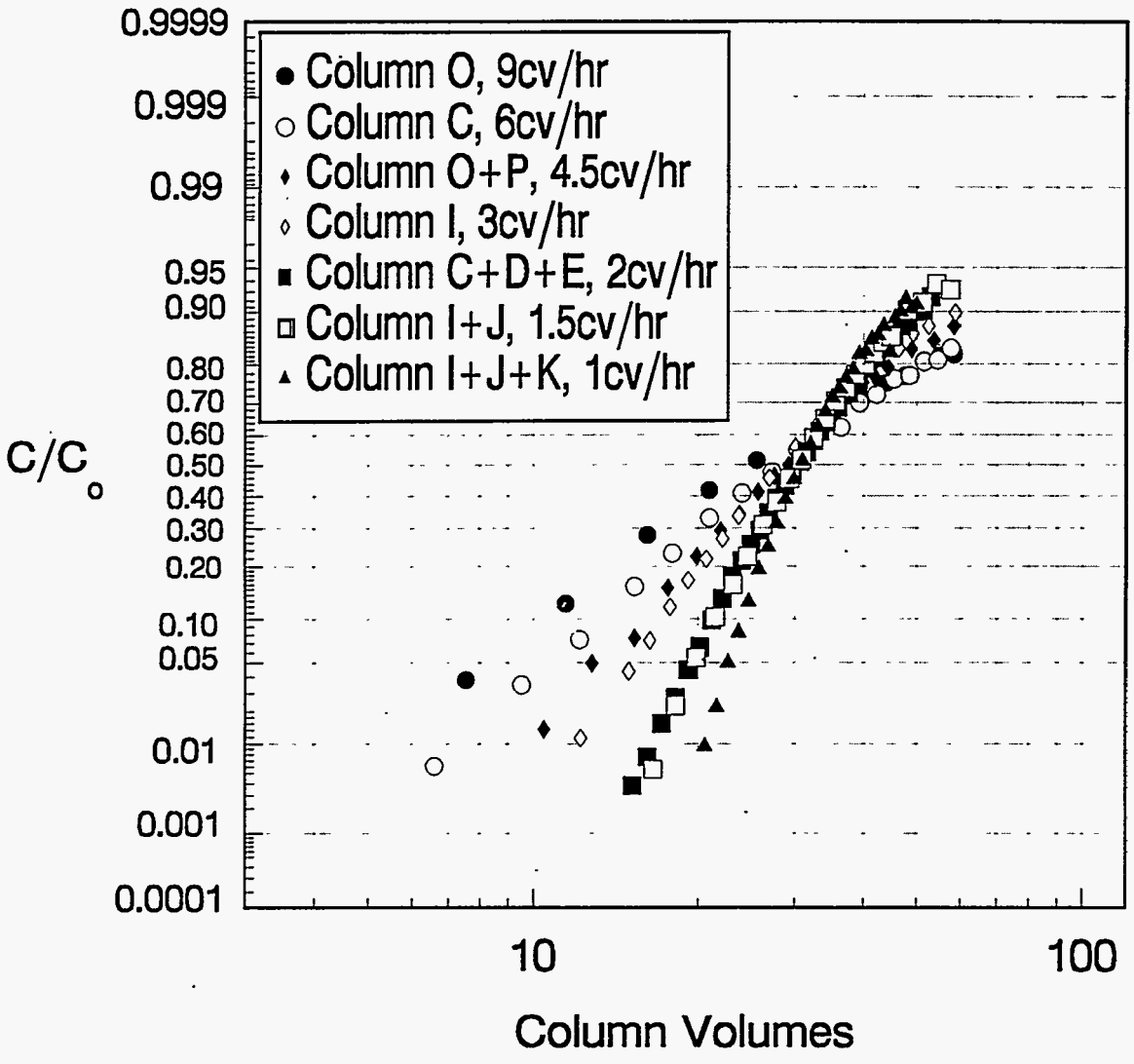

FIGURE 5.25. CS-100 Cesium Loading Results - Cs Breakthrough as a Function of Flow Rate for NCAW

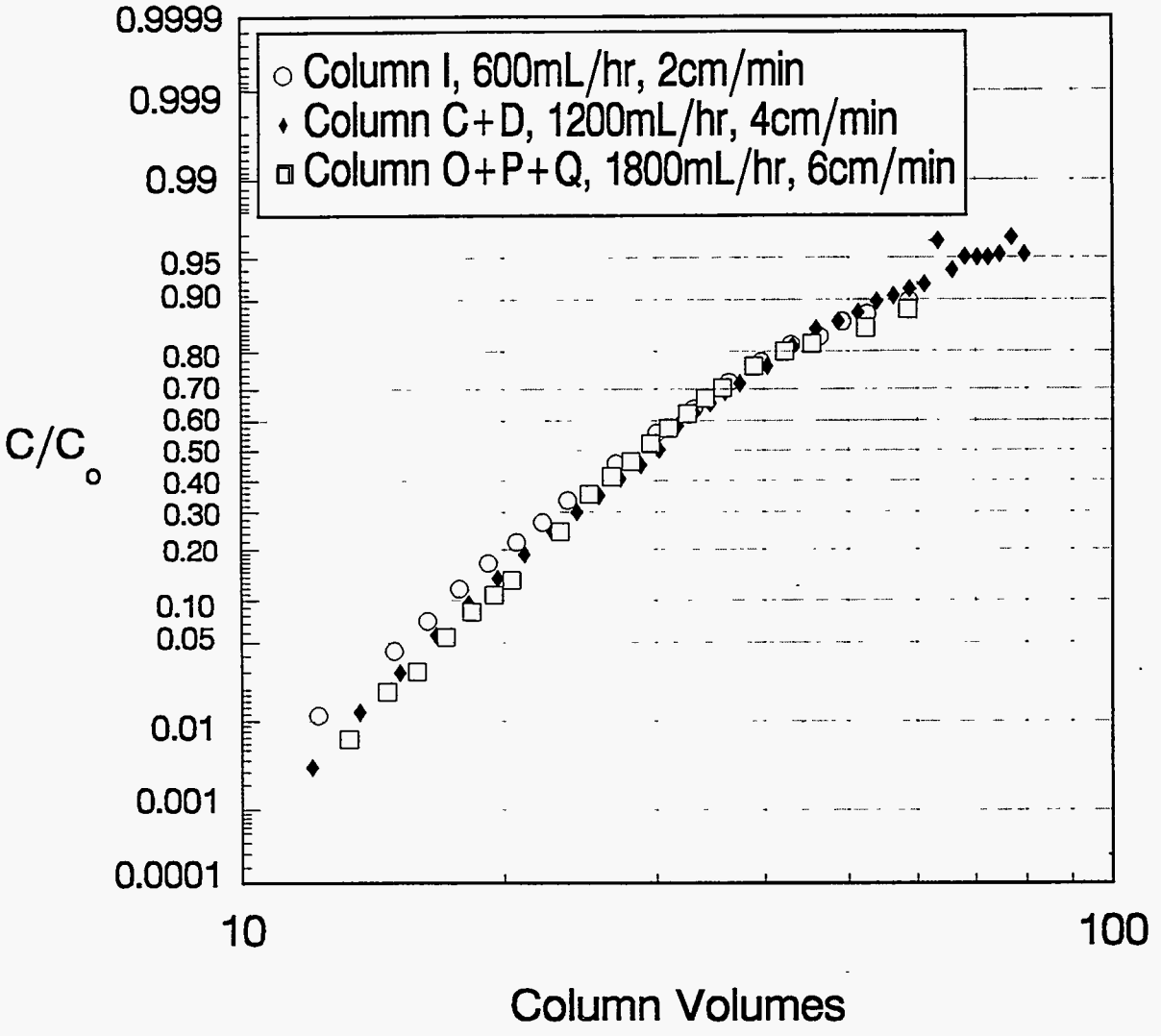

FIGURE 5.26. CS-100 Cesium Loading Results - Cs Breakthrough as a Function of Flow Velocity for NCAW

Figure 5.26 shows normalized cesium breakthrough curves for CS-100 loading at three superficial velocities (flow rate divided by cross-sectional area of column) of NCAW (2, 4, and 6 cm/min) at constant residence time (3 cv/h). The slight increase of the slopes with velocity suggests that mass transfer is primarily limited by diffusion in the particle but that an element of film diffusion is also present. The weak dependence of cesium breakthrough on superficial velocity also suggests that these data, obtained from 200 mL laboratory-scale columns, can be used directly for scale-up.

Experimental difficulties caused unexpected variations in the breakthrough curves for Runs 1, 3, 5, and 7. The counting instrument appeared to drift, resulting in a leveling off of breakthrough curves at $C/C_0 < 1$. The counter was periodically recalibrated during subsequent runs. Also, flow rate was difficult to control in 3-column series. Large variations in flow rate (as much as 100%), often a result of column plugging by small amounts of solides in the waste simulant, caused discontinuities in the breakthrough curves. This problem has been partially resolved by raising the feed inlet off the bottom of the feed tank.

5.2.1.2 CS-100 Loading Studies with DSSF

Cesium loading of CS-100 with DSSF simulants was carried out in three sets: Runs 11, 12, and 13 (Figures 5.27, 5.28, 5.29). DSSF simulant has high concentrations of sodium (7-10M Na^+, $[Na^+]:[Cs^+] = 10^5$) and potassium (1M K^+). Run 11 (AA, BB, CC) was performed with DSSF-2, and Runs 12 (EE, FF, GG) and 13 (II, JJ, KK) with DSSF-7. DSSF-2 contained less hydroxide and more nitrate and sodium (8M rather than 7M Na^+) than DSSF-7 (Section 4).

The DSSF-2 composition resulted in a lower column distribution coefficient (Cs λ) and a slower rate of cesium ion-exchange than that of DSSF-7. The average Cs λs were about 7 for run 11 and about 13 for runs 12 and 13. Much of this difference was probably due to the lower hydroxide content (see Figure 5.7) of the waste and the higher sodium content (See Figure 5.5) of the

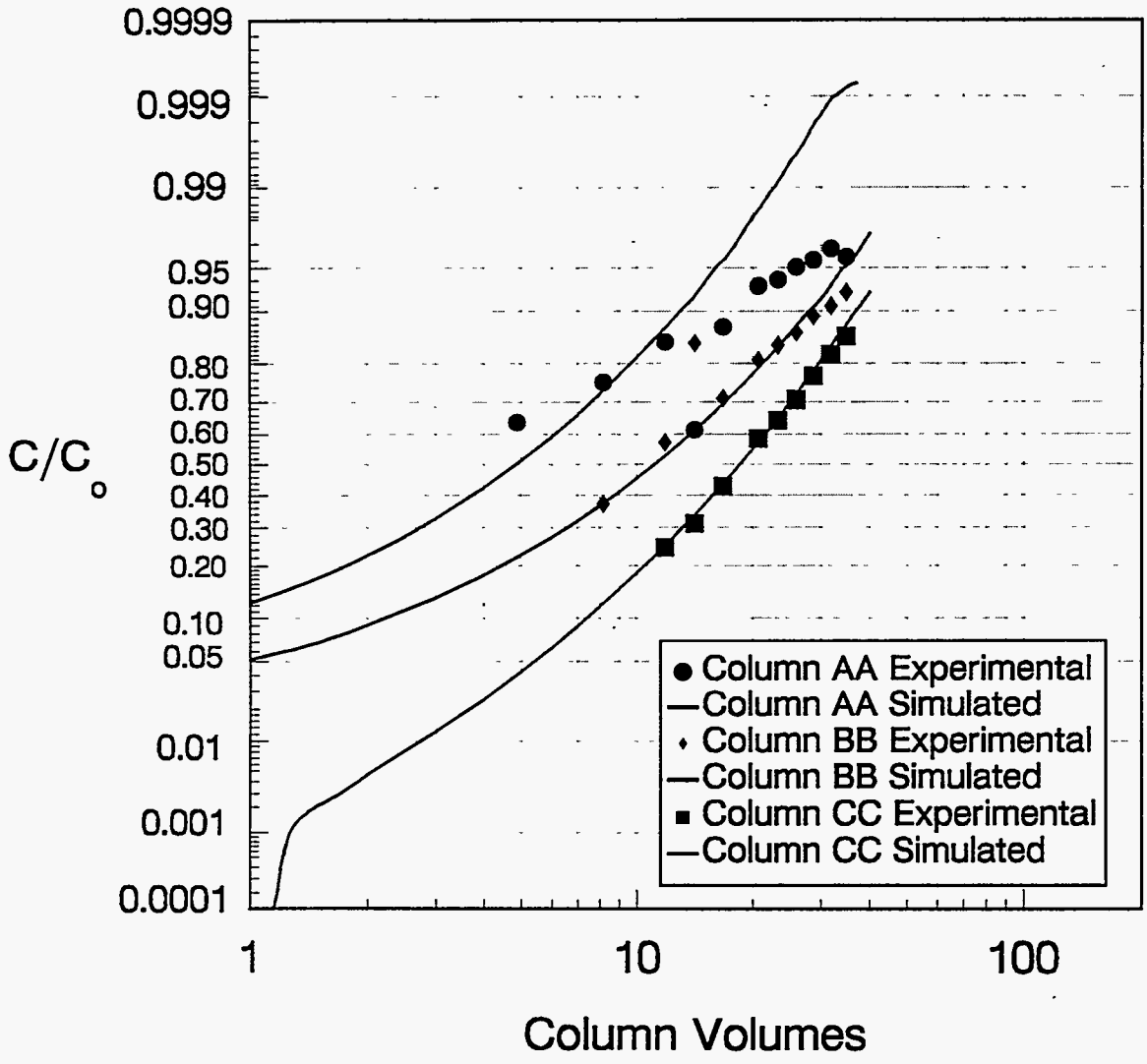

Resin: CS-100
Feed: DSSF-2
Flow rate: 6 cv/h, 1200 mL/h
Basis: 1 cv = 200 mL
Temperature: 25°C
Run 11: Columns AA,BB,CC (3 columns in series)

NOTE: Solution precipitated during run. Apparently, the OH^- concentration was not high enough to keep the sodium aluminate in solution.

FIGURE 5.27. Cesium Ion Exchange Column Loading Experiment

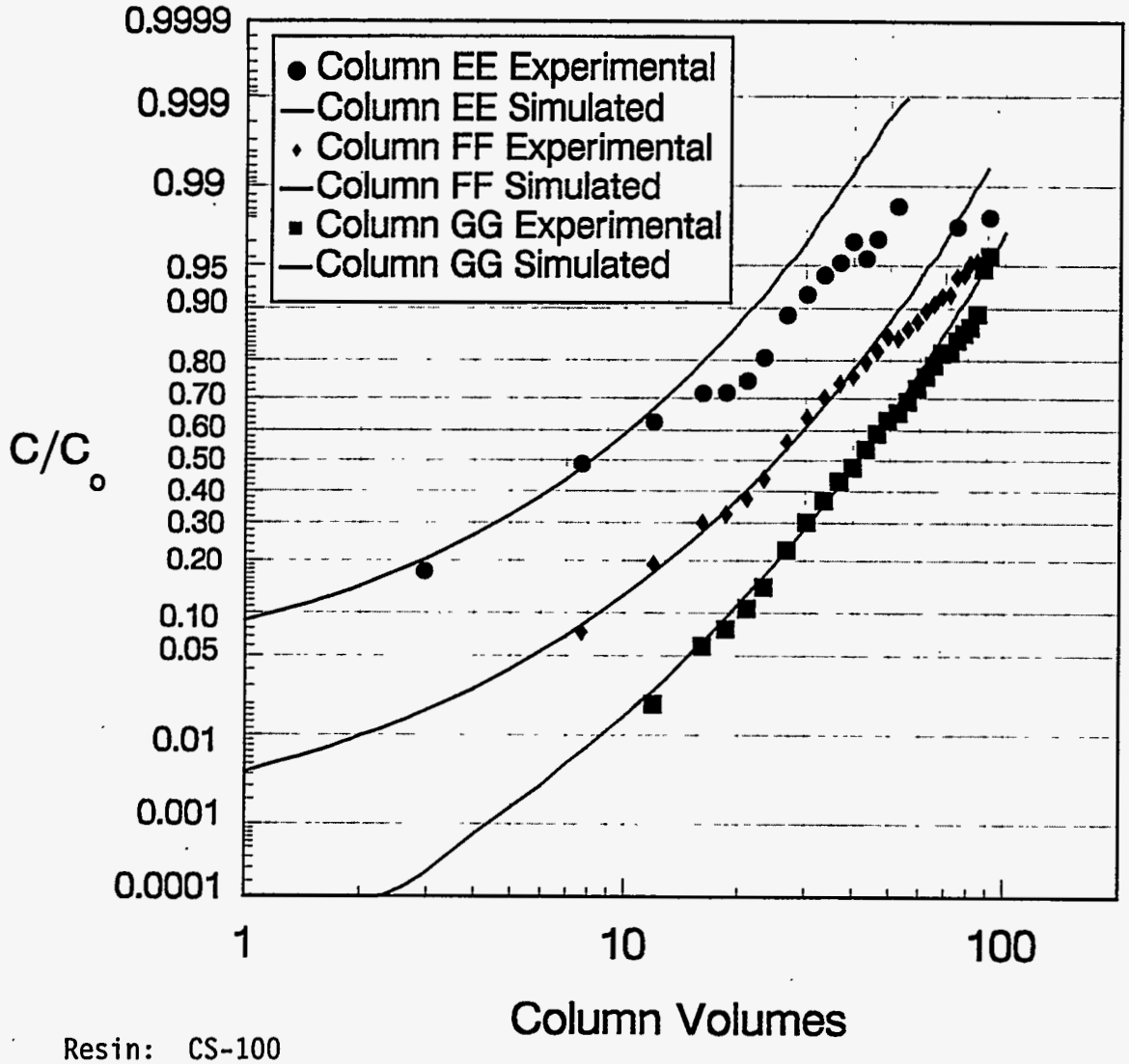

Resin: CS-100
Feed: DSSF-7
Flow rate: 6 cv/h, 1200 mL/h
Basis: 1 cv = 200 mL
Temperature: 25°C
Run 12: Columns EE,FF,GG (3 columns in series)

NOTE: No difficulties encountered.

FIGURE 5.28. Cesium Ion-Exchange Column-Loading Experiment

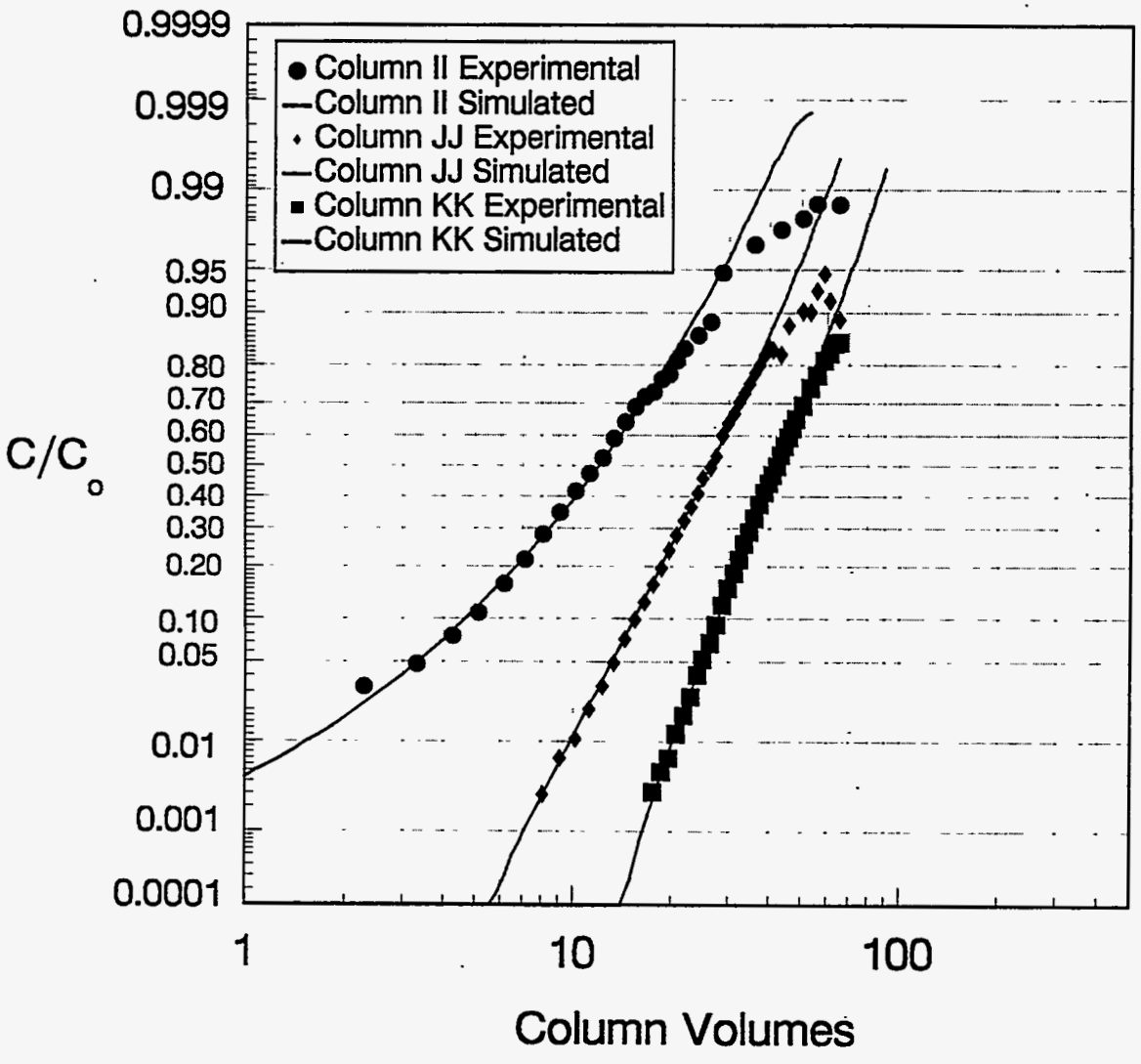

Resin: CS-100
Feed: DSSF-7
Flow rate: 2 cv/h, 400 mL/h
Basis: 1 cv = 200 mL
Temperature: 25°C
Run 13: Columns II,JJ,KK (3 columns in series)

NOTE: No difficulties encountered.

FIGURE 5.29. Cesium Ion-Exchange Column-Loading Experiment

during the run fouled the resin and appeared to reduce the rate of cesium ion exchange, as indicated by a comparison of the slopes of the breakthrough curves. The fouling may also have contributed to the low λ by blocking access to some of the ion-exchange sites.

The decrease in flow rate from 6 cv/h for Run 12 to 2 cv/h for Run 13 significantly changed the slopes of the breakthrough curves. At the higher flow rates, breakthrough in all three columns preceded the first sampling. At the lower flow rate, breakthrough occurred immediately in the first column but not until 7 and 18 cv in the second and third columns, respectively. Column 12 (Figure 5.28) illustrates the effect of fluctuating flow rate on the shape of the breakthrough curve. At approximately 16 cv, the flow rate was temporarily decreased by approximately 3 cv/h and restored at 26 cv. The result is a dip in the breakthrough curve of each column. A significant fraction of data scatter may be the result of varying flow rates.

Figure 5.30 shows the normalized cesium breakthrough curves for DSSF (Runs 12 and 13). Similar to the NCAW runs, the slope of the breakthrough increases as the flow rate (in cv/h) decreases. The curves intersect at a DSSF-2 composition. Precipitation of what is thought to be sodium aluminate C/C_0 of ~0.7 and at 17 cv. The average Cs λ for Runs 12 and 13 was about 13, which is unexpectedly lower than the Cs λ of 25 (Figure 5.2 $[Na^+]:[Cs^+]$) predicted from the batch equilibrium data.

Figure 5.31 compares breakthrough curves for CS-100 and DSSF-7 at two superficial velocities and constant residence time (2 cv/h). The different slopes of the curves suggest that resistance to mass transfer in the fluid phase (film diffusion) is significant.

5.2.1.3 CS-100 Loading with Other Wastes

Loading characteristics of West Valley alkaline supernatant (Bray et al. 1984) on CS-100 were studied. The simulant used in these experiments contained 7.2M sodium (similar to DSSF), low potassium (similar to NCAW), and

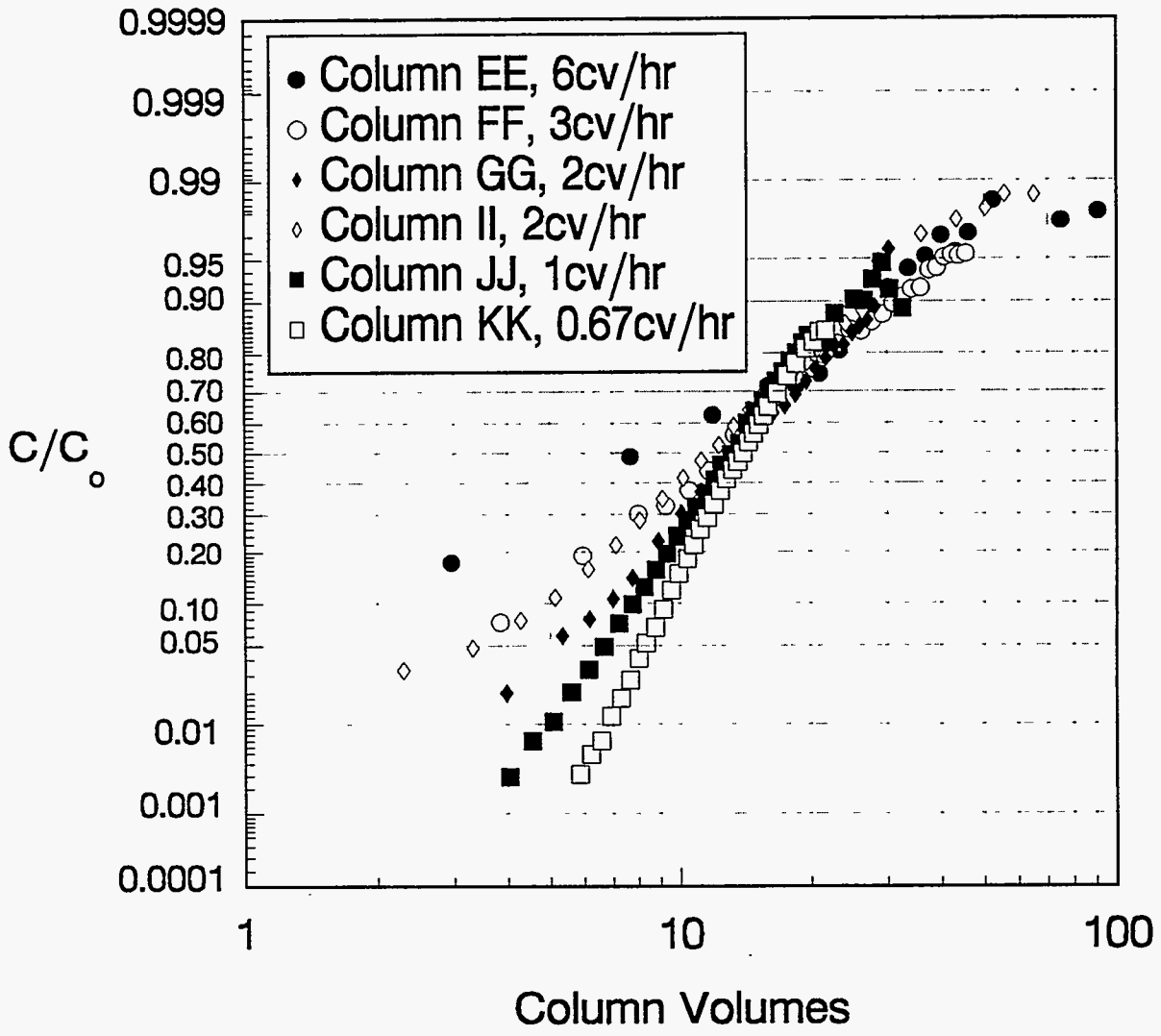

FIGURE 5.30. CS-100 Cesium-Loading Results - Cs Breakthrough as a Function of Flow Rate for DSSF. (Run 12, Columns EE, FF, and GG; Run 13, Columns II, JJ, and KK)

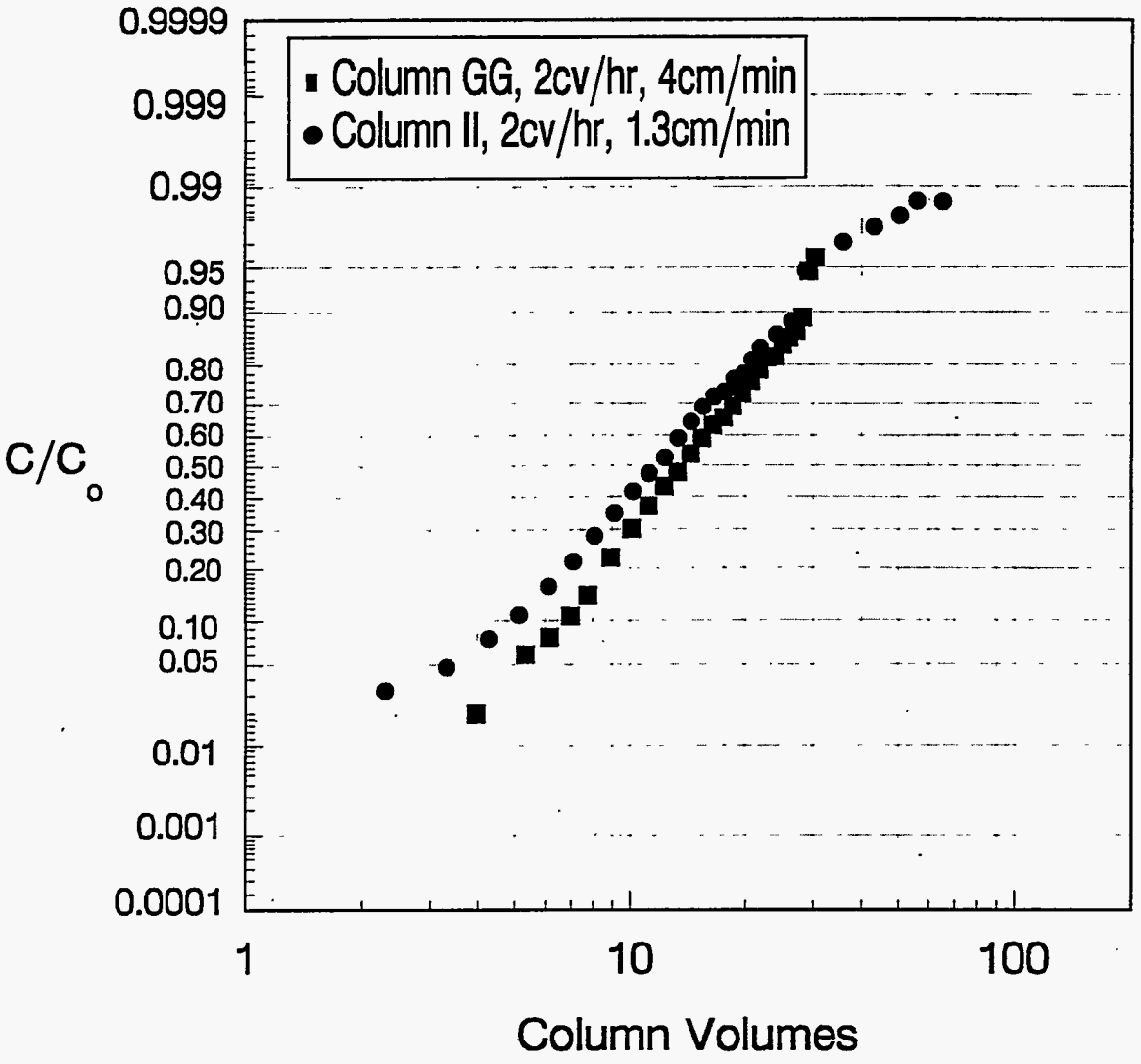

Note: Column GG is the third column in series (Run 12) and the column volume is based on 3 columns (1 cv = 600 mL); Column 11 is the first column in series (1 cv = 200 mL)

FIGURE 5.31. CS-100 Cesium-Loading Results - Cs Breakthrough as a Function of Flow Velocity for DSSF (Runs 12GG and 13II)

1.0 x 10^{-3}M cesium (twice that found in NCAW). In these 100-mL column-loading runs, lower temperatures improved cesium loading; λ increased from 8.5 to 11.5 as temperature fell from 25°C to 6°C. Temperature seemed to have little effect on mass transfer, since the breakthrough curve slope remained fairly constant over the temperature range (6° to 26°C). Lower temperature increases the equilibrium concentration of cesium on the resin (Section 5.1) and thereby shifts the breakthrough curve to later time. Mass transfer dramatically improved at smaller particle sizes (Figure 5.32). As the resin size decreased from 20 to 40 mesh to 80 mesh, the slope of the breakthrough curve increased, reflecting better mass transfer.

5.2.1.4 R-F Loading Studies Using NCAW

Three R-F resin ion-exchange columns were operated in series for Runs 8 (R, S, T) and 9 (U, V, W). Run 10 was operated with 1 column (Column Y) loaded with a new batch of R-F resin, BSC-210, produced by Boulder Scientific. The nominal flow rates were 1800 mL/h (or 9 cv/h) for Run 8, 2600 mL/h (13 cv/h) for Run 9, and 2400 mL/h (12 cv/h) for Run 10.

For Run 8 (Figure 5.33), the initial detectable cesium breakthrough (C/C_0 = 0.002) was at 100 cv. The column volumes of feed processed at C/C_0 = 0.5 is 190 (Column R), 380 (Column S), and 570 (Column T). These results indicate a Cs λ of 190 for each column, which agrees well with that predicted from batch equilibrium data (batch Cs λ = 180). When plotted in normalized form (Figure 5.34), the initial detectable cesium breakthrough (C/C_0 = 0.002) increased from 100 cv to 160 cv as the flow rate slowed from 9 to 3 cv/hr; the breakthrough curves intersected at ~0.6 C/C_0 and 190 cv.

Results in Run 9 (Figures 5.35) were similar to those of Run 8. Because the flow rate was higher, initial breakthrough for Column 9V occurred sooner (at 80 cv rather than 100 cv in Run 8). The initial breakthrough for Columns W and X occurred at 250 and 450 cv, respectively. The column volumes of feed processed at C/C_0 = 0.5 indicate a Cs λ of 190 for each column.

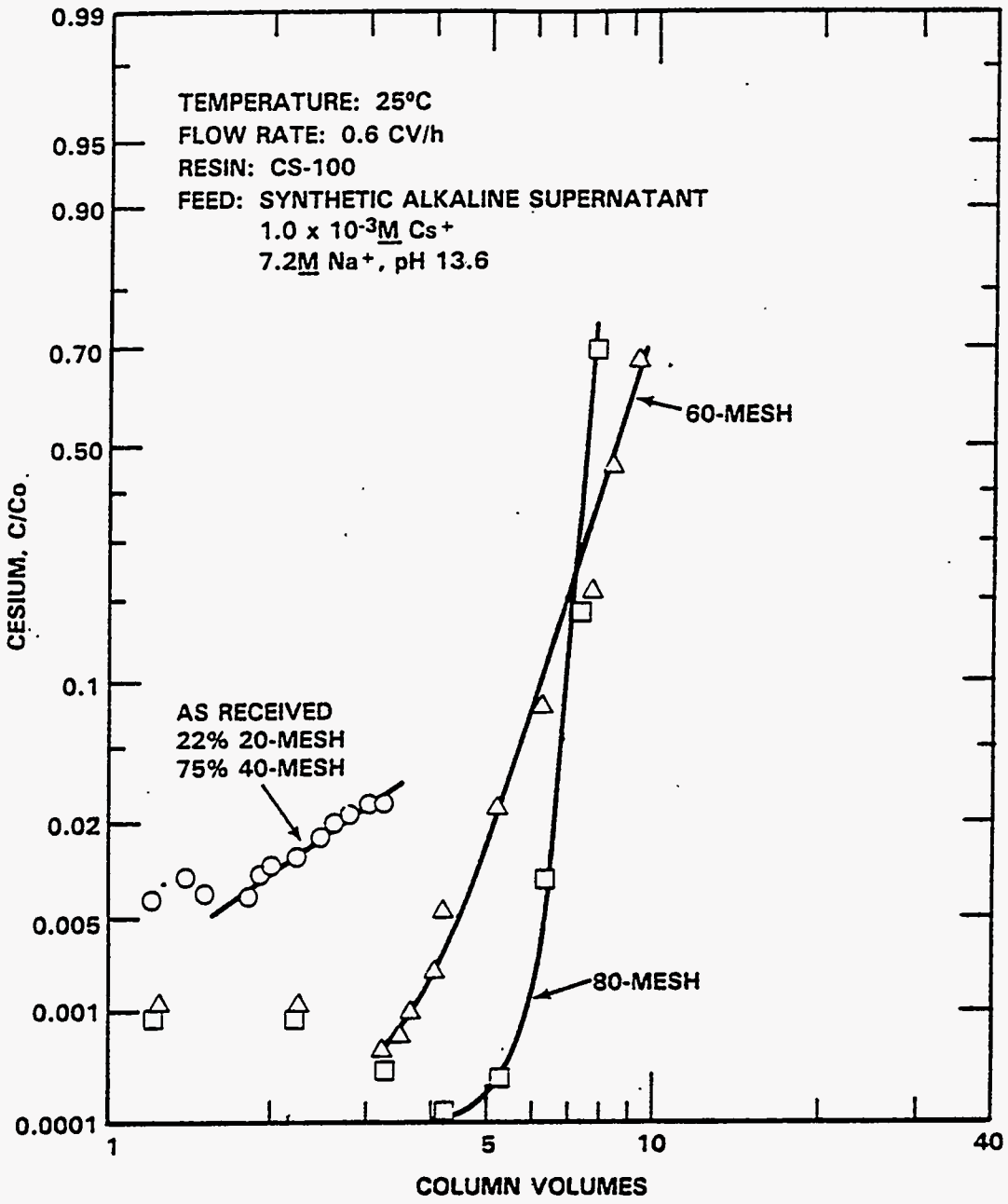

Resin: CS-100
Feed: Synthetic Alkaline Supernatant
1.0×10^{-3}M Cs^+
7.2M Na^+, pH = 13.6
Flow rate: 0.6 cv/h, 60 mL/h
Basis: 1 cv = 100 mL
Temperature: 25°C

FIGURE 5.32. Cesium Breakthrough as a Function of Mesh Size (Bray et al. 1984)

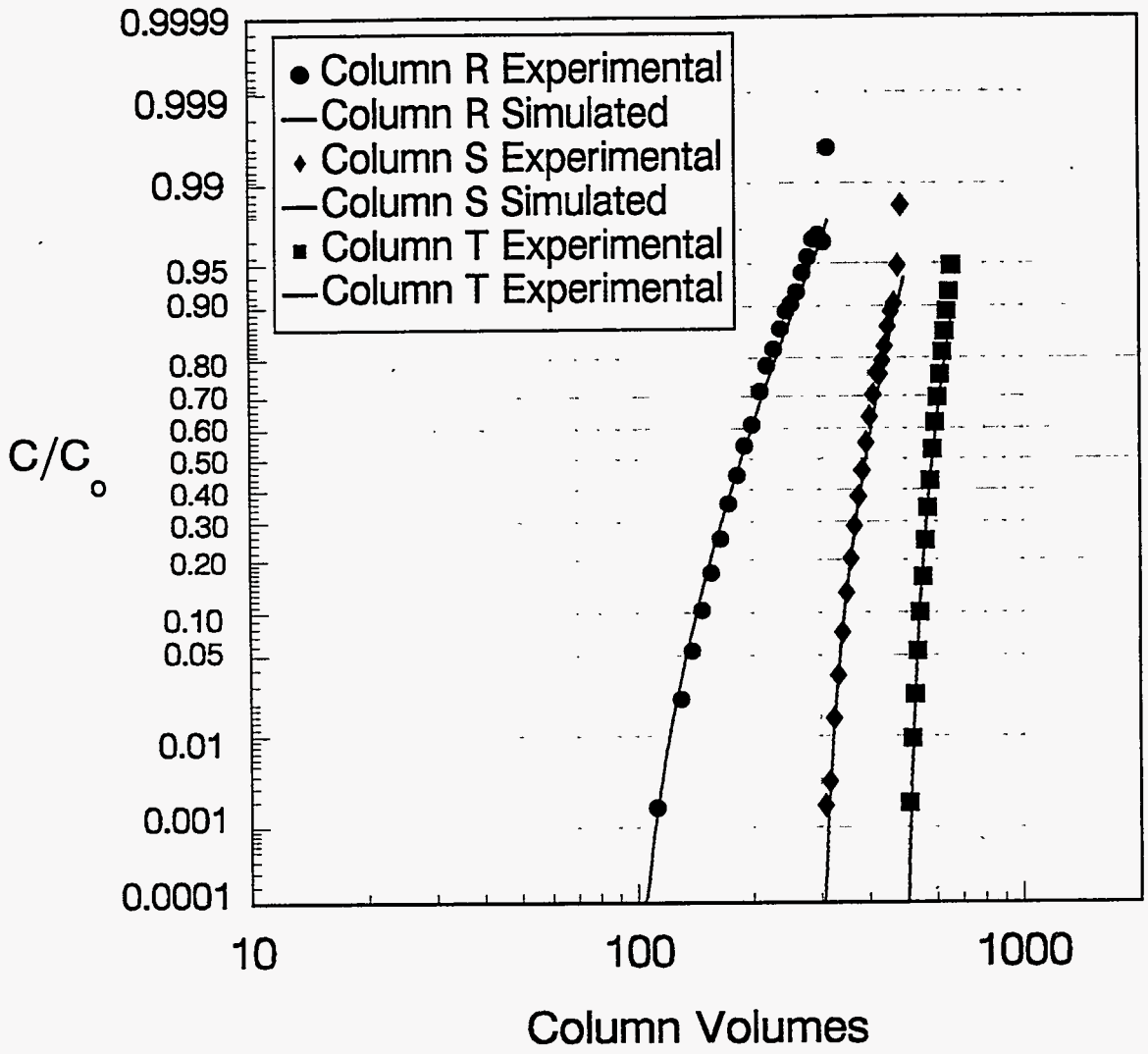

Resin: R-F
Feed: NCAW
Flow rate: 9 cv/h, 1800 mL/h
Basis: 1 cv = 200 mL
Temperature: 25°C
Run 8: Columns R,S,T (3 columns in series)

NOTE: No difficulties encountered.

FIGURE 5.33. Cesium Ion-Exchange Column-Loading Experiment

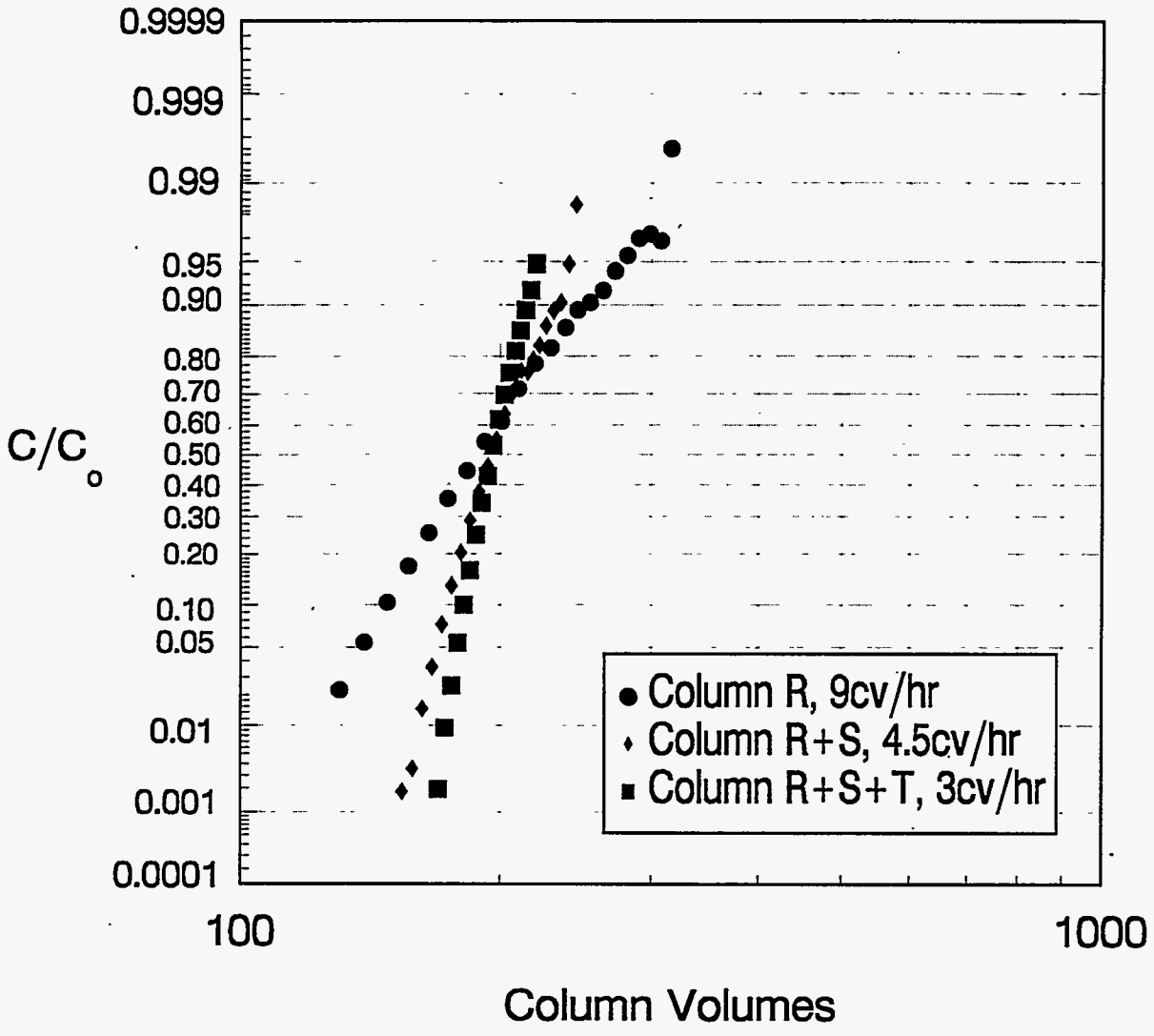

FIGURE 5.34. Normalized R-F(BSC-182) Cesium-Loading Curves for NCAW with Run 8, Columns R, S, T

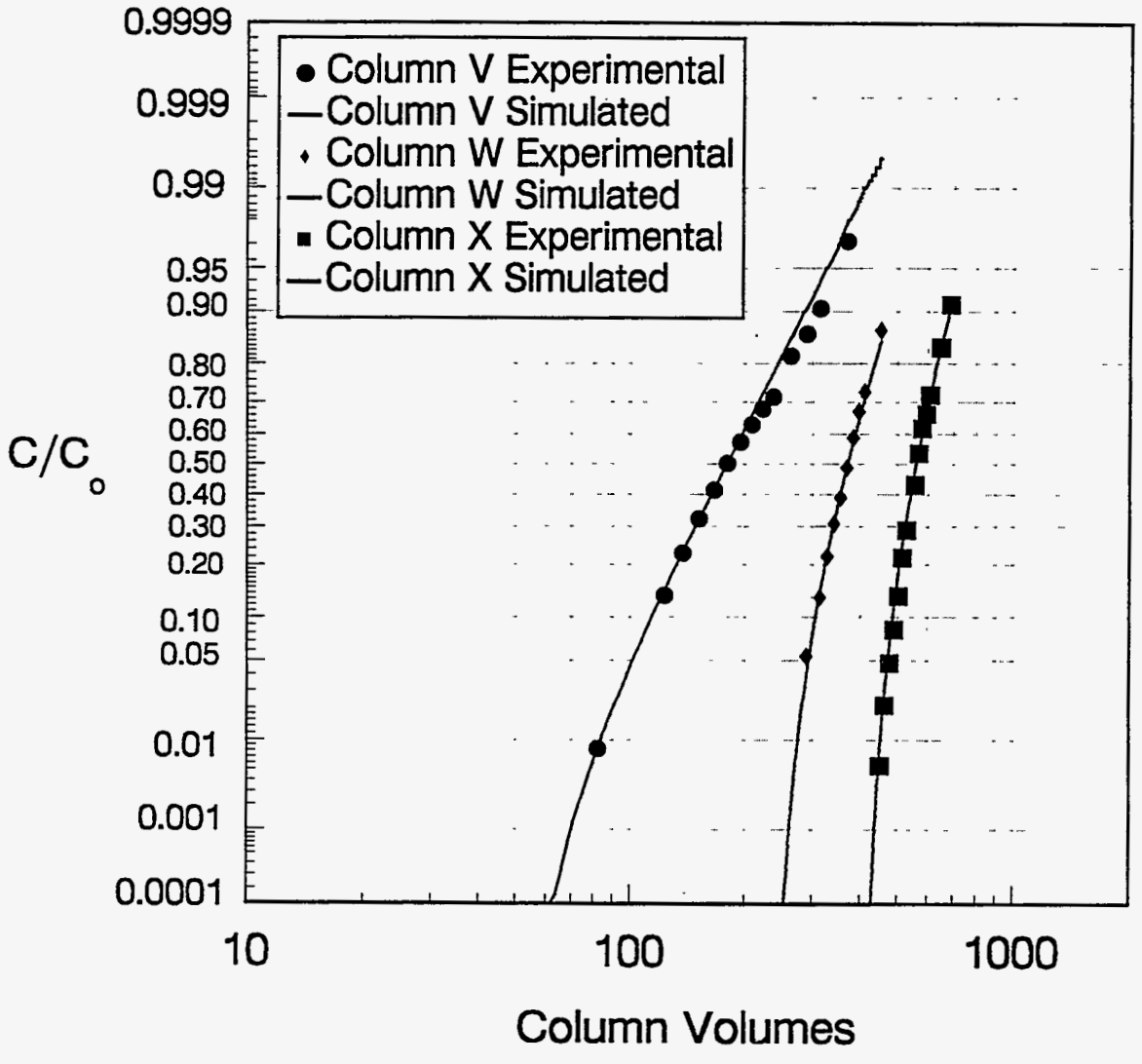

Resin: R-F
Feed: NCAW
Flow rate: 13.5 cv/h, 2700 mL/h
Basis: 1 cv = 200 mL
Temperature: 25°C
Run 9: Columns V,W,X (3 columns in series)

NOTE: First column (U) developed a severe leak after loading with approximately 7 cv and was taken offline. Column X was added as the last column of the series, Column V became the first column in line, and flow was restarted at zero. Based on the column loading, it appears that Column V did not load significantly before the restart.

FIGURE 5.35. Cesium Ion-Exchange Column-Loading Experiment

Figure 5.36 compares breakthrough curves of new (BSC-210) and original (BSC-187) batches of R-F resin . These runs were operated under similar flow conditions (2600 mL/h nominal rate). BSC-210 had better loading kinetics, as indicated by the steeper slope; equilibrium cesium loadings (cv at 50% C/C_0) were nearly identical (Cs λ = 190). The slightly better loading kinetics of the BSC-260 is probably due to the slightly smaller particle size.

For all R-F runs with NCAW, detectable breakthrough of the succeeding column never preceded 0.95 C/C_0 breakthrough of the initial column, even though the flow rates were relatively high compared to CS-100 runs. Therefore, the R-F resin can process higher flow rates while maintaining a high Cs DF.

Figure 5.37 shows the effect of superficial velocity on breakthrough by comparing normalized breakthrough curves for Column S (6 cm/min) and Column X (9 cm/min) for the same residence time (4.5 cv/hr). The similarity of the slopes suggests that mass transfer is primarily limited by diffusion in the particle but that an element of film diffusion is present (as for CS-100). The weak dependence of cesium breakthrough on superficial velocity also suggests that these data, obtained from 200 mL columns can be used directly for scale-up.

5.2.1.5 R-F Loading Studies with DSSF

Run 14 was performed with R-F resin, DSSF-7 simulant, and three columns in series at 9 cv/h. The 50% breakthrough occurred at 140, 280, and 490 cv (Figure 5.38), for an average of Cs λ of 160, compared to a Cs $\lambda$of 190 with NCAW. Similar to the situation with CS-100, R-F loads less DSSF than NCAW, and the initial appearance of cesium in the effluent from R-F occurs much earlier with DSSF than with NCAW. The initial breakthrough in the first column (MM) occurred after 7 cv, in the second column (NN) at 50 cv, and in the third column (OO) at 160 cv. The low slopes of these curves indicate strong resistance to mass transfer. The curves for DSSF show more scatter than the NCAW curves, due in part to variations in flow rate.

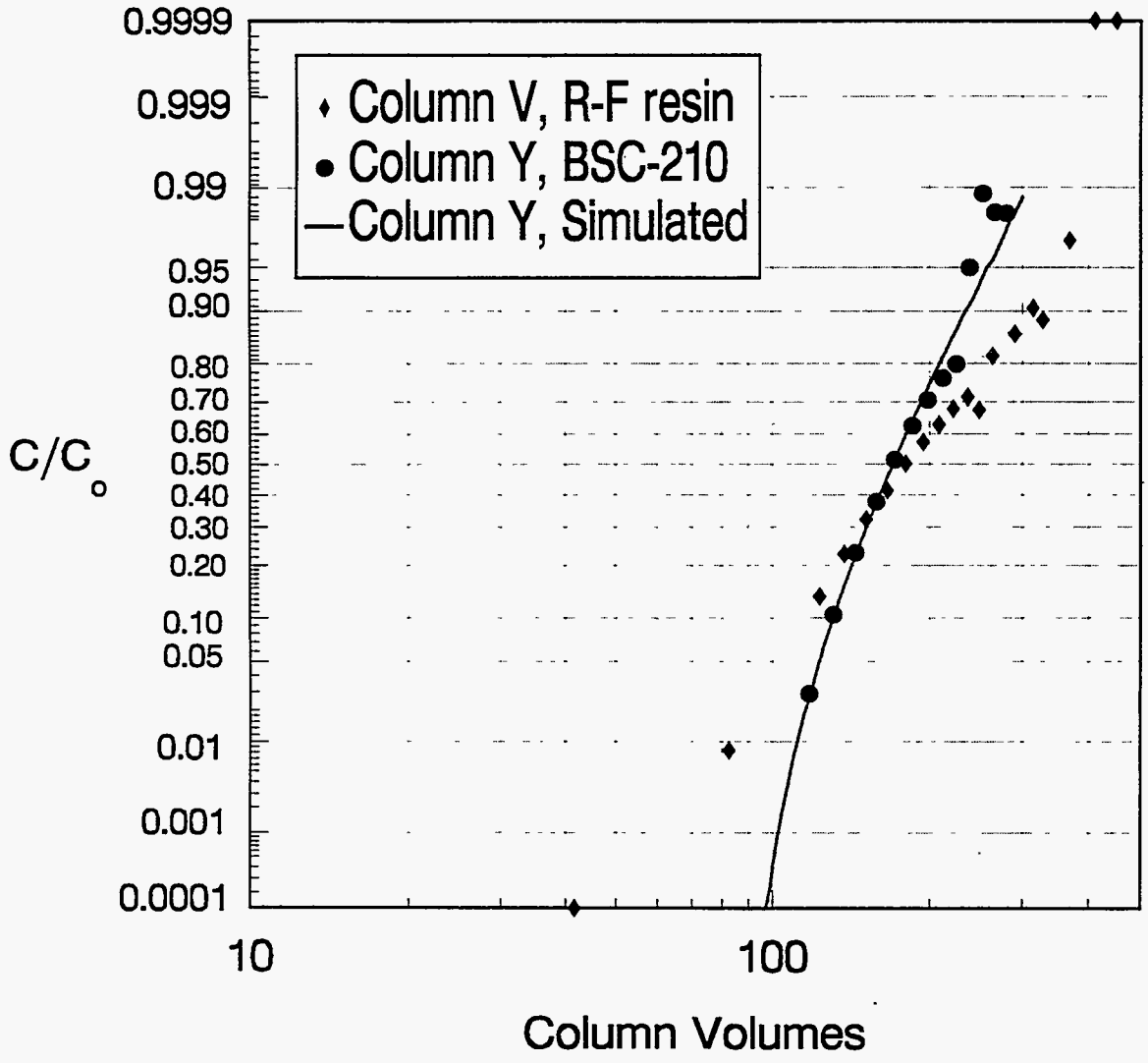

Resin: R-F (BSC-210)
Feed: NCAW
Flow rate: 13 cv/h, 2600 mL/h
Basis: 1 cv = 200 mL
Temperature: 25°C
Run 10: Column Y (1 column)

NOTE: Column Y was loaded with BSC-210, which is a different resin batch from that used for Runs 8 and 9. No difficulties encountered.

FIGURE 5.36. Cesium Ion-Exchange Column-Loading Experiment

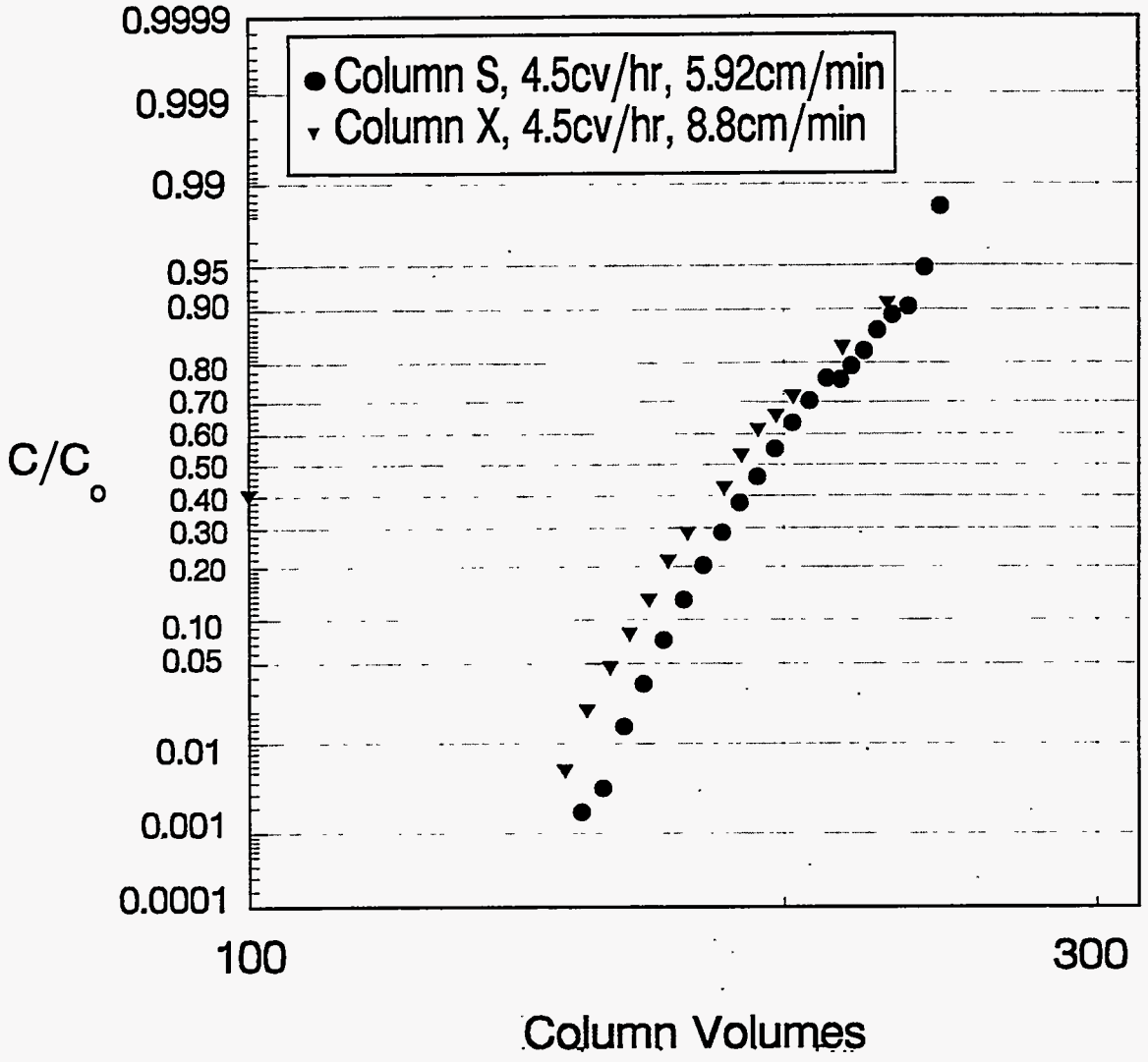

Note: Column S is the second column in series for run 8 (cv = 400 mL); column X is the third column in series for Run 9 (cv = 600 mL)

FIGURE 5.37. Cesium-Loading Results for R-F Resin. Breakthrough as a function of velocity for NCAW (Column S and X).

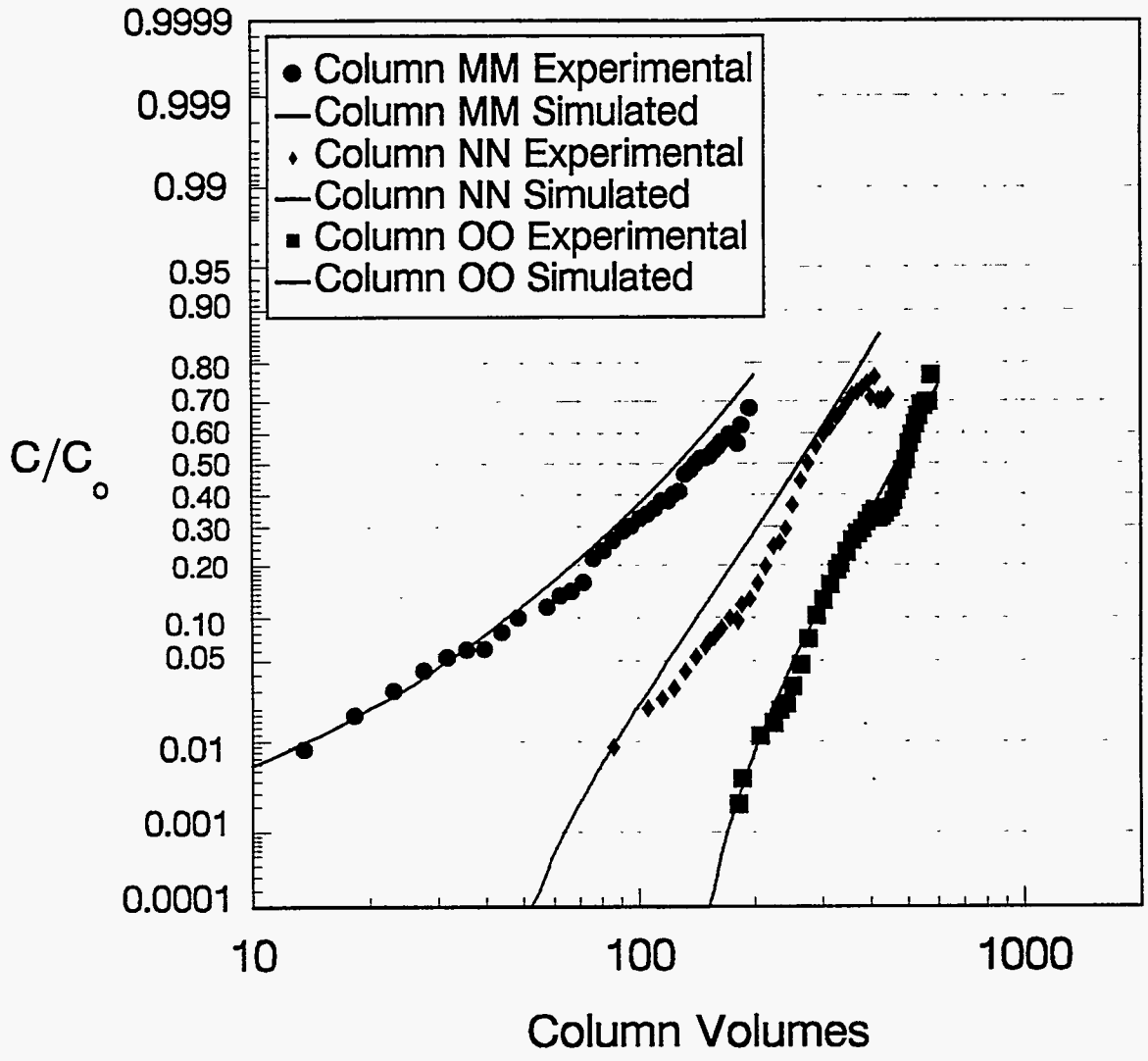

Resin: R-F
Feed: DSSF-7
Flow rate: 9 cv/h, 1800 mL/h
Basis: 1 cv = 200 mL
Temperature: 25°C
Run 14: Columns MM, NN, OO (3 columns in series)

NOTE: Removed Column MM from the series at 195 cv due to severe leakage through the bottom screen. Column NN plugged due to very cloudy feed: about 0.0625 in. of white precipitate on top of the resin bed. At approximately 450 cv, flow was stopped for 1.25 h.

FIGURE 5.38. Cesium Ion-Exchange Column-Loading Experiment

Run 15 was carried out with three columns of R-F in series (PP, QQ, RR) loaded at 3 cv/h (Figure 5.39). Even at the lower flow rates, initial detection of cesium was relatively early: 2 cv for Column PP, 80 cv for QQ, and 230 cv for RR. The column effluent reached C/C_0 = 0.5 at 170, 340, and 500 cv for the 3 columns, respectively. This indicates an average Cs λ of about 170, which is consistent with the Cs λ of 160 in run 14.

Run 16 was carried out with a single column of R-F resin (BSC-210) at a DSSF-7 feed rate of 12 cv/hr (Figure 5.40). This run was performed so that the loading characteristics of batch BSC-210 could be compared with those of batch BSC-187 with DSSF-7. As shown in Figure 5.40, the column distribution ratio is about 130, which is a bit lower than for the DSSF-7 runs on BSC-187.

Figure 5.41 shows the effect of superficial velocity on cesium-exchange kinetics of DSSF with R-F. The slightly different slopes in the normalized breakthrough curves for Columns OO (6 cm/min) and PP (2 cm/min) at a constant residence time (3 cv/h) suggest an element of fluid-phase resistance to ion exchange.

5.2.1.6 Comparison of CS-100 and R-F Cesium Loading

Column-loading tests and batch equilibrium measurements consistently show that R-F resin is superior to CS-100 for cesium ion exchange. Cesium λs in Section 5.1 and λ (cv at 50% C/C_0) from column-loading curves show that R-F resin loads more cesium than CS-100 (Table 5.10). Table 5.10 also indicates that λ for R-F column loading and CS-100 with NCAW are consistent with the equilibrium Cs λ. The reason for the difference between Cs λ and the column volumes at 50% C/C_0 for CS-100/DSSF is not known.

Higher cesium loading by R-F is also indicated by a larger volume of waste processed before initial detection of cesium. At 9 cv/hr NCAW (Figure 5.42), initial detection of cesium is much earlier for CS-100 (4 cv) than for R-F (100 cv). For DSSF (Figure 5.43), breakthrough occurs at approximately 20 cv with R-F resin, but at <2 cv with CS-100, even though CS-100 flow rate was less.

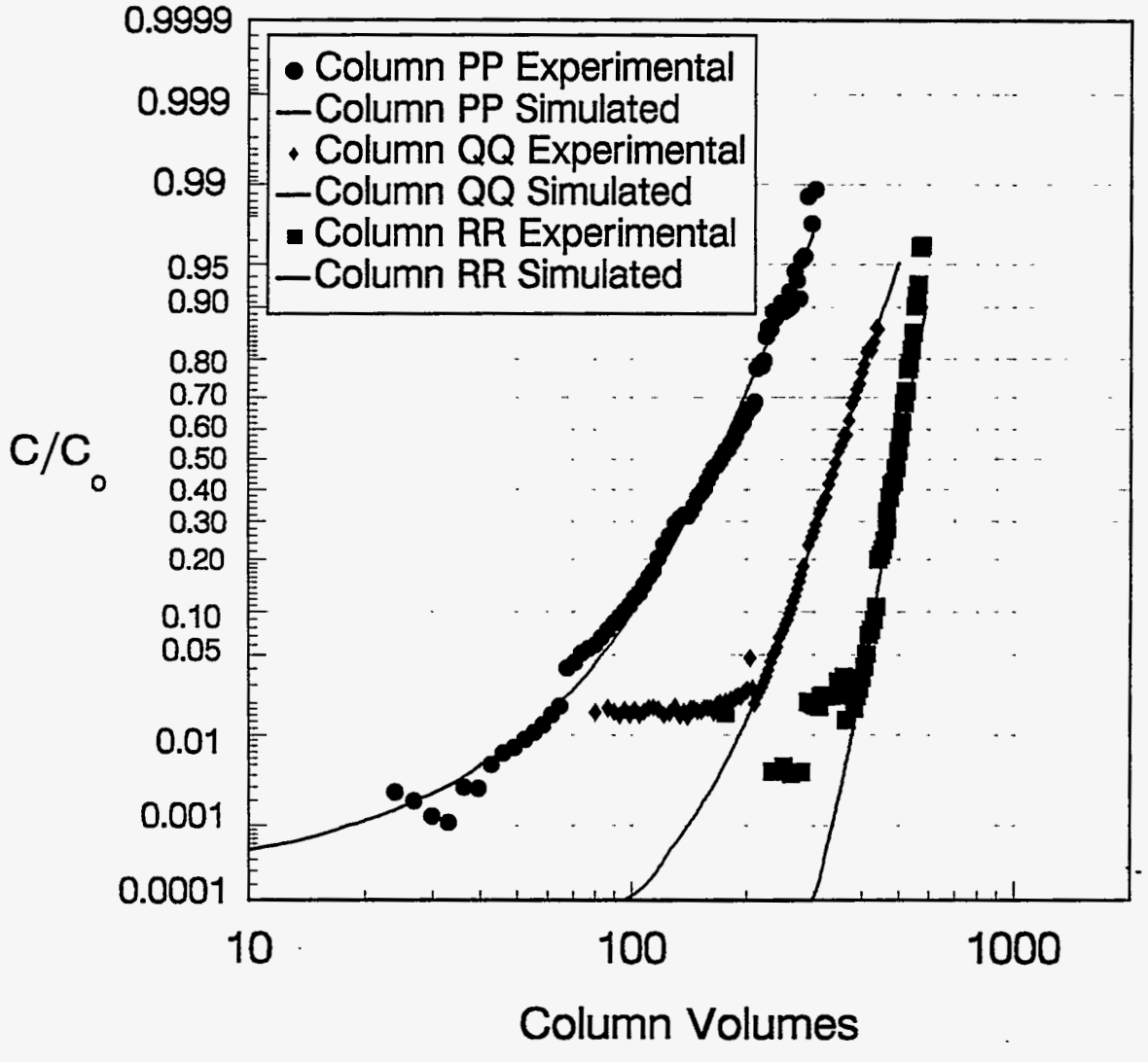

Resin: R-F (BSC-187)
Feed: DSSF-7
Flow rate: 3 cv/h, 600 mL/h
Basis: 1 cv = 200 mL
Temperature: 25°C
Run 15: Columns PP,QQ,RR (3 columns in series)

NOTE: There was a slight leak in Column PP; it did not halt operation. Column RR was pulled offline temporarily and stirred with a piece of wire at 581 cv to remove void spaces. Stirring did not appear to affect C/C_0. Initial high C/C_o was due to a radiation source inadvertantly placed under the counter.

FIGURE 5.39. Cesium Ion-Exchange Column-Loading Experiment

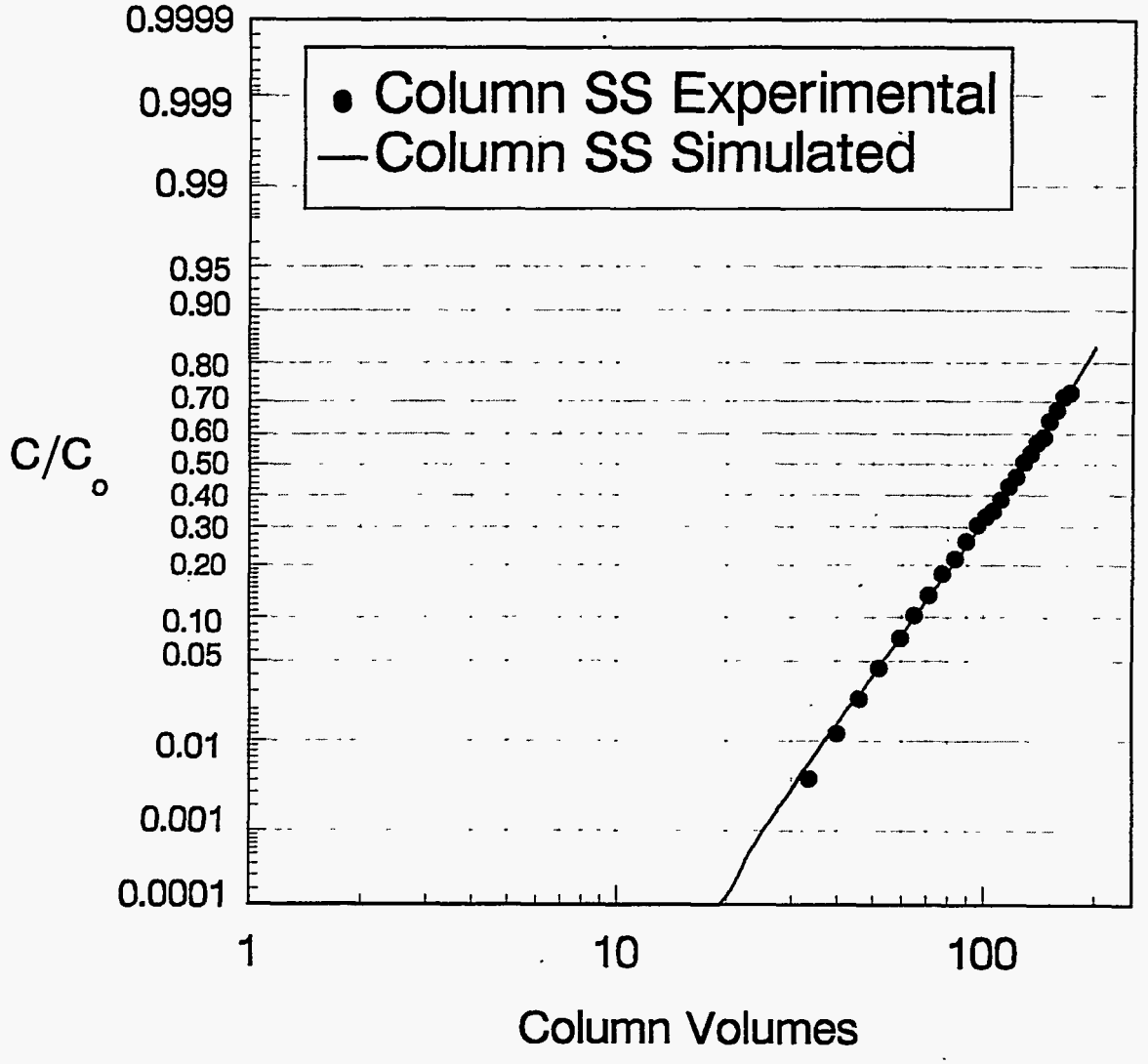

Resin: R-F (BSC-210)
Feed: DSSF-7
Flow rate: 9 cv/h
Basis: 1 cv = 200 mL
Temperature: 25°C
Run 16: Columns SS

FIGURE 5.40. Cesium Ion-Exchange Column-Loading Experiment

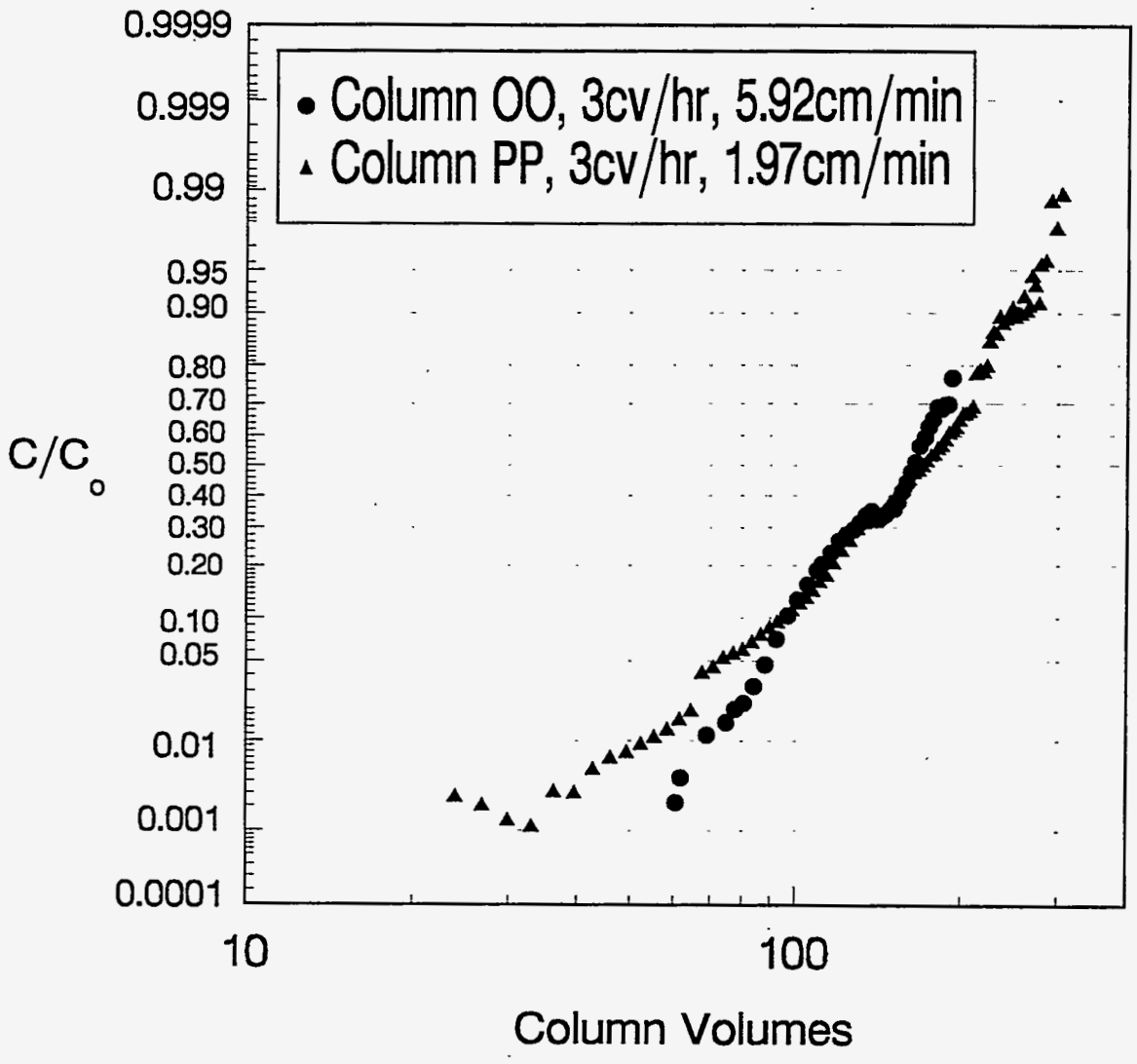

Note: Column OO is the third column in series (run 14) and the column volume is based on 3 columns (1 cv = 600 mL).

Column PP is first column in series (1 cv = 200 mL).

FIGURE 5.41. Cesium-Loading Results for R-F Resin. Breakthrough as a Function of Velocity for DSSF (Column OO and PP)

TABLE 5.10. Comparison of λ from Column Loading with Cs λ from Batch Equilibirium Experiments

Resin	Waste Simulant[a]	Column Distribution Ratio (Cs λ)[b]	Column Volumes at 50% C/CO (λ)[c]
CS-100	NCAW	34	30
CS-100	DSSF-7	25	13
R-F	NCAW	180	190
R-F	DSSF-7	170	160

(a) See Section 4 for composition.
(b) Interpolation of Section 5.1 data to simulant. composition.
(c) Average values.

Figures 5.44 and 5.45 compare the NCAW and DSSF simulants on CS-100 and R-F resins. In both cases, the slope of the breakthrough curve is lower for DSSF simulant, although R-F resin shows a larger difference. In this case, the change from NCAW to DSSF results in a 50% decrease in the column volumes to reach 70% C/C_0 for CS-100, but only a 20% decrease for R-F resin.

Figure 5.46 compares loading curves of two batches of R-F resin with DSSF. As indicated by the steeper slope, BSC-210 (Column SS) showed better mass-transfer properties than BSC-187, but loaded less volume of waste. Smaller particle size of BSC-210 (Table 5.2) may account for these differences. Higher DSSF flow rate was probably not the reason for improved mass transfer of BSC-210, since higher flow rates decrease the slope of the breakthrough curve and cause earlier initial breakthrough.

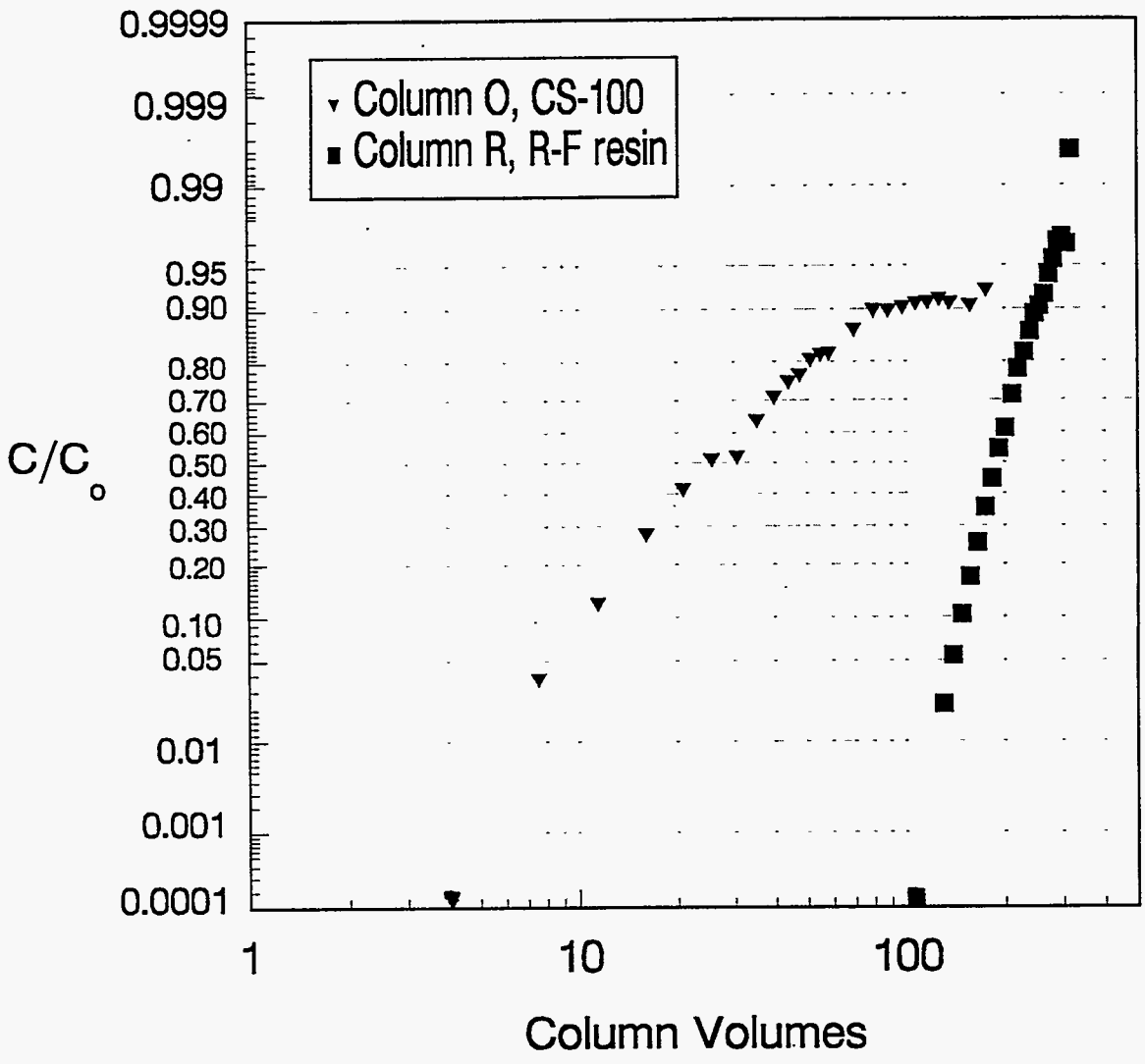

FIGURE 5.42. Comparison of CS-100 and R-F Loading Curves with NCAW Simulant at 9 cv/h and 25°C. (Column 70 and 8R)

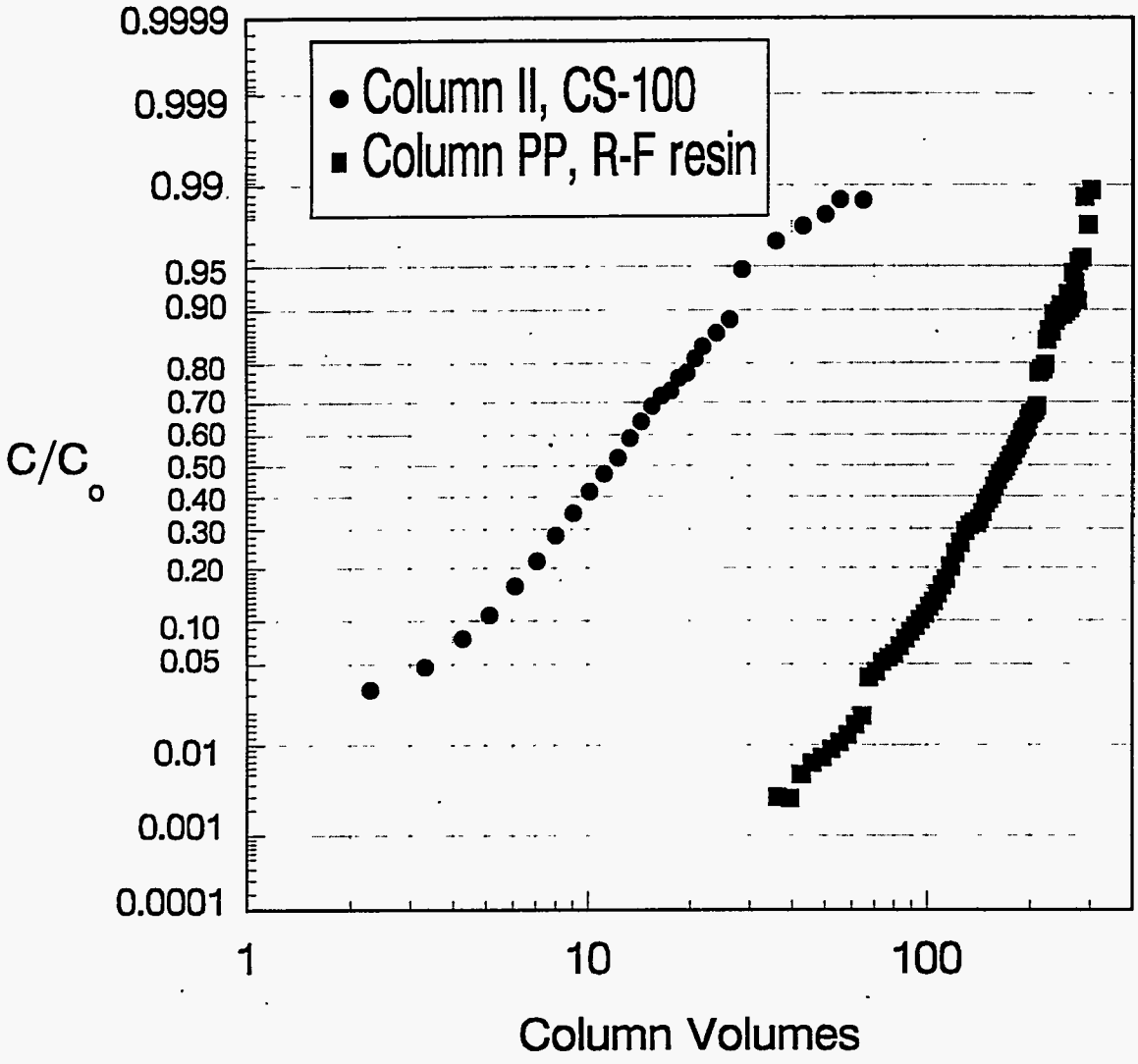

FIGURE 5.43. Comparison of CS-100 and R-F Loading Curves with DSSF-7 Simulant at 2 cv/h and 3 cv/h, Respectively. (Column 13II and 15PP)

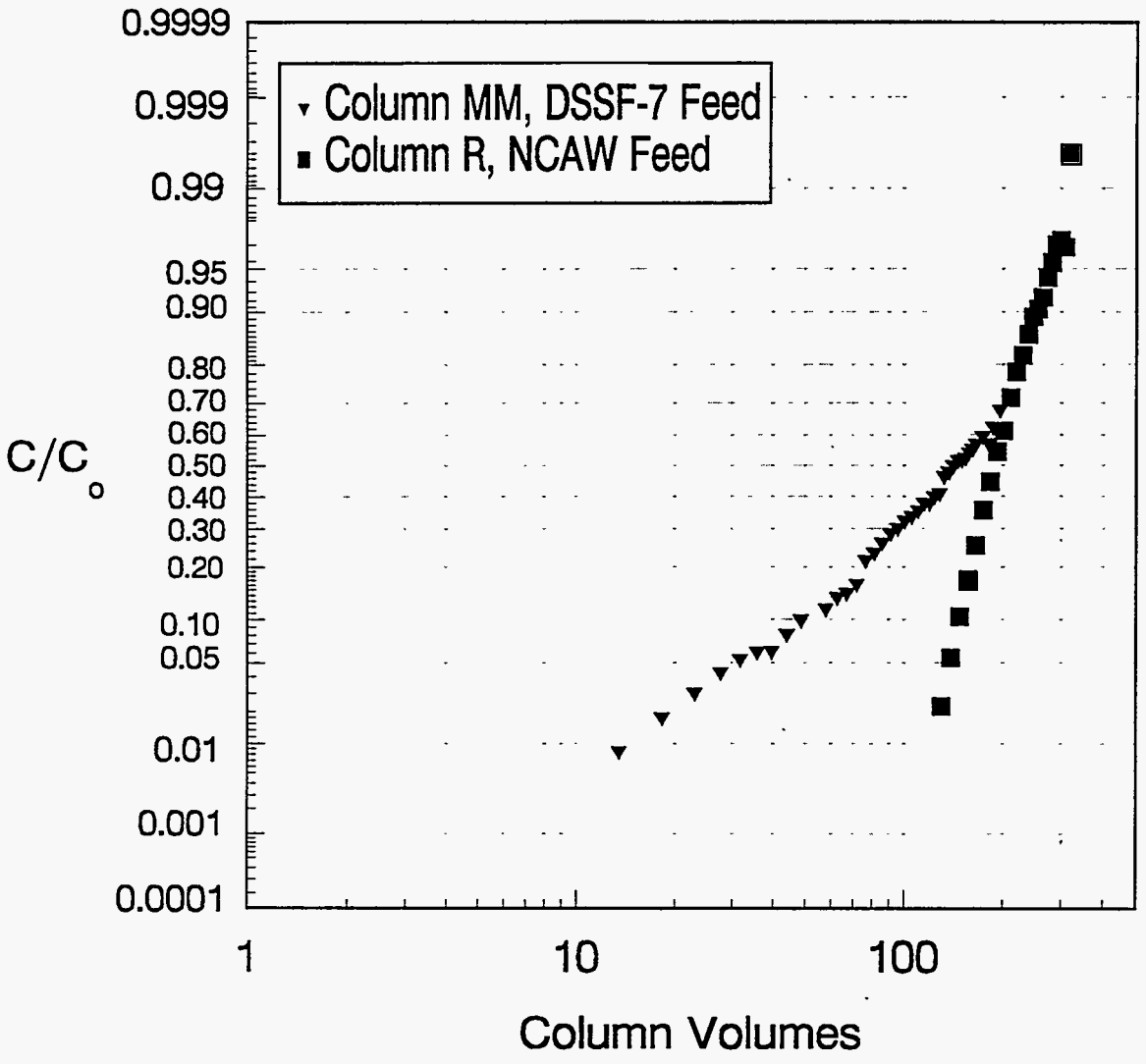

FIGURE 5.44. Comparison of the Loading Curves of the R-F Resin Using NCAW and DSSF-7 Simulants at 9 cv/h and 25°C. (Column 8R and 14MM)

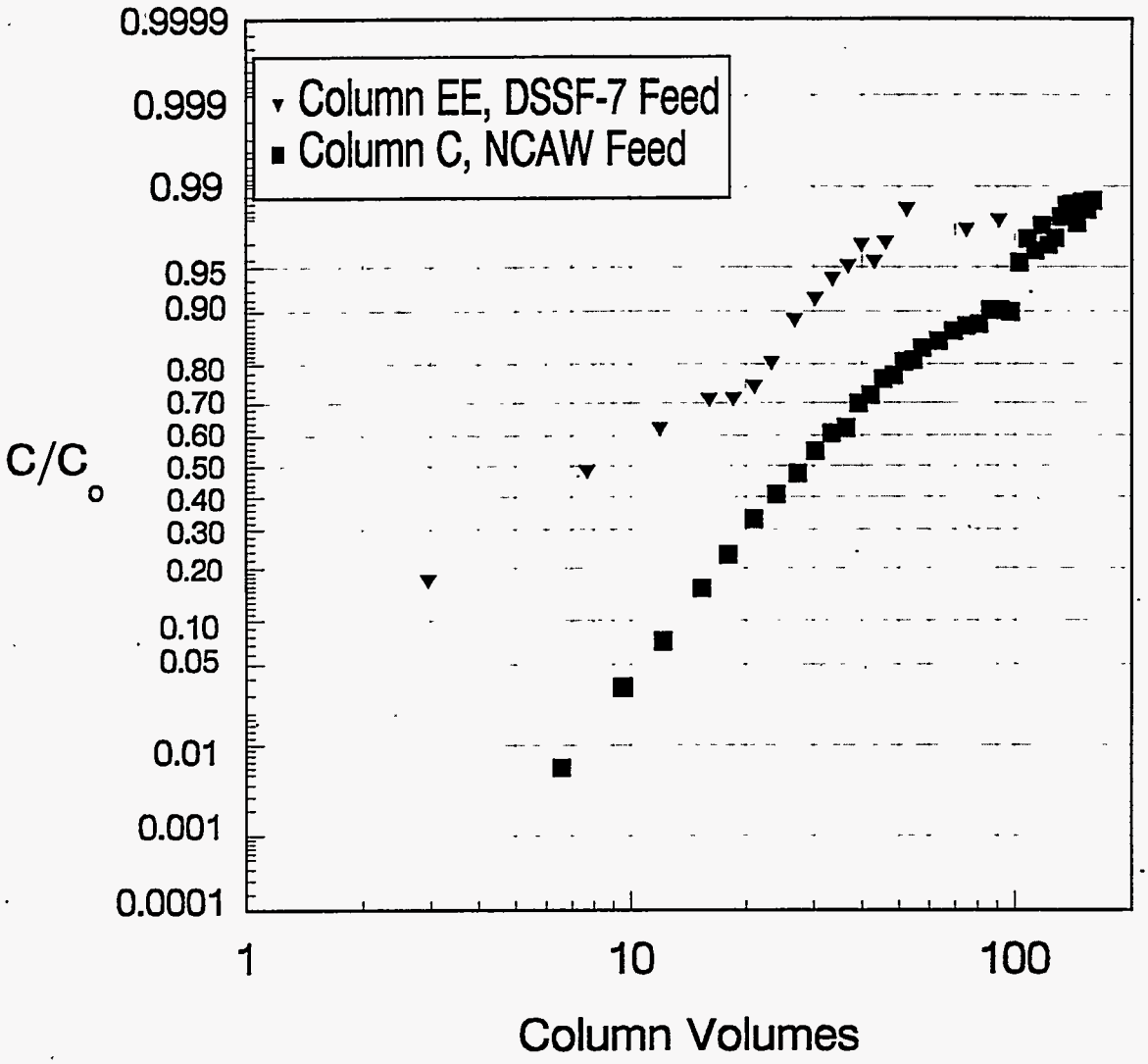

FIGURE 5.45. Comparison of the Loading Curves of the CS-100 Resin Using NCAW and DSSF-7 Simulants at 6 cv/h and 25°C. (Column 3C and 12EE)

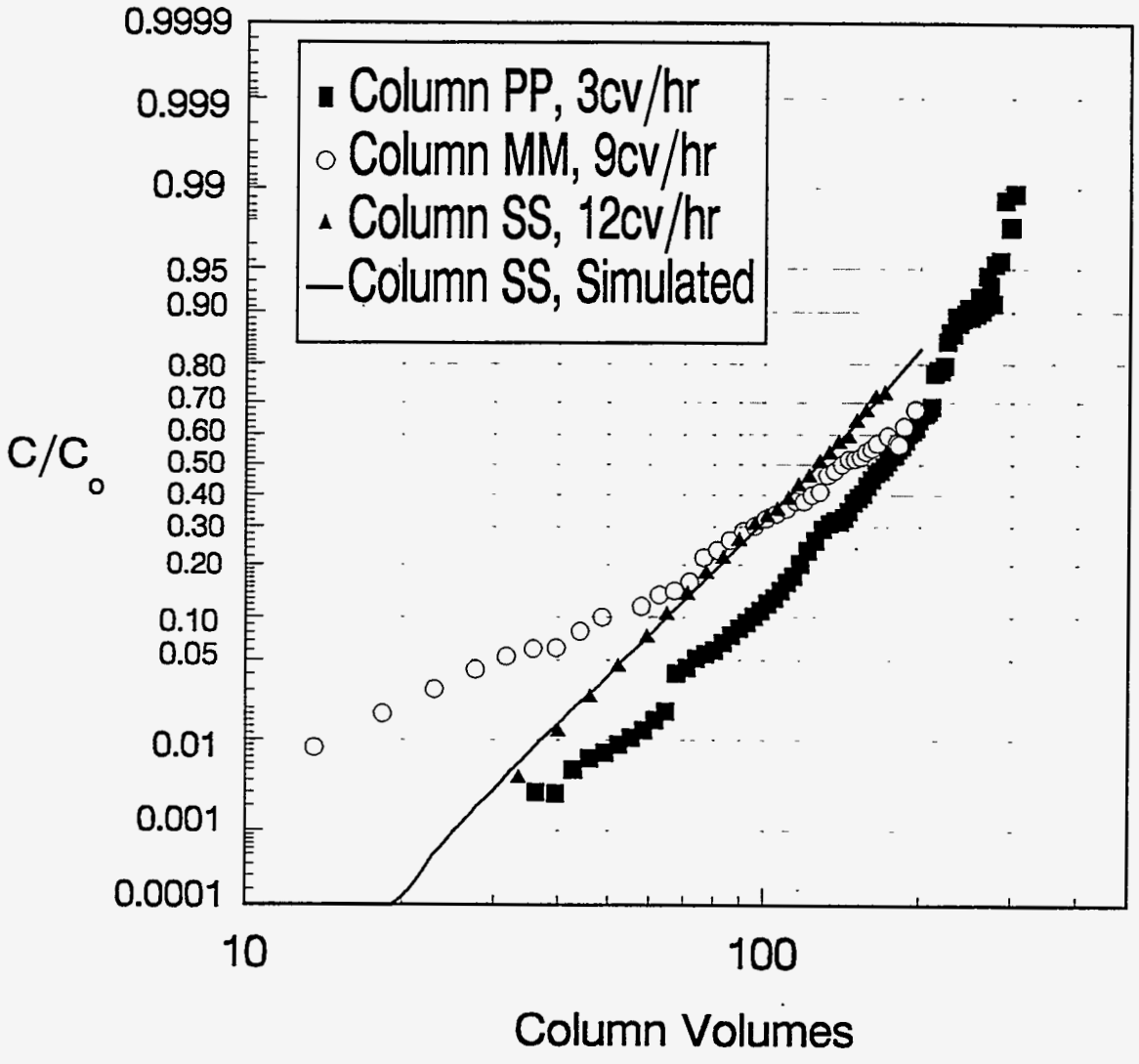

Note: Columns PP and MM = BSC-187
Column SS = BSC-210

FIGURE 5.46. Comparison of the Loading Curves of R-F Resin BSC-187 and BSC-210 with DSSF-7 Simulant at 3, 9, and 12 cv/h and 25°C. (Columns PP, MM, and SS)

5.2.2 Column-Loading Model and Evaluation

This section describes the mathematical model used to analyze the ion-exchange column-loading data. The modelling extend experimental data by providing a means to predict performance at other process conditions. The PNL model equations coupled with an equation solver (Simusolv™, Dow Chemical) provide simulated breakthrough curves. The mathematics of the PNL model are validated by comparing breakthrough curves with curves generated by a commercial ion-exchange code (Verse-LC©, Purdue University). The PNL model regresses model parameters for each experimental breakthrough curve and generates simulated curves from the regressed parameters. Trends in regressed parameters are discussed in relation to experimental conditions.

5.2.2.1 Description of the Model

Dr. R. S. Skeen of PNL developed the column-loading model and coupled it with Simusolv™ for bioremediation. The modified PNL model treats ion exchange as an adsorption phenomenon and is based on the one-dimensional, unsteady state transport equation for cesium.

Equation (5.10) accounts for cesium transport to the solid phase and convection and dispersion in the liquid phase. The dispersion coefficient is calculated from the Peclet number, particle size, and fluid velocity using a correlation (Perry 1984) which assumes that the dispersion coefficient (D_A) is a linear function of fluid velocity (U_z).

$$\frac{\partial C_A}{\partial t} + U_z \frac{\partial C_A}{\partial z} + \frac{1-\varepsilon}{\varepsilon} \frac{\partial C_{As}}{\partial t} = D_A \frac{\partial^2 C_A}{\partial z^2} \qquad (5.10)$$

where C_A = liquid cesium concentration (mol/ml)

C_{As} = solid cesium concentration (mol/cc)

t = time (min)

z = distance from column entrance (cm)

U_z = superficial liquid velocity (cm/min) = Q/A

Q = flow rate (mL/min)

A = cross-sectional area of column (cm^2)

ε = void fraction

D_A = effective dispersion coefficient (cm^2/min)

The PNL model further assumes that variations in cesium concentration with respect to radial and angular coordinates are negligible, or that ion exchange in a cylindrical column can be modelled by considering only the z-component of mass transport. The model also assumes that variations in fluid velocity and temperature are negligible.

A linear driving force is assumed for mass transfer to the solid phase. Two mechanisms for mass transport are considered: film-diffusion-controlled [Equation (5.11)] and particle-diffusion-controlled [Equation 5.12)].

$$\frac{\partial C_{As}}{\partial t} = K_f a \left(C_A - C_A^*\right) \qquad (5.11)$$

$$\frac{\partial C_{As}}{\partial t} = K_p a \left(C_{As}^* - C_{As}\right) \qquad (5.12)$$

where $K_f a$ = overall film-phase mass-transfer coefficient (min^{-1})

C_A^* = equilibrium cesium concentration in the liquid (mol/ml)

$K_p a$ = overall particle-phase mass-transfer coefficient (min^{-1})

C_{As}^* = equilibrium cesium concentration in the solid (mol/cc).

Cesium adsorption is modelled by the Freundlich isotherm [(Equation 5.13)]. The exponent in the Freundlich isotherm (N) can be obtained from an exponential curve fit of equilibrium cesium concentrations in solution and on the resin. The exponential fit also gives the Freundlich pre-exponent (K), but for column modeling, K was an adjustable parameter.

$$C_{As}^{*} = K\, C_{A}^{*N} \tag{5.13}$$

where K = Freundlich pre-exponent

N = Freundlich exponent

The boundary conditions are based on the assumptions that (1) just outside the column entrance, no adsorption of cesium occurs, and (2) the cesium concentration just outside the column exit is equal to the cesium concentration in contact with the last part of resin at the column exit. Therefore, from (1), dispersion and convection must be balanced at the entrance [Equation (5.14)] and from (2), the concentration gradient must be zero at the exit [Equation (5.15)].

$$-D_A \frac{\partial C_A}{\partial z} + U_z C_A = U_z C_{Ao} \text{ at } z = 0 \text{ for all } t \tag{5.14}$$

$$\frac{\partial C_A}{\partial z} = 0 \text{ at } z = L \text{ for all } t \tag{5.15}$$

where C_{Ao} = feed cesium concentration (mol/mL)

L = column exit (cm)

The initial conditions set the cesium concentrations in the column (Equation 5.16) and on the resin (Equation 5.17) to zero before flow is started.

$$C_A = 0 \text{ for } 0 < z \leq L \text{ at } t = 0 \tag{5.16}$$

$$C_{As} = 0 \text{ for } 0 < z \leq L \text{ at } t = 0 \tag{5.17}$$

The ability of the PNL model to characterize cesium ion-exchange column loading may be limited by the assumptions of the model in relation to actual conditions. First, the model assumes that the resin particles are uniform in size and shape. However, the crushing process during manufacture produces nonuniform particles. Second, the mass-transfer mechanism may not follow a linear driving force. Third, the Freundlich isotherm is a simple adsorption model, but cesium ion exchange is more complicated than adsorption. Finally, the model assumes a constant fluid velocity, but significant fluctuations occurred during the experiments.

A sensitivity analysis was performed to elucidate the effects of dispersion on model curves. Curves were generated using the PNL model with zero and nonzero values of the dispersion coefficient. The nonzero value was $0.16U_z$ cm^2/min, where U_z is the superficial fluid velocity, and was based on CS-100 average particle size (Table 5.1), expected flow rates, and column cross-sectional area (Perry 1984). As expected, dispersion tended to spread the breakthrough curve, although the effects were small.

Breakthrough curves approach 100% C/C_0 sooner in the case of film-diffusion control than in particle-diffusion control. The curves would appear identical in linear coordinates, but the earlier breakthrough for film-diffusion is clearly shown in log-probability coordinates (Figure 5.47). To create these curves with similar slopes, the ratio of the mass-transfer coefficients ($k_f a/k_p a$) was equal to the nondimensional distribution coefficient (Cs λ) of the feed.

Mathematics of the PNL model were validated by comparing model curves with breakthrough curves generated with Verse-LC©, which uses differential equations similar to the PNL model. For several film-diffusion-control cases, the results of the two models were identical. Particle-diffusion-control cases were not compared, because Verse-LC© does not model diffusion in the particle phase.

5.2.2.2 Fitting Column-Loading Data to PNL Model

This section summarizes CS-100 and R-F ion-exchange column modeling with the PNL model. Fitting the column data and simulating breakthrough curves are discussed. Regressed mass-transfer coefficients and Freundlich pre-exponents used to generate the simulated curves are presented and discussed in relation to experimental conditions. Simulated breakthrough curves for each run were presented with the column data (Section 5.2.1).

General Approach to Fitting Data. Each set of raw column data (C/C_0 vs. cv) was fit to the PNL column model with an optimization routine in Simusolv™. The mass-transfer coefficient and Freundlich pre-exponent were the adjustable parameters. Variation of the Freundlich pre-exponent allowed better fitting of the data, because the unavoidable differences between an empirical fit of equilibrium data and the equilibrium behavior of the column can be eliminated. The Freundlich pre-exponent is a crucial parameter because changes in it cause the entire breakthrough curve to shift as a function of column volumes of feed processed. The mass-transfer coefficient is a key variable in determining the slope of the breakthrough curve on log-probability plots.

Adjustment of the Freundlich pre-exponent may also have provided for better fits because cesium concentrations are outside the range of the Freundlich isotherm during part of the loading process. During initial loading when solution concentrations are dilute inside the column, the Freundlich isotherm derived from available equilibrium data (Table 5.11) likely overpredicts solid cesium concentration. Furthermore, the Freundlich

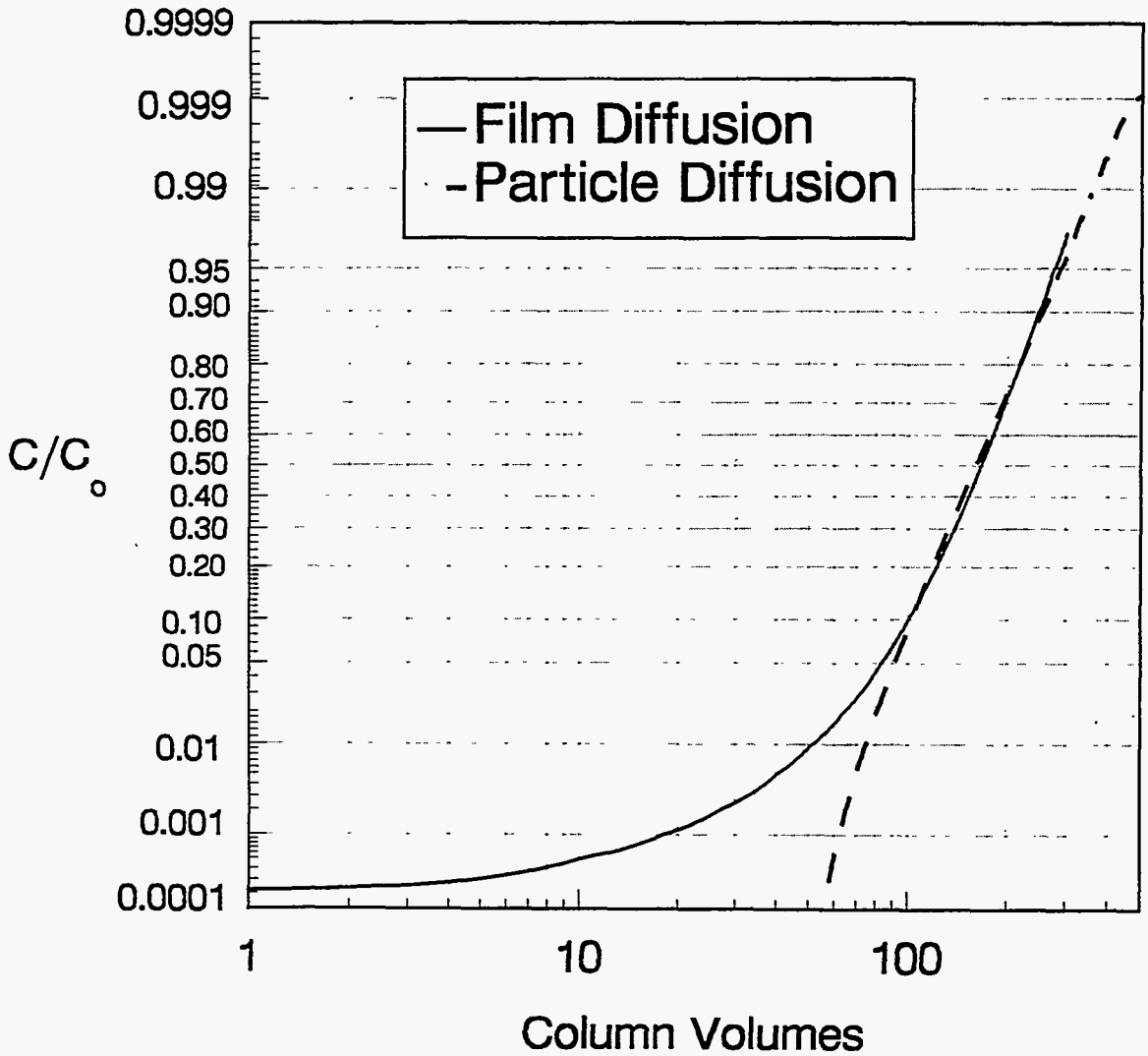

FIGURE 5.47. A Sample Plot of Loading Breakthrough Curves Using the Mathematical Model Based on the Assumption of Diffusion Limited by Transport in the (a) Particle Phase and (b) Film Phase

isotherm may overpredict solid cesium concentration during the final stages of loading, as the resin becomes saturated with cesium. A better model for equilibrium needs to be developed, because the Freundlich isotherm applies only to a subset of the cesium concentrations encountered during column loading.

Except in Runs 8 and 9, the cesium C/C_0 data were fit with column volumes as the unit of time. In previous work, use of minutes as the unit of time often resulted in a poor fit when minutes were converted to column volumes (using an average flow rate) and the data were plotted in column volumes. Because flow rate fluctuated significantly during the experiments, the difference between minutes and column volumes was not constant. Fitting with column volumes as the unit of time made conversion of time units unnecessary and allowed direct comparison between the fit and experimental data (Section 5.2.1). (Run 8 and 9 simulations obtained in minutes also fit the data well in column volumes, so that refitting the data in cv was unnecessary.) To fit the data in column volumes, the flow rate in the model was set to 200 mL/cv (conversion factor = 200/Q). With data input as C/C_0 versus column volumes, model equations coupled with Simusolv fitted the mass-transfer coefficient in units of cv^{-1}. A factor of $Q_{avg}/200$ was then used to convert the mass-transfer coefficient to units of min^{-1}, where Q_{avg} was the average flow rate over the range of experimental data best fit by the model. Selected data were used to fit breakthrough curves with significant scatter (such as Run 14) and known experimental error.

Most of the cesium breakthrough curves were fit well (Section 5.2.1) using the PNL model with particle-diffusion-controlled mass-transfer. The DSSF runs were the most difficult to fit, particularly Run 15. As discussed later in this section, Run 15 was fit best by the film-diffusion-control mass-transfer model.

TABLE 5.11. Freundlich Parameters from Equilibrium[a]

Resin	Waste	Pre-Exponent (K)[d]	Exponent (N)
CS-100[b]	NCAW	5.7	0.879
CS-100[c]	DSSF-7	1.3	0.845
R-F[c]	NCAW	5.2	0.735
R-F[c]	DSSF-7	2.4	0.754

(a) Units of $[Cs]_s$ and $[Cs]_l$ for Freundlich isotherm are mol/cc and mol/mL, respectively.
(b) From CS-100 correlation in Section 5.1.4 converted to units in (a).
(c) From exponential curve fit of equilibrium data at sodium concentration for specific waste.
(d) These values were allowed to vary during the curve-fitting process.

In the early column runs, the model was unable to fit high C/C_0 data, probably as a result of drift in the counting instrument. Instrument drift appeared to cause experimental C/C_0 to level off below 100%, which implied that cesium was loading at better-than-equilibrium conditions (see Figure 5.24, for example). Instrument drift is now accounted for by recalibrating the gamma counter periodically during each experiment.

Regressed Mass-Transfer Coefficients and Freundlich Pre-Exponents. Table 5.12 shows the regressed values of the particle-diffusion-controlled mass-transfer coefficient and Freundlich pre-exponent for CS-100 column data, and Table 5.13 shows regressed K_pa and K for R-F resin. (K_pa values for Run 15 were obtained by dividing K_fa by Cs λ determined from Freundlich isotherm.) Tables 5.12 and 5.13 also give the average flow rates used to convert K_pa from units of cv^{-1} to min^{-1}.

TABLE 5.12. Fitted Values of Mass-Transfer Coefficients and Freundlich Pre-Exponents for CS-100 Column Data

Run	Column	Waste	Average Flow		Freundlich Pre-exponent, K	Mass Transfer Coefficient $K_p a$, min^{-1}
			mL/h	cv/h[(a)]		
1	A	NCAW	1160	5.8	5.10	0.0281
3	C	NCAW	1120	5.6	5.21	0.0197
3	D	NCAW	1160	2.9	5.28	0.0175
3	E	NCAW	1140	1.9	5.31	0.0184
5	I	NCAW	590	2.9	4.95	0.0191
5	J	NCAW	600	1.5	5.25	0.0154
5	K	NCAW	610	1.0	5.31	0.0166
7	O	NCAW	1280	6.4	4.56	0.0200
7	P	NCAW	1730	4.3	5.14	0.0219
7	Q	NCAW	1780	3.0	5.14	0.0230
11	AA	DSSF-2	1090	5.4	0.43	0.0357
11	BB	DSSF-2	1150	2.9	0.49	0.0187
11	CC	DSSF-2	1150	1.9	0.50	0.0209
12	EE	DSSF-7	1590	7.9	0.74	0.0318
12	FF	DSSF-7	1330	3.3	1.06	0.0154
12	GG	DSSF-7	1320	2.2	1.13	0.0138
13	II	DSSF-7	390	2.0	0.99	0.0113
13	JJ	DSSF-7	430	1.1	1.04	0.0116
13	KK	DSSF-7	440	0.73	1.11	0.0102

(a) Based on total volume of resin (200 mL for 1 column, 400 mL for 2 columns, and 600 mL for 3 columns in series).

TABLE 5.13. Fitted Values of Mass Transfer Coefficients and Freundlich Pre-Exponents for R-F Resin Column Data

Run	Column	Waste	Average Flow rate mL/h	Average Flow rate cv/h[(a)]	Freundlich Pre-exponent, K	Mass Transfer Coefficient K_pa, min^{-1}
8	R	NCAW	1810	9.0	4.08	0.0114
8	S	NCAW	1780	4.5	4.19	0.0121
8	T	NCAW	1780	3.0	4.19	0.0134
9	V	NCAW	2740	13.7	3.98	0.00991
9	W	NCAW	2740	6.8	4.02	0.0127
9	X	NCAW	2690	4.5	4.03	0.0115
10	Y	NCAW	2640	13.2	3.67	0.0191
14	MM	DSSF-7	1790	8.9	2.76	0.00315
14	NN	DSSF-7	1870	4.7	2.45	0.00327
14	OO	DSSF-7	1970	3.3	2.84	0.00263
15	PP	DSSF-7	616	3.1	2.90	0.00265
15	QQ	DSSF-7	614	1.5	3.00	0.00238
15	RR	DSSF-7	605	1.0	2.90	0.00331
16	SS	DSSF-7	2350	11.8	2.36	0.00785

(a) Based on total volume of resin (200 mL for 1 column, 400 mL for 2 columns, and 600 mL for 3 columns in series).

For cesium exchange with CS-100, the mass-transfer coefficients show an upward trend with flow rate of NCAW (Figure 5.48) and DSSF (Figure 5.49), indicating that film diffusion is significant at these flow rates. However, for NCAW, this trend may be spurious because of data scatter.

For R-F resin (BSC-187), the lack of significant variation in the mass-transfer coefficient with flow rate (Figures 5.50 and 5.51) indicates that the cesium exchange rate is controlled by particle diffusion. The larger mass-transfer coefficients with smaller R-F particle size (BSC-210 = 0.29 mm vs BSC-187 = 0.34 mm) also suggest that particle diffusion is significant. Limited data indicate that the mass-transfer coefficient proportional to $d^{-2.6}$

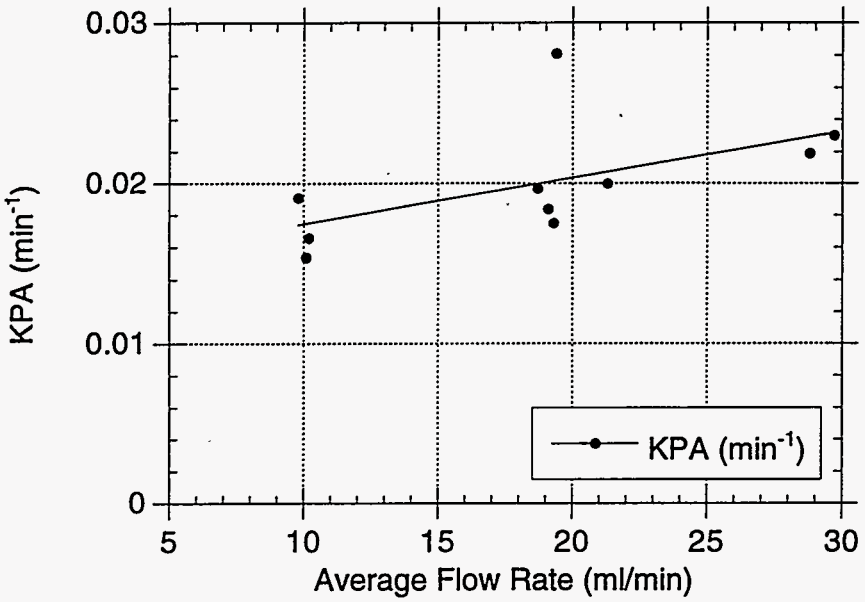

FIGURE 5.48. Mass-Transfer Coefficients for Cesium Ion Exchange as a Function of Flow Rate, CS-100 and NCAW

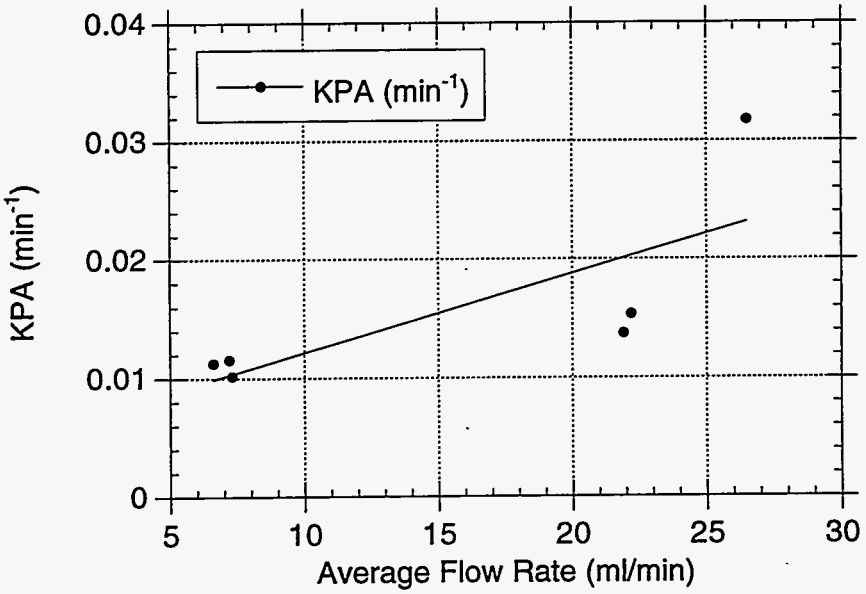

FIGURE 5.49. Mass-Transfer Coefficients for Cesium Ion Exchange as a Function of Flow Rate, CS-100 and DSSF-7

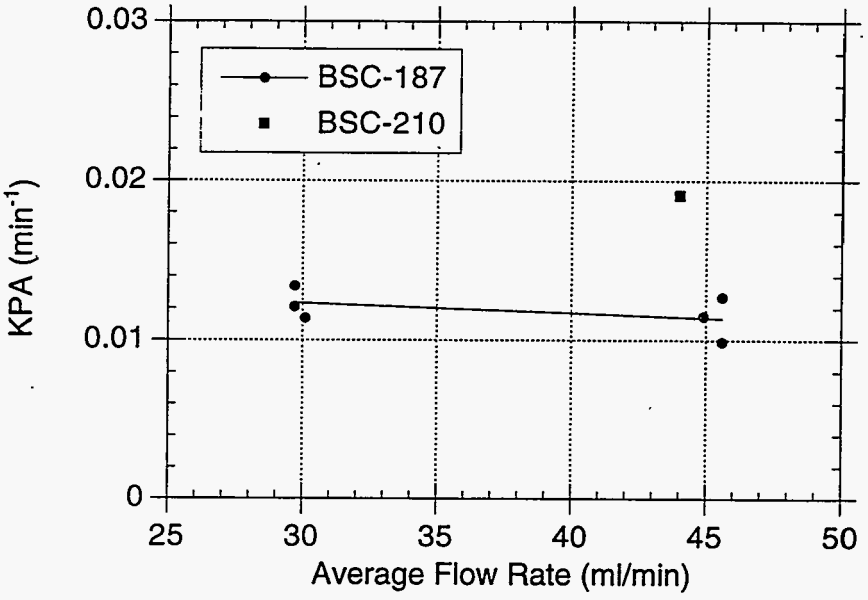

FIGURE 5.50. Mass-Transfer Coefficients for Cesium Ion Exchange as a Function of Flow Rate, R-F resin and NCAW

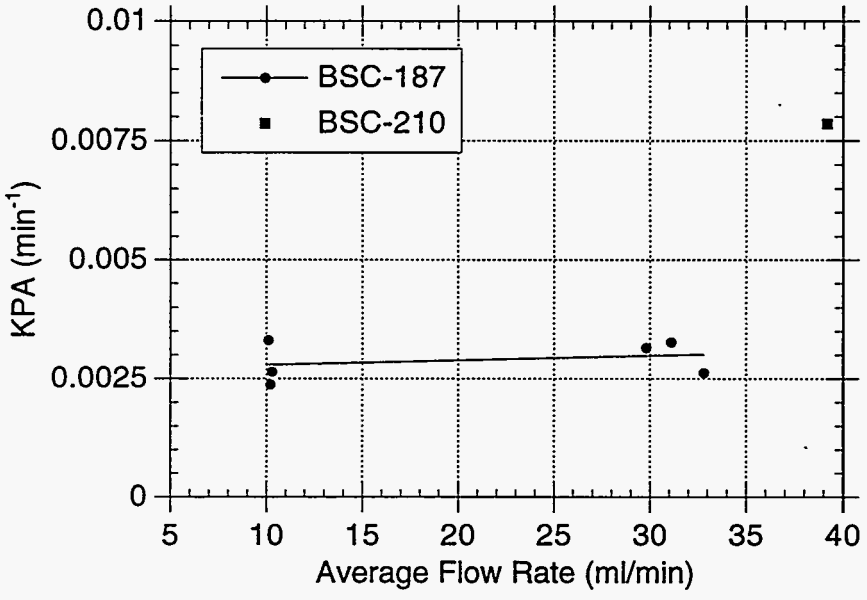

FIGURE 5.51. Mass-Transfer Coefficients for Cesium Ion Exchange as a Function of Flow Rate, R-F resin and DSSF-7

for NCAW and d^{-6} for DSSF, where d is particle diameter. Theory suggests that the mass-transfer coefficient is proportional to d^{-2} in particle-diffusion controlled systems (See Equation 2.21).

Run 15, which had the lowest DSSF flow rate, was fit the best by the film-diffusion-controlled mass-transfer model. Figure 5.52 compares film-diffusion and particle-diffusion models for Run 15, Column PP. At low flow rates (<3 cv/hr), film diffusion may be significant for R-F resin.

Mass-transfer coefficients for cesium exchange are significantly lower with R-F resin than with CS-100. Since the smaller particle size of R-F resin would favor a higher mass-transfer coefficient, the lower $K_p a$ for R-F are probably due to a lower cesium diffusivity inside the resin particles.

Mass-transfer coefficients for DSSF were generally lower than for NCAW. The reason, which remains unclear, may be related to the high ionic strength of DSSF relative to that of NCAW. The viscosity of DSSF-7 at 25°C (4.7cp) was slightly greater than that of NCAW (3.4 cp). This difference, which would be important only for film-phase control, does not appear to be great enough to account for the difference in $K_p a$.

The fitted values of the Freundlich and mass transfer coefficients for Run 12 Column EE differ significantly from the other DSSF-7 columns. The Freundlich coefficient for Column EE is lower and the mass-transfer coefficient is higher, probably because at the higher flow rate the concentration profile in the column is still developing.

The Helfferich number (He) can be used to estimate whether film or particle diffusion controls the process. The He number was calculated to be between 1 and 3 for CS-100 in NCAW, suggesting that the process contains elements of both film- and particle-diffusion control. A calculated Helfferich number of approximately 10 for R-F resin with DSSF indicates film-diffusion control.

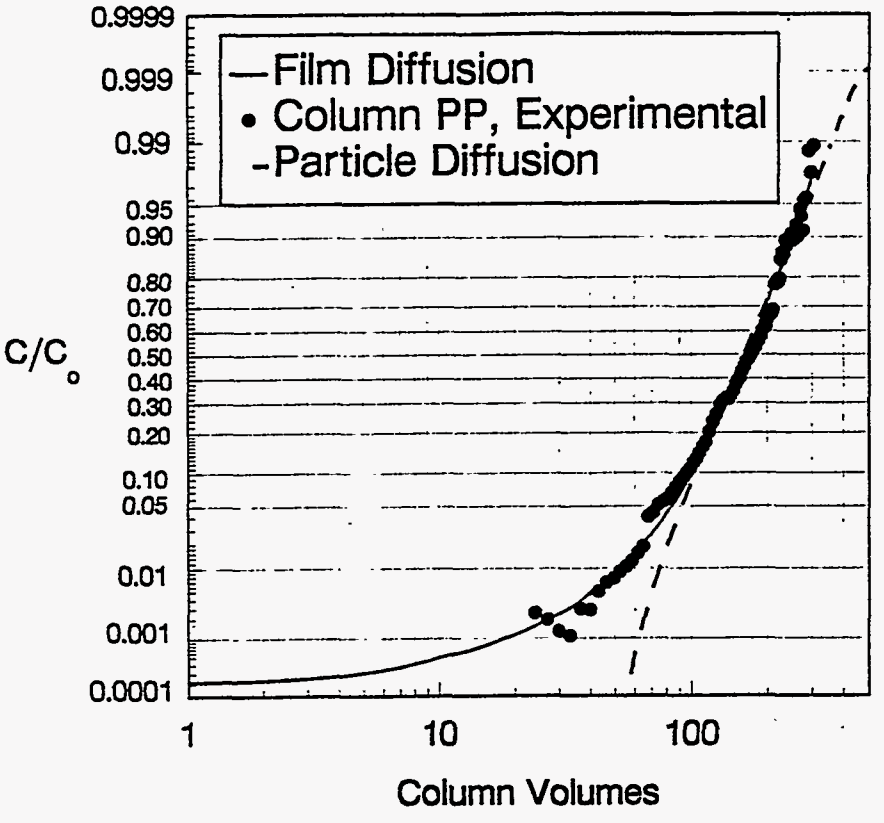

FIGURE 5.52. Comparison of Film- and Particle-Diffusion-Controlled Mass-Transfer Models for Run 15, Column PP

5.2.3 Column-Elution Studies

Cesium-elution experiments were performed on CS-100 and R-F resins loaded with cesium (Section 5.2). The experiments were designed to determine the effect of flow rate, temperature, and type of eluant on the elution characteristics of cesium. Eluants were nitric acid and formic acid. The concentration of nitric acid was kept below 0.5M to minimize the potential for oxidation of the resin at higher acidities. Conditions for the elution tests after loading from NCAW or DSSF feeds are shown in Table 5.14. All elutions were performed downflow with the exception of Column W (Run 9), which was performed in the upflow configuration.

5.2.3.1 CS-100 Elution Tests (NCAW)

The CS-100 resin ion-exchange Columns O, P, and Q were eluted at 1 cv/h and 25°C with nitric or formic acid (Figure 5.53). The initial column resin

TABLE 5.14. Cesium-Elution Experiments

test (run)	Resin	Eluant	Flow Rate (mL/h)	cv/h (200 mL/col.)	Temperature (°C)
A(1)	CS-100	0.1 M HNO_3	1200	6	25
C(3)	CS-100	0.05 M HNO_3	1200	6	25
D(3)	CS-100	1 M HCOOH	1200	6	25
E(3)	CS-100	0.5 M HCOOH	1200	6	25
I(5)	CS-100	0.1 M HNO_3	1200	6	40
J(5)	CS-100	0.05 M HNO_3	1200	6	40
K(5)	CS-100	1 M HCOOH	1200	6	40
O(7)	CS-100	0.1 M HNO_3	200	1	25
P(7)	CS-100	0.05 M HNO_3	200	1	25
Q(7)	CS-100	1 M HCOOH	200	1	25
R(8)	R-F	0.1 M HNO_3	200	1	25
S(8)	R-F	1 M HCOOH	200	1	25
T(8)	R-F	0.5 M HCOOH	200	1	25
V(9)	R-F	1 M HCOOH	200	1	25
W(9)	R-F	1 M HCOOH	200	1 (upflow)	25
X(9)	R-F	0.4 M HNO_3	200	1	25
Z(9)	R-F	0.4 M HNO_3	200	1	40
Y(10)	BSC-210	1 M HCOOH	200	1	40
AA(11)	CS-100	1 M HCOOH	1200	6	40
BB(11)	CS-100	1 M HCOOH	1200	6	25
II(13)	CS-100	0.4 M HNO_3	1200	6	40
JJ(13)	CS-100	0.1 M HNO_3	1200	6	40
KK(13)	CS-100	0.1 M HNO_3	1200	6	25
NN(14)	R-F	1 M HCOOH	1200	6	40
PP(15)	R-F	1 M HCOOH	200	1	25
SS(16)	R-F	1 M HCOOH	200	1	40

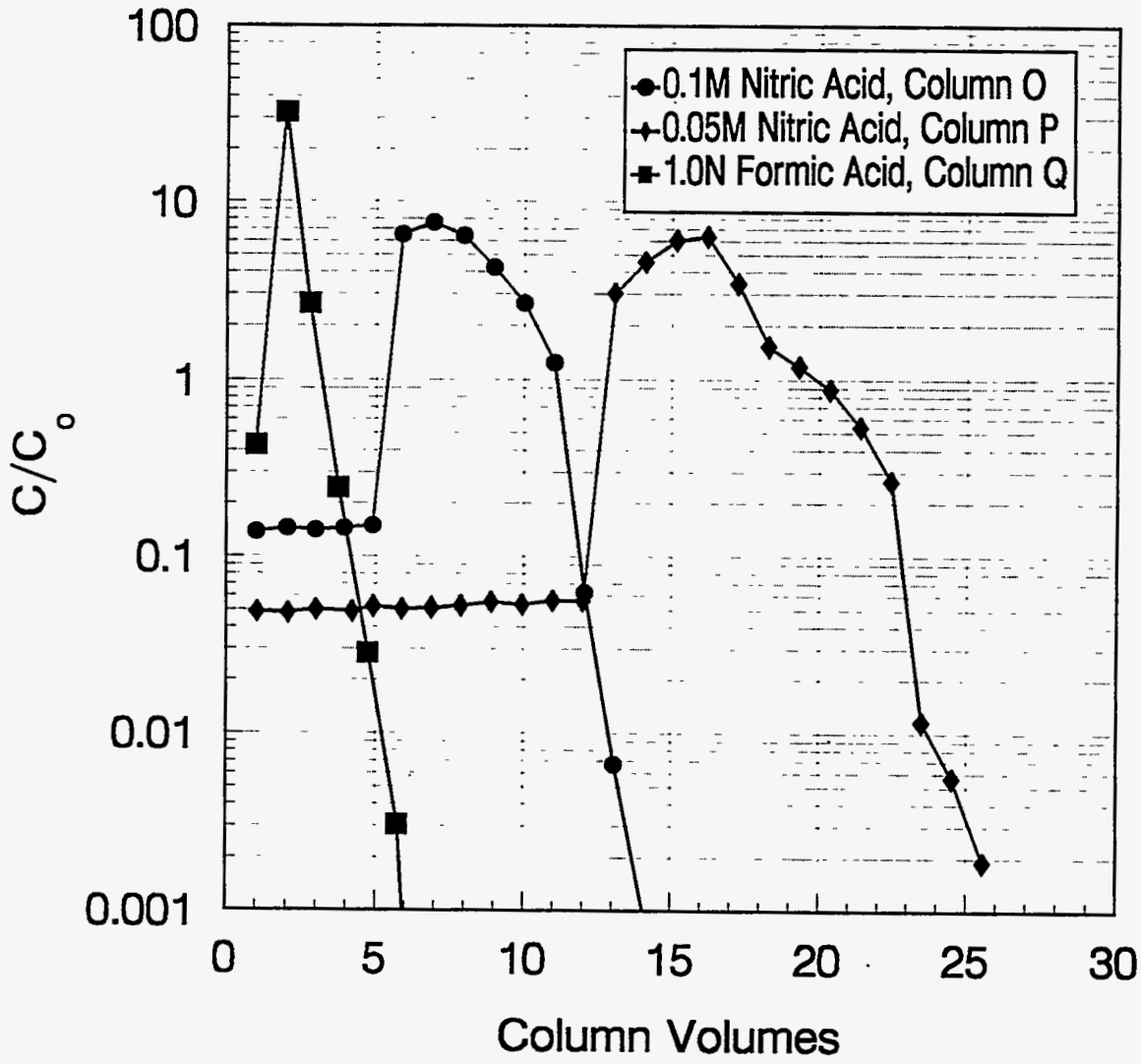

Resin: CS-100
Loaded with: NCAW
Eluant for Column O: 0.1M HNO_3
Eluant for Column P: 0.05M HNO_3
Eluant for Column Q: 1.0M HCOOH
Flow rate: 1 cv/h, 200 mL/h
Temperature: 25°C.
Run 7: Columns O, P, Q (3 columns in series)

Notes: No difficulties encountered.

FIGURE 5.53. Elution of CS-100 Resin Loaded with NCAW as a Function of Acid

had been loaded to a value equal to the cesium contained in 30 cv of NCAW (Loading Test #7). 1M HCOOH efficiently eluted the cesium in 6 cv of acid, concentrating the cesium 5-fold. However, 0.05M (Figure 5.54) and 0.1M HNO_3 required 5 to 12 cv of dilute acid to produce an acidic effluent, as verified by the change in pH. There appears to be residual hydroxide in the column even after washing it with several column volumes of water prior to elution. This neutralization is difficult to observe when 1M HCOOH is used (Figure 5.55) because of its higher acid concentration.

When the elution tests were performed at a higher flow rate (6 cv/h vs. 1 cv/h), the volume of 1M HCOOH or 0.1M HNO_3 required to obtain the same elution efficiency doubled (Figure 5.56). The required volume of the more dilute acid (0.05M HNO_3) did not change with flow rate. When tests were performed at a higher temperature (40°C vs. 25°C) the formic acid requirement did not change, but less nitric acid was required to reach $C/C_0 = 0.01$ (Figure 5.57).

5.2.3.2 CS-100 Elution Studies (DSSF)

Elution tests were also carried out for CS-100 with the runs on Columns AA, BB, II, JJ, and KK (Figures 5.58 and 5.59). These tests were performed to determine if the potassium that had loaded onto the resin affected the elution properties. Columns AA and BB were loaded with 8 and 13 cv of waste and contained less cesium than the columns loaded with NCAW. When loaded with DSSF, they eluted very quickly with 1M HCOOH, at rate similar to that of columns loaded with NCAW. For example, Column BB was eluted with less than 10 cv; Column O (loaded with NCAW) was eluted in 12 cv under similar conditions. Thus, as mentioned in Section 2.3, the quantity of cesium loaded on the column will not significantly influence the time (or cvs) required to elute it since the total number of cations that must be removed is the same.

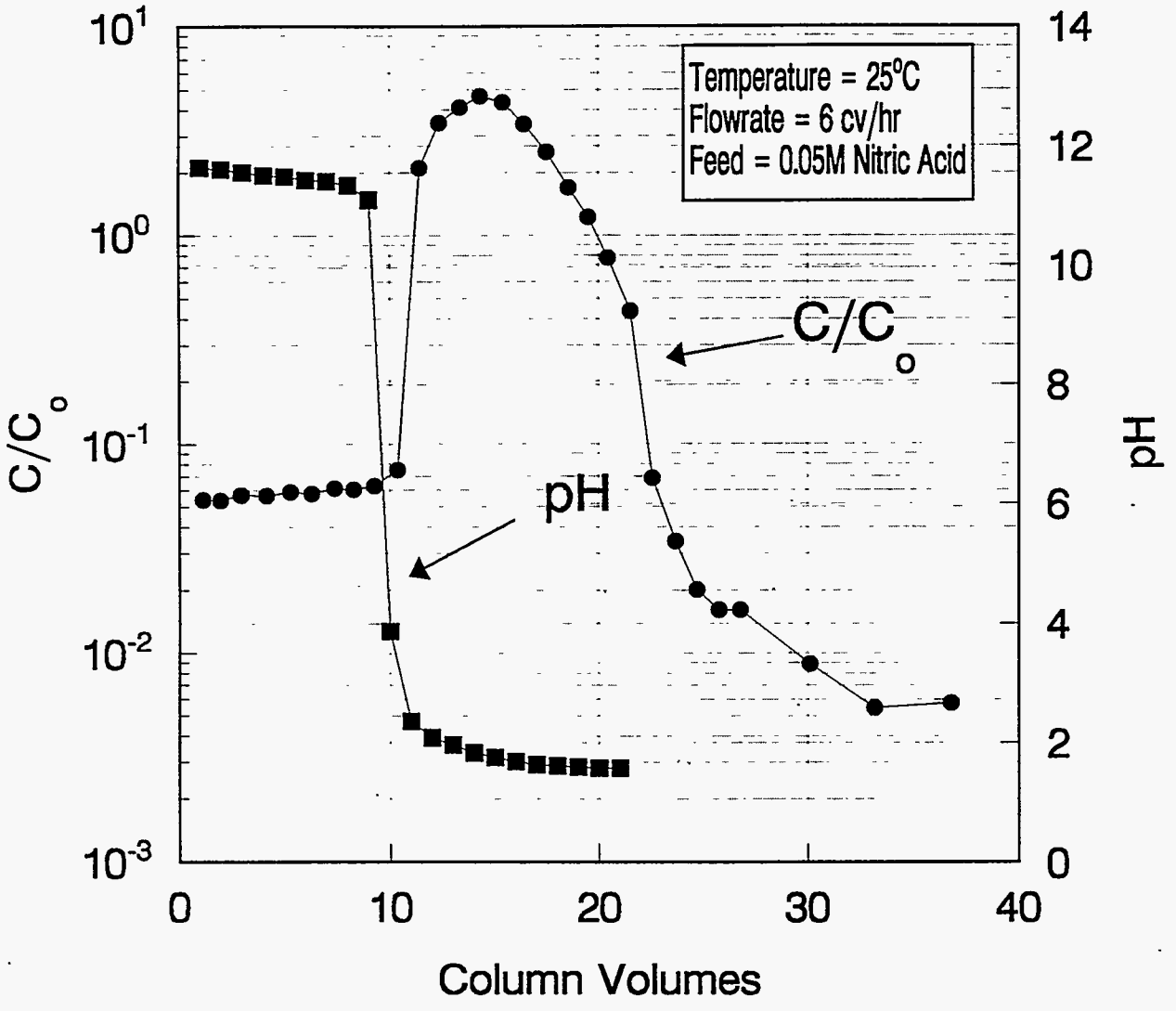

FIGURE 5.54. CS-100 Elution with 0.05M HNO_3 as a Function of pH (Column 3C)

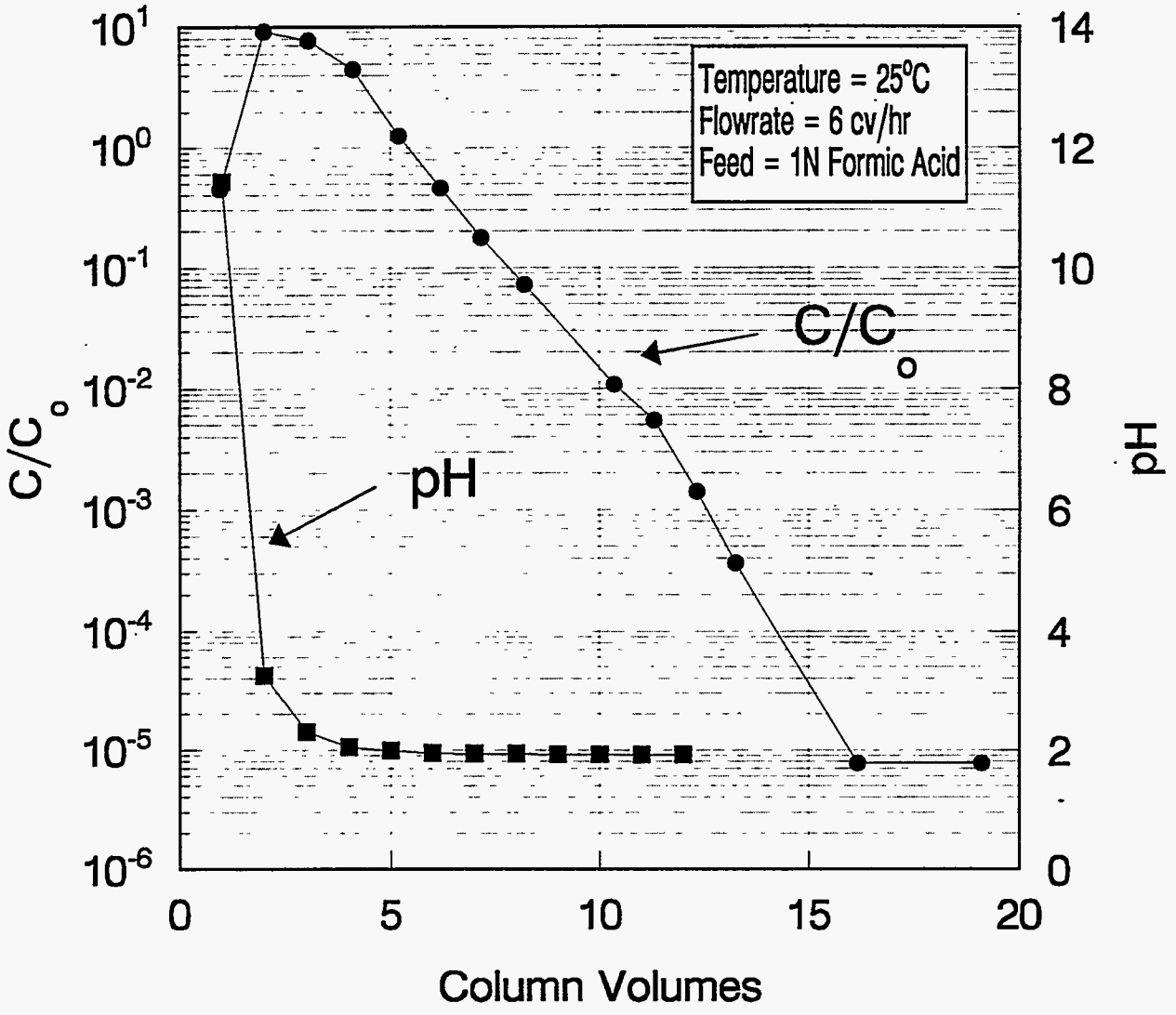

FIGURE 5.55. CS-100 Elution with 1M HCOOH as a Function of pH (Column 3D)

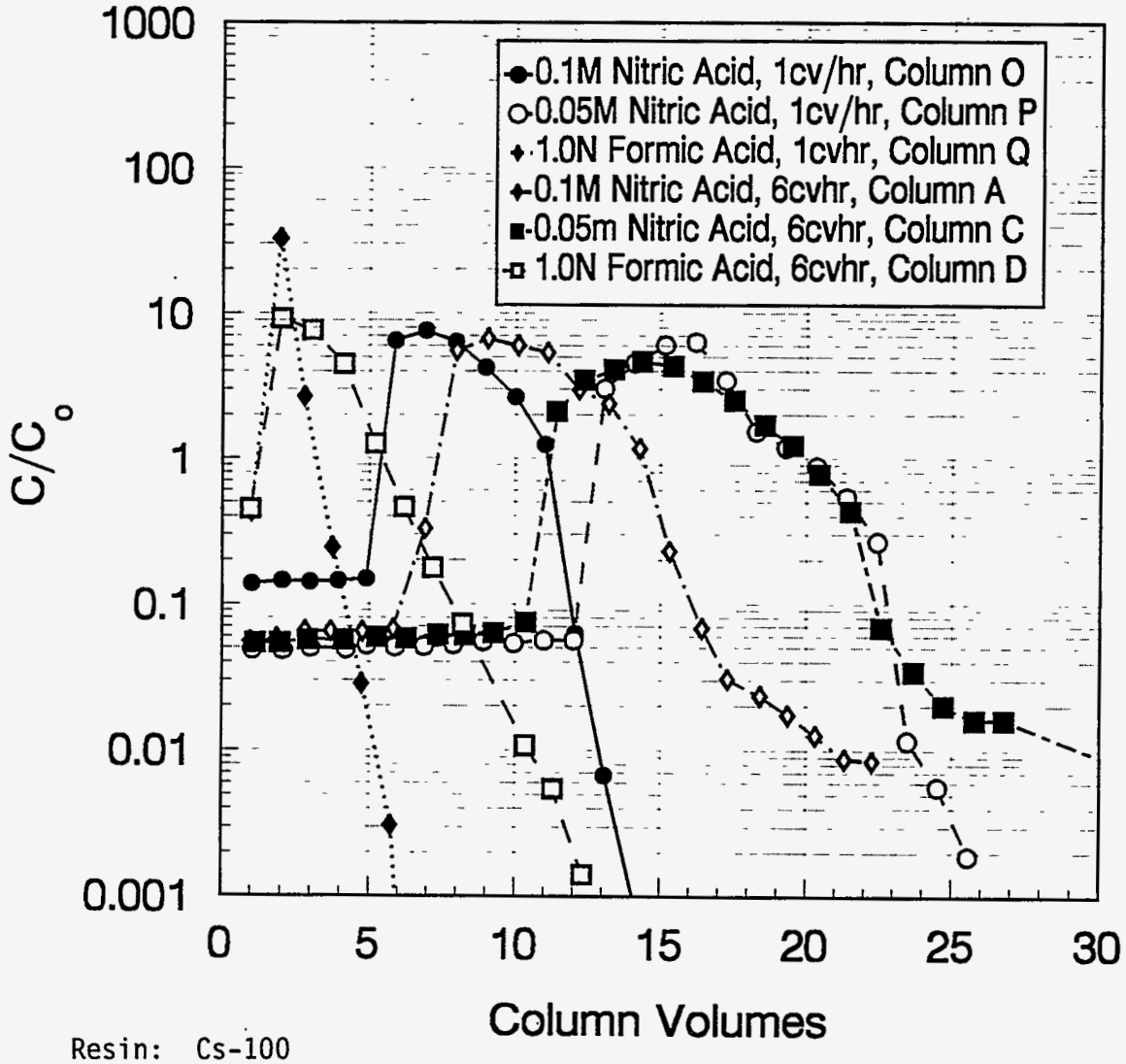

Resin: Cs-100
Loaded with: NCAW

Eluant for Column A:	0.1M HNO_3	Flow rates:	200 mL/h & 1200 mL/h
Eluant for Column C:	0.05M HNO_3	Temperature:	25°C
Eluant for Column D:	1.0M HCOOH	Run 1 at 6 cv/h, Column A	
Eluant for Column O:	0.1M HNO_3	Run 3 at 6 cv/h, Columns C, D, E	
Eluant for Column P:	0.05M HNO_3	Run 7 at 1 cv/h, Columns O, P, Q	
Eluant for Column Q:	1.0M HCOOH	(3 columns in series)	

NOTE: No difficulties encountered.

FIGURE 5.56. Elution of CS-100 Resin Loaded with NCAW as a Function of Flow Rate and Acid

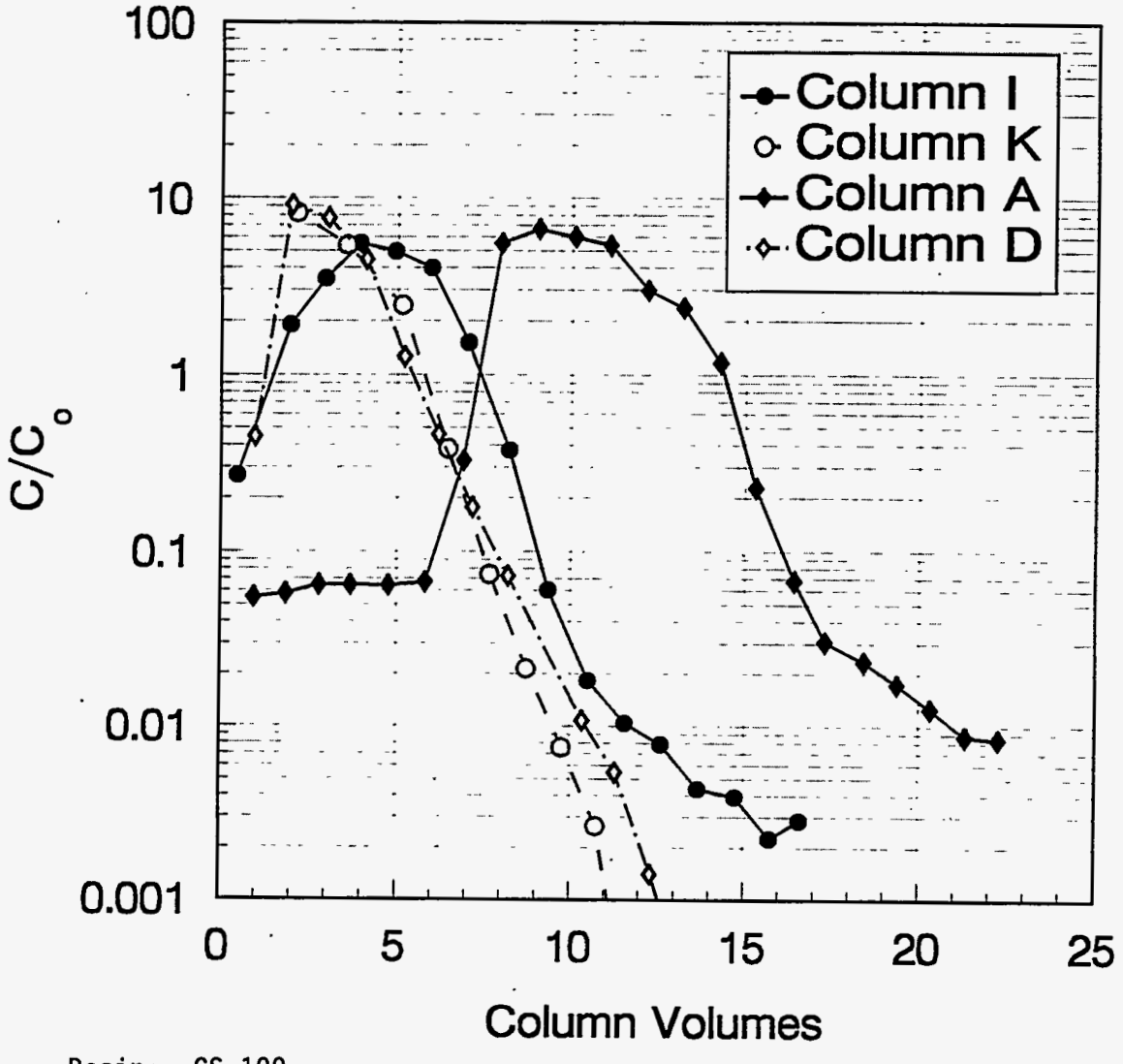

Resin: CS-100
Loaded with: NCAW
Flow rate: 6 cv/h, 1200 mL/h
Basis: 1 cv = 200 mL
Temperature: 40°C
Eluant for Column I: 0.1M HNO_3
Eluant for Column K: 1.0M HCOOH
Temperature: 25°C
Eluant for Column A: 0.1M HNO_3
Eluant for Column D: 1.0M HCOOH

NOTE: No difficulties encountered.

FIGURE 5.57. Elution of CS-100 Resin as a Function of Temperature

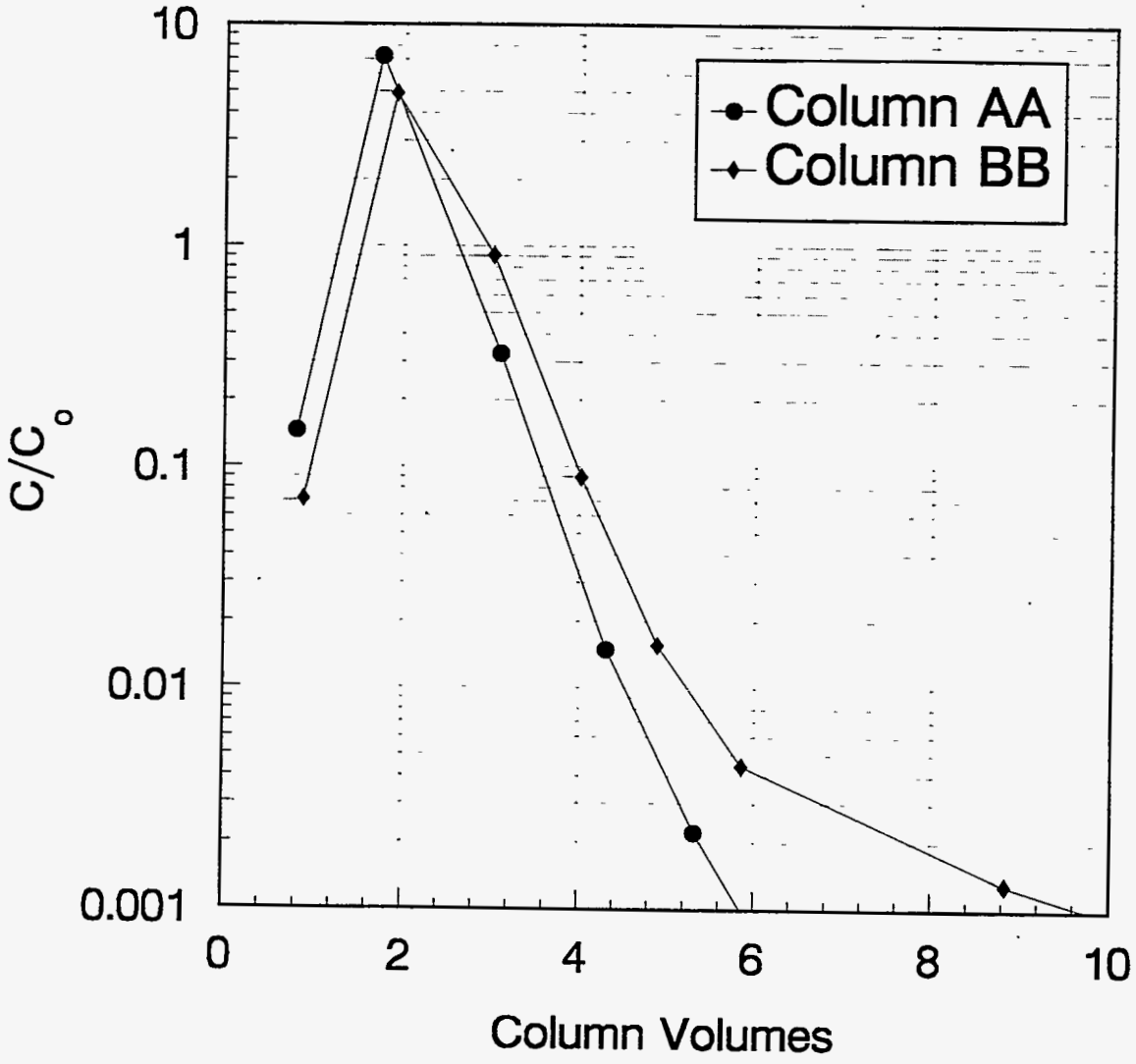

Resin: CS-100
Loaded with: DSSF-2
Temperature Column AA: 40°C
Eluant for Column AA: 1M HCOOH
Temperature Column BB: 25°C
Eluant for Column BB: 1M HCOOH
Flow rate: 6 cv/h, 1200 mL/h
Basis: 1 cv = 200 mL
Run 11: Columns AA, BB, CC (3 columns in series)

NOTE: Precipitation of what was probably sodium aluminate occurred during loading.

FIGURE 5.58. CS-100 Resin Elution as a Function of Temperature

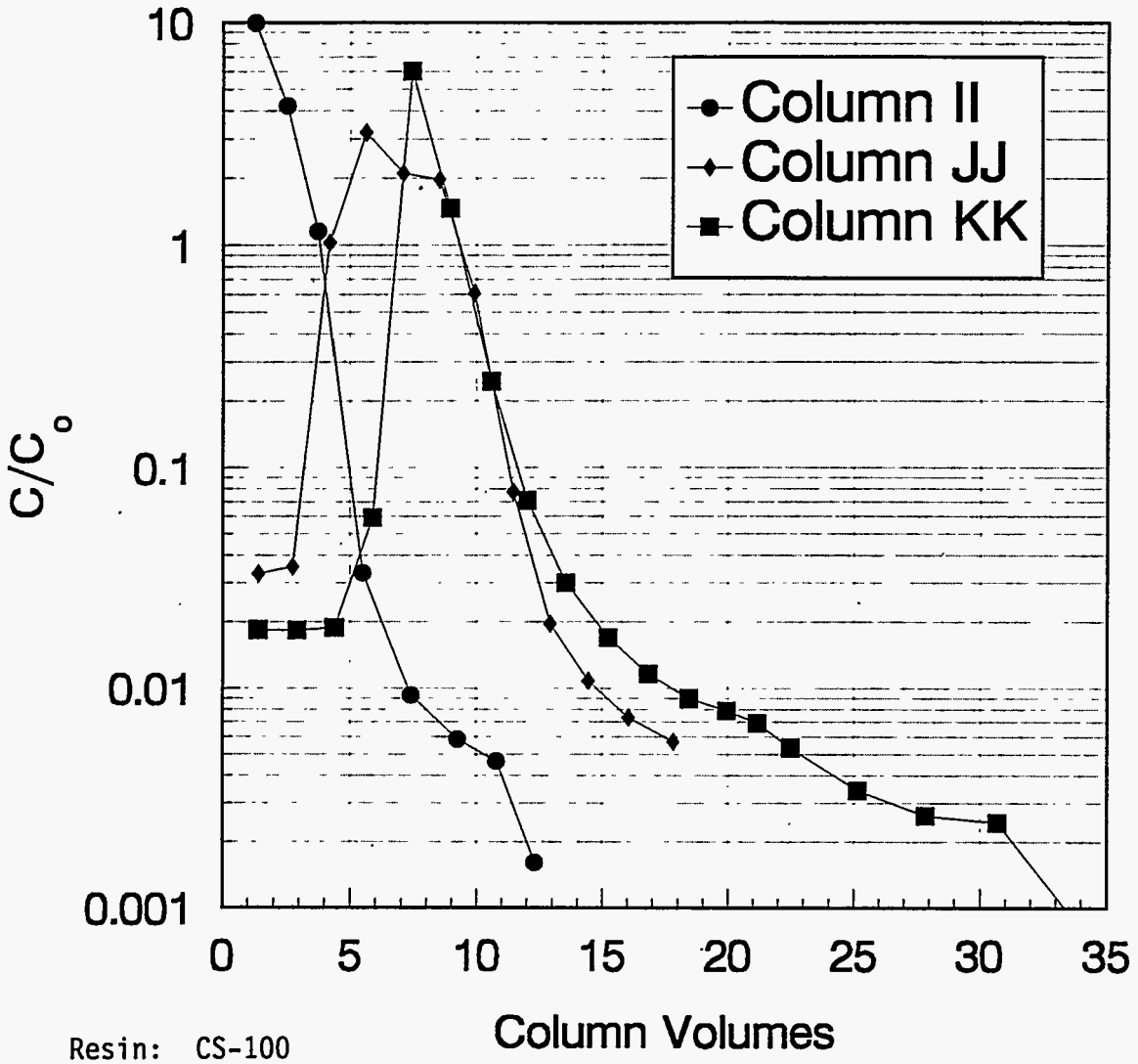

Resin: CS-100
Loaded with: DSSF-7
Temperature Column II: 40°C
Eluant for Column II: 0.4M HNO_3
Temperature Column JJ: 40°C
Eluant for Column JJ: 0.1M HCOOH
Temperature Column KK: 25°C
Eluant for Column KK: 0.1M HNO_3

Flow rate: 6 cv/h, 1200 mL/h
Basis: 1 cv = 200 mL
Run 13: Columns II, JJ, KK (3 columns is series)

NOTE: Flow was stopped in Column KK for 7-10 min at 21 cv to refill eluant feed vessel.

FIGURE 5.59. CS-100 Resin Elution as a Function of Temperature and Eluant Concentration

Higher temperatures enhance elution. Approximately 6 cv of 40°C formic acid eluted the cesium from Column AA down to a C/C_0 of 0.001. A similar elution for BB at 25°C required 10 cv (Figure 5.58). Note that for Column BB, the cesium in the eluate is more dilute than in the column feed.

Figure 5.59 shows the elution of the columns from Run 13. The resin was eluted with 0.4M HNO_3 at 40°C and 1200 mL/h (Column II); 0.1M nitric acid at 40°C and 1200 mL/h (Column JJ); and 0.1M nitric acid at 25°C and 1200 mL/h (Column KK). Results were similar to those of earlier tests performed on NCAW-loaded CS-100 columns. Column KK, eluted with 0.1M HNO_3, required approximately 5 cv of acid to neutralize before the effluent began to contain significant amounts of cesium. The time to neutralize the column and the rate that cesium was removed from Column KK are close to those of Column A, which was eluted under similar conditions. The behavior of the CS-100 columns loaded with DSSF or NCAW suggests that the concentration of potassium on the resin has no affect on the elution characteristics of CS-100.

Comparison of the three tests shows that higher nitric acid concentration (0.4M HNO_3) and higher elution temperature speed the elution process. However, increasing nitric acid concentration actually increases the total moles of acid required for elution. Channeling due to shrinkage of the resin was not observed.

5.2.3.3 R-F Elution Tests

Most elutions performed on cesium-loaded R-F resin (BSC-187), including Runs 8, 9, 14, and 15, exhibited double peaks or tailing of effluent C/C_0 to a large value (>0.01 C/C_0). Figure 5.60 compares 1M formic acid elution curves of BSC-187 and a new batch of R-F resin, BSC-210. Unlike BSC-187, BSC-210 showed no double peaks or tailing. BSC-210 (Column Y) effluent reached C/C_0 <0.01 in 11 cv, similar to the CS-100 elution results, and the BSC-187 (Column V) eluate tailed only to $C/C_0 = 0.1$ even after 35 cv. The results of Column SS confirm the superior performance of the new batch of resin. The effluent from this column reached C/C_0 <0.02 in 8 cv (See Figure 5.61).

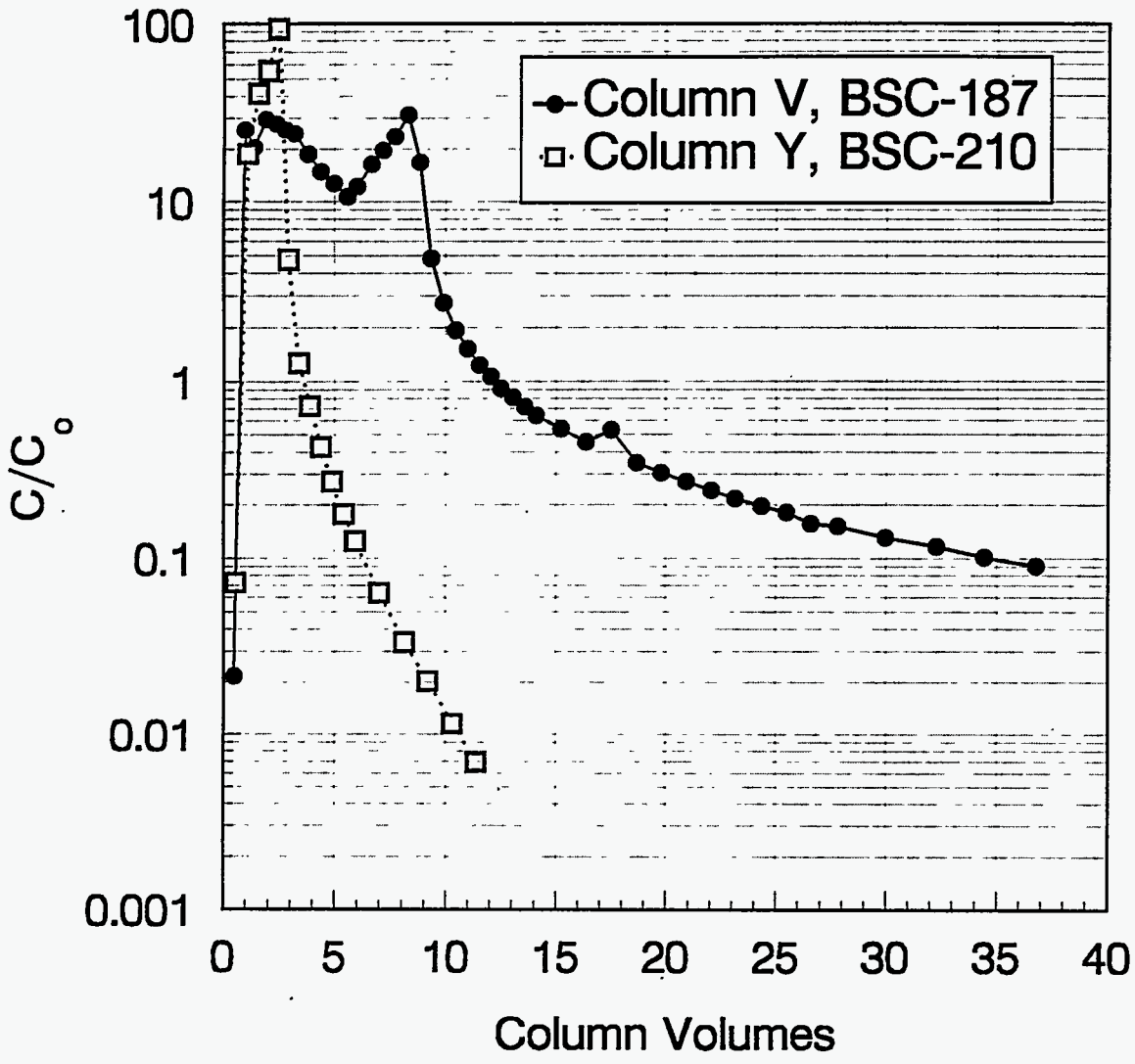

Resin: R-F
Loaded with: NCAW
Temperature Column V: 25°C
Temperature Column Y: 40°C
Eluant: 1M HCOOH
Flow rate: 1 cv/h, 200 mL/h
Run 9: Columns V, W, X (3 columns in series, BSC-187)
Run 10: Column Y (1 column in series, BSC-210)

FIGURE 5.60. R-F Resin Elution for Two Different Batches of Resin

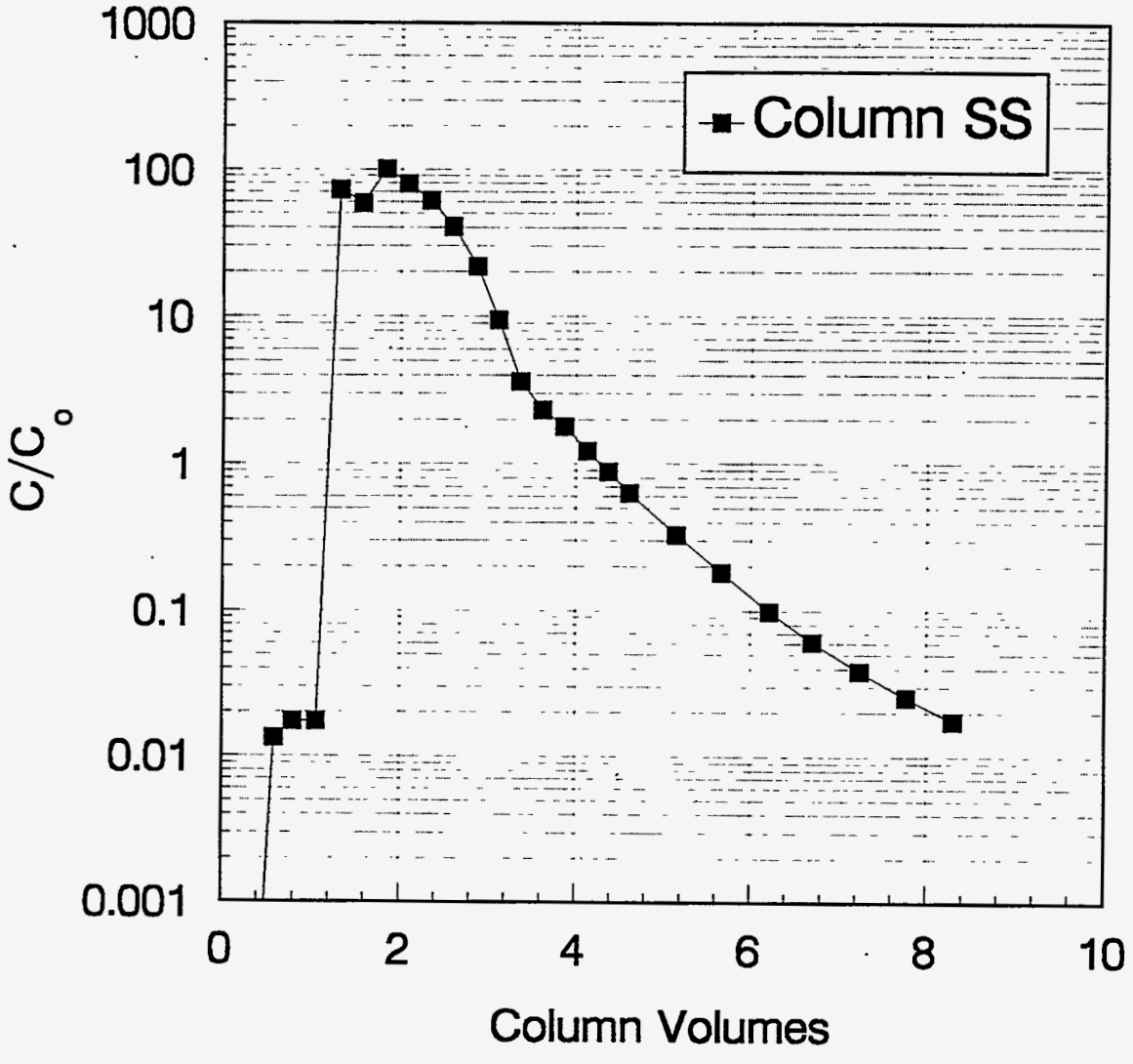

Resin: R-F (BSC-210)
Loaded with: DSSF
Temperature Column SS: 40°C
Eluant: 1M HCOOH
Flow rate: 1 cv/h, 200 mL/h
Run 16: Column SS (1 column in series, BSC-210)

FIGURE 5.61. R-F Resin Elution using the New Batch of Resin (BSC-210)

The relatively poor elution behavior of R-F appears to be due to the ~35% volume shrinkage during elution when H^+ replaces Na^+, K^+, and Cs^+. When R-F resin is eluted with acidic solution, the resin shrinks, agglomerates, and pulls away from the walls of the column, thereby increasing channeling of solution along the column walls. A visible void space forms between the resin and the wall of the ion-exchange column during elution, and the resin appears to contract toward the center of the column. In a larger column, where the weight of the resin is much greater, the resin may settle under its own weight.

Elution of BSC-187 was improved somewhat by stirring the resin. Figure 5.62 compares elution curves of Column QQ and Column Z, both of which were eluted at 40°C with 0.4M HNO_3. Column QQ was stirred before each sample of eluate was taken and Column Z was not stirred. The eluate of Column QQ reached 0.1 C/C0 in 10 cv versus 27 cv for Column Z.

In an earlier study (Figure 5.63), BSC-187 was loaded with cesium (Savannah River Site simulant) and eluted with 1M formic acid at 35°C to 50% C/C_0 (Bray et al. 1990). There is evidence of tailing in the first set of runs (Runs 1, 2, and 3). Even after 28 cv, the columns had still not reached $C/C_0 < 0.01$. This resin was loaded and eluted once again under similar conditions. Surprisingly, the second elution cycle (Runs 4, 5, and 6) required significantly less eluant to reach a C/C_0 of 0.1 than the first cycle runs and showed little evidence of tailing. For all runs, approximately 99% of the cesium was eluted in less than 10 cv.

The causes of the double peak in C/C_0 during the more recent BSC-187 resin runs remain unknown. One possible cause is a chromatographic effect. The initial peak would be caused when acid elutes cesium from the bottom of the column. Cesium eluted from the top of the column would not leave in the eluate, but would move to the bottom of the column, where its elution would cause the second peak. Another possible cause of the initial decrease in cesium elution is that the bed begins to shrink and agglomerate; a chemical or

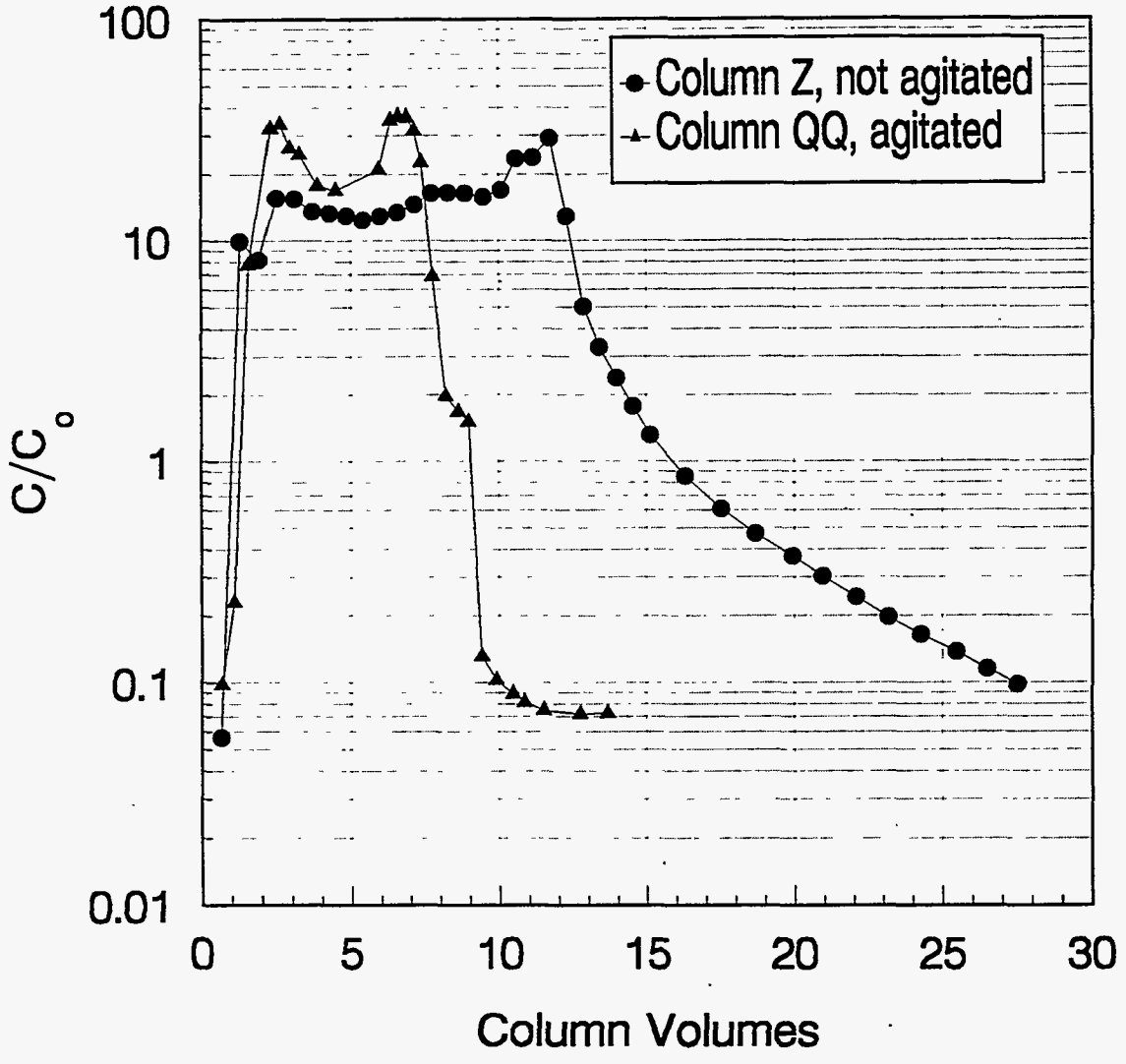

Resin: R-F
Loaded with: NCAW
Temperature: 40°C
Eluant: 0.4M HNO_3
Flow rate: 1 cv/h, 200 mL/h
Column QQ is stirred, Column Z is not
Run 9: Columns V, W, X, Z
Run 10: Columns PP, QQ, RR

Note: Column QQ was stirred after each sample was taken throughout the run to break up clumps of resin.

FIGURE 5.62. R-F Resin Elution With and Without Stirring

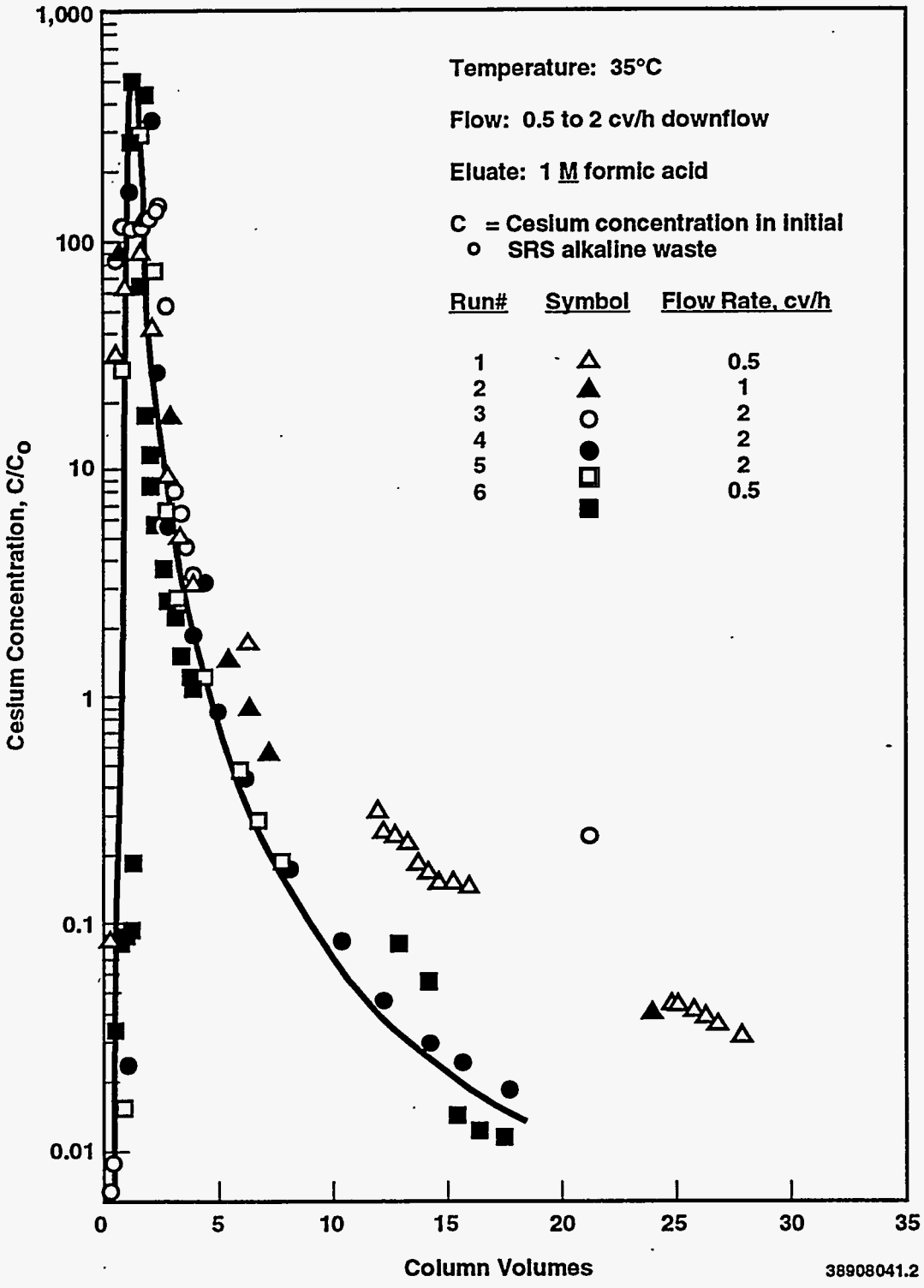

FIGURE 5.63. Cesium-Elution Profiles of SRS Simulant-Loaded BSC-187 Ion-Exchange Resin With Formic Acid

hydrodynamic effect then causes the bed to settle or shifts slightly, exposing the center of the agglomerated resin to the eluant. This, in turn, generates the temporary increase in cesium elution efficiency.

A third possible explanation for the double peak found in Runs 8 and 9 is that elution of another cation during the cesium "valley" slowed its elution. To investigate this possibility, the elution profiles of sodium, cesium, potassium, and rubidium during the elution of Run 9 Column V with 1M HCOOH were measured by flame atomic adsorption. Figures 5.64 to 5.66 show the cesium, potassium, sodium, and rubidium concentrations of the eluant as a function of column volumes of acid. No cation has a large concentration peak which would cause the cesium "valley" to occur. However, these curves have several other interesting features.

The cesium concentration profile shows a peak at 8.5 cv (Figure 5.64), consistent with the second peak in the corresponding C/C_0 elution curve (Figure 5.62). During elution, $[Na^+]$ in the eluant drops rapidly during the first 5 cv and then more slowly (see Figure 5.65), and $[Cs^+]$ begins to rise to its second peak just after the decrease in the slope of the $[Na^+]$ profile. Thus for the R-F resin, the cesium elution mechanism may be related to the amount of sodium remaining in the resin; once a critical amount of sodium has been exchanged with hydrogen, the cesium seems to elute at a faster rate. The rubidium ion concentration in the eluant increases to a second maximum at the same time (Figure 5.66). Thus, elution of rubidium and cesium may be controlled by similar mechanisms. Figure 5.67 shows $[Na^+]:[Cs^+]$ in the eluant as a function of column volumes of formic acid. The $[Na^+]:[Cs^+]$ is near 20 after 2 cv, and remains below 20 for the rest of the samples analyzed, up to 9.5 cv.

5.2.4 Elution Modeling

An elution model was developed to clarify some of the characteristics of column elution. This model is basically the same as the loading model, except for the boundary conditions. Rather than an assumed initial cesium concentration on the solid of zero, the column is assumed fully loaded.

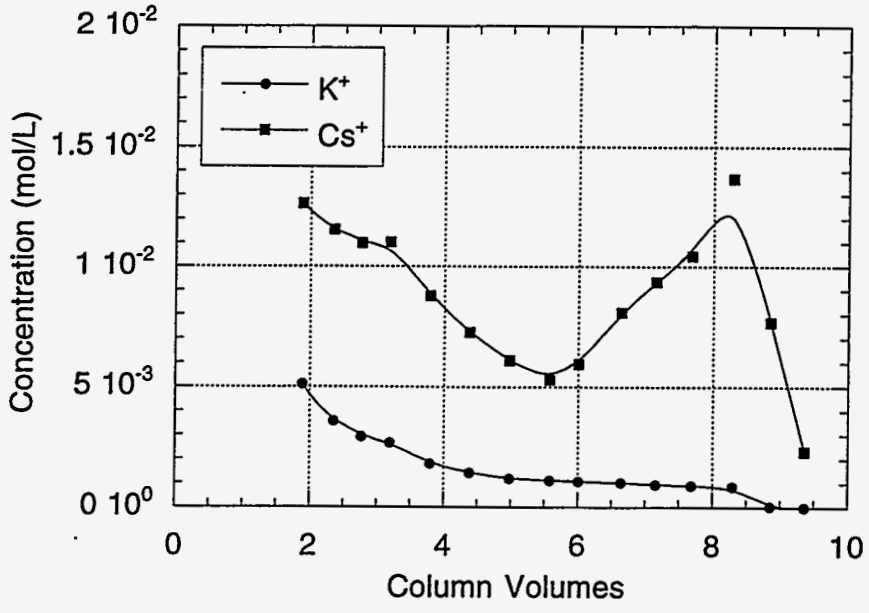

FIGURE 5.64. Cesium and Potassium Ion Concentration Profiles During the Elution of Column V. (R-F Resin, 1M HCOOH, 1 cv/h)

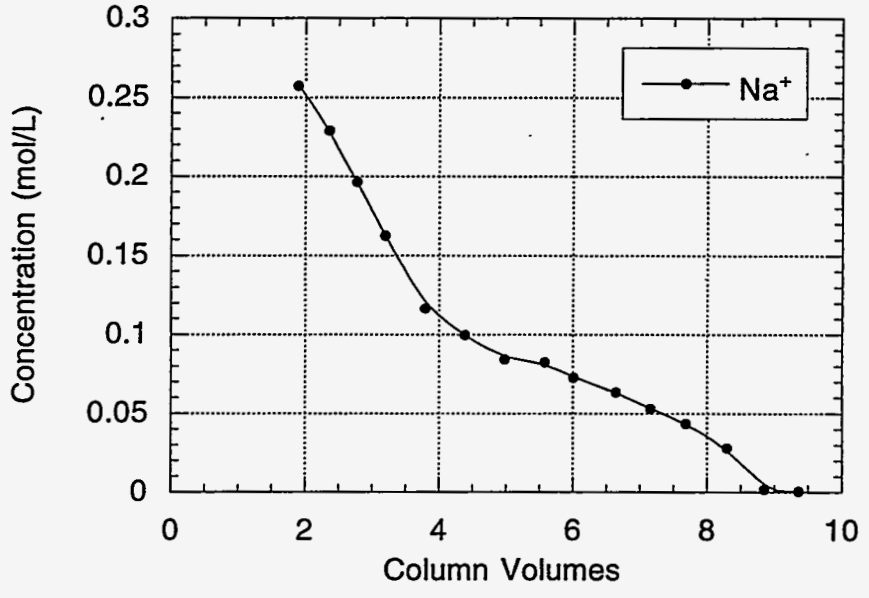

FIGURE 5.65. Sodium Ion Concentration Profile During the Elution of Column V (R-F Resin, 1M HCOOH, 1cv/h)

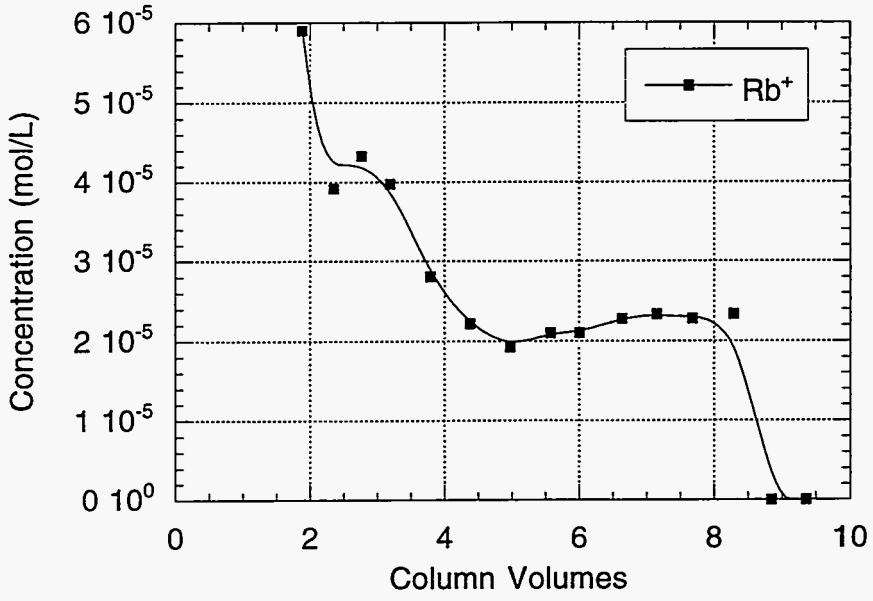

FIGURE 5.66. Rubidium Ion Concentration Profile During the Elution of Column V

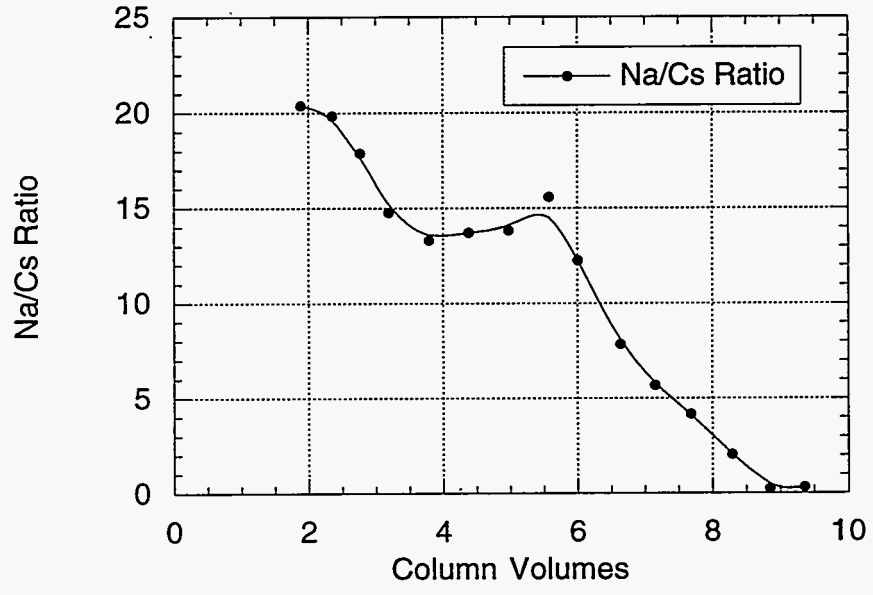

FIGURE 5.67. Sodium/Cesium Mole Ratio During the Elution of Column V

Furthermore, the eluant does not contain cesium. The driving force for cesium exchange is assumed to be linear and particle-diffusion control is assumed to be the rate-limiting step. A Freundlich isotherm is used to describe the equilibrium ratio of cesium in the liquid to cesium in the solid.

Dividing the elution curve into four sections (neutralization, peak, exponential decay, and tailing) helps explain the model. Based on the pH of the column effluent, the neutralization of the resin occurs during the initial flat portion of the elution curve before it rises to the peak C/C_0 value. This region is especially significant for 0.1M and 0.05M HNO_3 dilute eluant concentrations; several column volumes of acid pass through the column eluting very little cesium. The variations in acid concentration down the length of the column make it difficult to model this phenomenon; it has not been attempted here. Because neutralization is based almost entirely on the total moles of acid throughput rather than flow rate or acid concentration, higher flow rates and acid concentrations would be preferable.

After the elution curve reaches a peak, the cesium concentration drops until it reaches the exponential decay region. This region is associated with mass-transfer limitations and is the limiting case of fastest cesium removal. In this region, acid concentration does not impact the rate of cesium removal; thus lower concentrations may be warranted. Lower flow rates will decrease the amount of eluant required under these circumstances.

In some cases, the cesium concentration does not drop as quickly as predicted by exponential decay. Instead, cesium bleeds off over the course of several column volumes without a significant decrease in concentration. The reason for this "tailing" effect is not clear. Tailing at low concentrations could be the result of the background influencing the cesium count. It has also been postulated that cesium removal occurs quickly near the surface of the resin particles; as the elution progresses, the cesium deep within the particles is more difficult to remove. For the R-F resin, most of the "tailing" effect is due to channeling.

The elution model cannot describe all the sections of the elution curve because it cannot describe the behavior of the resin over the entire range of acid concentrations. The model assumes that throughout the run cesium is in equilibrium with a constant acid concentration all the way down the column. Therefore, the model rises to its maximum value in <1 cv. In reality, the concentration of acid in the elution experiments is not constant, even after the initial flat neutralization region. Thus, the model can describe the concentration gradient only after the acid concentration is constant, which is usually after the peak. This limitation creates the problem of determining the concentration of cesium throughout the bed after the peak, since a significant amount of cesium has already left the column. Due to this limitation, the model will be used to describe only the equilibrium and exponential decay regions of the elution curves. In addition to this limitation, the mathematical model of elution has all the same limitations as the loading model.

When eluting the column, it is necessary to determine the quantity of eluant required. Proper elution modeling will determine how much the waste can be concentrated and the quantity of waste that will be produced. The amount of eluant required is based on the level of cesium that DF requirements will permit on the solid at the exit of the column. Current laboratory experiments provide information about the concentration of cesium in the liquid exiting the column, but not the concentration of cesium on the solid during elution. The solid concentration can be determined experimentally by counting the solid sample after elution or by a cesium mass balance. It can also be determined through the use of mathematical modeling. The current elution model was created for this purpose.

The current model cannot fully describe the cesium concentration on the solid; however, the modeling efforts have clarified several important features of the elution process. For example, if the elution is mass-transport-controlled only (not controlled by the acid concentration), the concentration of cesium on the solid throughout the column can be described by

$$\frac{\bar{C}_s}{\bar{C}_{s,initial}} = e^{-k*t} \qquad (5.18)$$

where k is the mass-transport coefficient (which can be related to $k_p a$ or $k_f a$), $\bar{C}_s$ is the concentration of cesium on the solid, and t is time. For total equilibrium control (relatively fast exchange rate), the cesium concentration on the solid can be determined by

$$\bar{C}_s = C_{effluent} \lambda \qquad (5.19)$$

where λ is the nondimensional distribution coefficient at the appropriate pH condition and $C_{effluent}$ is the cesium concentration exiting the column. Most cases have both mass-transport and equilibrium influences, making modeling even more difficult and analytical expressions impossible. The current model can account for both of these influences, but not the "tailing" and neutralization region of the elution curve. Future efforts will focus on describing the entire elution process.

5.2.4.1 Elution Modeling of CS-100

Three tests of CS-100 resin eluted with 1M HCOOH and 0.1M HNO_3 (Runs 3, 5, and 7) were compared to the elution model. The model was used to describe only the characteristics of the mass transfer (exponential decay) region. The particle-phase-controlled mass-transfer coefficients derived from fitting the model to the data are shown in the Table 5.15. A six-fold flow rate increase results in a 2.5- to 3-fold increase in mass-transfer coefficient, which is roughly equivalent to the square root of 6 (2.449) increase predicted by the film-diffusion-controlled correlation. If the system were particle-phase

TABLE 5.15. Mass-Transfer Coefficients During Elution of CS-100

Run #	Eluant	Temperature (°C)	Flow rate (cv/h)	Mass Transfer (min^{-1})
7Q	1 M Formic	25	1	0.04
3D	1 M Formic	25	6	0.10
5K	1 M Formic	40	6	0.14
7O	0.1 M HNO_3	25	1	0.05
1A	0.1 M HNO_3	25	6	0.14
5I	0.1 M HNO_3	40	6	0.18

controlled, it would require equal time to elute the columns at both flow rates and thus 6 times the volume. An example of the fitting of the elution curve for Run 70 is shown in Figure 5.68.

A 15°C increase in temperature also resulted in an increase in mass-transfer coefficient, which is consistent with increased ion diffusivity. Mass transfer appears to be similar for both formic and nitric acid, although slightly higher for nitric acid.

The mass-transfer coefficient for eluting is much higher than that for similar runs during loading. The increased mass transfer could be the result of higher diffusivities during elution both in the particle and film phases. Furthermore, the process appears to be controlled by film diffusion rather than particle diffusion during elution.

Modeling the elution curve peak required that the equilibrium behavior of the resin be determined. Fitting the results of the 0.1M HNO_3 runs yielded λ values ranging from 4.0 to 5.0 ($\bar{C}_s/C_l$). The 0.05M HNO_3 runs should yield slightly higher λ values based on their maximum peak values. These λ values are not unreasonable when compared to Figure 5.5. The formic acid runs do not appear to be equilibrium-based, thus they were not included. The tailing effect was seen only in those runs which had higher flow rates or lower acid concentration.

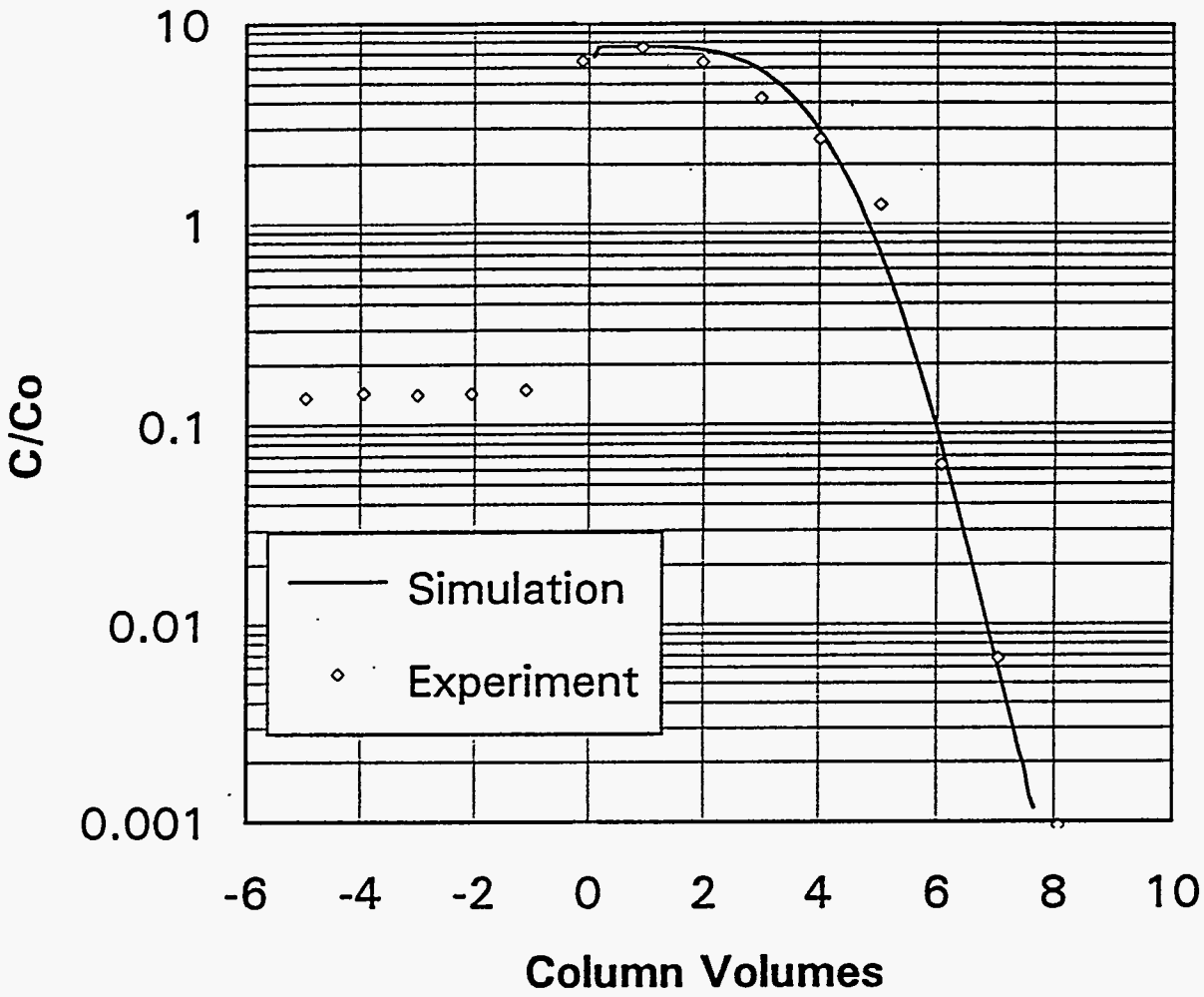

FIGURE 5.68. Comparison of Experimental Cesium Elution Results for Run 7 (Column 0) with CS-100 and Simusolv™ Elution Model

In an attempt to determine approximate quantities of effluent required to remove the cesium to the levels required, Column 7Q and 7O models were analyzed. Assuming a decontamination factor of 55,200 for 5M Na^+ NCAW and an initial cesium concentration of 5×10^{-4}M in the feed, the maximum concentration of cesium in the liquid during loading that can exit the column is 9.1×10^{-9}M. Extrapolating the equilibrium data to a $[Na^+]:[Cs^+]$ ratio of 5.5×10^8, the cesium concentration on the solid at the exit of the column after elution should be 1.8×10^{-6} moles/L of bed.

Column Q is assumed to be limited by mass transfer, therefore the concentration is related to the time of elution. With the mass-transfer coefficient determined previously and a loading of 30 cv of NCAW, the resin should be eluted for 233 min or 4 cv after reaching the mass-transfer-limited region. The C/C_0 in the effluent at this concentration on the solid is 9×10^{-3}. Column O is assumed to be equilibrium-controlled with an initial λ in the acidic eluant of 4. With the mass-transfer coefficient determined previously and a loading of 30 cv, the resin in this case should be eluted for 13 cv or 780 min after neutralization. The C/C_0 for the elution of Column O is 8.6×10^{-4}.

5.2.4.2 Elution Modeling of R-F Resin

Most of the elution curves for the R-F resin are not as well behaved as the CS-100 curves. All of the BSC-187 runs had double peaks and/or tailing effects, apparently because the resin agglomerated. Only the two column runs performed with the newer BSC-210 batch provided acceptable elution curves and could be appropriately modelled. Both were eluted at 40°C and 1 cv/hr using 1M formic acid. Column 10Y was originally loaded with NCAW and the particle-phase diffusion mass-transfer coefficient was 0.01 min^{-1}. Column 16SS was loaded with DSSF and the particle-phase diffusion mass-transfer coefficient was 0.02 min^{-1}. Similar to loading, the mass-transfer coefficient during elution of R-F is significantly lower than CS-100 resin. It is not known if the difference between mass-transfer coefficients of the two runs is significant.

5.3 CHEMICAL AND RADIATION STABILITY

The chemical and radiation stability of resins is an important variable in assessing their useful life. The organic resins are degraded by the chemical cycling between the sodium form (loading phase) and the hydrogen form (elution) and by radiation damage. Their loss of capacity may be either from loss of ion-exchange sites or from loss of the characteristics that give the resin selectivity for cesium.

It is typical of organic resins that the capacity decreases exponentially with the number of the cycles according to the following:

$$\lambda = \lambda_o \exp(-aN) \qquad (5.20)$$

where N = the number of cycles

a = the empirical coefficient

The value of a is determined by a regression of the λ values as a function of the cycle number.

Resin performance was determined as a function of exposure to radiation in a ^{60}Co source gamma pit. Deterioration of resin performance typically follows an exponential decay curve. The distribution coefficient (K_d) for cesium uptake was used as an indicator of radiation damage to the resin material. Gases released during the experiment and organic materials found in the aqueous solution were measured and identified. Stainless steel coupons were placed in the reaction vessels to assess corrosion during testing.

5.3.1 Chemical Stability of CS-100 Resin

An extensive investigation into the chemical stability of the CS-100 resin was performed at ORNL (Chilton 1981). In these experiments, two columns of the CS-100 were cycled simultaneously through 30 cycles. One column was regenerated with 0.1M NaOH (converted to the sodium form) before loading and the other was loaded with resin in the hydrogen form. The composition of the feed to the columns was not given, but it apparently contained sodium, calcium, ^{90}Sr, and ^{137}Cs and had a pH >11.85. The number of column volumes processed to the 50% breakthrough point suggests that the feed was dilute relative to the tank wastes. Adding an alkaline feed to a column of resin in the hydrogen form would also convert the resin to the sodium form. The volume of feed processed was recorded at 10% and 50% breakthrough with similar results

for both columns. Each loaded column was eluted with 10 cv of 0.5M nitric acid and rinsed with water.

From the graphical presentation of the data in the report, it appears that the resin capacity (or selectivity for cesium) decreased at a rate of approximately 2% to 3% per cycle. Thus, the value of a in Equation (5.20) was 0.02 to 0.03. There was considerable variability during the testing, but no reason was suggested. A likely possibility is changing feed composition, since the performance of the two columns varied in a similar manner. It is not known how applicable those results are to the existing CS-100 resin since it is now prepared by a different manufacturer. However, since the polymer structure is quite similar, it is likely that the resin degradation will be similar.

5.3.2 Chemical Stability of the R-F Resin

Testing with the R-F resin was less extensive (Bray et al. 1990). In this work, a reasonable estimate of the capacity loss was 20% after the completion of 7 loading/elution cycles, or about 3%/cycle. Considerable uncertainty was associated with this value as the λ values varied considerably from run to run.

5.3.3 Radiation Stability of the CS-100 Resin

Cesium distribution coefficients were determined for untreated (no gamma) CS-100 resin and resin that had been irradiated for various intervals up to ~10E9 Rad. The resin was tested under flowing conditions or in a static solution. Gases generated during static testing of CS-100 resin were collected and analyzed. A coating formed on the test corrosion coupons for the static-irradiation test; in the static-nonirradiation test, no coating layer or visible corrosion was observed. The initial radiation study yielded the following findings:

- The Cs K_d values for the static tests were always lower than for the flowing system.

- A small decrease in Cs K_d as a function of radiation dose occurred in both the flow and static tests. In the flow tests the Cs K_d values were still within 10% of the initial untreated resin value after a dose of $>10^8$ Rad.

- Hydrogen was the most abundant gas produced (0.021 moles/kg of resin after 5.4E8 Rad), followed by nitrogen, nitrous oxide, and oxygen. The relative amounts of the production of these gases is consistent with the organic resin material acting as a source of reductant within the system.

- The observed coating on the irradiated coupons was a precipitated oxide of aluminum. During nonflowing conditions in plant operations, the precipitate could foul the resin and clog the facilities, requiring costly and time-consuming repairs.

5.3.4 Radiation Stability of R-F Resin

The only information available for the R-F resin is the gas generation work and the corrosion studies.

- Gases generated during static testing of R-F resin were collected and analyzed. The results for the R-F resin were similar to those observed for the CS-100, with the exception that the R-F resin did not release oxygen during the test. Instead, the R-F resin scavenged the hydroxide radical. which is the product of the radiolysis of water. In a solution containing no resin, the hydroxide radical can interact with other hydroxide radicals and hydrogen radicals to form oxygen, hydrogen, and water. When the R-F resin is present, the hydroxide radical interacts with hydrogen atoms on the aromatic ring, causing oxidation of the resin material.

- As occurred in the CS-100 test vessel, a coating formed on the test corrosion coupons only during the static-irradiation test. No coating layer or visible corrosion was observed after any other test.

6.0 ASSESSMENT OF PROCESS CONDITIONS

Several alternative operating conditions and process configurations for removal of cesium from NCAW and DSSF by ion exchange are now under investigation. Comparisons among them are based on the experimental work and mathematical models of Section 5.0. This section describes trends and potential uses of the data without formally recommending any choice of resin or operational scenario. Analytical approach and assumptions are presented in Section 6.1. Sections 6.2 and 6.3, respectively, examine possible operating conditions for NCAW in detail and for DSSF only in contrast with NCAW. Finally, Section 6.4 presents alternatives to the baseline processing configurations.

6.1 ANALYTIC APPROACH AND ASSUMPTIONS

The baseline scenario is a semi-continuous, regenerable ion-exchange system in which several columns are loaded in series in a carousel configuration. The lead column is taken offline for elution and regeneration when it is nearly loaded or when the breakthrough on the last column reaches a specified C/C_0. While the columns are being loaded with waste, one reserve column is being eluted and regenerated. The second column then takes the lead, and the freshly regenerated column is placed last in the series, so that the resin with the least cesium is the last to contact the feed. The carousel arrangement permits continual operation, if the elution-and-regeneration cycle time is balanced with the loading time.

The elution-and-regeneration cycle for this baseline scenario can be described as follows.

- Following the loading cycle, the column is washed with 3 cv of 2M NaOH to remove the feed solution from the column and prevent aluminate precipitation.
- Wash with 6 cv of H_2O to remove the NaOH.
- Elute with acid to remove the Cs^+ and Na^+ ions from the resin. The quantity required varies according to the resin, eluant and loading characteristics and the required extent of elution.
- Wash with 6 cv of H_2O once again to remove any residual acid.

- Regenerate with 3 cv of 2M NaOH to load the sites with Na^+ ion. The column is now ready for loading waste once again.

With the exception of elution, these steps are assumed to be carried out at a flow rate of 2 cv/hr. Thus, excluding the elution time, the regeneration cycle requires 9 hours. The above quantities and flow rates were used in the experimental work described in Section 4.4 and are believed to be very conservative. It is thought that the volumes could be reduced to 1 cv of 2M NaOH and 2 cv for each of the washes for a total offline time of 3 hours plus the elution time. Optimized values should be sought in future work.

The design objectives of the ion exchange process are 1) achieving the Cs DF, 2) minimizing the impact on the HLW-glass product, 3) minimizing the quantity of eluant (volume and moles of acid), 4) allowing continuous operation, and 5) minimizing the size and number of ion-exchange columns. All the objectives are interrelated, and each must be adjusted to achieve an optimum.

The feed to the columns is assumed to be NCAW containing 5M sodium or DSSF containing 7M sodium. The cesium concentrations in the feed (based on the simulant composition given in Table 4.1 and the isotopic ratio given in Table 3.2) are 2.25 Ci/L for NCAW and 0.208 Ci/L for DSSF. The limit for ^{137}Cs in the glass is Class A or <0.4 Ci/m^3 at 5M sodium in the effluent from the ion-exchange system. The required DF is estimated to be 5600 for NCAW and 520 for DSSF.

It is assumed that scale-up can be based solely on the residence time of the feed in the column, as discussed in Section 2.3. Data from Table 6.1 were used to model column loading and breakthrough curves. The Fruendlich parameters and the mass-transfer coefficients are based on data from Section 5.2. The maximum cesium concentration in the liquid is based on the cesium in the feed and the required DF.

The quantity of eluant required is based on the estimated amount required to elute the resin to the extent that the maximum cesium concentration is not exceeded on the next loading cycle. The maximum cesium concentrations on the resin at the conclusion of the elution were determined using the equilibrium data (Cs λ at the required [Na^+:Cs^+]). The cesium concentration in the liquid used was determined using the required DF during

TABLE 6.1. Data Used to Model Column Loading

Parameter	Resin	NCAW	DSSF
Freundlich Exponent	CS-100	0.834	0.845
	R-F	0.734	0.754
Freundlich Coefficient (moles, cm^3)	CS-100	2.70	1.07
	R-F	3.82	2.80
Mass Transfer Coefficient (min^{-1})	CS-100	0.02	0.013
	R-F	0.01	0.0029
Max. Final Cesium Concentration on Resin, elution (M)	CS-100	1.2×10^{-5}	3.2×10^{-6}
	R-F	1.3×10^{-4}	8.6×10^{-5}
Max. Cesium Conc. in Liquid in Last Column in Series, loading (M)	--	9.0×10^{-8}	1.9×10^{-7}

loading. The elution rate of the cesium is assumed to be limited by mass transfer with the cesium evenly distributed throughout the column.

The estimated impact of cesium ion exchange on HLW-glass production is based on $[Na^+ + K^+]:[Cs^+]$ in the eluate. Section 3.2 showed the $[Na^+ + K^+]:[Cs^+]$ in the eluant can be as high as 1500 without affecting the total volume of glass. If sodium and potassium have similar properties in the glass, the same ratio can be applied to the processing configurations.

6.2 OPERATING CONDITIONS FOR NCAW

Although the baseline of the NCAW waste is a 5M sodium solution, results of the distribution coefficient measurements in Section 5.1 permit comparisons of the amount of waste that can be processed at various dilution factors. Table 6.2 shows that, for both CS-100 and R-F resins, more original concentration waste can be processed at 5M Na^+ than at 1M Na^+. Similar trends exist for CC waste. Therefore, in the case of CS-100 and R-F there is a benefit to not diluting the waste prior to processing. In some cases, it may even be beneficial to concentrate the waste before processing although too much concentration will precipitate waste components.

TABLE 6.2. Effect of Dilution: Volume of Original Concentration* Waste Processed

Sodium Molarity	Dilution Factor	Liters of Waste for CS-100	Liters of Waste for R-F
5	1	33	204
3	1.667	29	183
1	5	22	145

* Assuming 5M initial feed, $[Na^+]:[Cs^+] = 10^4$, and 25°C.

Figure 6.1 shows the relationship between exit C/C_0 and percent loading of CS-100 or R-F resin in a single column. For the more selective R-F resin, percent loading is much higher than the percent loading on CS-100. As the flow rate is increased, percent loading decreases for a given C/C_0. Increased flow rate impacts CS-100 more strongly than R-F.

Figure 6.2 shows the relationship between flow rate, column loading, and number of columns required in series if the final column is taken offline just before breakthrough at the Class A limit. Percent loading on the first column

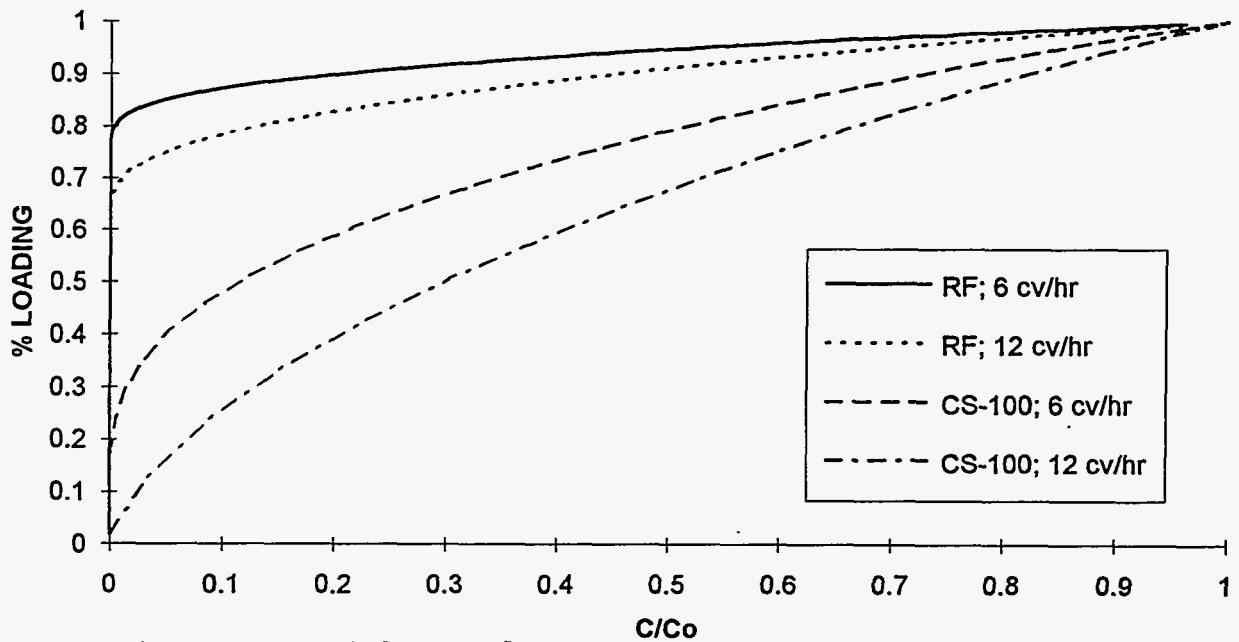

Note: C/Co at exit of first column
Waste is assumed to be NCAW

FIGURE 6.1. Loading on the First Column as a Function of Breakthrough

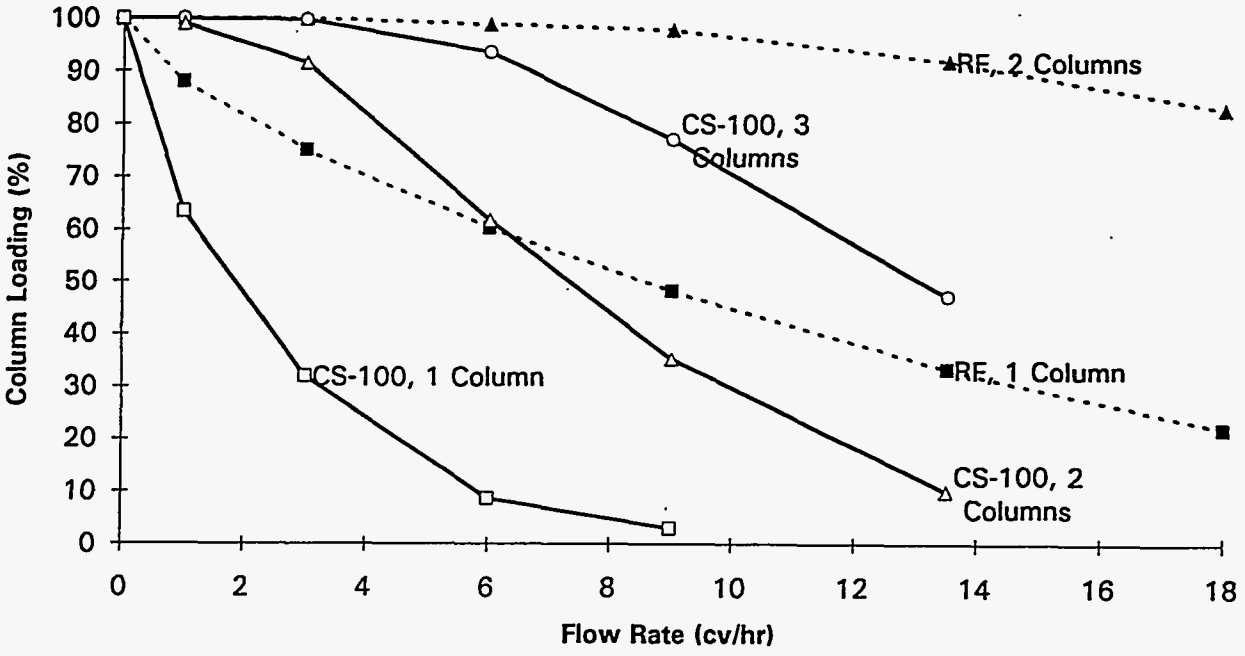

Note: Breakthrough on the last column corresponds to Class A limit in LLW Waste is assumed to be NCAW

FIGURE 6.2. Loading on the First Column as a Function of Flowrate and Number of Columns

increases if flow rate is decreased or if the number of columns in series is increased. With R-F resin, two columns in series would be sufficient for reasonably high loadings over a wide range of flow rates (>90% loading of first column for flow rates up to 14 cv/h); CS-100 would require a 3-column series unless the flow rate were low (>90% loading of first column for flow rates up to 4 cv/hr). For either resin using a single-column system, higher percent loadings are only possible at flow rates of less than 1 cv/hr.

The total online amount of CS-100 (3 columns) and R-F resin (2 columns) and the corresponding processing rate (column volumes per hour) required to process NCAW at 20 gpm (76 L/min) are shown in Table 6.3. Decreasing the flow rate increases either the time or the size of the columns required to process a given quantity of waste. The incentive for very high column throughput rates with CS-100 will probably be limited by the time required for washing, elution, and regeneration of the columns (Table 6.4). With R-F resin,

TABLE 6.3. Loading Conditions with NCAW (5M Na^+)

	CS-100: 3 Columns		R-F: 2 Columns	
Flow Rate (cv/h)	Loading Time (h)	Total Resin Volume* (gallons)	Loading Time (h)	Total Resin Volume* (gallons)
2	15	1800	94	1200
3	10	1200	63	800
6	5	600	31	400
9	3	400	21	270
13.5	1	270	13	180

* Resin volume is based on minimum bed required for 20 gpm flow rate.

continuous loading (with single-column elution) should be achievable even at the higher flow rates, because the time for elution (See Table 6.5) is less than the loading time. The total volume of resin would be significantly higher for CS-100 than for R-F, both because of its requirement for more columns and its lower throughput.

TABLE 6.4. Elution Conditions for CS-100 Resin Loaded with NCAW

Flowrate (cv/h)	Eluant	cv required to elute*	Total Acid Used (moles)+	Total Hours to Elute and Regenerate Column**
1	1M HCOOH	4	0.8	13
1	0.1M HNO_3	12	0.24	21
1	0.05M HNO_3	23	0.23	32
6	1M HCOOH	8	1.6	10.3
6	0.1M HNO_3	16	0.32	11.7
6	0.05M HNO_3	23	0.23	12.8

* Based on Runs 1, 3, and 7.
+ Assuming a 200 mL column.
**Includes 9 hours for washing and regeneration steps; washing and regeneration time can probably be reduced to 3 hours.

Table 6.4 shows the elution conditions for CS-100 loaded with NCAW. Fewer moles of acid are required when CS-100 is eluted with nitric acid than with formic acid. At higher acid concentration, both the volume of eluant and the time to elute is reduced. However, the total number of moles of acid required to elute is increased. Higher flow rates also reduce elution time but increase the total moles and volume of eluant required. The acid concentration and flow rate will be adjusted according to the tank farm specification and final waste form requirements.

As mentioned in Section 5.2, most of the elution runs for R-F failed to elute the cesium sufficiently. Column Y, which contained a new batch of R-F (BSC-210), gave the only acceptable elution curve for NCAW-loaded R-F resin (see Table 6.5). Roughly 2 times more total moles of acid are needed to elute R-F resin than CS-100. However, because R-F loads more cesium, it requires less acid to process the same volume of waste.

TABLE 6.5. Elution Conditions for R-F Resin Loaded with NCAW

Flowrate (cv/h)	Temp (°C)	Eluant	cv required to elute*	Total Acid Used (moles)+	Total Hours to Elute and Regenerate Column**
1	40	1M HCOOH	6	1.2	15

* Based on run 10.
+ Assuming a 200 mL column.
** Includes 9 hours for washing and regeneration steps; washing and regeneration time can probably be reduced to 3 hours.

To determine if elution impacts the quantity of HLW glass produced, $[Na^+ + K^+]:[Cs^+]$ in the eluate was measured for the two resins. Estimation of $[Na^+]:[Cs^+]$ was based on the assumption that the lead column was 100% loaded to equilibrium and that the sites not occupied by cesium are occupied by sodium or potassium. The resin capacity given in Section 5.1.2 suggests that $[Na^+ + K^+]:[Cs^+]$ in the eluate will be approximately 65 for CS-100 and 11 for R-F. Since these values are significantly lower than the suggested limit of 1500, the NCAW eluate is not likely to increase the amount of HLW glass. In order to neutralize the acidic eluant for tank farm specifications,

significant quantities of NaOH would be required. This analysis assumes that such a neutralization of the eluant is not required.

6.3 OPERATING CONDITIONS FOR DSSF

Figure 6.3 shows the percent column loading and number of columns in series required as a function of DSSF flow rate for CS-100 and R-F resin. As in Figure 6.2, these data assume that the final column is taken offline just before breakthrough to produce a Class A final-waste form. Although these curves are similar in shape to those of NCAW, the loading at any given flow rate is substantially less. For CS-100, a three-column configuration for DSSF processing would require less than 2 cv/hr to obtain high column loading on the first column, in contrast to the 6 cv/hr required for NCAW processing. For DSSF flow rates >2 cv/hr, a 4-column series may be more appropriate, so that more column capacity is used.

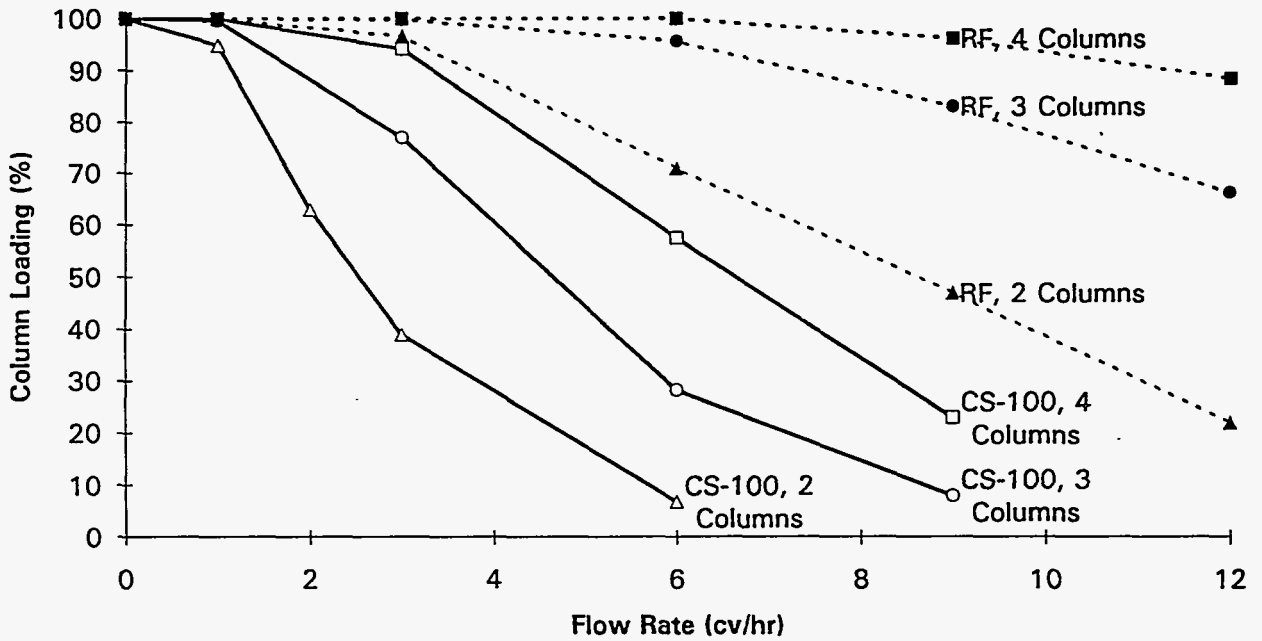

Note: Breakthrough on the last column corresponds to Class A limit in LLW Waste is assumed to be NCAW

FIGURE 6.3. Loading on the First Column as a Function of Flowrate and Number of Columns

Effects are similar, but less dramatic, when R-F resin is loaded with DSSF simulant. A 2-column system for DSSF operating at 6-12 cv/hr would make inefficient use of column capacity, and at least three R-F columns should be used for flow rates >9 cv/hr. Processing DSSF with even a 2-column R-F system would use resin capacity more efficiently than would a 4-column CS-100 system.

Table 6.6 shows the effect of DSSF flow rate on loading time and resin volume required at a flowrate of 20 gpm. A greater total online resin volume is required to process DSSF at the same flow rate as NCAW (Table 6.3), because a slower flow rate and more columns in series are needed. The loading time is greater than the regeneration cycle for loading rates of < 1 cv/hr or < 9 cv/hr for CS-100 or R-F resin, respectively. At these rates, the loading portion of the process could be operated continuously.

TABLE 6.6. Loading Conditions with DSSF (7M Na^+)

	CS-100: 4 Columns		R-F: 3 Columns	
Flow Rate (cv/h)	Loading Time (h)	Total Resin Volume* (gallons)	Loading Time (h)	Total Resin Volume* (gallons)
1	13.7	4800	161	3600
3	4.3	1600	53	1200
6	1.3	800	26	600
9	0.3	530	15	400
12	--	--	9	300

* Resin volume is based on minimum bed required for 20 gpm flow rate.

The elution conditions for CS-100 loaded with DSSF are shown in Table 6.7. All elutions were performed at 6 cv/h and 25° or 40°C. As with NCAW, higher acid concentrations require less volume of eluant and time to elute but more total moles of acid. The 0.1M nitric and 1M formic acid data show that less eluant is required at the higher temperature. This could be caused by greater hydrogen ion activity, cesium diffusivity, or both at the higher temperature.

TABLE 6.7. Elution Conditions for CS-100 Resin Loaded with DSSF

Flow Rate (cv/h)	Eluant	Temp (°C)	cv required to elute*	Total Acid Used (moles)+	Total Hours to Elute and Regenerate Column**
6	1M HCOOH	25	4.5	0.9	9.8
6	1M HCOOH	40	3.8	0.76	9.6
6	0.1M HNO_3	25	22	0.45	12.8
6	0.1M HNO_3	40	15	0.31	11.6
6	0.4M HNO_3	40	7.4	0.59	10.2

* Based on Runs 11 and 13.
+ Assuming a 200 mL column.
** Includes 9 hours for washing and regeneration steps; washing and regeneration time can probably be reduced to 3 hours.

Column SS was filled with a new batch of R-F resin, BSC-210, and loaded with DSSF. The column was then eluted with 1M formic acid (Table 6.8). As with NCAW, elution of R-F required more acid than did CS-100, but because R-F resin is more selective during loading, the cesium concentration factor is much higher than CS-100.

TABLE 6.8. Elution Conditions for the R-F Resin Loaded with DSSF

Flow Rate p(cv/h)	Temp. (°C)	Eluant	cv required to elute*	Total Acid Used (moles)+	Total Hours to Elute and Regenerate Column**
1	40	1M HCOOH	4.2	0.7	13.2

* Based on Run 16.
+ Assuming a 200 mL column.
** Includes 9 hours for washing and regeneration steps; washing and regeneration time can probably be reduced to 3 hours.

For processing DSSF on CS-100 or R-F resin, the estimated $[Na^+ + K^+]:[Cs^+]$ is 1200 or 100, respectively. The R-F value is acceptable, but the CS-100 value may be unacceptably high if neutralization of the eluate is

required before disposal. Methods to decrease the $[Na^+]:[Cs^+]$ will be discussed in Section 6.4.

Overall composition of the Hanford tank wastes that will be sent to cesium ion exchange can also be evaluated. Column loading and the $[Na^+]:[Cs^+]$ can be approximated from an enhanced sludge wash of the overall contents of DST or SST. At [Na] = 5M and $[Na^+]:[Cs^+] = 2.3 \times 10^5$, a λ value of 58 and 650 can be assumed for CS-100 and R-F, respectively (based on the equilibrium data from NCAW). Therefore, the estimated $[Na^+ + K^+]:[Cs^+]$ for an enhanced sludge wash is approximately 770 and 70 for CS-100 and R-F resins. With CS-100, there may be concerns about the quantity of cations in the eluate, if neutralization of the eluate is required. For R-F resin, on the other hand, the low sodium concentration should not affect the HLW glass.

6.4 PROCESSING CONFIGURATIONS

Achieving optimal performance during loading and elution requires that several processing configurations be evaluated and compared to the baseline operational scenario. A few of these options and their advantages and disadvantages are discussed.

6.4.1 Once-Through Processing

The simplest ion-exchange configuration is the once-through process. When the lead column is fully loaded, it is taken offline, and the exchanger is sent to disposal as HLW. The column is loaded with new exchanger and placed online as the trailing column. This approach is used with the zeolite system at West Valley, New York (Kurath 1989). The advantages to this approach are as follows.

- High decontamination factors can be achieved since new clean resin is used for each cycle.
- Low volume of cesium concentrate (in solid form) is produced.
- Selection of exchange material can be based solely on cesium-loading properties, since elution properties are unimportant.
- Safety issues associated with acid eluants (auto-oxidation of organic resins by nitric acid, H_2 generation from the formic acid in the melter) do not exist.

- Equipment and maintenance requirements are reduced because less valving is required.

The disadvantages are as follows.

- The volume of HLW glass may be excessive, depending on the amount of discarded resin relative to the total organic carbon allowed in the high-level glass feed.
- Interim storage of cesium-loaded organic resins creates a safety hazard because of risk of gas generation due to resin radiolysis.
- The large quantity of resin (possibly more than 10 times that required for a regenerative system) required increases cost.
- Frequent and complete removal of resin from the column to maintain the required decontamination factor increases cost.

If disposal of the exchanger is unacceptable as a HLW, the cesium can be eluted and the resin can be disposed of after once through as LLW. Using this approach, both the interim storage requirements can be simplified and high DFs can be achieved.

6.4.2 Combined Once-Through and Regenerative System

In some cases, it is difficult to completely elute the ion-exchange columns in a regenerable system and still maintain the high required DFs. A combined regenerable/once-through approach may help address this problem by providing the "polishing" column following the regenerated columns to catch any residual cesium bleed. Thus, this hybrid could attain the high DFs of a once-through system and minimize resin use with a regenerative system.

Although such a system sounds promising, it is not without limitations. In most cases the λ value does not increase significantly at low cesium concentrations, but remains relatively constant. Thus, in some cases, the number of column volumes (λ) that can be processed at the high cesium concentration in the feed would be nearly the same as the number of column volumes that can be processed at the low cesium concentration sent to the polishing column. Therefore, the "polishing" column would load as quickly as the regenerable columns and would have to be removed as often. As a result, this system may require as much resin as the nonregenerable system.

The advantages of this approach are as follows.

- The guard column may provide higher decontamination factors than are possible for a regenerative system.
- The amount of resin to be disposed of would be reduced if the non-regenerable column loaded less rapidly than the regenerable column.
- The quantity of eluant might be reduced if the regenerable resin in the hybrid system requires less complete elution than the standard regeneration system.

Disadvantages are as follows.

- The polishing column might require changing as often as the regenerable columns, so that more exchange material would be used than in a once-through approach.
- The system equipment requirements would be at least as large as those of the regenerative system. Using two different types of resins may require even more equipment.

6.4.3 Elute Column and Reload Onto Exchanger

A fourth processing option is to follow an elution procedure similar to that for the regenerable column configuration. The resin would be loaded, taken offline, and eluted. However, rather than being sent its final disposal form, the eluate would be neutralized (if necessary) and passed through another set of ion exchangers. Because the eluate contains much less sodium and much more cesium than the original feed, it may be possible to further concentrate the cesium on either once-through or regenerative secondary columns. This process has the most merit if the cesium is reloaded onto an inorganic exchanger. The inorganic material would then be the final waste form.

The advantages to this approach are as follows.

- The once-through reloading process would yield less exchange material for disposal than the standard once-through approach.
- The volume of eluate and amount of sodium and potassium in eluate would be less for the regenerable reloading process.

Disadvantages are as follows.

- The analyses in Sections 6.2 and 6.3 suggest that $[Na^+ + K^+]:[Cs^+]$ in the resins is usually so low as not to warrant such an approach.

- Additional chemicals would be needed and more secondary waste would be produced; the eluate may need to be neutralized before passing through the secondary columns.

- Such a configuration would require at least one additional column, with piping, valving, pumps, tanks, and instrumentation.

- Higher concentrations of cesium on the column would increase the need for shielding and the possibility of radiolytic generation of gases in the column and eluate. Premature degradation of an organic secondary resin could also result.

6.4.4 Elute Two Columns in Series

A method of minimizing eluant use is to elute two columns in series. As discussed in Section 5.2, at the beginning of elution the resin requires some neutralization of residual NaOH before the cesium will begin to elute from the column. Near the end of elution, the acid removes only trace quantities of cesium and does not become neutralized. This configuration would use the relatively clean acid at the end of column elution to neutralize the residual NaOH in a second column being eluted. Thus, one column is undergoing the neutralization phase while the cesium is being eluted from the second column in series.

Advantages of such an approach are as follows.

- The quantity of eluant used would be reduced by using the same eluant to elute two columns.

- The columns could be better eluted than with simple regeneration, improving column DF.

Disadvantages are as follows.

- The equipment, operating, and maintenance costs would be higher than for single-column elution.

- The $[Na^+]:[Cs^+]$ would not be minimized using this approach. Thus, there would be no reduction in quantity of HLW glass produced.

6.4.5 Other Processing Options

The ion-exchange process could also be improved through more novel approaches. These approaches may be capable of reducing the quantity of eluant which will require storage and disposal as HLW glass. Although

numerous approaches exist, the three to be discussed are acid recycle, electrochemical elution, and electrochemical salt splitting.

After the eluant has passed through the column, it contains still contains large amounts of nitric acid. Both the water and the nitric acid can be removed from the cesium and sodium salts using an acid fractionator. The acid can be concentrated and used for future elutions. Furthermore, the volume of eluant is reduced, facilitating its storage.

When electrodes are placed in an aqueous solution, hydrogen ion is produced at the anode and hydroxide ion is produced at the cathode. In a salt solution, the cations are attracted to the cathode forming a metal hydroxide near its proximity. The anions are attracted to the cathode, producing the respective acid. Cation and anion exchange membranes are used to separate the anion, salt, and cation solutions, respectively. Thus, the salt solution can be converted to two separate streams: an acid and a base solution. Using this approach for ion exchange, nitric acid can be separated from the sodium and cesium even if the acid has been neutralized in the column during elution.

If an electrical field is produced in the presence of an ion-exchange resin, the cesium and sodium will leave the resin and move towards the cathode, allowing the hydrogen ion produced at the anode to replace the cations and elute the column. This process is called electrochemical elution. It can be coupled with standard acid elution to improve its efficiency and reduce the quantity and volume of eluant required.

6.4.6 Optimizing the Process Conditions

The simplest method to improve the process and reduce volume of waste is to optimize temperature and flow rate of eluant. Increase temperature tends to improve the elution process without increasing the amount of acid required and should be employed where possible to reduce the eluant requirements. The flow rate during elution need not be constant, but can be adjusted to minimize the use of eluant. A high flow rate could be used initially, until the neutralization (of residual hydroxide in column) and equilibrium phases of elution have been completed. As mass transfer begins to control cesium elution, flow rate could then be decreased. In some cases it might be beneficial to stop the flow of eluant and allow the cesium in the resin to

equilibrate with the eluate. These approaches would minimize both volume of eluant and time to elute the column.

The concentration of the eluant also does not have to be constant during operation. During neutralization, the total moles of acid are important, not the acid concentration. High acid concentration is needed only during the neutralization phase; at later stages, use of lower acid concentrations will minimize total moles of acid.

Some studies with other ion-exchange resins precede elution with a low-acid wash, called a "sodium scrub." In low concentrations, the acid will remove the sodium, leaving cesium on the resin until elution with the more concentrated acid begins. Use of the "sodium scrub" will reduce the $[Na^+ + K^+]:[Cs^+]$ in the effluent. In treating DSSF, this procedure may be necessary to get the $[Na^+ + K^+]:[Cs^+]$ below the point where it increases the volume of HLW.

7.0 CONCLUSIONS

This chapter presents the main conclusions and observations based on the information presented in the report. The conclusions are grouped into the categories of equilibrium behavior, kinetic (rate) behavior, radiation stability, chemical stability, resin fouling, elution behavior, and processing considerations.

Equilibrium Behavior

- Low temperature favors high cesium loading. The average cesium column distribution ratio (Cs λ) of the CS-100 resin doubles as the temperature decreases from 40°C to 10°C. For the same temperature change the Cs λ of the R-F resin increases about 40%. The actual percentage increase is a function of the experimental conditions and ranges from 65% to 150% for CS-100 and from 15% to 95% for R-F.

- Dilution of the waste decreases the cesium loading on the resins. For the wastes (NCAW, CC, DSSF) and conditions studied ([Na] <7M, T = 10° to 40°C), it appears that dilution of the waste decreases both cesium loading and the amount of waste that can be processed per quantity of exchanger. If D is the dilution factor (initial volume:final volume) the actual amount of waste that can be processed is proportional to D^{a} where a is about 0.24 for the CS-100 resin and ranges from 0 (no effect) for $[Na^+]:[Cs^+]$ >100,000 to 0.21 for $[Na^+]:[Cs^+]$ <10,000 for the R-F resin.

- Potassium inhibits cesium loading on the resins. The potassium present in DSSF ($[Na^+]:[K^+]$ = 7.4) appears to act through the competing cation effect. The Cs λ was about 14 in the column runs with DSSF (7M Na, $[Na^+]:[Cs^+] = 10^5$, 25°C) on CS-100 resin and about 38 in runs with CC (low potassium) waste at the same conditions. In the column runs with DSSF (7M Na, $[Na^+]:[Cs^+] = 10^5$, 25°C) using the R-F resin Cs λ is about 160, and for CC waste (low potassium) at the same conditions, Cs λ based on batch equilibrium data was about 400.

Kinetic Behavior

- The rate-limiting step in the loading of the resins in the laboratory-scale columns with NCAW type wastes (5M Na, low K) appears to be diffusion in the particle phase. This conclusion is supported by the fact that the breakthrough curves showed little to no dependence on the velocity of the fluid through the exchanger bed, by a flow interruption test, and by values of the mass-transfer coefficients that were nearly independent of the flow rate. Further, the shape of the breakthrough curve is largely a function of the residence time of the feed in the column.

- The rate-limiting step in the loading of the resins in the bench-scale columns with DSSF-type wastes (7M Na, high K) appears to be diffusion in the particle phase with an element of film diffusion. This may be due to the fact that DSSF has a higher viscosity than the NCAW; diffusion in viscous liquids is slower.

- The implication for scale-up is that the breakthrough curves from runs with small columns can be expected to be reasonably similar to the breakthrough curves for full scale columns if the feed composition, operating temperature and the flow rate (cv/h) are similar. Theoretically, the column dimensions (L:D) have no impact when the loading process is limited by diffusion in the particle phase although it is a common practice to design columns with an L:D >1.5 to minimize problems associated with channeling and feed distribution.

- A new batch of the R-F resin (BSC-210) was tested and exhibited improved kinetics over the older batch of resin (BSC-187). The improved kinetics was reflected by a steeper breakthrough curve. One reason for the improved kinetics is that the new resin has a smaller average particle size. Since the rate of the ion-exchange process is largely limited by diffusion in the particle, it is reasonable to expect the new resin to have faster loading kinetics.

Elution Behavior

- The elution curve is characterized by four separate regions: 1) an initial phase in which residual hydroxide is neutralized and little cesium is eluted, 2) a rapid increase to a high concentration of cesium, sometimes with a plateau, 3) exponential decrease of the cesium concentration, and 4) a tailing effect observed at low residual amounts of cesium.

- The CS-100 resin can be eluted with either nitric acid or formic acid. The amount of chemicals added as eluant can be minimized by eluting at a slower rate, raising the temperature, and decreasing the acid concentration. While using a lower acid concentration results in addition of fewer chemicals to the system, the actual volume is larger because the acid concentration is lower.

- During many runs, significant channeling of the eluant in the column was observed with the R-F resin (batch BSC-187, produced in 1988) in 200 mL columns. During elution, the resin shrinks 35% and tends to adhere to itself, causing the resin to pull away from the column walls. The result is a poor elution curve requiring excessive quantities of eluant and incomplete elution of the cesium. The resin does not appear to be very sticky, as the bed settled and excellent elution profiles were obtained after light stirring of the resin. It is not known if this will be a problem in full-scale columns, but a larger bed might settle under its own weight.

- A new batch of the R-F resin (BSC-210) presented no difficulty in elution. The material did not appear to stick together, and tailing of

the elution curve was not observed. The reason(s) for the different elution performance of the two batches of resin is not known.

- In the absence of channeling, the R-F resin can be eluted by either nitric or formic acid.

- It was not possible to determine the extent of elution by measuring the cesium in the eluant because the residual cesium on the resin is a complex function of the elution conditions: temperature, eluant type and concentration, flow rate, and resin type.

Radiation Stability of CS-100

- There was a decrease in resin selectivity or capacity as a function of radiation dose, although the decrease was small in both flow and static tests. The selectivity or capacity of the CS-100 resin appears to decrease less than 10% for a radiation dose of $>10^9$ Rad.

- Gases generated during the static radiation testing of the CS-100 resin were collected and analyzed. Hydrogen was the most abundant gas produced, followed by nitrogen, nitrous oxide, and oxygen. The relative amounts of the production of these gases are consistent with the organic resin material acting as a source of reductant.

Radiation Stability of R-F

- Preliminary K_d data indicate that the R-F resin has a slight decrease in selectivity or capacity as the radiation dose increases. The extent of this loss appears to be similar to that observed in radiation testing of CS-100.

- The rate of gas evolution from R-F resin during radiation exposure was identical to that of CS-100 resin for hydrogen, nitrogen, and nitrous oxide. The amount of oxygen produced was two orders of magnitude less than in the CS-100 resin case. This is due to the scavenging of the hydroxide radical (produced by radiolysis) by the R-F resin and results in oxidation of the resin material.

Chemical Stability

- According to the manufacturer's technical data sheet for the CS-100 resin, contact with nitric acid concentrations greater than 1M at 25°C is not recommended. Although not yet defined, a similar limit is probably appropriate for the R-F resin based on the chemical similarities of the materials. It is reported that the R-F resin can be dissolved in 3M nitric acid.

- Published data suggest that both resins lose capacity at a rate of 2 to 3% per loading/elution cycle. Considerable uncertainty is associated with this estimate of capacity loss, since the estimate for the R-F resin is based on only 7 cycles, the data for the CS-100 resin were obtained in 1979, and the resin is now made by a different manufacturer.

Resin Fouling

- A comparison of equilibrium data for CC waste (high organic complexant) to NCAW (low organic) suggests that the complexants have little effect on the equilibrium behavior of the resins. This is plausible because the organic complexants are probably present as anions and do not participate in the ion-exchange reaction. Additionally, the complexants are likely to bind with divalent ions, such as strontium, but not with monovalent ions, such as cesium. It is possible, although not considered likely, that repeated exposure of the resins to the complexants could result in fouling.

- Resin fouling with inorganic precipitates is a potential problem, especially when processing more concentrated waste streams (DSSF at 7M sodium). Many of the wastes in the tank are at roughly 40°C and generate significant volumes of precipitate when cooled to room temperature. Adequate dilution is one potential solution, although aluminum hydroxide ($Al(OH)_3$) may precipitate on dilution of some waste streams that are low in free hydroxide.

Processing Considerations

- Decontamination requirements were estimated for several waste types and for NRC Class C, A, and 1/10th of Class A limits in LLW. The decontamination requirements to meet 1/10th of Class A limits range from about 900 for an average SST waste supernate (5M sodium feed) to about 55,200 for NCAW. The DF required to meet the 1/10th of Class A limit for an estimated blended aqueous phase (includes all supernates and sludge wash solutions) from an ESW process is about 1700. For Class C limits, the only waste requiring cesium removal appears to be the NCAW, which has a required DF of approximately 2.

- Large DFs are expected to be difficult to achieve with a regenerable system because of the increasing elution requirements. However, DFs in excess of 10,000 were achieved with a 200 mL laboratory-scale system for two cycles of SRS waste-simulant on R-F resin.

- There appears to be little incentive for using a regenerable ion-exchange system with a polishing column rather than a once-through column system. At low cesium concentrations, which is the case for most expected feeds, the isotherm is approximately linear, and the Cs λ is a constant. Thus, the amount of exchanger required is independent of the cesium concentration, and nearly the same amount of resin would be required for a regenerable ion-exchange system with a polishing column as for a once-through column system.

- A limited effort at defining the compositional requirements of the eluate indicates that the ratio of the total moles of monovalent cations (Na^+, K^+, Rb^+) to moles of cesium must be <1500. This number is arrived at by assuming that the sodium that would normally be added as glass formers (or frit) is replaced by sodium in the eluate from the ion-exchange process. It is further assumed that sludge from an enhanced

sludge wash process is loaded at 50 wt% waste oxides in a HLW glass with a glass former composition of 92 wt% SiO_2 and 8 wt% Na_2O. Considerable uncertainty is associated with this value because of the evolving characteristics of the rest of the tank waste treatment system. The two areas of primary importance in setting the eluant composition are 1) the quantity of washed solids to be vitrified as HLW glass and 2) the characteristics of the HLW glass.

- A preliminary examination of a 4-column carousel operation indicates that the R-F resin requires about 10% of the total number of column loadings as the CS-100 resin for a given quantity of waste. For processing a NCAW feed of average composition, the [total cation]:[Cs^+] would be about 11 in eluate from an R-F loading and about 65 in eluate from the CS-100 resin. For processing a DSSF feed of average composition, the [total cation]:[Cs^+] would be about 100 in eluate from an R-F loading and 1200 in the eluate from the CS-100. Both resins appear capable of providing an eluate with [total cation]:[Cs^+] <1500 for these wastes unless the acidic eluate must be neutralized.

- A preliminary examination of the column-loading characteristics indicates that use of CS-100 resin will require larger columns or more columns than use of R-F resin.

- A preliminary examination of the elution data indicates that the moles of acid required for elution to a given C/C_0 can be minimized by reducing the acid concentration, reducing the flow rate, and raising the temperature.

- It is apparent that processing of waste at concentrations greater than about 7M sodium will be difficult. The DSSF simulant was near the solubility limit at 7M sodium (@ 25°C), and further concentration would increase the risk of precipitation and fouling of the resins. Perhaps more significantly, the R-F resin floats in DSSF at 8M sodium, and this would require a restraining device in the columns to keep the bed from fluidizing and mixing.

8.0 REFERENCES

Barney, G. S. 1976. *Vapor-Liquid-Solid Phase Equilibria of Radioactive Sodium Salt Wastes at Hanford.* ARH-ST-133. Atlantic Richfield Hanford, Richland, Washington.

Bibler, J. P. (SRL), R. M. Wallace (SRL) and L. A. Bray. 1990. "Testing A New Cesium-Specific Ion Exchange Resin For Decontamination of Alkaline-High Activity Waste." In *Proceedings of Waste Management '90*, Vol. 2, p. 747-751, Tucson, Arizona.

Boomer K. D., S. K. Parker, A. L. Boldt, J. D. Galbraith, and J. S. Garfield. 1993. *Tank Waste Technical Options Report.* WHC-EP-0616, Westinghouse Hanford Company, Richland, Washington.

Bray, L. A., K. J. Carson, and R. J. Elovich. 1993. *Initial Evaluation of Sandia National Laboratory-Prepared Crystalline Silico-Titanates for Cesium Recovery.* PNL-8847, Prepared by Pacific Northwest Laboratory for Westinghouse Hanford Company, Richland, Washington.

Bray, L. A., R. J. Elovich, and K. J. Carson. 1990. *Cesium Recovery Using Savannah River Laboratory Resorcinol-Formaldehyde Ion Exchange Resin.* PNL-7273, Pacific Northwest Laboratory, Richland, Washington.

Bray, L. A., L. K. Holton, T. R. Myers, G. M. Richardson, and B. M. Wise. 1984. *Experimental Data Developed to Support the Selection of a Treatment Process for West Valley Alkaline Supernatant.* PNL-4969, Pacific Northwest Laboratory, Richland, Washington.

Chilton, J. M. 1981. *The Use of a Phenolic-Carboxylic Acid Cation Resin in the Treatment of Low-Level Liquid Waste at Oak Ridge National Laboratory.* ORNL/TM-7524, Oak Ridge National Laboratory, Oak Ridge, Tennessee.

Coulson, J. M., and J. F. Richardson. 1991. *Chemical Engineering.* Vol. 2, 4th Ed., Pergamon Press, New York, New York.

Dixon, W. J., and F. J. Massey, Jr. 1969. *Introduction to Statistical Analysis.* 3rd Ed., p. 116, McGraw-Hill Book Company, Inc., New York, New York.

Freundlich, H. 1926. *Colloid and Capillary Chemistry.* Dutton, New York.

Helfferich, F. 1962. *Ion Exchange.* McGraw-Hill Book Company, Inc., New York, New York.

Hoza, M. 1994. "Multipurpose Optimization Models for High Level Waste Vitrification." In *Proceedings of Nuclear and Hazardous Waste Managment International Topical Meeting, Spectrum '94*, Vol. 2, pp. 1072-77, Atlanta, Georgia.

Koble, R. A., and T. E. Corrigan. 1952. "Adsorption Isotherms for Pure Hydrocarbons." *Industrial Engineering Chemistry*, **44**:383-7.

Langmuir, I. 1918. "The Adsorption of Gases on Plan Surfaces of Glass, Mica, and Platinum." *Journal of American Chemical Society*, **40**:1361.

Perry, R. H., and C. H. Chilton. 1973. *Perry's Chemical Engineers' Handbook.* 5th Ed., McGraw-Hill Book Company, New York, New York.

Perry, R. H., and D. W. Green. 1984. *Perry's Chemical Engineers' Handbook*, 6th Ed., p. 16-27, McGraw-Hill Book Company, New York, New York.

Popovich, R. P. 1964. *Ion Exchange Recovery of Cesium from Alkaline Supernatant Waste--Scaleup Studies.* HW-83461, General Electric Company, Richland, Washington.

Van Vleet, R. J. 1993. "Radionuclide and Chemical Inventories for the Double Shell Tanks." WHC-SD-WM-TI-543, Rev. 1, Westinghouse Hanford Company, Richland, Washington.

APPENDIX A

CESIUM DISTRIBUTION COEFFICIENTS

APPENDIX A

CESIUM DISTRIBUTION COEFFICIENTS

Appendix C plots Cs λ as a function of the equilibrium $[Na^+]:[Cs^+]$ at several sodium concentrations and temperatures for CS-100 and the R-F resin. Figures C.1 through C.6 plot Cs λ for NCAW and Figures C.7 through C.12 plot Cs λ for CC waste. The Cs λ values consistently increase as the equilibrium $[Na^+]:[Cs^+]$ is increased and as the temperature is decreased. The Cs λ values are lower for higher waste concentrations, as indicated by sodium concentration. The Cs λ values for R-F are higher than for CS-100, sometimes by more than a factor of 10 for a given equilibrium $[Na^+]:[Cs^+]$.

The R-F resin exhibits more complex behavior than CS-100 because the R-F data were taken over a broader range of $[Na^+]:[Cs^+]$. At high $[Na^+]:[Cs^+]$ (above 10^6), the R-F resin approaches a constant value of Cs λ. Thus, relatively small gains in cesium selectivity for the R-F resin are expected for higher than 10^6 $[Na^+]:[Cs^+]$. It appears that the leveling off of Cs λ for $[Na^+]:[Cs^+]$ is a result of saturation of the resin with sodium.

The R-F data were taken under conditions where the resin is being significantly loaded, while the CS-100 was probably not significantly loaded. For a more complete characterization of the equilibrium behavior of CS-100, the data should be taken over a wider range of $[Na^+]:[Cs^+]$.

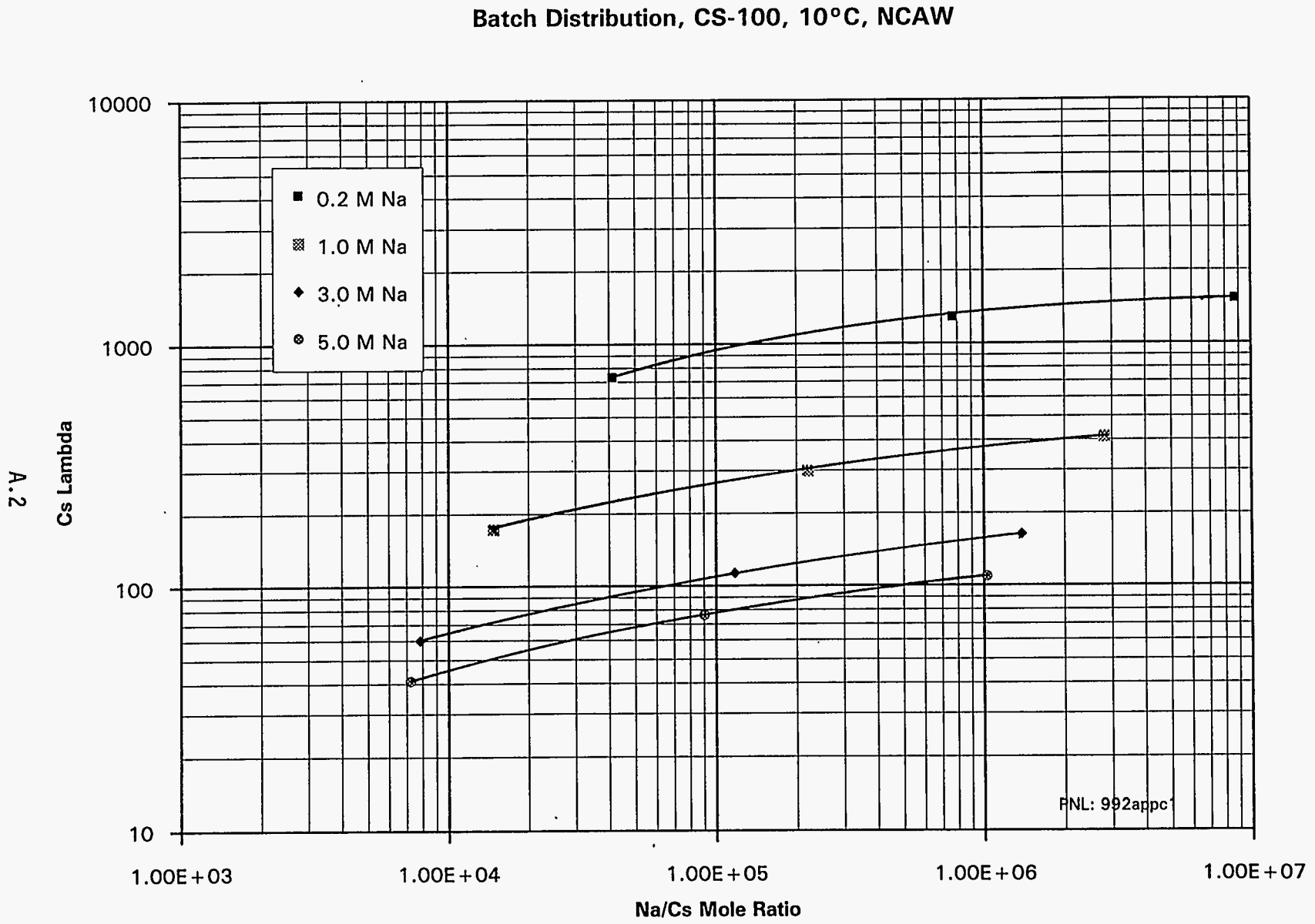
Batch Distribution, CS-100, 10°C, NCAW
10000
1000
100
10
Cs Lambda
0.2 M Na
1.0 M Na
3.0 M Na
5.0 M Na
PNL: 992appc1
1.00E+03
1.00E+04
1.00E+05
1.00E+06
1.00E+07
Na/Cs Mole Ratio

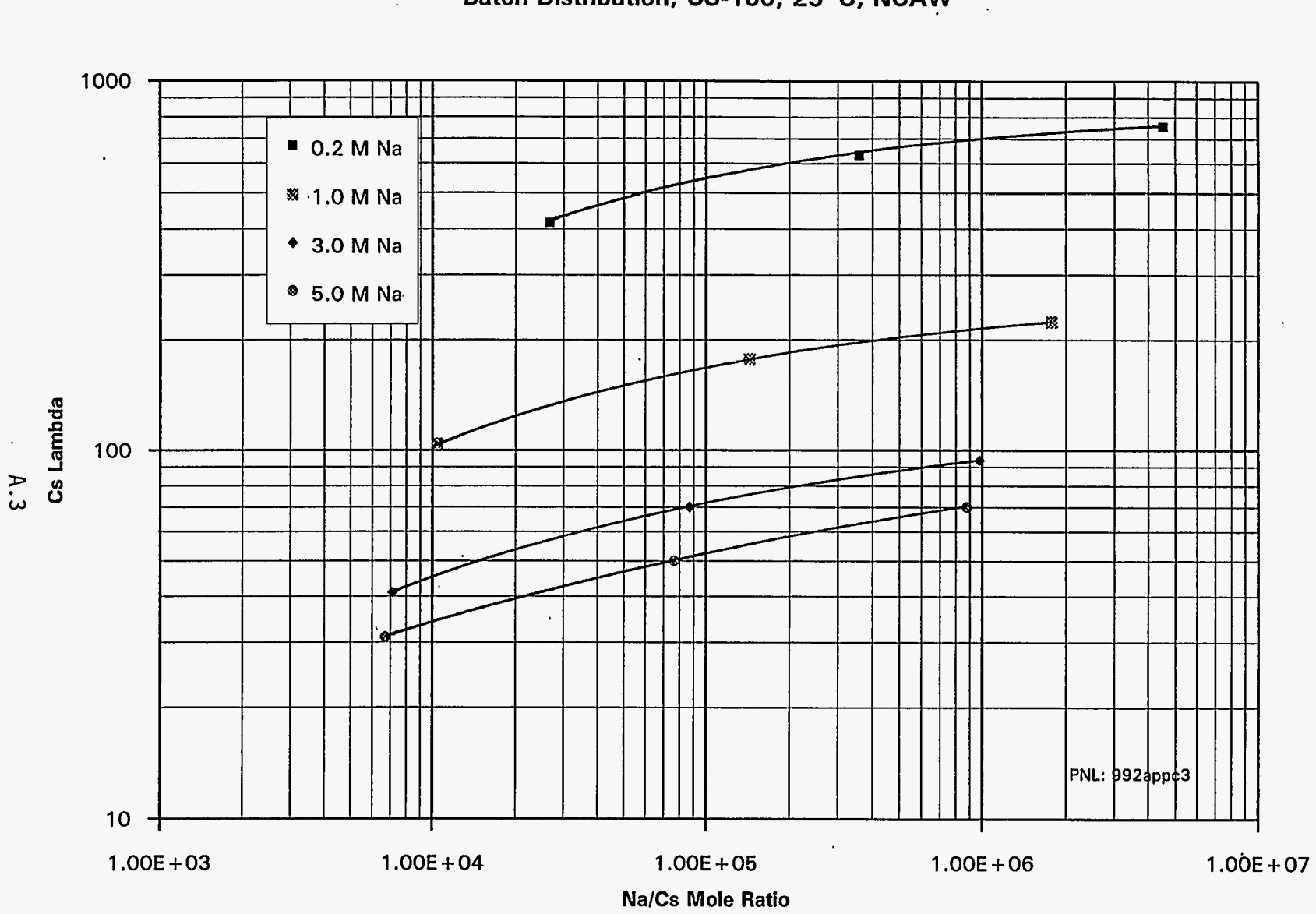
Batch Distribution, CS-100, 25°C, NCAW
1000
100
10
Cs Lambda
0.2 M Na
1.0 M Na
3.0 M Na
5.0 M Na
PNL: 992appc3
1.00E+03
1.00E+04
1.00E+05
1.00E+06
1.00E+07
Na/Cs Mole Ratio

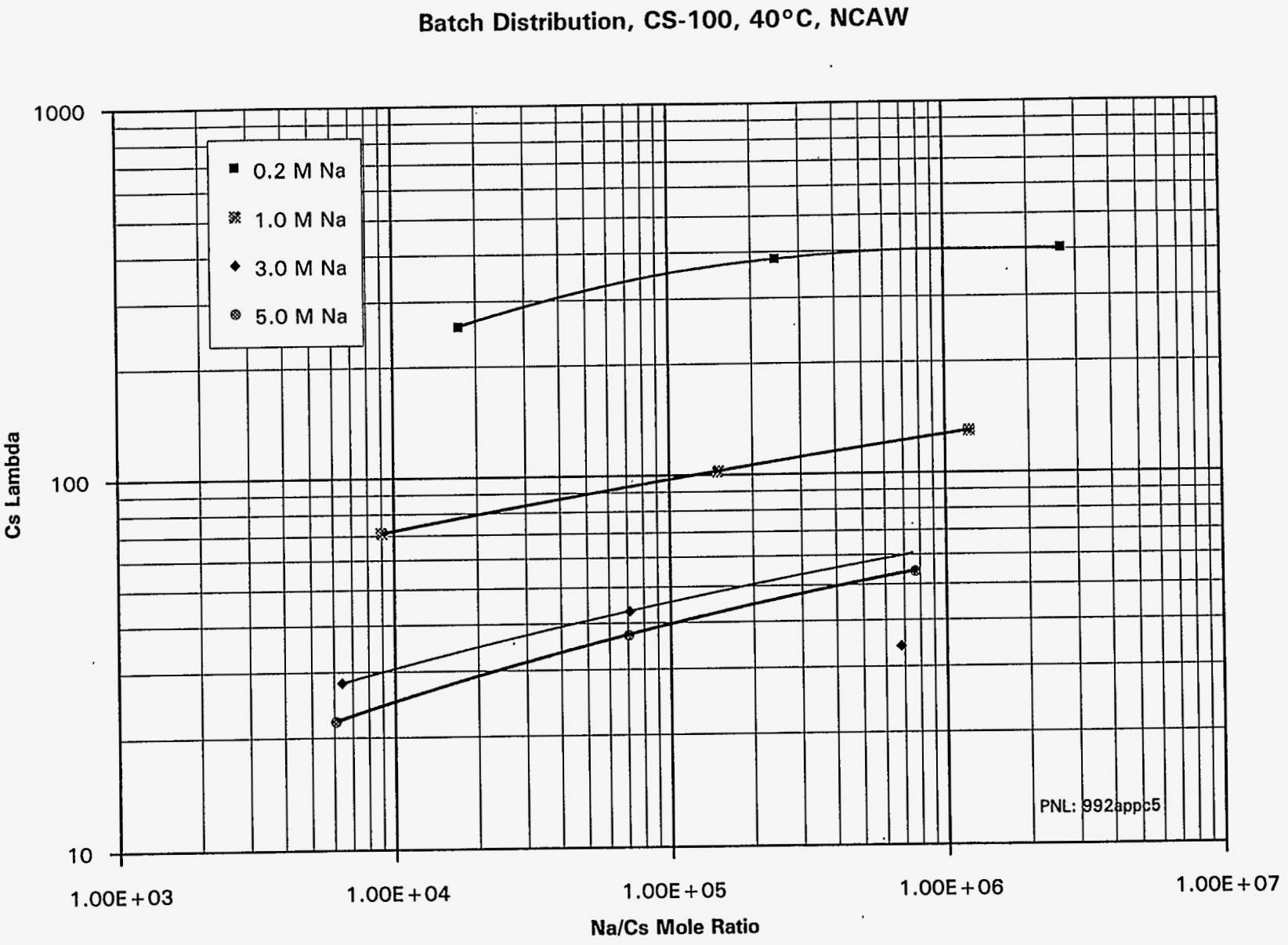
Batch Distribution, CS-100, 40°C, NCAW
1000
100
10
Cs Lambda
0.2 M Na
1.0 M Na
3.0 M Na
5.0 M Na
PNL: 992appc5
1.00E+03
1.00E+04
1.00E+05
1.00E+06
1.00E+07
Na/Cs Mole Ratio

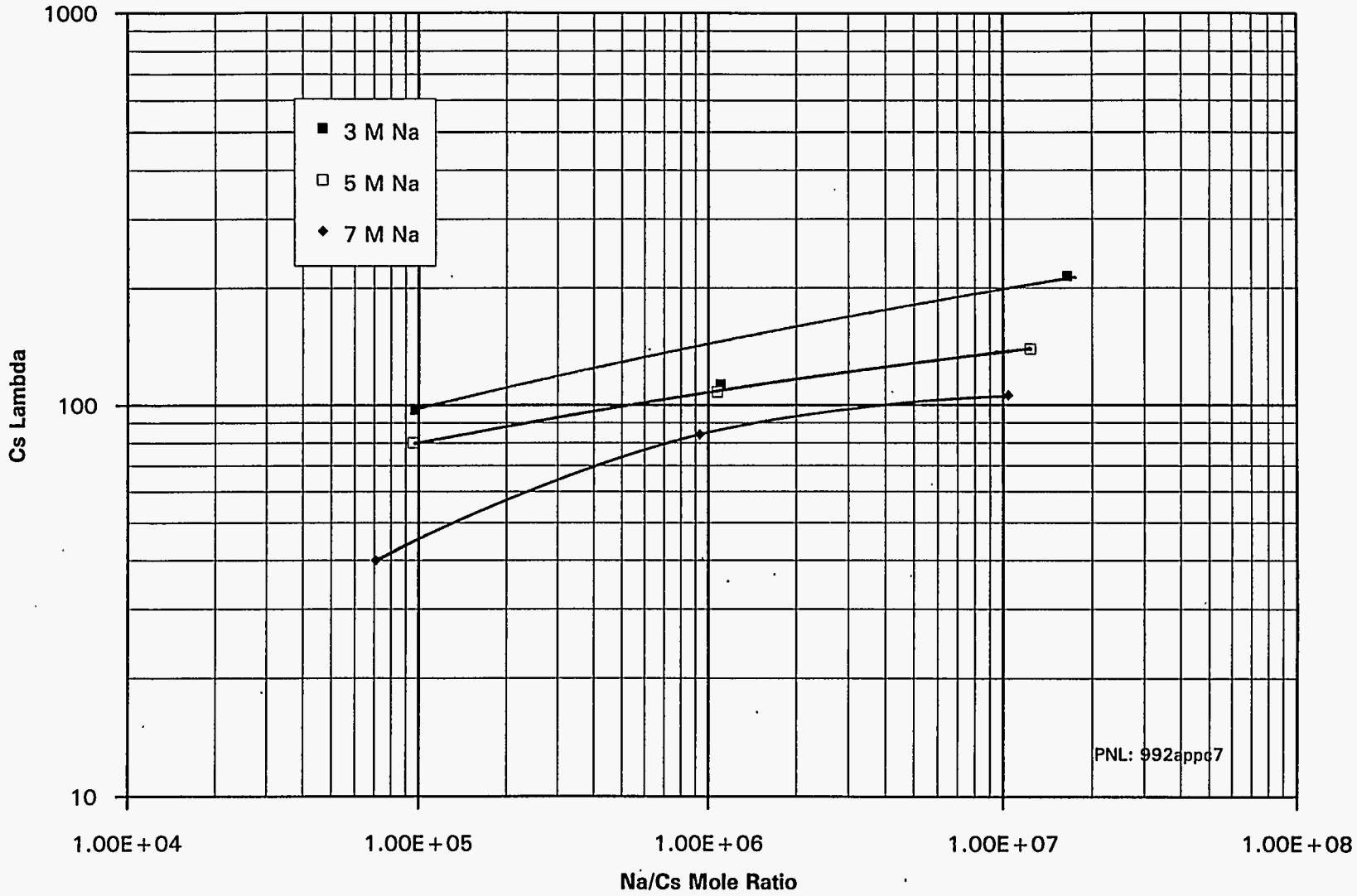
Batch Distribution, CS-100, 10°C, CC
1000
100
10
Cs Lambda
3 M Na
5 M Na
7 M Na
PNL: 992appc7
1.00E+04
1.00E+05
1.00E+06
1.00E+07
1.00E+08
Na/Cs Mole Ratio

Batch Distribution, CS-100,25°C, CC

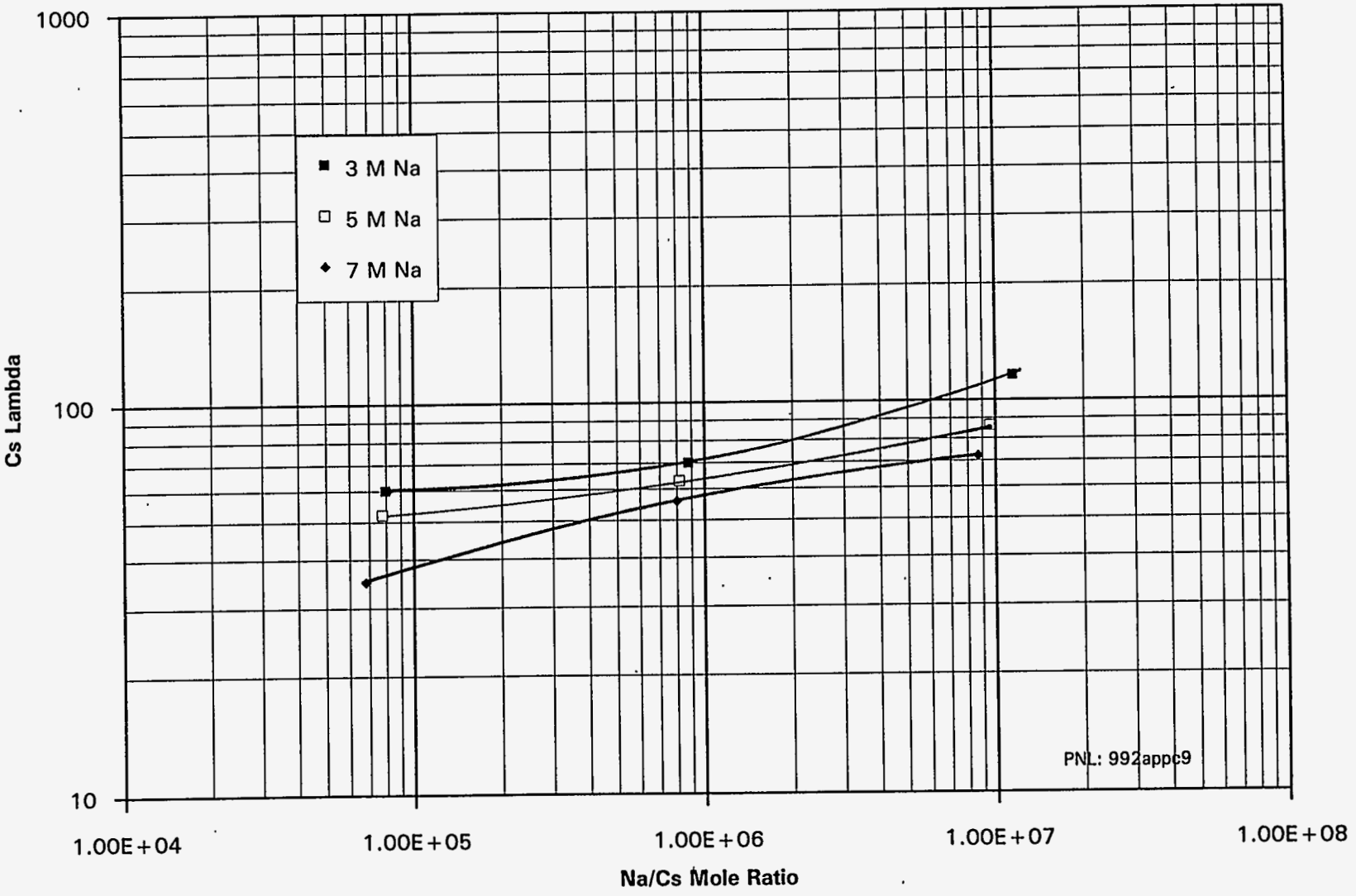

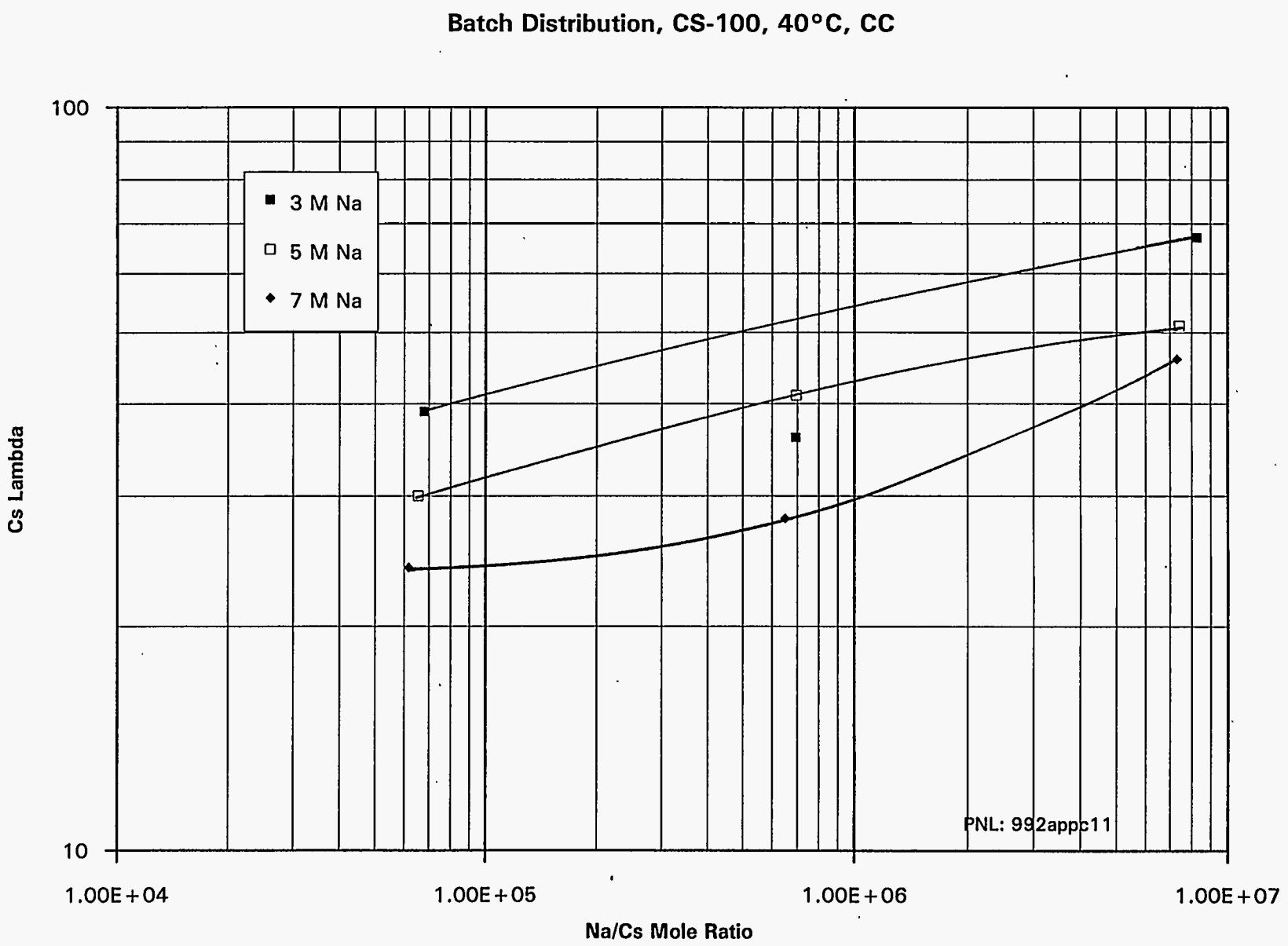
Batch Distribution, CS-100, 40°C, CC
100
10
3 M Na
5 M Na
7 M Na
Cs Lambda
PNL: 992appc11
1.00E+04
1.00E+05
1.00E+06
1.00E+07
Na/Cs Mole Ratio

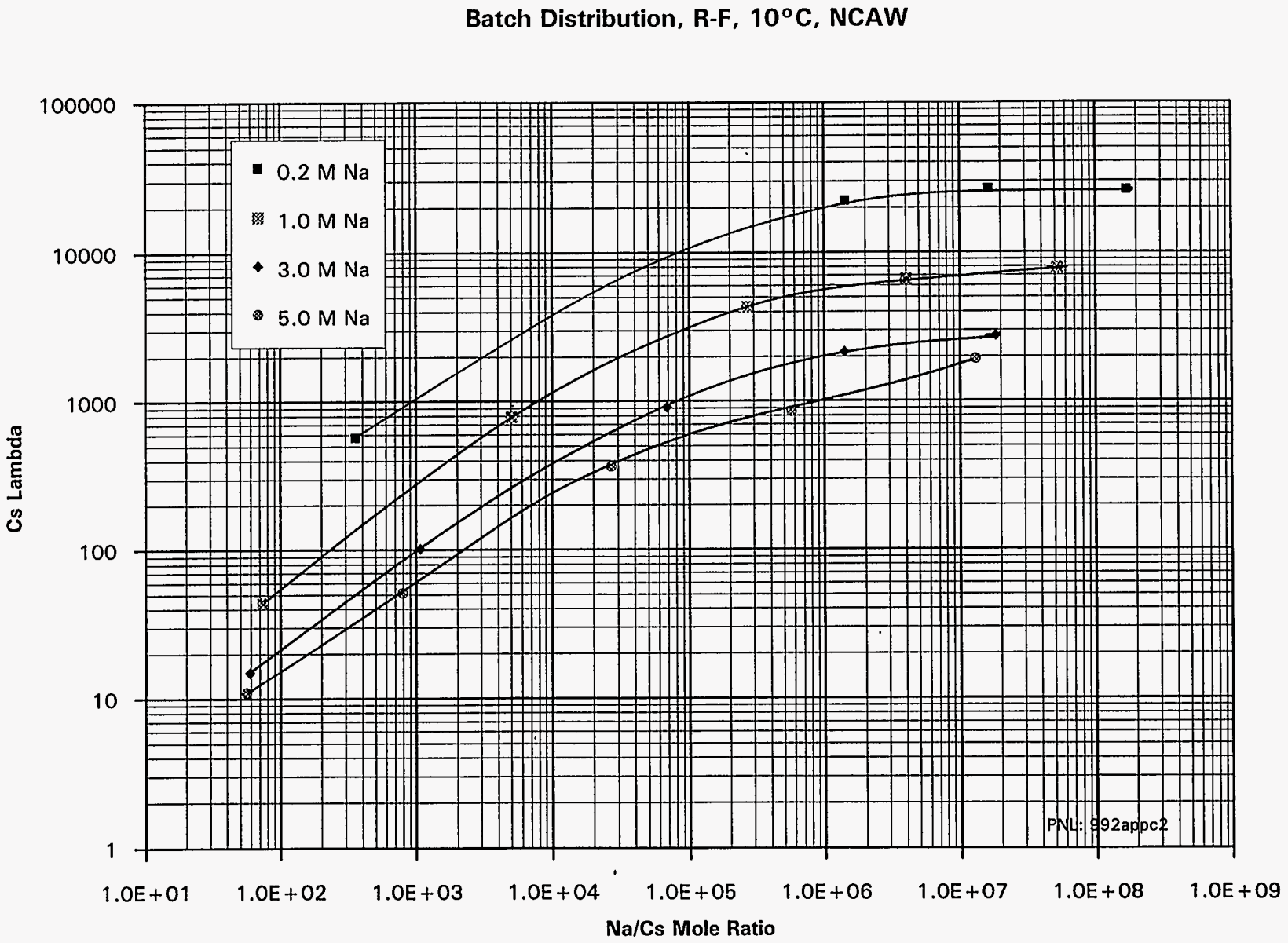
Batch Distribution, R-F, 10°C, NCAW
100000
10000
1000
100
10
1
Cs Lambda
0.2 M Na
1.0 M Na
3.0 M Na
5.0 M Na
PNL: 992appc2
1.0E+01
1.0E+02
1.0E+03
1.0E+04
1.0E+05
1.0E+06
1.0E+07
1.0E+08
1.0E+09
Na/Cs Mole Ratio

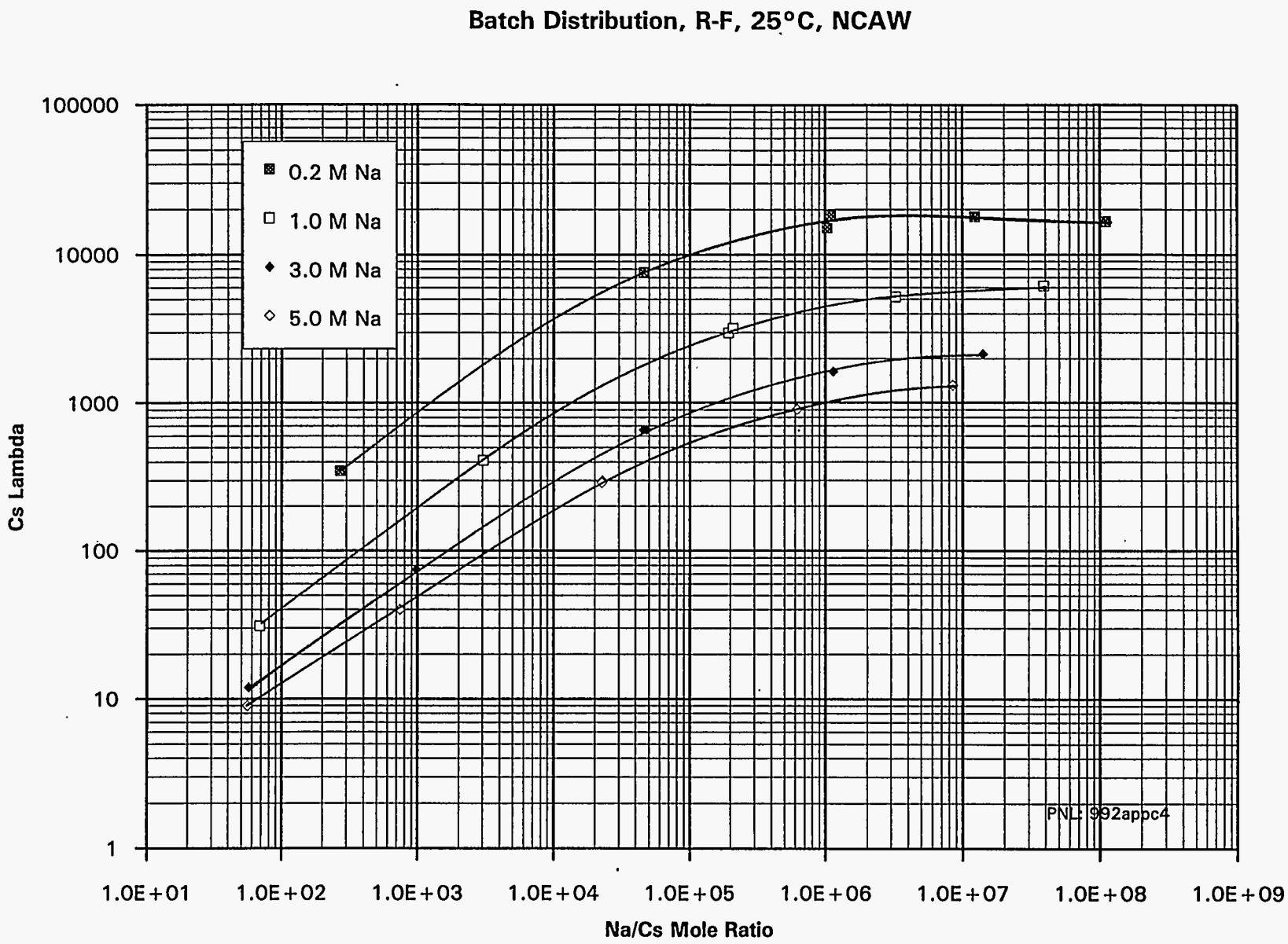
Batch Distribution, R-F, 25°C, NCAW
100000
10000
1000
100
10
1
Cs Lambda
0.2 M Na
1.0 M Na
3.0 M Na
5.0 M Na
PNL: 992appc4
1.0E+01
1.0E+02
1.0E+03
1.0E+04
1.0E+05
1.0E+06
1.0E+07
1.0E+08
1.0E+09
Na/Cs Mole Ratio

Batch Distribution, R-F, 40°C, NCAW

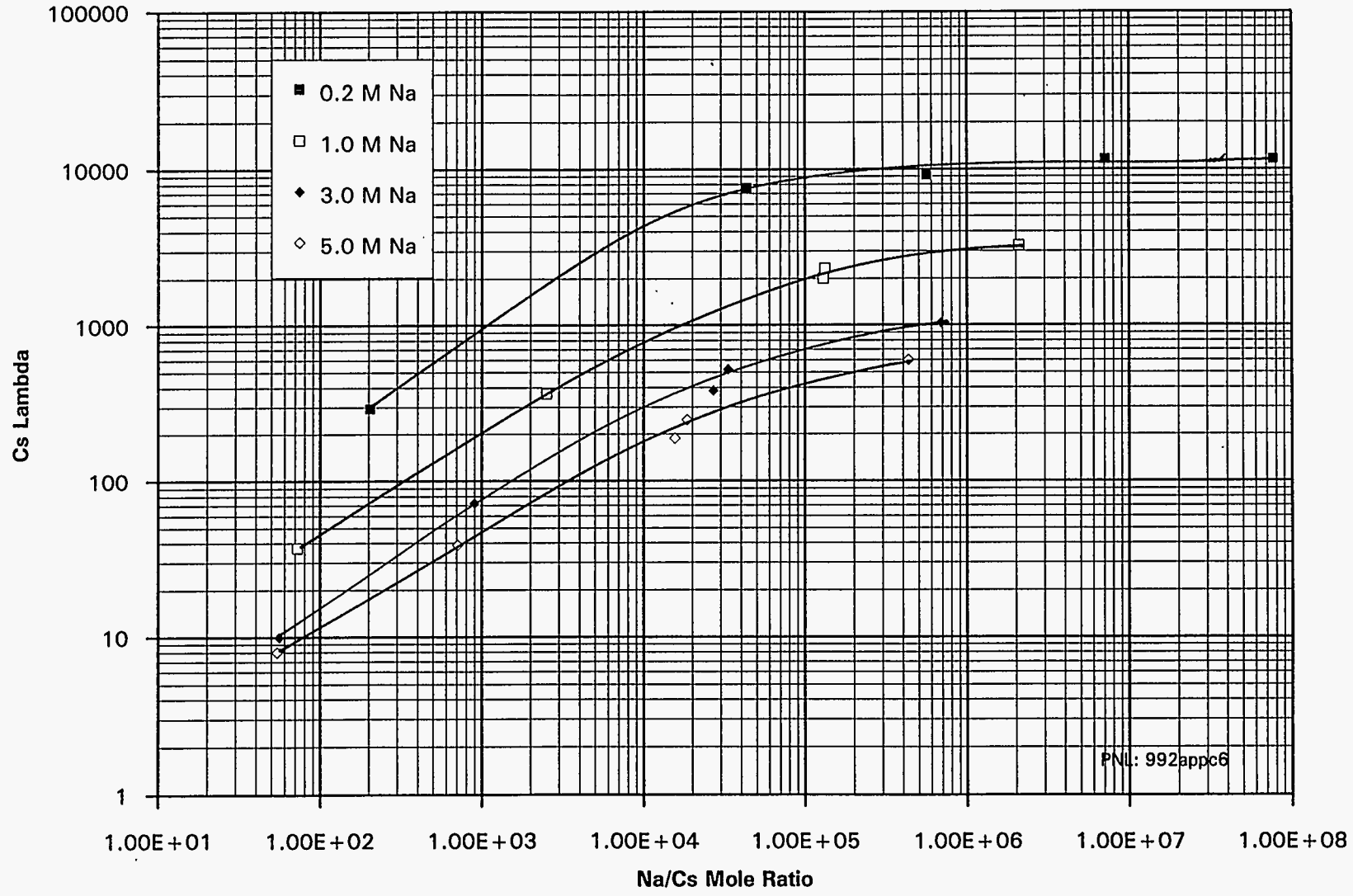

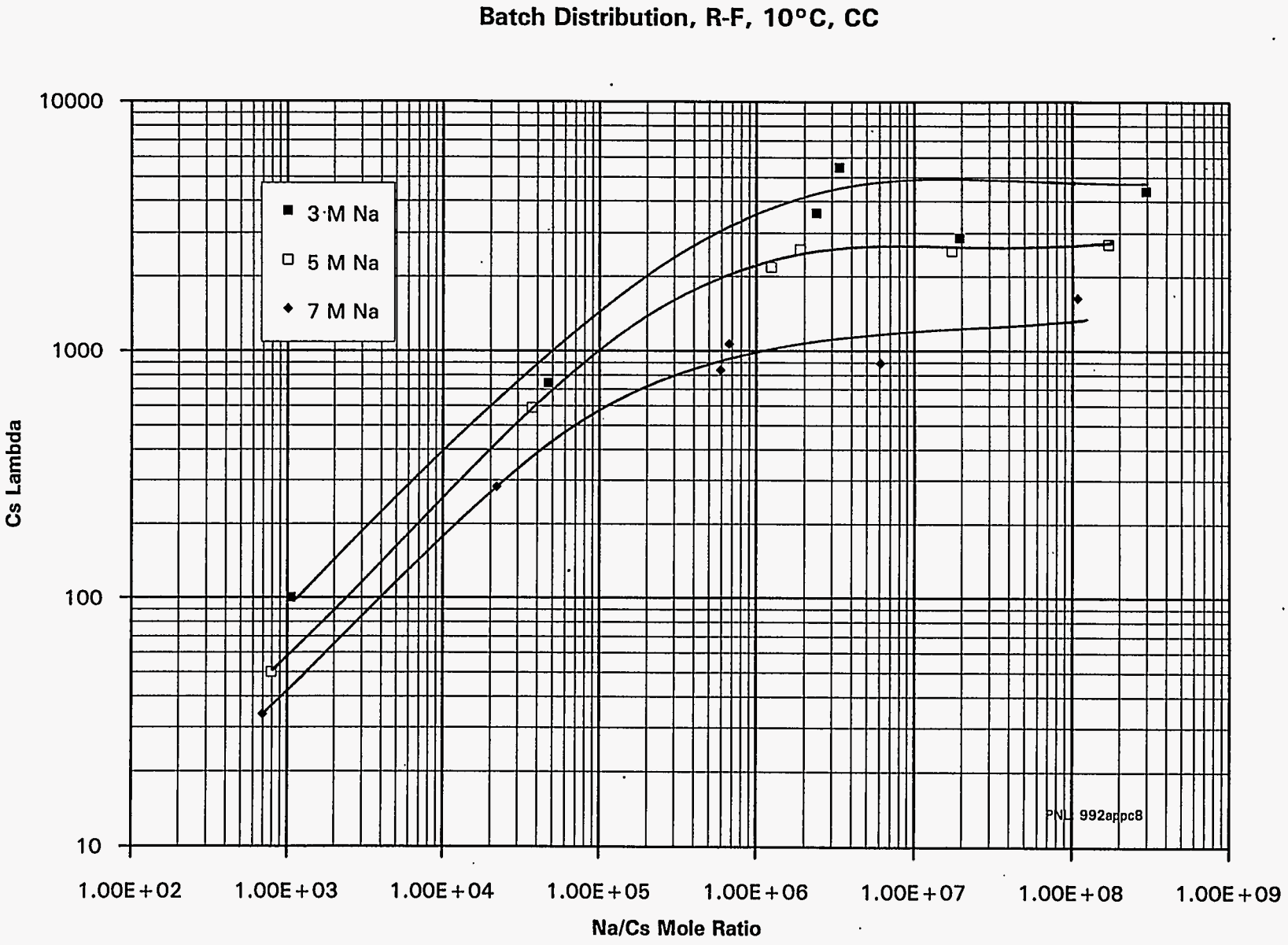
Batch Distribution, R-F, 10°C, CC
10000
1000
100
10
3 M Na
5 M Na
7 M Na
Cs Lambda
1.00E+02
1.00E+03
1.00E+04
1.00E+05
1.00E+06
1.00E+07
1.00E+08
1.00E+09
Na/Cs Mole Ratio
PNL 992appc8

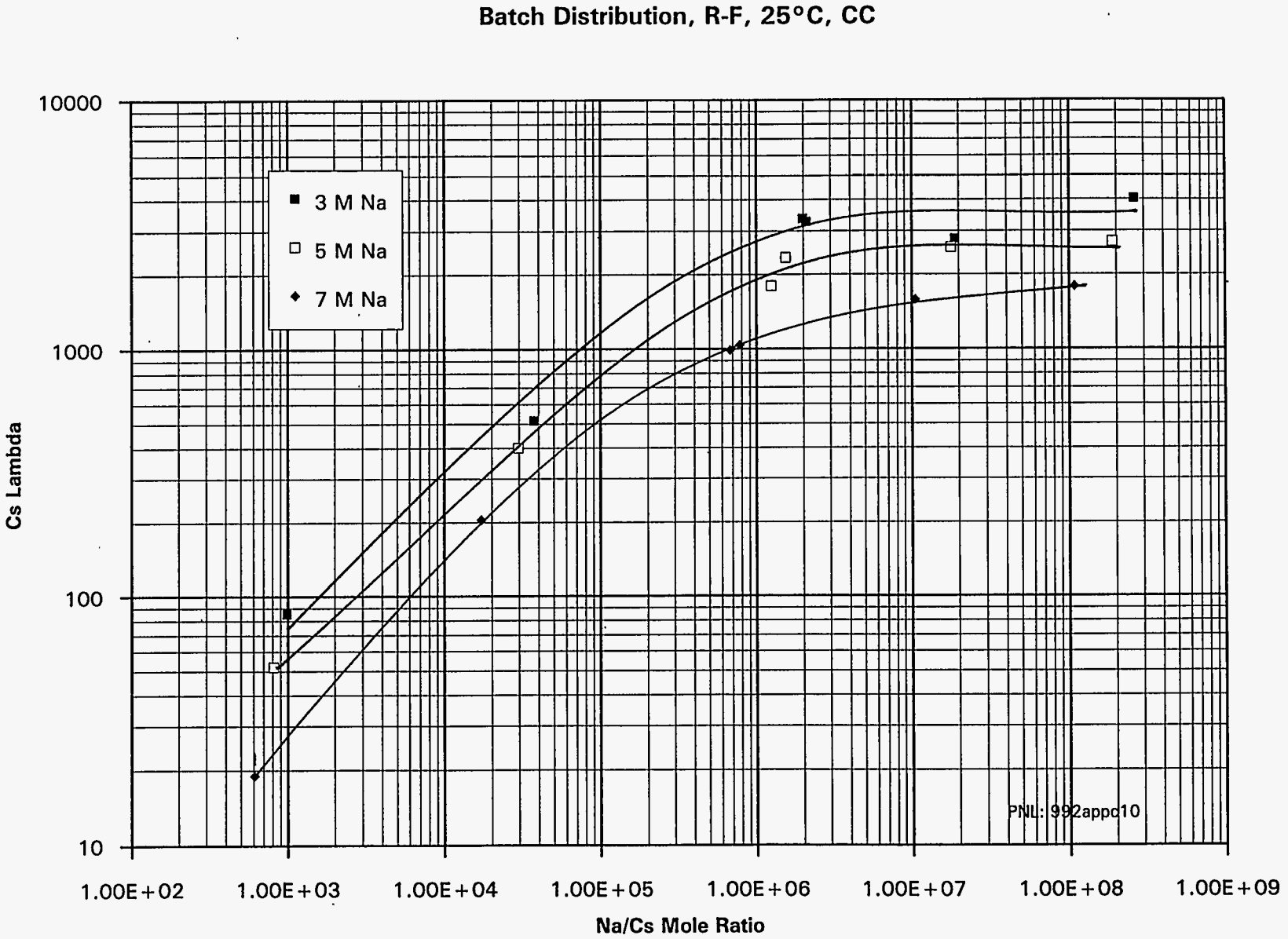
Batch Distribution, R-F, 25°C, CC
10000
1000
100
10
Cs Lambda
3 M Na
5 M Na
7 M Na
PNL: 992appc10
1.00E+02
1.00E+03
1.00E+04
1.00E+05
1.00E+06
1.00E+07
1.00E+08
1.00E+09
Na/Cs Mole Ratio

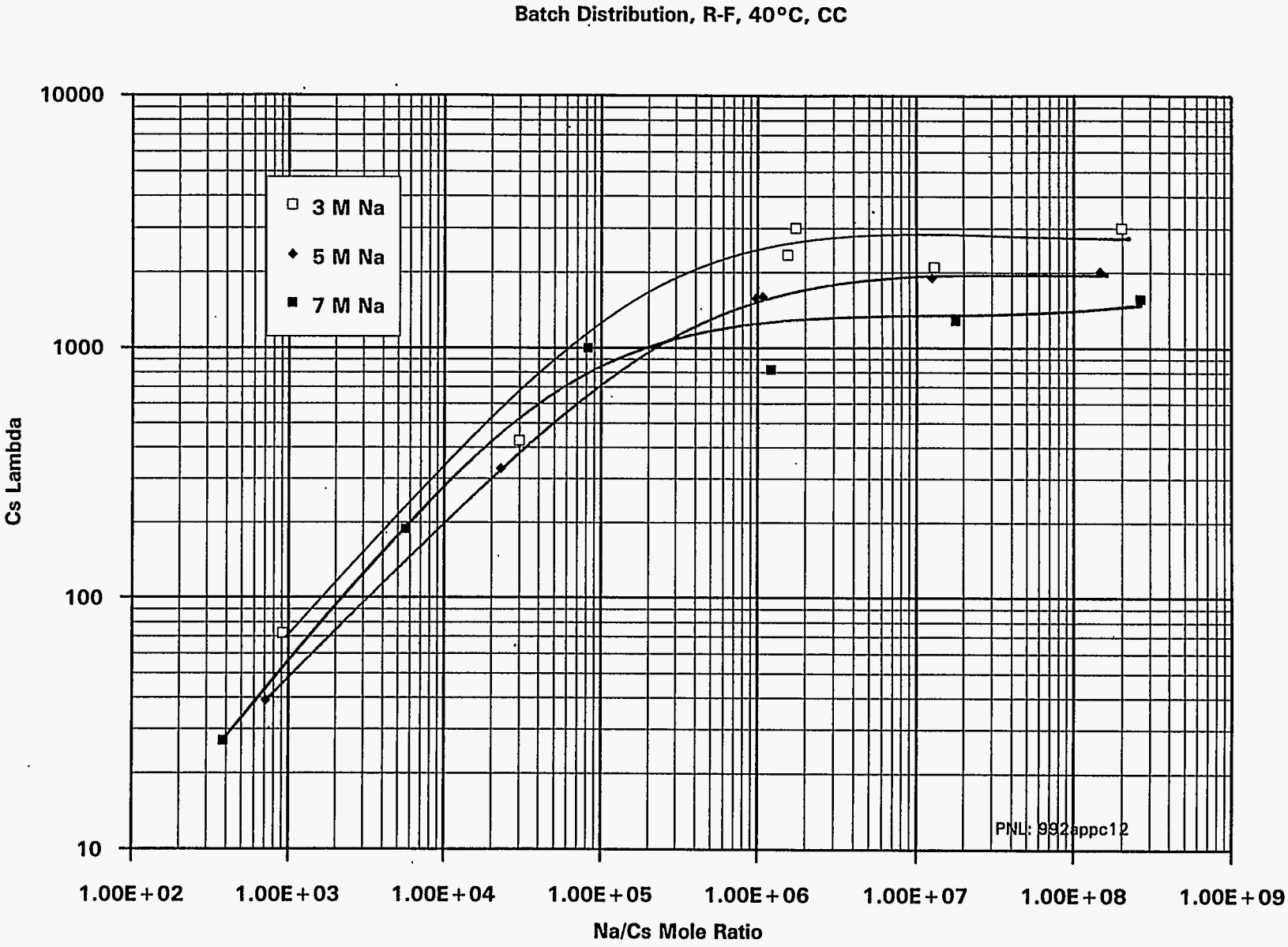
Batch Distribution, R-F, 40°C, CC
10000
1000
100
10
Cs Lambda
3 M Na
5 M Na
7 M Na
PNL: 992appc12
1.00E+02
1.00E+03
1.00E+04
1.00E+05
1.00E+06
1.00E+07
1.00E+08
1.00E+09
Na/Cs Mole Ratio

Distribution

No. of Copies

Offsite

12 DOE/Office of Scientific and Technical Information
P.O. Box 62
Oak Ridge, TN 37831

J.P. Bibler
MS 773-A
Westinghouse Savannah River Laboratory
Aiben, SC 29808

Robert King
Washington Department of Ecology
P.O. Box 47600
Olympia, WA 98594-7600

Suki Meris
BDM Federal, Inc.
20300 Gentury Blvd.
Germantown, MD 20874

Edward I. Rizkalla, PE
EM-36, Trevion II
U.S. Department of Energy
Washington, D.C. 20585

Dennis Wynne
EM-361, Trevion II
U.S. Department of Energy
12800 Middlebrook Road
Germantown, MD 20874

Onsite

4 **DOE Richland Operations Office**

S.T. Burnum, S7-53
P.T. Furlong, S7-52
R.A. Gilbert, S7-53
L.S. Waldorf, S7-53

No. of Copies

Onsite

16 **Westinghouse Hanford Company**

J.N. Appel, G3-21
L.D. Arnold, B2-35
S.A. Barker, G3-20
W.B. Barton, H5-27
K.M. Eager, H5-27
R.R. Gadd, G3-20
K.A. Gasper, G3-21
R.A. Kirkbride, H5-27
M.J. Klem, H5-27
C.J. Lyons, G3-20
P.A. Ombrellaro, G3-20
R.M. Orme, H5-27
D.L. Penwell, H5-27
I.E. Reep, G3-21
J.P. Sloughter, H5-27
D.J. Washenfelder, H5-27

45 **Pacific Northwest Laboratory**

L.A. Bray, P7-25
K.P. Brooks, P7-43
G.N. Brown, P7-25
S.A. Bryan, P7-25
B.C. Bunker, K2-45
C.D. Carlson, P7-25
J.A. Franz, K2-38
R.T. Hallen, P8-38
L.K. Holton, P7-43
T.L. Hubler, P8-38
B.M. Johnson, K1-78
A.Y. Kim, K2-45
W.L. Kuhn, K2-21
D.E. Kurath, P7-43 (20)
J.P. LaFemina, K2-25
G.J. Lumetta, P7-25
B.M. Rapko, P7-25
B.A. Reynolds, P7-43

No. of Copies

Onsite

W.G. Richmond, P7-35
D.W. Wester, P7-25

No. of Copies

Onsite

Publishing Coordination
Technical Report Files (5)